Microstrip Antennae with Various Substrate Thicknesses

by

Mehmet Kara

Dipl.-Ing. (M.Sc.Eng) (Konstanz, West Germany)

Dipl.-Ing. (M.Sc.Eng) (West Berlin, West **Germany)**

A thesis submitted in fulfilment of the requirement for the degree of

Doctor of Philosophy

The University of Adelaide

Department of Electrical and Electronic Engineering

Faculty of Engineering

May, 1996

The bitter and the sweet come from the outside,
the hard from within, from one's own efforts.

ALBERT EINSTEIN

Contents

Abstract

Microstrip antennae have been in the spotlight ever since their introduction in early sixties. A strong demand has arisen in many areas for small, lightweight and low profile antennae, for example in mobile communications, satellite communication terminals, covert communications, phased array, electronic warfare, missile seekers, missile telemetry, altimeters, biological telemetry, navigation, radar, surveillance, radiometers, and low probability of intercept - systems.

The effective design, analysis and application of microstrip antennae presupposes a quantitative knowledge of their properties as both elements and arrays on substrates of various sizes, thicknesses and permittivities. The significant advantages of printed circuits are somewhat offset by the electromagnetic complexity of the structure, because inherent inhomogeneity makes accurate analysis and performance prediction rather difficult. In particular, antennae with thick substrates require a detailed analysis of both radiated and surface waves. Many models have been proposed for microstrip antenna analysis, from simple static and quasistatic approximations to full-wave integral formulations solved by sophisticated computer techniques. None of these methods can be used to calculate all the physical and electrical properties of a microstrip antenna. This means that approximations and modifications may be needed when using the methods and this is inevitable when thick antenna element design is considered.

The research presented in this thesis principally addresses probe fed classical rectangular microstrip antenna elements and arrays, that are fabricated on substrate materials with various thicknesses and relative permittivities. A fundamental requirement for the design and analysis of microstrip antennae is the development of accurate and versatile analytical tools. Formulae have been developed for calculating the patch dimensions, the resonant input resistance, the resonant frequency, the bandwidth and the radiation patterns of elements, as well as the mutual coupling coefficients of arrays. The research has to some extent been driven by identifying methods capable of delivering fast and reliable numerical results, and which can be modified for calculating physical and electrical properties of thick antennae. To demonstrate the capability of the methods developed in this thesis, antenna elements and arrays with various substrate sizes, thicknesses and

permittivities were constructed and tested. The experimental results agree well with those calculated by the developed methods.

Increasingly stringent system requirements have led to a shift in focus to the design of novel miniaturised rectangular and ring broad-band and dual-band antenna elements. The size reduction and cost effective implementation of such antennae for microwave operation requires extensive experimental and numerical research. Novel configurations of patch antennae have been presented in this thesis, which provide dual-band and broad-band operations. Progress and achievement on unproved characteristics and miniaturisation is ultimately judged by its overall size reduction, cost effectiveness and reliability, as well as the specified microwave performance requirements. This thesis achieves several successes in further miniaturising of microstrip antennae, and in doing so has shown the potential for a new generation of antenna systems.

Useful information has been obtained which reveals the influence of the physical and effective dimensions of the patch, thickness, size and permittivity of the substrate, surface wave, radiation, dielectric and conductor losses, and feed point location on the antenna characteristics. The information is of sufficient detail to enable an engineering design that exploits these effects to optimise performance. The principles and results of the research presented in this thesis are in a form which is intended to be easily understood by all who wish to use it, irrespective of their level of mathematical skill. Numerical results, pertaining to the analysis of microstrip antenna elements satisfactorily indicate the accuracy and utility of the developed techniques for designing microstrip antennae and calculating mutual coupling coefficients between two rectangular antenna elements.

Statement of Originality

This work contains no material which has been accepted for the award of any degree or diploma in any University or other tertiary institution and, to the best of the author's knowledge and belief, contains no material previously published or written by another person, except where due reference has been made in the text.

The author gives consent to this copy of his thesis, when deposited in the University Library, being available for loan and photocopying.

Mehmet Kara

Signed. Date: May 29, 1996

Acknowledgments

Dr Donald. W. Griffin, the author's supervisor, deserves special thanks for his guidance.

Acknowledgment is due to the author's wife Mufide, and his children, Ela Konstanze, Emren Edwin, Denise Eren and Ervin Ender for their unfailing support. It is their unselfish effort that has allowed him to work with so little distraction for the many hours necessary to complete such a degree.

Many thanks must go to Dr D. Nandagopal, Research Leader, Weapons Systems Division, DSTO, for his regular encouragement and to Dr Colin S. Coleman, Head of the Guidance and Control Group of the Weapons Systems Division, DSTO, and Dr Peter D. Simms for helping proofread the thesis.

Messrs G. W. Pook and G. L. Allison are to be thanked for their skilled technical and mechanical assistance.

List of Author's Related Publications

The following is a list of the author's publications which are related to the research reported in this thesis.

Chapter 3

M. Kara, "A new method for computing the physical parameters of rectangular Microstrip Antenna Element", *Proceedings of IREECON International Convention*, Melbourne, Australia, pp. 642-645, September 1989.

M. Kara, "Design principles of physically thick microstrip antenna elements for missile applications", *Third Australian Symposium on Antennas*, Sydney, Australia, February 1991.

M. Kara, "Effective permittivity of rectangular microstrip antenna elements with various thicknesses of substrates", *Microwave and Optical Technology Letters*, Vol. 10, No. 4, pp. 244-247, 1995.

M. Kara, "Formulae for the computation of the physical properties of rectangular microstrip antenna elements with various substrate thicknesses", has been accepted for publication in *Microwave and Optical Technology Letters* and will appear in the *July 1996 issue.*

M. Kara, "A new formula for patch resonant length",to be published in *International Journal of Electronics.*

Chapter 4

M. Kara, "The input resistance of rectangular microstrip antenna elements with various substrate thicknesses," to be published in *Microwave and Optical Technology Letters.*

M. Kara, "An efficient technique for the computation of the input resistance of rectangular microstrip antenna elements with thick substrates," to be published in *Microwave and Optical Technology Letters.*

Chapter 5

M. Kara, "The resonant frequency of rectangular microstrip antenna elements with various substrates thicknesses", M*icrowave and Optical Technology Letters,* Vol. 11, No. 2, pp. 55-59, February 1996.

M. Kara, "Closed-form expression for the resonant frequency of rectangular microstrip antenna elements with thick substrates", has been accepted for publication in *Microwave and Optical Technology Letters* and will appear in the June 20, 1996 issue.

Chapter 6

M. Kara, "A simple technique for calculating the bandwidth of rectangular microstrip antenna elements with various substrate thicknesses", *Microwave and Optical Technology Letters* Vol. 12, No. 1, pp. 16-20, May 1996.

M. Kara, "A novel technique for computation the bandwidth of rectangular microstrip antenna elements with thick substrates", has been accepted for publication in *Microwave and Optical Technology Letters* and will appear in the June 5, 1996 issue.

M. Kara, "Thick patch on a thin substrate improves the bandwidth of microstrip antennas", *Fourth Australian Symposium on Antennas*, p. 23, Sydney, February 1994.

Chapter 7

M. Kara, "Examination of far field characteristics of rectangular microstrip antenna elements", *Proceedings of RADARCON 90*, Adelaide, Australia, pp. 407-414, April 1990.

M. Kara and N. M. Martin, "Measuring the near-field of rectangular microstrip antenna elements", *Fourth Australian Symposium on Antennas*, p.18, Sydney, Australia, February 1994.

N. M. Martin, M. Kara and D. Nandagopal, "Apparatus for the measurement of microstrip antenna near-fields", *Asia-Pacific Microwave Conference*, Adelaide, Australia, pp. 803-806, August 1992.

M. Kara, "The calculation of the far-field radiation patterns of rectangular microstrip antenna elements with various substrate thicknesses", to be published in *Microwave and Optical Technology Letters.*

D. W. Griffin and M. Kara et al. "Quantitative comparison of near electric field measurement methods relevant to microstrip integrated microwave structure design", *Proceedings of IREECON International Convention*, Sydney, Australia, pp. 318-321, September 1987.

Chapters 8 and 9

M. Kara, "A novel broad-band rectangular microstrip antenna element", *Microwave and Optical Technology Letters*, Vol. 7, No. 15, pp. 685-687, October 1994.

M. Kara, "Novel dual-band rectangular microstrip antenna element" *International Journal of Electronics*, Vol. 78. 2, pp. 417-422, 1995.

M. Kara, "Novel microstrip antenna elements for radar and satellite systems applications", *Workshop on Applications of Radio Science*, Canberra, Australia, June 1995.

M. Kara, "Miniaturised microstrip antenna elements for surface and space borne vehicles applications", to be published in *Journal of Electrical and Electronics Engineering, Australia.*

Chapter 10

M. Kara, "A novel tiny microstrip ring antenna element", *Microwave and Optical Technology Letters*, Vol. 10, No. 5, pp. 259-261, December 1995.

M. Kara, "Miniaturised microstrip antenna elements", *Fifth Australian Symposium on Antennas*, p. 18, Sydney, Australia, February 1996.

Chapter 11

M. Kara, "Novel technique for computation of mutual coupling between two rectangular microstrip antenna elements with thick substrates", to be published in *IEE Proceedings, Microwaves, Antennas and Propagation.*

M. Kara, "A simple technique for the computation of the mutual coupling between two rectangular microstrip antenna elements with various substrate thicknesses", *Fifth Australian Symposium on Antennas,*p. 14 Sydney, Australia, February 1996.

Other Related Publications

M. Kara and D. W. Griffin, "An investigation of microstrip patch antennas using various thickness of dielectric", *Proceedings of IREECON International Convention*, Sydney, Australia, pp. 339-342, September 1987.

D. W. Griffin and M. Kara, "Experimental evidence that microstrip patches and flat dipoles on grounded substrates are same type of element", *IEEE Antennas and Propagation Symposium Digest, Syracuse,* USA, pp. 458-461, June 1988.

M. Kara, "Directivity and gain of electrically thick rectangular microstrip antennas", *Second Australian Symposium on Antennas*, Sydney, Australia, February 1989.

M. Kara, "Functional dependence of directivity and gain of rectangular microstrip antenna elements of their structural parameters", *Proceedings of IREECON International Convention*, Melbourne, Australia, pp. 164-167, September 1989.

M. Kara, D. Nandagopal, N. M. Martin and B. Bates, "Antenna options for missile seekers", *Third Australian Symposium on Antennas*, Sydney, Australia, Feb. 1991.

M. Kara, "Considerations for X- and Ku band rectangular microstrip antenna elements", *Proceedings of IREECON International Convention*, Sydney, Australia, pp. 688-691, September 1991.

N. M. Martin, D, Nandagopal, M. Kara, V. N. Tran and S. Hamilton, "Body fixed antenna options for seekers", *Proceedings of RADARCON 92, Brighton, United Kingdom,* pp. 272-275, 1992.

M. Kara, "Effects of substrate thickness on performance characteristics of rectangular microstrip antenna elements", *Asia-Pacific Microwave Conference*, Adelaide, Australia, pp. 203-206, August 1992.

M. Kara, "Microstrip antenna element with thick Patch conductor", to be published in *Electronics Letters.*

List of Principal Symbols

Symbols and acronyms used in the text are defined below. In each instance, the symbols has been defined on introduction to avoid misinterpretation of its meaning.

Symbol	Description
a	inset distance: distance between the feed probe and the nearest end of a rectangular antenna element
A	area of an antenna element
B_a	input susceptance of an radiating aperture
BW	bandwidth expressed in percent
C_{10}	patch capacitance for the fundamental mode
C_b	static main field capacitance of an antenna element
C_1	edge capacitance on one side of an antenna element's length
C_2	edge capacitance on one side of an antenna element's width
c_o	velocity of electromagnetic waves in free space
C_p	coupling coefficient
C_{pE}	coupling coefficient in the E-plane
C_{pH}	coupling coefficient in the H-plane
C_T	total capacitance of a patch
D	outer diameter of a ring patch
d	inner diameter of a ring patch antenna
d_o	diameter of the feed probe (3.04 mm)
$E_\theta(\theta)$	total radiated field in the E-plane
$E_\phi(\theta)$	total radiated field in the H-plane

$\underline{E}$	electric field intensity vector
$(E_\theta)_o$	total electric field induced on the second patch
f_r	resonant frequency
f_{mn}	resonant frequency of the m,n mode
f_{10}	resonant frequency from the dominant mode
$F_H(\theta)$	far field radiation pattern in the H-plane
$F_E(\theta)$	far field radiation pattern in the E-plane
G_a	conductance contributed by the radiation field
$\overline{G_a}$	normalised radiation conductance
G_r	radiation conductance
G_s	conductance due to substrate surface waves
h	substrate thickness
I_D	polarisation current induced in the second patch
$I_E(0)$	input current of the fed patch
k_o	free space wavenumber
k_{mn}	wave number of the m,n mode
k_x,k_y	eigen values
k_1,k_2	surface wave propagation coefficients
L	length of a transmission line or a rectangular antenna element
L_e	electrical length
L_{ef}	effective length
L_{eq}	equivalent patch length
M	magnetic current
Q_c	quality factor due to ohmic losses
Q_d	quality factor due to dielectric losses
Q_s	quality factor associated with surface wave propagation
Q_r	quality factor due to radiation losses
Q_T	total quality factor that includes internal and external losses
P_r	power lost to radiation
P_s	power lost to surface waves
R_c	equivalent resistance due to ohmic losses
R_d	equivalent resistance due to losses in the dielectric

R_s	equivalent resistance for the surface waves
R_r	radiation resistance
R_{in}	input rsistace of antenna
R_T	total input resistance
R_N	normalised resistance
R_o	free space impedance = $120\pi\Omega$
S	distance between two antenna elements
$S_{11},S_{12},S_{21},S_{22}$	scattering matrix parameters
S_{11}	return loss coefficient
S_{21}	scattering transfer coefficient
$\tan\delta$	loss tangent of a dielectric material
$\underline{u}_x$	unit vector in the x-direction; similarly $\underline{u}_y,\underline{u}_z,\underline{u}_p,\underline{u}q,\underline{u}f$
U_o	input induced voltage
v_{pL},v_{pw}	phase velocities of a quasi transverse electromagnetic (TEM) mode on a microstrip line
VSWR = S	voltage standing wave ratio
W	width of a microstrip antenna element
W_{ef}	effective patch width
W_{eq}	equivalent patch width
Y_a	aperture admittance
X_L	lumped series reactance of the feed
Y_c	characteristic admittance of a microstrip line
Y_{in}	input admittance
Z_{aw}	characteristic impedance of an air filled microstrip line of width
Z_{aL}	characteristic impedance of an air filled line of length
Z_{cw}	characteristic impedance of a dielectric filled microstrip line of width
Z_{cL}	characteristic impedance of a dielectric filled microstrip line of length
Z_{in}	input impedance of a microstrip antenna element
Z_{12}	mutual impedance
$\overline{Z_{12}}$	normalised mutual impedance

ΔW	edge extension as a function of the patch width
ΔL	edge extension as a function of the patch length
β	propagation constant
ε_{dyn}	dynamick permittivity
ε_{ew}	effective relative dielectric constant as a function of the patch width
ε_{eL}	effective relative dielectric constant as a function of the patch length
ε_{edL}	effective dynamic dielectric constant as a function of the patch length
ε_o	permittivity of free space $= 8.854\ 10^{-12}$ F/m
ε_r	relative dielectric constant of a dielectric substrate
η	antenna efficiency in percent
λ_d	wavelength in a dielectrically filled medium
λ_o	wavelength in free space
μ_o	free-space permeability
θ_{BE}	half power beamwidth in the E-plane
θ_{BH}	half power beamwidth in the H-plane
Ω	ohm
ω	resonant angular frequency ($2\pi f_r$)

Chapter 1

Introduction

1.1 Microstrip Antennae and Arrays

The vast scope of the work published on microstrip antennae and arrays since the early 1970's makes evident the broad range of research and development being undertaken in this field throughout the world. In fact, rapidly developing markets in warfare systems, navigational aids systems, personal communications systems, mobile satellite communications, direct broadcast satellite systems, intelligent vehicle highway systems, wireless local area networks, the global positioning system, medical hypothermia and remote sensing, suggest that the demand for microstrip antennae and arrays will increase even further. Such research covers many different structural shapes of microstrip antenna elements and arrays [1-16] with various types of substrate materials with different values of dielectric constant operating over a broad frequency range. However, the range of substrate thickness of most of the antennae designed so far is thin compared with the range considered in this thesis.

A microstrip antenna element, also called a patch antenna or printed circuit antenna, in its simplest form commonly consists of a metal patch on one side of a single thin dielectric sheet, and a ground plane on the other side. Patch antennae can be fed in many ways [1 - 5]. The feed type

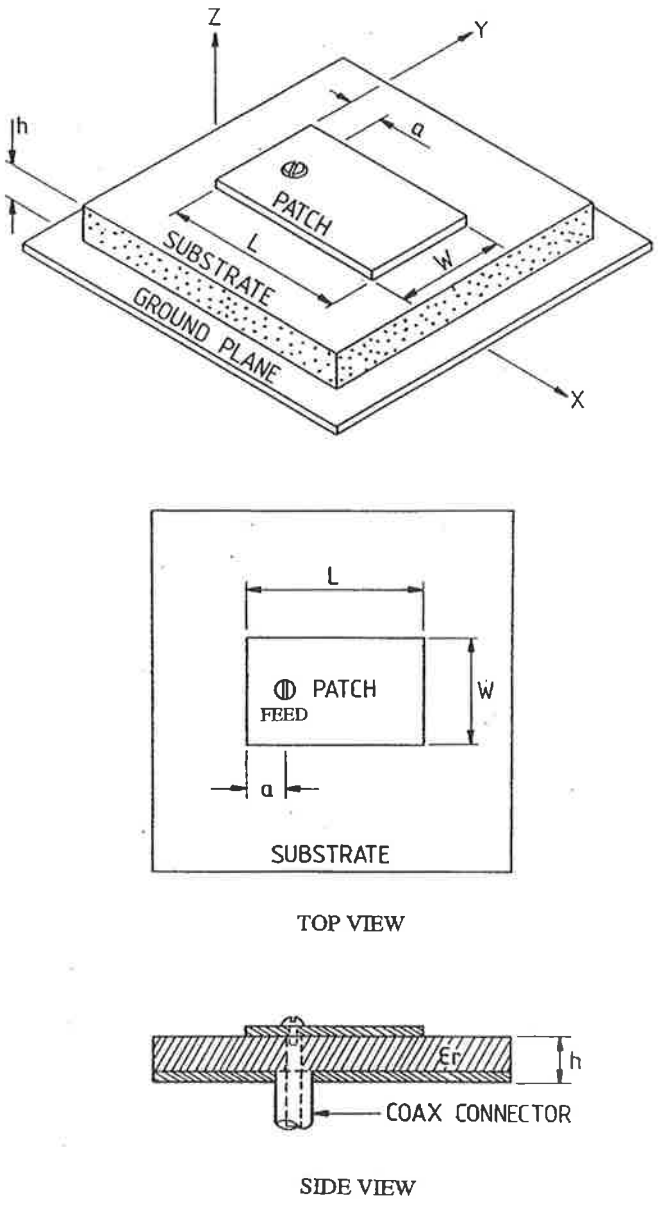

Figure 1.1: Geometry of a rectangular microstrip antenna element with dimensional parameters

used for antenna elements considered in this thesis is the probe feed. Here the inner conductor of the standard 50 ohm coaxial feeding line is extended to form a probe through thesubstrate to the patch. However, the structural simplicity of such antenna elements belies a very difficult analysis problem in electromagnetics. The configuration of a rectangular microstrip antenna element with dimensional parameters and feed is shown in Figure 1.1.

Generally, the analysis of a conventional microwave antenna often involves formidable difficulties, but the nature of a microstrip antenna element introduces an additional complexity. This

complexity is partly due to the presence of an inhomogeneous dielectric, whose loading loss, surface wave effects and the high quality factor nature of the antenna are often critical.

Although several analysis techniques, using different levels of approximation, are available in the literature to extensively analyse microstrip antennae [1 -75], a number of physical and electrical properties of these antennae are not readily available. For example, while methods are known for calculating the properties of antenna elements on very thin substrates, there appear to be no detailed methods which treat the physical and electrical properties for antennae on thick substrates. Because of the above difficulties and also the effect of the thickness and relative permittivity of the substrate material, the principles underlying the physical and electrical design properties of thick antennae differ from those of thin ones. Most of these analysis techniques can be separated into three broad categories: the classical methods based on simplifying assumptions, the solutions that are full-wave and other methods, which are a hybrid of empirical and full-wave analyses.

As far as microstrip antenna design is concerned, the use of the full-wave solutions and other methods is somewhat limited. For example, would not be able to provide a solution readily if it were desired to find the physical parameters of a patch for a given frequency, bandwidth, polarisation and some radiation characteristics. Even for the simplest antenna configuration, the numerical treatment requires considerable computational effort and is time consuming and expensive.

In addition, many of the existing analysis techniques have shown good quantitative agreement for the cases cited in the open literature, but the limits of the ranges of validity are not generally known. The calculated results may not be sufficiently accurate for many practical values of substrate thickness and relative permittivity, or for variations in patch geometry. Therefore, the microstrip antenna designer needs a simple and reliable method of analysis, that is neither too time consuming nor complex, to calculate the physical and electrical properties of interest for microstrip antenna elements on various substrate thicknesses and permittivities.

After a comprehensive survey in which the more prominent analysis techniques in microstrip antenna design were studied, the transmission line model, TLM, and the cavity model, CM, are selected for computing the physical and electrical properties of antenna elements with various thickness and permittivity of substrates These two models have a clear advantage in terms of computational simplicity, flexibility and speed, and providing a physical insight that is usually missing in more numerical solutions.

The classical models have been validated with a large amount of experimental data, with good results for both the physical and the electrical properties for antenna elements with thin substrates.

Using a technique which compares experimentally derived and computed results, it was found that a boundary at 0.0815 λ_o exists, beyond which the existing design equations fail to accurately predict the antenna physical dimensions or electrical properties. This thesis seeks to remedy this situation by deriving a number of formulae which take into account all substrate material properties and the physical and effective patch dimensions. From these formulae, new results are obtained either by empirical studies or by the modifications of existing theories that can be applied to rectangular microstrip antenna elements with thick substrates.

In recent years, a broad spectrum of applications has been proposed for microstrip antennae, because they have unique advantages and attractive features over conventional microwave antennae. Commonly acknowledged advantages of microstrip antennae are: their light weight, thin profile, compatibility with monolithic integrated circuits, ability to be made conformal and easily mounted on an arbitrary surface, integrability with other units such as signal processing circuits, and low cost. Unfortunately these antennae have some disadvantages including their narrow bandwidth, typically in the order of 2% or 5% for a voltage standing wave ratio, VSWR, of 2:1 or less; limited power handling capability, typically in the order of a Watt or less [1-16]; extraneous radiation from feeds, junctions and surface waves, and they require a quality substrate and good temperature tolerance.

For many practical applications, the advantages of microstrip antennae far outweigh their disadvantages. Almost without exception the employment of microstrip technology arises because of a system demand for thin low-profile radiators. Some of the applications include [1 - 2]:

- *Aircraft antennae*: Communication and navigation Altimeters, Blind-landing systems,
- *Missile guidance and telemetry*: Seeker monopulse arrays, Integrated radome arrays, Stick-on-sensors, Proximity fuzes, Millimetre devices,
- *Battlefield communications and surveillance*: Flush-mounted on vehicles,
- *Adaptive arrays*: Multi-target acquisition, Semiconductor integrated array,
- *Mobile radio*: Pagers and hand telephones, Manpack systems,
- *Remote Sensing*: Large lightweight apertures,
- *SATCOMs*: Domestic direct broadcast system receiver, vehicle-based antenna, Switched-beam arrays,

- *Covert antennas*: Intruder alarms, Personal communication systems,
- *Reflector feeds*: Beam switching,
- *Biomedical*: Applications in microwave cancer therapy,
- *Mobile satellite communications,*
- *Global positioning system,*
- *Wireless local area network,*
- *Intelligent vehicle highway systems.*

Throughout this thesis antenna elements with substrates thinner than approximately $0.0815\lambda_0$, which corresponds approximately to $0.13\ \lambda_d$ for $2.22 \leq \varepsilon_r \leq 10.2$, will be considered as thin, where λ_0 is the free space wavelength, λ_d the wavelength in the dielectric substrate at resonant frequency and ε_r the relative permittivity of the substrate material. All others are considered to be thick. These approximations were obtained experimentally. Similarly, Wood [76] also considered antenna elements to be thin if $h < 0.07\ \lambda_0$ for $\varepsilon_r = 2.3$ and $h < 0.023\ \lambda_0$ for $\varepsilon_r = 10$ and he also estimated that surface wave excitation in this case was not important, where h is the substrate thickness. Similarly, this thesis will take the surface waves into consideration only if the substrate is thick. It is important to note that antenna elements can be built on substrates which can be electrically thick, but physically thin.

To overcome some of the problems of thin antenna elements without unduly sacrificing their principal advantages, they can be built on thick substrates. To determine the characteristics of such antennae the methods available in the literature become less applicable. Unfortunately, some constraints also exist in the design of thick antennae. These include: extraneous radiation from the feed, generation of surface waves in the dielectric substrate, losses through radiation, dielectric losses, and conductor losses. Whereas for thin substrates surface wave excitation is generally not important, as the substrate becomes thicker, more surface wave modes can exist, and more power can be coupled into the waves. The effect of surface waves and the losses on the performance properties of the antenna elements will be discussed in the subsequent chapters.

For any given microstrip antenna a few formulae have been developed to calculate the physical dimensions corresponding to the required radiation properties, while many analysis techniques using different levels of approximation have been developed to compute the electrical characteristics. However, some of these models and methods ignore the dielectric substrate while others either come short of obtaining solutions for the current distribution on the patch or do not explicitly

include the feeding arrangement in the formulation, and are complex and computationally demanding. Furthermore, none of the analysis techniques can be used to calculate all the performance characteristics of an antenna. Some of the more popular methods are addressed and the two methods that are widely used are reviewed in this thesis because they deliver fast and reliable results. The models are the TLM and the CM. These two methods are mostly used in this thesis to calculate the physical and electrical characteristics of thin microstrip antennae.

One of the *aims* of this research is to extend existing design methods for microstrip patch antennae so that radiation and circuit characteristics as a function of all material properties and physical properties are better understood and more accurately taken into account. Most analytical models are greatly simplified at the present time by assuming that the dielectric substrate thickness is small enough to be ignored and yet it is known from experimental work that the bandwidth of operation can be improved by increasing the substrate thickness. Particular attention will be given to the problem of generalising the design model to include the influence of substrate thickness on element and mutual coupling characteristics. The validity of the analytical models that are formulated will be tested by using computer controlled microwave measurement facilities to investigate representative antennae fabricated within the practical range of physical dimensions and material properties.

An important electromagnetic characteristic of an antenna array is the mutual coupling between its elements. Mutual coupling involves the transfer of power from one element to a nearby element by space waves, or by surface waves, or a combination of the two [2,16,17]. Such mutual coupling affects the performance characteristics and therefore the design of the arrays. Many modern system applications impose stringent specifications on the performance of the array antenna, and as a consequence, the analytical model for mutual coupling must be accurate. This thesis will introduce a modified method for calculating the mutual coupling taking into account the effective properties of the patch and also the mismatches between elements. This method provides quite accurate results.

The search for novel microstrip antenna designs with better physical and operational properties has been a dominant feature of the literature, because conventional microstrip designs inherently have a narrow impedance bandwidth and are not suitable for dual band operation. A dual band antenna is useful in situations where it is required to operate at two distinct frequencies which may be too far apart for a conventional microstrip antenna to perform efficiently at both frequencies. The typical size of conventional antenna structures is quite large, making them unsuitable for such

applications. A study of published microstrip antenna designs reveals that it is still desirable to reduce size without sacrificing performance properties. Three novel antenna elements will be introduced, designed manufactured, measured and described, namely the broad band, the ring, and the dual band microstrip antenna elements. These antennae consist of a metal ring or rectangular patch on one side of a dielectric sheet, in which the dielectric substrate is restricted to the same size as the metal ring or rectangular patch, and a ground plane on the other side. They are fed by a coaxial line from the back through the ground plane. These antennae have improved electrical performance, are economical, occupy a minimum space and can be distributed over or embedded in the surface of space and surface borne vehicles.

This thesis describes methods, designs, constructions and measurements of

- rectangular antenna elements with dielectric substrates ranging in electrical thickness, h/λ_d, from 0.0065 to 0.2284, and physical thickness from 0.17 mm to 2.81 mm, and operating over a frequency range of 2.980 GHz to 8.450 GHz. The size of the substrate material was 100 mm square and the ground plane 700 mm square. Note that substrate thicknesses were increased by stacking two or more double sided etched substrate slabs together,
- a novel miniaturised broad-band microstrip antenna element,
- a novel miniaturised dual-band microstrip antenna element,
- a novel miniaturised microstrip ring antenna element.
- mutual coupling between two antenna elements in an array is investigated theoretically and experimentally. The substrate thickness of the elements was varied from $0.037\ \lambda_d$ to $0.225\ \lambda_d$, the separation between the edges from $0.2\ \lambda_o$ to $1.4\ \lambda_o$ and operating over the frequency range 3.960 to 5.900 GHz. The range of the physical thickness of the substrate was varied from 1.50 mm to 9.92 mm.

1.2 Outline of the thesis

The effective design, construction, measurement and application of microstrip antennae presupposes the quantitative knowledge of their physical and electrical properties as both the elements and arrays with various thickness and relative permittivity of substrate materials. This thesis provides results of extensive research into both the properties associated with rectangular and ring antenna elements and their solution by analytical, numerical, and experimental means. In the study several antenna

elements with various relative permittivity and thickness of substrates at different frequencies were designed and measured. For the investigation the dimensions as well as the feed point locations were varied. Additional care has been taken for the exact positioning of the feed during the design process, to match the antenna element to 50 Ohm. This additional effort is compensated by a higher attainable bandwidth.

To design a microstrip antenna element the physical dimensions are needed for a specified substrate material and operating frequency. The performance of such an antenna element is found by calculating and measuring such characteristics as: input impedance, resonance frequency, bandwidth, E- and H- plane radiation patterns, and beamwidth. If the performance of the antenna satisfies all of specifications for the characteristics mentioned above then the design is successful. For these reasons the thesis is organised into twelve chapters addressing each one of these characteristics, novel antenna elements and mutual coupling in turn.

The remainder of this section reviews what can be found in each of the ten technical chapters 2 to 11. Section 1.3 provides a point summary of the main new results obtained in this thesis.

Some of the analysis techniques available in the open literature, with some indication of limitations and considerations that must be kept in mind when designing microstrip antennae at microwave frequencies, are itemised in *Chapter 2*. This chapter reviews some useful parts of two suitable models, namely the transmission line and the cavity models and reviews some of the formulae applied in this thesis for designing and analysing microstrip antenna elements. For the sake of completeness other methods are summarised without mathematical derivations and formulations. In addition, the well known mathematical details are avoided to limit the size of the text .

Chapter 3 discusses the formulae available in the literature on the design of physical properties of rectangular microstrip antenna elements, and assesses their suitability and the threshold of their applicability. Their variations have been experimentally examined by analysing a set of new constructed antenna elements with various thicknesses and relative permittivity of substrates material over wide a frequency band.

A formula based on the TLM is used to determine the resonant length of these antennae. It also derives new empirical formulae based on a curve fitting technique that can determine the width and the feed point location of thin antennae. While such a method was proposed and implemented by the author in previous work [79 - 80], a second method for determining the resonant length and

width of antenna elements with thicker substrates is empirically derived by using a similar curve fitting technique in the second half of this chapter.

A new expression for calculating the effective permittivity of rectangular microstrip antenna elements with various thickness and relative permittivity of substrate materials is also derived in this chapter. The results obtained from this technique confirm with those calculated from formulae reported elsewhere. This chapter also studies the effects of the substrate thickness on the patch dimensions.

The contents of Chapter 3 has been published in [77 - 83].

The resonant input resistance is usually one the most difficult to predict accurately, primarily because of the narrow bandwidth of most microstrip antenna elements, but also because of dielectric material tolerances.

Three methods for the calculation of the resonant input resistance of rectangular microstrip antenna elements are introduced in *Chapter 4*. The first method is based on the refinement of the CM and the TLM considering the antenna in the fundamental mode, modelled by a simple resonant parallel RLC circuit. Due to the resonant nature of the investigated antenna elements, their resonant input resistance is related to the quality factors associated with the system losses. This technique has been successfully used to calculate the resonant input resistance of rectangular antenna elements with thin substrates. A second method based on the modified cavity model has been developed for computing the resonant input resistance for antenna elements with thick substrates by considering the antenna in the fundamental mode, modelled by a simple resonant parallel RLC circuit. It takes into account the effective dimensions, dynamic permittivity, resistance due to power loss in surface wave, the radiation resistance of the patch, and the resistances due to losses in the conductor, and dielectric. A third method is an alternative formula derived empirically using experimentally derived resistance data for computing the resonant input resistance for antenna elements with thick substrates. The proposed formulae for computing the resonant resistance have been validated with a large amount experimental data obtained from antenna element investigated in Chapter 3.

The contents of Chapter 4 has been published in [81 - 82, 84 - 85, 131 - 132].

Formulae based on the TLM, the CM and the magnetic wall models to determine the resonant frequency of a rectangular microstrip antenna element are investigated in *Chapter 5*. Their

respective regions of validity in theory and applicability are also established by analysing a set of data obtained experimentally from the antenna elements given in Chapters 3 and 4. For thin antenna elements, the formula based on the TLM is successfully used to calculate the resonant frequencies for given dimensions.

Three closed-form expressions are presented for the calculation of resonant frequencies of rectangular microstrip antenna elements with thick substrates. They are derived by modifying the TLM, the CM, and by the curve fitting technique. The results of all proposed expressions are compared with measurements obtained from antenna elements investigated in Chapters 3 and 4.

The contents of Chapter5 has been published in [86 - 88].

In *Chapter 6* several formulae based on the CM and the TLM are combined to produce a closed-form expression for calculating the bandwidth of antenna elements with thin substrates. The formula takes into account the effects of radiation, conductor and dielectric losses, with their quality factors. The results obtained from this technique confirm those calculated from the MSAnt program [14], and results obtained from measured return loss plots of antenna elements with thin substrates. A novel closed-form expression based on the cavity model and the exact Green's function for a grounded dielectric slab has been developed for computing the bandwidth of thick antenna elements taking into account both the power radiated in the space waves and the power radiated in surface waves and a correction factor. The results obtained from the derived formula are compared with measurements made using the antenna elements investigated in Chapters 3, 4 and 5, and excellent agreement is obtained.

The contents of Chapter 6 has been published in [86], [89 - 90].

Chapter 7 discusses formulae based on the two-slots model (the TLM), the CM and the electric surface current model available in the literature for calculating both the E-plane and H-plane far field patterns for both thin and thick antenna elements. It also identifies their suitability and the threshold of their applicability. For thin antenna elements, formulae based on either the two-slots model, or CM can be used to calculate both the E-plane and H-plane patterns. These formulae are also useful for calculating the H-plane patterns for thick antenna elements but fail to give satisfactory results for E-pane radiation pattern. To get improved calculated results on the E-plane patterns of thick antenna elements the line extension is incorporated in the formula based on the two-slot model to account for the inhomogeneity of medium and fringing field, respectively. Comprehensive

measurements confirm the validity of the modified formula. The half-power beamwidth in the E- and H-plane have also been determined for each investigated antenna element.

Some of the material in Chapter 7 has been published in [86], [91 - 94].

Design details and experimental observation of a novel miniaturised microstrip antenna element, which provides a large bandwidth is presented in *Chapter 8*. This antenna consists of a rectangular metal patch on one side of a dielectric sheet in which the dielectric substrate is restricted to the same size as the metal patch and a ground plane on the other side. It is fed by a coaxial line from the back through the ground plane. This chapter also reports a simple and accurate design procedure based on the TLM and the CM for this antenna. Good agreement between numerical and experimental results is achieved.

Designed, measured and calculated data on the physical and electrical properties of this miniaturised antenna element are presented and compared with properties of a conventional microstrip antenna element having the same patch dimensions in order to highlight the merit of the former in respect of cost, size, weight, bandwidth, and radiation patterns.

The design and results in this chapter have been reported in [80], [95 - 96].

A dual-band antenna is useful in situations where it is required to operate in two distinct frequencies which may be too far apart for a conventional microstrip antenna to perform efficiently at both frequencies. For applications in which saving space and weight is a premium, a single layer, microstrip radiating structure is desirable. A novel miniaturised patch antenna design, which provides dual-band operation has advantages with respect to other patch antenna solutions for dual-band applications is presented in *Chapter 9*. It consists of a rectangular metal patch on one side of a dielectric sheet in which the dielectric substrate is restricted to the same size as the metal patch and ground plane on other side. The antenna is fed by a coaxial line from the back through the ground plane. The physically intuitive CM and the TLM are used for analysis. A relatively simple design scheme is included.

A novel analytical technique is developed for the dimensions and operational properties for these antennas. Measured performance data of this miniaturised antenna element is presented and compared with the calculated results. Good agreement between numerical and experiment results was achieved.

The design and results in this chapter have been reported in [82], [95 - 97].

Chapter 10 introduces a design, testing and analysis for a novel miniaturised broad-band microstrip ring antenna, consisting of a metal ring on one side of a dielectric sheet, in which the dielectric substrate is restricted to be the same size as the metal ring, and a ground plane on the other side. The ring antenna is fed by a coaxial line from the back through the ground plane. A method based on TLM and CM is developed for the dimensions and operational properties and design predictions are compared with measured results for this antenna element. Very good agreement between theory and experiment was achieved.

The design and results in this chapter have been reported in [84, 95].

In *Chapter 11* several formulae, based on the volume equivalence theorem, classical Schelkunoff theory and a theoretical model equivalent to a lossy transmission line, are combined to produce a new closed-form expressions for calculating mutual coupling coefficients between two identical probe fed rectangular microstrip antenna elements in both the E- and H-plane configurations for the dominant TM_{10} mode. The measured mutual coupling coefficients are compared with those obtained from these formulae. Good agreement is obtained.

As the substrate becomes thick the differences between the measured and calculated results become large. Thus, modifications to these formulae are made, in order to increase the accuracy of the predictions for the mutual coupling coefficient. These modifications take into account the surface wave contribution, mismatching that may occur between the elements, the thickness and relative permittivity of the substrate material and the effective dimensions of the antenna elements. These are applied to a number of antenna arrays that have been designed, constructed, and tested for both the E-and H-plane coupling configurations for the dominant TM_{10} mode resulting in good agreement.

Note that, the formulae given in Chapter 3 are applied to determine the dimensions and the feed point locations of the antenna elements used in the array design.

The contents of Chapter 11 has been published in [85, 98]

Finally, *Chapter 12* the major conclusions of this research are summarised and some recommendations for further research are given.

Some supporting formulae for the derivation of far-field radiation pattern in the E- and H-plane are given in Appendix A and some analysis of mutual coupling are given in Appendix B.

1.3 Point Summary of Contributions

The major part of each chapter is dedicated to directly applicable, useful formulae and comprehensive graphical representations, which have been selected for practical design applications. These formulae are given with error bounds, and they can be easily used for CAD. The values for the diagrams and tables have been calculated by programs written in Pascal. In the interests of clarity, each chapter concludes with a detailed summary of its content. As far as is known, no other comparable work on microstrip antennae exists.

In summary, the major contributions made in this thesis are as follows:

- A review of the advantages and drawbacks associated with microstrip antenna elements.
- A review of applications and developing markets for microstrip antenna technology.
- A listing of the analysis techniques along with a some indication of limitations and references.
- The determination of the threshold of applicability of some formulae available in the literature for designing microstrip antennae and computing *mutual coupling coefficients* of arrays.

- The derivation of empirical formulae by curve fitting techniques to calculate the
    - *resonant lengths* of antennae elements with *thick* substrates,
    - *resonant widths* of antenna elements with *thin* substrates,
    - *resonant widths* of antenna elements with *thick* substrates,
    - *feed point locations* of antenna elements with *thin* substrates.

- The derivation of a new formula for the *effective relative permittivity* of the substrate material by considering the relation of velocities of the electromagnetic waves in the air and the substrate material (inhomogeneity condition).

- The development of methods to calculate the *input resistance* at resonance of
    - *thin* antenna elements, and
    - *thick* antenna elements.

- The development of methods to calculate the *resonant frequency* for
    - *thin* antenna elements, and
    - *thick* antenna elements.

- The development of methods to calculate the *bandwidth* for
    - *thin* antenna elements, and
    - *thick* antenna elements.

- The development of methods to analyse the *E- and H-plane far field radiation pattern* for
    - *thin* antenna elements, and
    - *thick* antenna elements.

- The introduction, design, analysis and implementation of a *novel broad-band miniaturised microstrip antenna element* which offer tiny dimensions and better performance characteristics compared to a classical microstrip antenna element having the same patch size.

- The introduction, design, analysis and implementation of a *novel dual band miniaturised microstrip antenna element* which offer tiny dimensions and betterperformance characteristics compared to a classical dual band microstrip antenna element having the same patch size.

- The introduction, design, analysis and implementation of a *novel miniaturised microstrip ring antenna element* which offer tiny dimensions and betterperformance characteristics compared to a classical microstrip antenna element having the same ring size.

- The development of computationally efficient methods for the analysis of *mutual coupling coefficients* between two rectangular antenna arrays with
    - *thin* substrates, and
    - *thick* substrates considerably thicker than those reported in the literature.

- The discovery of the small *mutual coupling coefficient* for widely separated antenna elements with *thick* substrates.

- The application of the developed formulae, over a wide range of substrate thicknesses, to rectangular microstrip antenna arrays of practical significance.

- An understanding of the fundamental effects of very thick substrates on mutual coupling.

- The constructing and testing of thirtythree new antenna elements with various thickness and relative permittivity of substrate materials.

- Experimental measurements are used to test, verify and validate analysis techniques that are developed.

- The effect of substrate thickness and patch physical dimensions on the antenna operational properties is described, and some of the characteristics are exploited to optimise the antenna properties.

Chapter 2

Analytical Techniques for Microstrip Antennae

2.1 Introduction

Microstrip antenna analysis is important, because it can aid the design process by reducing the time and cost involved in the trial by error procedure and it is also useful when optimising an antenna design over one or more design parameters. In addition, it provides an understanding of the operating principles of an antenna as well as helping to determine the limitations in performance and/or modification to an existing antenna design.

Generally, microstrip antenna structures are inhomogeneous. Consequently, the analysis of such structures is normally difficult, due primarily to the presence of a dielectric substrate to support the patch conductor. Since radiation occurs from the patch edges, some researchers replaced the microstrip structure with apertures, or slots, connected to each other by a transmission line [1 - 6], [17 - 26], [99 - 100]. In addition, the patch acts as a low impedance microstrip transmission line.

Another approach replaces the structure by a dielectric cavity bounded by four magnetic walls. The magnetic walls are along the perimeter and the electrical walls are on the top and bottom of the patch. The radiation occurs from slots formed by the periphery of the patch and ground plane [1 - 9], [27 - 38].

Some researchers use the full wave analyses [13 - 5], [39 - 56] utilising the moment method solutions that use the exact Green's function pertaining to the grounded dielectric slab for the derivation of a set of integral equations for the unknown current on the patch, as well as solutions based on the finite difference time domain method, and the finite element method. Such models are very time consuming computationally, due to numerical integrations of Sommerfeld type integrals (very slow convergent integrals), in either space domain or spectral domain form. They do not readily provide a solution [101]. Furthermore, one of the typical features of an analytical technique is the amount of mathematical work required for it to be implemented. The less the analytical processing, the easier the implementation of the analytical technique.

In the following section some of the analytical techniques available in the literature for analysing microstrip antennae are mentioned and briefly described. Two methods considered important in evaluation of the basic properties of microstrip antennae are summarised, namely, the transmission line model, and the cavity model. Note that the design formulae that can be relied upon to give a stated degree of design precision will be given only.

2.2 Analytical Techniques

There are many different approaches to microstrip antenna analysis. Unfortunately, these methods possess different levels of complexity and require vastly different computational efforts. The accuracy of each method is also difficult to determine and will depend on how accurately the method can be implemented and how well the antenna is modelled. The application of each method has its advantages and disadvantages and therefore no single method is appropriate for predicting all the fundamental properties of an antenna.

In general, a good antenna design method should have the following characteristics:

- its applicability must suit the given problem,
- it should be easy to implement, while providing the necessary fundamental properties of an antenna,
- it should be capable of computing the necessary parameters for the antenna element under test speedily,

- its results should be accurate enough for the intended purposes,
- it should lend itself to interpretation in terms of intuitive models (the simplest solution often provides the best physical insight),
- its numerical treatment should not require considerable computational effort,
- it must not time consuming and expensive,
- it must give an idea about the behaviour of the antenna,
- it must provide a good insight into the physics of the antenna.

Considerably progress has been recently made in the numerically modelling of microstrip antennae in the framework of different techniques, such as the

1. *Classical models (Physical models)*

    - Transmission-line model,
    - Cavity and modal expansion models.

2. *Full-wave analysis*

    - Method of Moments, MoM,
    - MoM in Space Domain,
    - MoM in Spectral Domain,
    - Finite-element technique,
    - Finite-difference time-domain method,
    - Transform Domain Analyses,
    - Mixed Potential Integral Equation Approach,
    - Conjugate Gradient Fast Fourier Transform Technique.

3. *Other methods*

    - The Dyadic Green's Function Technique,
    - Wire-grid method,
    - Segmentation and desegmentation techniques,

- Electric Surface Current Model,
- The Vector Potential approach,
- The Variation Approach,
- Hankel Transform Technique,
- The Radiating Aperture Method,
- Generalised Edge Boundary Condition Technique,
- Generalised Variational Approach,;
- Dual Integral Equation Approach.

The two methods which are the most useful for practical design as well as providing a good intuitive explanation of the operation of microstrip antennae, are TLM and CM as they are based on some fundamental simplifying assumptions regarding the radiation mechanism of antennae. Most of the calculations throughout this thesis are based on both methods and are briefly discussed in the following sections. Unfortunately, the methods, as reported in the literature, are satisfactorily accurate only for antenna elements with substrates thinner than approximately 0.0815 λ_o and at frequencies typically up to the X-band [2 - 4], [79, 87, 89], where λ_o is the free space wavelength. However, as the thickness of the substrate increases, the accuracy of these methods decreases rapidly [88, 90]. The analytical and numerical treatment of other methods; however, requires considerable computational effort and is time consuming and expensive. As far as design is concerned most of the methods available do not provide a solution readily for finding the physical properties of a microstrip antenna element for a given frequency and they are also unable to predict all the electrical properties of such antenna.

2.2.1 Classical Models (Physical models)

It is crucial to initially have a good understanding of the physical mechanisms that reign the antenna elements, that are considered to be designed for a given application. It is well known, that the best physical insight of an antenna element is given by the TLM and the CM. The TLM is considered first.

2.2.1.1 Transmission Line Model

The TLM is based on the observation that a rectangular patch antenna is simply an open-circuit microstrip line, in which the radiation leaks through the open ends. It models the antenna element as a transmission line section lumped loads at the radiating edges as shown in Figure 2.1. The TLM leads to results that are adequate for most engineering purposes and requires less computation. Structures such as printed dipoles and nonrectangular patches cannot be accommodated by this model.

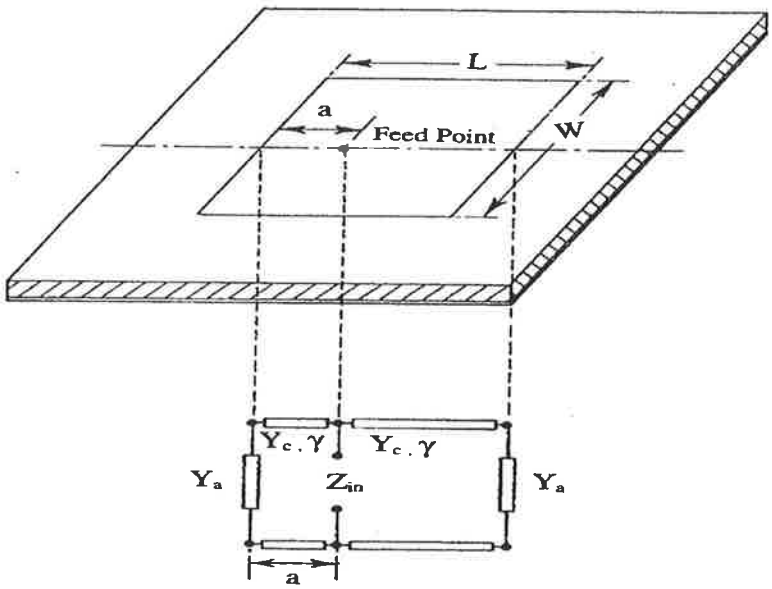

Figure 2.1: Probe fed rectangular microstrip antenna element with its equivalent transmission line circuit.

The TLM offers a reasonable interpretation of the radiation mechanism, while simultaneously giving a simple expression of the antenna's characteristics. In this method, the rectangular antenna element is modelled as a resonant section of a uniform microstrip transmission line with a length, L, width, W, and thickness, h, loaded with impedances at the two ends. These impedances represent the radiated power that emanates from the open ends and the stored energy by fringing fields. The basic concept is shown in Figure 2.1, which illustrates the TLM for a rectangular microstrip patch antenna.

This model assumes that

- there no currents transverse to the resonant length of the patch,
- the fields are uniform along the width of the patch, and
- the transverse currents are caused by the feeding mechanism and are invariable present.

Furthermore, the TLM prescribes that the antenna element must have two parallel radiating slots, known as radiating edges, with dimension W, h, located within the dielectric for thin antenna elements [3, 6, 19, 21]. The slots are characterised by their equivalent admittance, Y_a. The equivalent susceptance, due to end affects, is represented by a capacitor. However, the application of this model is limited to antenna configurations in which the thickness and the relative dielectric constant are sufficiently small to avoid considerable excitation of surface waves, because it does not include surface waves in the calculations [2]. Also, this model does not consider the actual nature of the feed. Fortunately, this is not a severe limitation for antenna elements with thin substrates satisfying the criteria $h \leq 0.0815\ \lambda_o$ for $2.22 \leq \varepsilon_r \leq 10.2$, where ε_r is the relative permittivity of the substrate material, as will be shown in subsequent chapters of this thesis. The TLM has direct provided applicable design formulae for thin antennae. These have been used in their current form, in this thesis.

From the equivalent circuit given in Figure 2.1, the input impedance at the feed point can be written as [4]

$$Z_{in} = \left(\frac{Z_{cw}}{g_1 + g_2} \right) + jX_L = \frac{1}{Y_{in}} \tag{2.1}$$

with

$$g_1 = \frac{Z_{cw} \cos(\beta a) + jZ_a \sin(\beta a)}{Z_a \cos(\beta a) + jZ_{cw} \sin(\beta a)} \tag{2.2}$$

and

$$g_2 = \frac{Z_{cw} \cos[\beta(L-a)] + jZ_a \sin[\beta(L-a)]}{Z_a \cos[\beta(L-a)] + jZ_{cw} \sin[\beta(L-a)]} \tag{2.3}$$

where **a** is the distance from the radiating edges to the feed position. Z_{cw} is the characteristic impedance of the microstrip line as a function of W, h and ε_r is given as [102]

for W/h≤3.3

$$Z_{cw} = \frac{R_o}{\pi\sqrt{2(\varepsilon_r+1)}}\left[\ln\left(\frac{4h}{W}+\sqrt{\frac{16h^2}{W^2}+2}\right)-\frac{(\varepsilon_r-1)}{(\varepsilon_r+1)}\left(0.2258+\frac{0.1208}{\varepsilon_r}\right)\right] \tag{2.4}$$

and for W/h≥3.3

$$Z_{cw} = \frac{R_o}{2\sqrt{\varepsilon_r}}\left[\frac{W}{2h}+0.4413+\frac{0.0823(\varepsilon_r-1)}{\varepsilon_r^2}+\frac{(\varepsilon_r+1)}{\varepsilon_r}\right.$$

$$\left.\cdot\left(0.231+0.1592\ln\left(\frac{W}{2h}+0.94\right)\right)\right]^{-1} \tag{2.5}$$

where $R_o = 120\,\pi\Omega$ is the wave impedance in free space.

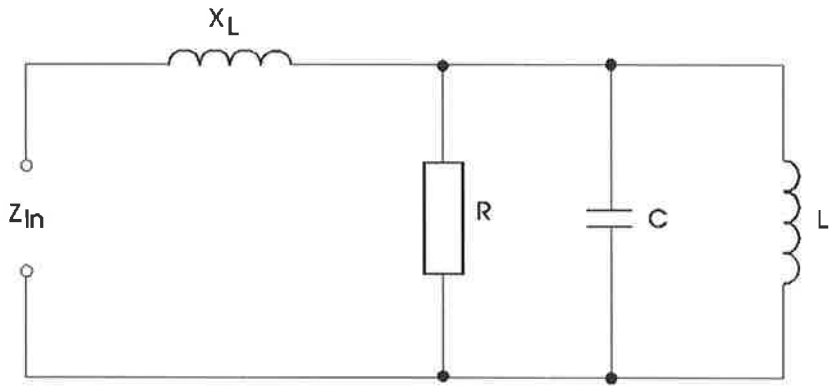

Figure 2.2: Simplified circuit model valid over the band of a single, isolated mode.

Y_a is the aperture admittance or Z_a the aperture impedance is given by

$$Y_a = G_a + jB_a \tag{2.6}$$

G_a is the conductance contributed by the radiation field associated with each edge. If $W/\lambda_o \ll 1$ and $h \ll \lambda_o$ the G_a is placed across the centre of each slot and is given by the formula [1, 8, 18].

$$G_a = \frac{W^2}{90\lambda_o^2} \qquad \text{for } W << \lambda_o$$

$$G_a = \frac{W}{120\lambda_o} \qquad \text{for } W >> \lambda_o \tag{2.7}$$

Another formula yielding quite a different conductance has been derived by Harrington [103]. It has been adopted to patch antennae by Munson [18] and Richards [8], assuming that radiation only

occurs at the edges of the patch (perpendicular to TEM propagation),and that each edge radiates individually and isolated from the other edges. In this case

$$G_a = \frac{\pi W}{R_o \lambda_o}\left[1 - \frac{(k_o h)^2}{24}\right] \tag{2.8}$$

The propagation constant β is given by

$$\beta = \frac{2\pi\sqrt{\varepsilon_{ew}}}{\lambda_o} \tag{2.9}$$

where ε_{ew} denotes the corresponding effective relative permittivity, and is related to the intrinsic relative permittivity ε_r of the substrate as follows [104]

$$\varepsilon_{ew} = \frac{(\varepsilon_r + 1)}{2} + \frac{(\varepsilon_r - 1)}{2}\left(1 + \frac{10h}{W}\right)^{-\frac{1}{2}} \tag{2.10}$$

ΔW signifies the line extension due to the fringing effect. This is because an open ended microstrip antenna does not perform as a perfect open circuit as shown in Figure 2.3. The value of ΔW can be approximated by using the following formula [105]:

$$\Delta W = 0.412\ h\ \frac{(\varepsilon_{ew} + 0.300)}{(\varepsilon_{ew} - 0.258)}\left(\frac{W}{h} + 0.264\right)\left(\frac{W}{h} + 0.813\right)^{-1} \tag{2.11}$$

The susceptance B_a accounts for the fringing field and is associated with the radiating edge of the width. The reactive part of the aperture admittance is capacitive and can be calculated using the edge extension formula, ΔW, for the microstrip transmission line open circuit truncation. The susceptance is given by [1, 3. 6. 21] as

$$B_a = k_o\ \Delta W\ \frac{\sqrt{\varepsilon_{ew}}}{Z_{cw}} \tag{2.12}$$

where k_o is the free-space wave number

$$k_o = \frac{2\pi}{\lambda_o} = \frac{2\pi f_r}{c_o} \tag{2.13}$$

where f_r is the resonant frequency.

The probe reactance in equation 2.1 is given as [4, 50]

$$X_L = \frac{120\pi h}{\lambda_o}\left[-\gamma + \ln\left(\frac{2\lambda_o}{d_o\pi\sqrt{\varepsilon_r}}\right)\right] \tag{2.14}$$

where d_o is the probe diameter, and $\gamma = 1.781072$ is Euler's constant.

At resonance, the imaginary part of Z_{in} goes to zero. This condition yields the following formula [1, 3, 6, 106]:

$$\tan\beta L = \frac{2B_a Y_{cw}}{B_a^2 + G_a^2 - Y_{cw}^2} \approx \frac{2B_a}{Y_{cw}} \tag{2.15}$$

where Y_{cw} is the characteristic admittance of the microstrip line. When considering this condition, equation 2.1 is reduced by substituting equation 2.15 into it as follows [1, 6]:

$$Y_{in} = 2G_a\left[\cos^2(\beta a) + \frac{G_a^2 + B_a^2}{Y_{cw}^2}\sin^2(\beta a) - \frac{B_a}{Y_{cw}}\sin^2(\beta a)\right]^{-1} \tag{2.16}$$

Also, the following condition is, in many cases, satisfied [1, 3, 6] $G_a, B_a \ll Y_{cw}$

So, equation 2.16 can be approximated by

$$Y_{in}(a) \approx \frac{2G_a}{\cos^2(\beta a)} \tag{2.17}$$

Further manipulation of equation 2.15 results in a more illustrative formula at resonance [3, 7]

$$L + 2\Delta W = \frac{n\pi}{\beta} \tag{2.18}$$

where n = 1, 2, 3, ...

The patch length at resonance can be shown to be slightly shorter than half a wavelength in the dielectric substrate by substituting equation 2.9 into equation 2.18:

$$(L + 2\Delta W) = \frac{\lambda_o}{2\sqrt{\varepsilon_{ew}}} \tag{2.19}$$

Equation 2.19 is useful in design as well as analysis. It allows the resonant length of the patch to be determined once the desired resonant frequency is specified and the substrate is selected.

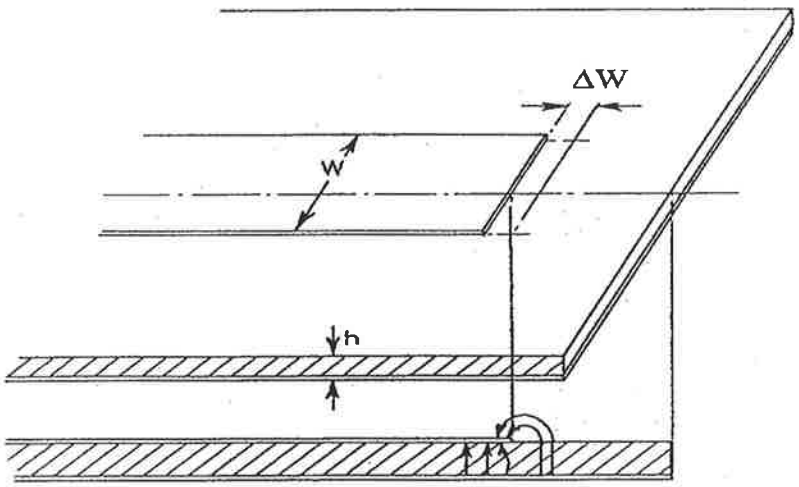

Figure 2.3: Open-ended microstrip line with line extension ΔW and aspect ratio W/h.

As mentioned previously, the rectangular patch antenna is represented by two slots separated by a distance L. In this case, each slot can be thought of as radiating the same field as a magnetic dipole with a magnetic current of [1, 6]:

$$M = 2E\hat{z} = \frac{2V_o}{h}\hat{z} \tag{2.20}$$

where the factor of 2 arises due to the positive image of magnetic current, which is near the ground, and V_o is the voltage at either of the two ends of the. The total radiation far field is obtained by multiplying the field due to a single slot by an array factor representing the arrangement of the two-slot array. When the coordinate system shown in Figure 2.1 is employed, the final result is [6]:
For the E-plane,

$$E(\theta) = -j4V_o W k_o \frac{e^{-jk_o R}}{4\pi R} F_E(\theta) \tag{2.21}$$

with

$$F_E(\theta) = \frac{\sin\left(\frac{k_o h}{2}\sin\theta\right)}{\frac{k_o h}{2}\sin\theta}\cos\left(\frac{k_o L}{2}\sin\theta\right) \tag{2.22}$$

where R is the distance from the antenna.

For the H-plane

$$E(\theta) = -j4V_o W k_o \frac{e^{-jk_o R}}{4\pi R} F_H(\theta) \tag{2.23}$$

with

$$F_H(\theta) = \frac{\sin\left(\frac{k_o W}{2}\sin\theta\right)}{\frac{k_o W}{2}\sin\theta}\cos\theta \tag{2.24}$$

The analysis does not include the effect of surface waves excited along the substrate (see Chapter 4). Therefore, the application is generally limited to antenna configurations for which the thickness and dielectric constant are small enough to avoid excessive excitation of those surface waves. Detailed discussion of the surface waves is omitted here.

Conversion of bandwidth from one Standing Wave Ratio, SWR, level to another can be accomplished by using the relation between bandwidth, BW, and total quality factor, Q_T [29]:

$$BW = \frac{SWR - 1}{Q_T\sqrt{SWR}}\,100\% \tag{2.25}$$

Finally, the half-power beamwidths in the E and H planes are [1, 4]

$$\theta_{BE} = 2\cos^{-1}\sqrt{\frac{7.03\lambda_o^2}{4\pi^2\left(3L^2 + h^2\right)}} \tag{2.26}$$

and

$$\theta_{BH} = 2\cos^{-1}\sqrt{\frac{1}{2 + k_o W}} \tag{2.27}$$

This thesis uses a TLM to determine the resonant patch length, resonant frequency and far-field radiation patterns for antenna elements with thin substrates. For thicker substrates however, the

formulae for computing the afore mentioned antenna characteristics have been modified either by the addition of empirically derived correction factors or the consideration of the effective patch dimensions.

An alternative for TLM is the CM, which takes into account higher order modes and provides much physical insight into the antenna's operation.

2.2.1.2 Cavity Model

A planar two-dimensional cavity model for microstrip patch antennae was first proposed by Lo et al [30] and Richards [8, 107]. It overcomes some of the shortcomings of the one-dimensional TLM discussed in the previous section and is capable of predicting the antenna performance accurately if the patch is not more than a few hundredths of a wavelength thick. In this case the TM modes are superior in the cavity region. However, it requires more computational effort than the TLM.

This model basically treats the antenna as a cavity of thickness h and a conducting patch having dimensions L and W with electric walls on the top and bottom and magnetic walls around the perimeter of the patch. The radiation is assumed to occur from the slots formed by the periphery of the patch and ground plane.

This method is the most suitable for analysing those antennae with structures for which the corresponding wave equation can be solved by the method of separation of the variables. However, the method is applicable to the analysis of arbitrarily shaped patch antennae in general.

The theoretical model is based on the following assumptions [3, 8]:

- The close proximity between the microstrip patch and the ground plane (Figure 1.1) suggests that the E-field consists only of the z-component and the H-field of only the xy-components in the region bounded by the microstrip patch and the ground plane.
- Fields in the cavity region do not vary with z.
- The tangential component of the H-field along the edge is negligible.
- The existence of a fringing field is taken into account by slightly extending the edges.

The CM method has been successfully used to predict the resonant frequency, radiation patterns and the input impedance of microstrip antennas with substrates thinner than approximately 0.02 λ_d, at any feed point. However, the method does not rigorously account for the presence of surface waves on the antenna substrate nor does it account for mutual coupling between closely spaced antenna elements [30, 34, 106, 108]. One advantage of this theory is that it can provide much physical insight into the field distribution under the patch. This understanding is useful in many new designs and applications. However, like the TLM, the CM analysis requires an empirical edge extension factor (line extension) to account for the fringing field effect and also an idealised excitation at the feed. As will be shown in the subsequent chapters, this is not a severe limitation for antenna elements specified as thin in this thesis.

Assuming an $e^{j\omega t}$ time variation, the electromagnetic fields associates with the z-directed current source located at the feed point (a, b) must satisfy the following relations derived from Maxwell's equations [6, 7, 28, 32]:

$$\left(\nabla_T^2 + k^2\right)E_z = -j\omega\mu_o J_z(a,b) \tag{2.28}$$

$$H = \frac{j}{\omega\mu_o}\nabla_T x\left(\hat{z}E_z\right) \tag{2.29}$$

where a and b are the widths of the feed in x and y directions, ∇_T is the transverse component with respect to the z-axis of the del operator and $\hat{z}$ is the unit vector in the z-direction. In the relations above, the electric wall condition is automatically satisfied because $E = E_z\hat{z}$. On the sides of the cavity, the magnetic wall condition can be satisfied by the following Newman boundary condition:

$$\frac{\partial E_z}{\partial n} = 0 \tag{2.30}$$

The inhomogeneous wave equation of equation 2.29 can be solved by finding eigenfunctions $j_{mn}(x,y)$, which satisfy the following homogeneous wave equation:

$$(\nabla_T^2 + k_{mn}^2)\varphi_{mn} = 0 \tag{2.31}$$

with $\frac{\partial \varphi_{mn}}{\partial n} = 0$ on the magnetic wall.

This is subject to the same boundary conditions as equation 2.30, where k_{mn} is the corresponding eigenvalue. That is, if N eigenfunctions are assumed, the solution of equation 2.28 is

$$E_Z(x,y) = \sum \sum A_{mn} \varphi_{mn}(x,y) \tag{2.32}$$

where m and n are the mode indices in the x and y directions, respectively. A_{mn} are the mode coefficients and the j_{mn} are the orthonormalised mode vectors, obtained by solving equation 2.31 as follows:

$$\varphi_{mn}(x,y) = \frac{X_{mn}}{\sqrt{\varepsilon h W L}} \cos k_x x \cos k_y y \tag{2.33}$$

where $X_{mo} = X_{on} = \sqrt{2}$ for $m \neq 0$ and $n \neq 0$, and $X_{mn} = 1$ for $m = n = 0$.

The mode vectors all satisfy the wave equation and the eigenvalues $k_x = \frac{m\pi}{W}$ and $k_y = \frac{n\pi}{L}$ satisfy the separation condition:

$$k_{mn}^2 = \omega_{mn}^2 \mu\varepsilon = k_x^2 + k_y^2 \tag{2.34}$$

so that the resonant frequencies are

$$f_{mn} = \frac{k_{mn}}{2\pi\sqrt{\varepsilon_r \varepsilon_o \mu_o}} \tag{2.35}$$

Impedance boundary conditions are imposed at the four walls, by considering the external stored and radiated energy effects as complex wall admittance, which result in the following complex transcendental equations [1, 28, 32] which hold for thin substrates:

$$\tan k_x W = \frac{2 k_x \alpha_x}{k_x^2 - \alpha_x^2} \tag{2.36}$$

and

$$\tan k_y L = \frac{2 k_y \alpha_y}{k_y^2 - \alpha_y^2} \tag{2.37}$$

with

$$\alpha_x = j\frac{2\pi Z_o}{\lambda_o}\frac{h}{L}Y_x F_x\left(\frac{L}{W}\right) \tag{2.38}$$

and

$$\alpha_y = j\frac{2\pi Z_o}{\lambda_o}\frac{h}{W}Y_y F_y\left(\frac{W}{L}\right) \tag{2.39}$$

Y_x is the wall admittance for x = 0, x = W walls, Y_y is the wall admittance for y = 0, y = L walls. The empirically derived aspect ratio factors F_x and F_y are approximate units [32]. For the TM_{10} mode,

$$F_y = 0.7747 + 0.5977\left(\frac{W}{L} - 1\right) - 0.1638\left(\frac{W}{L} - 1\right)^2 \tag{3.40}$$

Since accurate solutions have not yet been derived for the wall admittance, an approximation based on the wall conductance of a TEM parallel plate waveguide radiating into a half space and the wall susceptance of a uniform microstrip transmission line may be used [1, 28, 32]. This gives the following formulas:

$$Y_y = G + jB \tag{2.41}$$

where G is the total wall conductance given by

$$G = 0.00836\frac{W}{\lambda_o} \tag{2.42}$$

and B, the wall susceptance, is

$$B = 0.00678\frac{W}{\lambda_o}\frac{\Delta W}{h}\varepsilon_{ew} \tag{2.43}$$

ε_{ew} is given by equation 2.10 and ΔW by equation 2.11.

An approximation for the resonant frequency for the dominant TM_{10} mode ($k_x = 0$) is made by assuming that the radiating walls at y = 0 and y = L are perfect magnetic walls (open circuited with zero tangential magnetic field). This would give: $Y_y = 0$ and $a_y = 0$ so that the first non-zero root of equation 2.37 is $k_y = \pi/L$, ie. $L = \lambda_o/(2\sqrt{\varepsilon_r})$. This corresponds to an approximate resonant frequency for the dominant mode given by [28]:

$$f_r = \frac{c_o}{2L\sqrt{\varepsilon_r}} \tag{2.44}$$

The complex resonance frequency may be found from equation 2.36 and equation 2.37 assuming the TM_{10} condition that $k_x = 0$, and taking the substrate loss tangent, tanδ, into account [16]:

$$f_{r'} + jf_{i'} = f_r \frac{1 - \frac{\Delta}{\pi}}{\sqrt{1 - j\tan\delta}} \tag{2.45}$$

Δ is a complex root of a complex transcendent equation which does not have an exact value. This can be calculated from a simple iterative algorithm [28] ie.,

$$k_y = k_{10} = \frac{\pi - \Delta_4}{L} \tag{2.46}$$

with $\Delta_o = 0$ as the seed value. equation 2.44 is derived from equation 2.34, assuming TM_{10} condition, with tan(L k_{10})

$$\Delta_{p+1} = \frac{2\alpha_{10}L(\pi - \Delta_p)}{(\alpha_{10}L)^2 + 2\Delta_p\pi - \Delta_p^2 - \pi^2} - \frac{\Delta_p^3}{3} \tag{2.47}$$

expanded in the first two terms of a Taylor series about π.

Also,

$$\alpha_{10} = j\frac{2\pi Z_o h}{\lambda_o W Z_w} \tag{2.48}$$

with Y being the admittance of the radiating walls at y = 0 and y = L.

The input impedance for the TM_{mn} mode for a patch fed at position was calculated using a modal expansion method [1, 28], yielding

$$Z_{in} = -j\frac{h\omega}{\varepsilon LW}\sum_{m=0}^{\infty}\sum_{n=0}^{\infty}\frac{X_{mn}^2\cos^2 ak_y\cos^2 bk_x}{\omega^2 - \tilde{\omega}_{mn}^2}G_{mn} \tag{2.49}$$

ϖ_{mn} is the complex radian resonant frequency which is approximated by

$$\tilde{\omega} = \frac{c_o}{\sqrt{\varepsilon_r(1 - j\tan\delta)}} k_y \tag{2.50}$$

The factor G_{mn} in the series of equation 2.49 accounts for the finite width of the coaxial probe wire.

$$G_{mn} = \frac{\sin\left(\frac{b}{2}k_x\right)}{\frac{b}{2}k_x} \frac{\sin\left(\frac{a}{2}k_y\right)}{\frac{a}{2}k_y} \tag{2.51}$$

Alternatively, Richards [28] and Derneryd et al. [29] approximated the input impedance at any frequency f near a resonance f_r considering the total quality factor, Q_T, and the resistance due to radiating slot of the patch, R_{in}, as

$$Z_{in} = \frac{R_{in}}{1 + 2jQ_T\left(\frac{f}{f_r} - \frac{f_r}{f}\right)} \tag{2.52}$$

where Q_T is the quality factor associated with four loss mechanisms, namely, radiation, Q_r, the loss due to heating in the conducing elements and the ground plane, Q_c, the loss due to heating within the dielectric medium, Q_d, and the loss associated with surface wave propagation on a dielectric coated conductor, Q_s, [32, 108]:

$$Q_T = \left(Q_r^{-1} + Q_c^{-1} + Q_d^{-1} + Q_s^{-1}\right)^{-1} \tag{2.53}$$

The quality factor associated with the surface wave is negligible for thin substrates. For thicker substrates some other technique will be used to estimate the surface wave contribution. The Q factors due to conductor loss may be calculated from [32]

$$Q_c = h\sqrt{\pi f_r \mu_o \sigma} \tag{2.54}$$

where σ is the conductivity.

The Q factor due to dielectric loss may be calculated from

$$Q_d = \tan^{-1}\delta \tag{2.55}$$

The radiation Q factor is given by [22]

$$Q_r = \frac{c_o\sqrt{\varepsilon_{ew}}}{4h f_r} \tag{2.56}$$

Other characteristics of the patch may be defined by representing the microstrip antenna element as a parallel RLC lossy resonant circuit, Figure 2.2, comprising capacitance C, inductance L and resonant resistance R of the TM_{10} mode as given by Bahl et al. [1] and Carver [28]

$$L = \frac{1}{C\omega_r^2} \tag{2.57}$$

$$C = \frac{\varepsilon_{ew}\,\varepsilon_o LW}{2h}\cos^{-2}\left(\frac{\pi a}{L}\right) \tag{2.58}$$

$$R = \frac{Q}{\omega_r C} \tag{2.59}$$

The bandwidth is given by equation 2.25.

The radiation patterns in the E and H planes can be calculated by using equation 2.21 and equation 2.23 respectively. Alternatively, the radiation pattern of a rectangular microstrip antenna element for TM_{10} can be given as [6] :

in the E-plane

$$E_\theta(\theta,90°) = K_E\cos\left(\frac{k_o h}{2}\cos\theta\right)\cos\left(\frac{k_o L_e}{2}\sin\theta\right) \tag{2.60}$$

$$E_\phi(\theta,90°) = 0 \tag{2.61}$$

with

$$K_E = -j\frac{e^{-jk_oR}}{R}\frac{2W_e}{\lambda_o}V_{10}e^{j\frac{k_oL_e}{2}\sin\theta} \tag{2.62}$$

where V_{10} is the voltage at either of two ends of the patch and R is the distance from the antenna element. And in the H-plane:

$$E_\theta(\theta,0°) = 0 \tag{2.63}$$

$$E_\phi(\theta,0°) = K_H\cos\left(\frac{k_o h}{2}\cos\theta\right)\cos\theta\frac{\sin\left(\frac{k_oW_e}{2}\sin\theta\right)}{\left(\frac{k_oW_e}{2}\sin\theta\right)} \tag{2.64}$$

with

$$K_H = -j\frac{e^{-jk_o R}}{R}\frac{2W_e}{\lambda_o}V_{10}e^{j\frac{k_o W_c}{2}\sin\theta} \tag{2.65}$$

where W_e and L_e are the effective dimensions, taking into account the fringing fields at the edge of the patch. They will be given in the subsequent chapters.

2.2.2 Full Wave Analyses

Full wave analyses is a term that covers formulations that are electromagnetically rigorous as well as computationally extensive. These models usually assume that the substrate is infinite in extent in the lateral dimensions, and enforce the proper boundary conditions at the air-dielectric interface. Unfortunately, they require an extensive analytical and computational effort also a high computational cost. This effort is justified, however, by the reliability of the results, notwithstanding possible human error.

The full wave analyses, FW, are applicable, in principle, to microstrip antennas of any shape and thickness and is the most rigorous theory, though accurate results are not always assured. They utilise the dyadic Green's function pertaining to the grounded dielectric slab for the derivation of a set of integral equations for the unknown two components of the surface current of the patch. The technique can easily be extended to multiple dielectric layers. The Method of Moment is then used to solve the integrals numerically, commonly in the Fourier transform domain [3, 12, 40]. The FW analyses provide a theoretically exact model from which the resonant frequency and the radiation pattern can easily be extracted. However, the basic difficulty lies in the dubious definition of the input impedance of the antenna and in the modelling of the practical complex feed structure accurately. Therefore, the determination of the input impedance for a specified excitation appears to be less obvious. Furthermore, in published works, the computations were made only for some idealised excitations [3].

As far as design is concerned, the use of the FW theory is somewhat limited. For example, it would not be able to provide a solution readily if it were desired to find the physical parameters of a patch for a given frequency, bandwidth, polarisation and some radiation characteristics. Even for the simplest antenna configuration, the numerical treatment requires considerable computational effort and is time consuming and expensive.

2.2.2.1 Method of Moments

The method of moments, MoM, is a general procedure to convert the analytical formulation of a field problem into a numerical formulation in the form of a matrix equation. Many numerical methods may be considered a special forms of the MoM. The method of moments is generally applied to the solution of an integral equation. It is presently recognised as a good approach to the analysis of microstrip antenna configurations [12].

This technique transforms the integral equation into a matrix algebraic equation which can be solved on a computer. Overlapping rooftops can be used to develop the currents in the x and y directions, yielding pulse doublets for the surface charge density. The elementary rectangular cells of the division can take various sizes, so any kind of microstrip structure can be modelled [109].

2.2.2.2 Moment Method in Space Domain

Newman et al [39], Ney [48] and Huang [110] applied their formulation to compute antenna properties only at frequencies up to the S-band, and therefore did not notice any significant improvements in the accuracy of their results, as compared to the cavity model method.

This formulation depends on the solving of an integral equation which involves the patch surface current and the feed current as unknowns. The analysis is performed in several steps:

- assuming an air dielectric, using the image theory, the ground plane is removed from the analysis and the feed (for both probe-fed and end-fed examples) is replaced by an impressed current filament,
- the patch surface current is expanded in the terms of N suitably chosen expansion modes,
- the boundary condition that $[E_{incident} + E_{scattered}]_{tan} = 0$ is then used to generate the matrix equation for the unknown mode coefficients, which is then numerically solved for the patch and feed currents,
- once the currents are known, it is possible to easily calculate the antenna properties.

In the case of a non-air dielectric, the formulation can be modified in an appropriate way by using the volume equivalence theorem to replace the dielectric slab with a mix of free space and equivalent volume polarisation currents [39].

In order to use the moment method in the space domain, an extremely accurate numerical evaluation of the matrix elements is needed, posing the drawback that a significant increase in computational time is required.

2.2.2.3 Moment Method in Spectral Domain

The processes of the moment method in the spectral domain are as follows [42-47], [49-54], [111]. Firstly the integral equation containing the unknown patch current and the Green's function for the dielectric slab is formulated, and then the exact Green's function for the dielectric slab is derived. A numerical evaluation of the Sommerfeld type of integrals involved in the expression for the vector magnetic potential is then carried out, and Galerkin's procedure is used to formulate and compute the patch surface current (including the feed surface current in the case of an end-fed patch). The antenna properties are then determined. This method effectively involves the surface wave effects, as well as mutual coupling effects.

The moment method in the spectral domain is theoretically capable of analysing any arbitrary patch shape, as well as patch arrays. It's drawbacks seem to be the minor one of the loss of physical insight resulting from the transformation of the problem into the spectral domain, and that of the considerable computational and analytical effort required.

2.2.2.4 Finite-Element Method (FEM)

This method is related to the method of moments. The region of interest is subdivided into surface or volume elements, depending on whether a two - or three - dimensional structure is being examined. The unknown function, which may be a scalar potential or a vectorial field component, is approximated within each element by a polynomial function. Each of these functions must satisfy some particular boundary conditions such as continuity. Application of the Rayleigh-Ritz procedure

then transforms the functional minimisation into a linear system of equations. The equations to be solved are usually expressed in terms of an integral-type functional. The functional is chosen such that the field solution makes the functional stationary. The total functional is the sum of the integral over each element.

The FEM solution take a more 'brute force' approach by modelling the entire antenna, including dielectric and metal components, and some of the surrounding volume. This method allows a high degree of versatility for treating arbitrary geometries, including multilayer and inhomogeneous dielectric, but a high price is paid in terms of computer time [5] and human errors.

2.2.2.5 Finite-Difference Time-Domain Method (FDTD)

The finite difference method transforms a differential equation into a system of algebraic equations. Derivatives are simply replaced by finite differences. The region of interest is divided into nodes located on a two - or three dimensional grid. It requires, however, a large number of mesh points, thus a large memory storage, and numerical efficiency is rather low. Another shortcoming is the difficulty of fitting curved boundaries with a rectangular mesh [112-117].

The FDTD requires either large memory requirements making the solution procedure highly inefficient, or estimates of the propagation and decay behaviour of the field which can not be predicted in a systematic fashion for general applications

2.2.2.6 Transform Domain Analyses

Both the spectral domain approaches used by Itoh and Menzel for rectangular patches [40] and by Araki and Itoh for circular patches [41] come under the category of transform domain analyses.

Basically, this method, as applied to microstrip antennas involves the following procedures. Firstly, the coupled homogenous integral equations involving both the longitudinal and the transverse components of the patch surface current density as unknowns are derived. The resultant equations are then transformed into algebraic equations using the Fourier transform domain, and then the unknown patch surface current density components are solved using Galerkin's method.

Finally, the radiating characteristics of the antenna are computed. This formulation inherently takes into account the effects of surface waves. It is known to be efficient, but is generally restricted to well-shaped structures that involve infinitely thin conductors.

2.2.2.7 Mixed Potential Integral Equation (MPIE) Approach

This approach was proposed by Mosig [55] in order to analyse arbitrarily shaped patches. Basically, this method involves an adaptation of Harrington's work on wire antennas [40] into the field of microstrip antennas. The integral equation is a generalisation of the integral equations considered by other authors, involving both a scalar potential and a vector potential. The method of moments is used to solve the MPIE in the space domain. However, although several structures of practical interest are considered, such as a rectangular patch and an L-shaped patch, the results presented are not in a form that is directly useful to a designer.

2.2.2.8 Conjugate-Gradient Fast Fourier Transform (CGFFT) Technique

This technique, proposed by Willis and Sengupta [56] is novel in that it makes a distinction between the currents on the top and the bottom of the patch. The CGFFT proceeds according to the following steps. Firstly, the dyadic Green's function is derived for a ground plane covered with dielectric substrate, and then the integral equation for the total patch current is derived. The integral equation is then solved in the spectral domain by assuming the point of observation on the patch surface, and thus reducing it to a two dimensional problem. The CGFFT technique is used to solve the integral equation numerically.

From these procedures the surface current for both the top and the bottom of the patch is known, and the computation of the radiation characteristics of the antenna can then be performed using two dimensional stationary-phase integrals [66]. The rigorous modelling of the aperture admittance could be of some interest to a practicing engineer, but no exact or approximate analysis has ever been performed, owing to the complexity of the structure. Hence a tedious "cut and try" optimisation is necessary to realise a broad banding.

2.2.3 Other Methods

2.2.3.1 The Dyadic Green's Function Technique

An alternative technique for evaluating the characteristics of microstrip antenna is the dyadic Green's function technique with boundary admittance of the edge. For this technique, the feed pin size and location, the patch size, thickness and dielectric constant of the material are important in deriving the analytical expression for the input impedance. The boundary admittance can be obtained by considering the radiated power and the electric and magnetic stored energies in the fringe capacitance. As is well known, once the dyadic Green's function is known, the field from an arbitrary source distribution may be found by means of a superposition integral [1, 2, 57]. The main difficulty presented by this method resides in the calculation of Green's functions. It is mathematically cumbersome and does not lend itself to tractable analysis.

The negative aspect of this model is that it requires an extensive analytical and computational effort, the pay-off of which is the complete trust that the designer can get in the results, possible human error by the researchers involved notwithstanding.

2.2.3.2 The Wire Grid Method

This approach models the microstrip antenna element and its feed probe as a fine grid of wire segments immersed in a dielectric medium, and then applies Richmond's Reaction formulation to solve the piecewise sinusoidal currents distribution on the wire grid segments. Once the currents are known, all antenna characteristics of interest can be calculated [59].

This method takes the dielectric slab into account, using empirical frequency shift and impedance scaling information. Furthermore, it has the advantage of being amenable to other microstrip patches of more general shape such as the circular disc, circular segment, rectangular and triangular antenna elements.

Although this method gives good results for thin antenna elements if the grid is made sufficiently fine, design computations require considerable computer storage and time, which escalates design cost. However, it provides some physical insight into the operation of this class of antenna.

2.2.3.3 Segmentation and Desegmentation Techniques

For the segmentation and desegmentation method the antenna element is segmented into regular shapes for which Green's function can be determined. The effect of radiation losses can be taken into account by dividing the radiating aperture into a discrete number of ports and loading these ports by lumped resistors. This technique can be applied to any arbitrary microstrip geometry and is readily amenable to computer aided design based on optimisation methods
[60, 61].

Segmentation techniques can be combined with other theories, such as the generalised cavity method theory, to compute the properties of the antenna. However, the main limitation of the generalised cavity method using segmentation technique is that the effect of the dielectric substrate on the input impedance has not been considered [62].

2.2.3.4 Electric Surface Current Model

The electric surface current model involves an assumed current density distribution over the upper conductor in conjunction with the appropriate Green's function, and is applicable to relatively thick substrates. A computer analysis of the element near resonance is made possible by an approximation of the current distribution using lossles transmission line analysis. This model takes into account both the effect of the dielectric material and its effect on the antenna parameters, and also the surface wave effects, which are an inherent element of the model.

The electric surface current model was developed primarily with regards to rectangular patches [63] and conformal antennas [64], but can be easily adapted to analyse a printed dipole. It was also initially used for predicting the input impedance of a four element array in the calculation of the radiation pattern of a wire-grid microwave antenna. It is a model that, like the variational approach discussed in section 2.2.3.6, depends upon an educated guess. However, the two models vary significantly. Firstly, as the mathematical expressions for the components of the Green's function necessarily contain both space and surface wave components, the electric surface current model is valid for electrically thick substrates, whereas the variational approach is applicable only to antennas with electrically thin substrates. Secondly, the electric surface current model is applicable for patches of any shape where a reasonable guess of the current distribution can be made, unlike the variational approach method, which is mainly suitable only for a printed dipole. Thirdly, the variational approach analyses the structure in the space domain, as opposed to the electric surface current model, which uses the Fourier domain.

The electric surface current model offers both a consideration of the surface wave effects in the analysis, thereby extending its applicability to the millimetre wave band, and also ease of use. Its assumption of a constant transverse current (which may be of questionable accuracy for large W/λ_o values), its omission of the feed localities in the calculations of input impedance, and the assumption of an infinitely large ground plane, all constitute limitations on the model.

Some mathematical formulations of this method are given in Appendix A.

2.2.3.5 The Vector Potential Approach

In this approach, the mode theory of wave propagation developed by Sommerfeld is used to determine the electromagnetic field produced by a horizontal electric dipole, and the characteristics of the antenna are then evaluated by numerical techniques. The fields created by a horizontal electric dipole on the microstrip may be determined from the vector potential. Appropriate simplifications are required to obtain convergence. Further, it is difficult to obtain physically significant interpretations of the results [118].

2.2.3.6 The Variational Approach

The variational approach [66] follows the following two procedures:

- Derivation of the Green's function for a horizontal Herzian dipole printed on a ground substrate.

- Use of the Green's function and an assumed current distribution on the dipole, based on a quasi-TEM mode in the microstrip, to write a variational expression for the input impedance of the antenna.

The variational expression for the input impedance involves two dimensional improper integrals which are computed numerically. As has been demonstrated in the literature, the superposition of a space wave component and a surface wave component is the real part of the input impedance (which is equal to the radiation resistance of the antenna at resonance). Also derived are explicit closed form equations for the far field components of the radiated field.

The variational approach is valid primarily for thin substrates, that is, those with microwave frequencies.

2.2.3.7 Transmission-Line Matrix Method

The transmission line matrix method simulates the wave propagation in the time domain by discretizing the space into a two- or three-dimensional transmission line matrix. It provides a complete solution to the Maxwell equations It therefore has a number of similarities with the finite difference time domain method discussed in 2.6. The method is founded on the modelling of the spatial electromagnetic field in terms of a distributed transmission line network. Electric and magnetic fields equivalent to voltage and current on the network. The numerical calculation starts by exciting the matrix at specific points by voltage or current pulses. Propagation of pulses is then evaluated at discrete time intervals. Time synchronisation is required so that all pulses reach nodes at the same time [67, 68].

2.2.3.8 Hankel Transform Technique

The formulation is in the Hankel domain, and is applied to a situation where a concentric circular patch is in proximity with a similar patch, which functions as a parasitic element, widening the total antenna bandwidth by a factor of up to nine [69]. This analysis inherently accounts for the thickness of the substrate and the effects of surface waves, however, it neglects the connection of the two patches, the centre pin, hence limiting the usefulness of the results for the fundamental quasi TM_{110} mode. Another major shortcoming of this method is the considerable programming effort requires to duplicate the results.

The Hankel transform domain analysis can be applied for microstrip structure, as both the driving current and the feed have been removed, making the boundary value for the system a source free problem. Thus it is possible to solve the natural frequencies of the radiating/resonant system. The structure is actually fixed by a centre pin inserted between two disks, but this can be neglected if a resonant mode to be analysed is a quasi TM_{110} dominant mode, whose E_z component vanishes on the z-axis.

2.2.3.9 The Radiating Aperture Method

This method considers four slots surrounding the central conductor, which is located in the same plane. The width of the equivalent slots is determined empirically, and the magnetic current density is expanded over the complete set of resonant modes. Radiation resistances for each mode are then determined for a particular location of the excitation.

This model, using the Kirchhoff Vector relationship is mathematically precise if the aperture fields are known exactly [70, 71, 119]. In the absence of exact aperture field distributions, they may be reasonably approximated to produce good results for thin antennas. However, this model is, in principle, applicable only to approximate the radiation pattern of microstrip antennas terminated by open circuits. The main difference between this model and the TLM is that in the first one the far-field is produced by a slot surrounding the microstrip antenna element.

2.2.3.10 Reciprocity Method

The reciprocity method [72] may be applied to many different microstrip antenna configurations, and possesses satisfactory analytical rigour. This method is based on the reciprocity theorem, using the exact Green's functions (in the spectral domain) for the grounded dielectric slab and, for the unknown antenna current, a moment method solution. The necessary field components from electrical and magnetic currents in the presence of a dielectric slab are found by using the exact Green's functions in the spectral domain. The accuracy of the results, particularly in the millimetre wave band, are improved by obtaining the numerical solution for the antenna properties by incorporating a large number of expansion terms in the aperture field. This model seems to be limited only by its failure to acknowledge higher order microstrip modes in the expression for modal fields of the microstrip feed.

This method has been applied to the analysis of both printed slot and aperture coupled rectangular microstrip patches [72]. It is assumed that both these configurations are end-fed by a microstrip of infinite length, thus enabling the antenna to be modelled on a series impedance Z in the microstrip line. This compatibility applies to both the printed slot and the aperture coupled patch. This method does have some validity in the millimetre wave band, but the duplication of the results, requiring considerable programming effort, presents obstacles to the practising engineer.

The basic method can be extended to moment method solutions for slot antennas with numerous expansion modes in the slot, and for aperture coupled patch antennae with numerous expansion modes on the patch, resulting in a combination of the reciprocity analysis and a moment method structure, using the exact Green's functions for the planar structure. This combination provides a versatile technique that should find application in a number of printed antenna and planar circuit problems.

2.2.3.11 Generalised Edge Boundary Condition (GEBC) Technique

The GEBC technique [73] proceeds by decomposing an arbitrary patch shape, including the feed, into a discrete series of interrelated segments, and then, assuming a TEM mode of propagation, the equivalent voltage and current on each patch are defined. A generalised boundary condition in integral form thus relates the equivalent voltage and current everywhere along the patch edge. This technique accounts for the dynamic edge effects and mutual coupling between different edge points by implication.

Analysis of an arbitrary patch shape eventually results in a discrete version of the edge boundary conditions, which is convertible into the corresponding matrix form, in which the equivalent voltages and the equivalent current matrices are the unknowns. The solution for the equivalent voltage and currents (for various segments) can then be solved numerically. The computation of antenna properties then follows.

Two main steps are followed in this technique. Firstly, the edge of the patch and its feed line are discretised as a series of connected segments, and, secondly, an equivalent voltage and an equivalent current are defined on each patch. The resultant boundary of the patch and the feeding line can then be seen as an interface between two separate networks, the first taking into account the coupling under the patch, and the second presenting the dynamical edge effects and the coupling over the top side of the patch. This general and computer efficient method can then be satisfactorily applied to the determination of the input impedance of some commonly used probe fed antenna strip fed patch resonators.

The basic limitation of the GEBC method is that it assumes a thin substrate, limiting the method's application to mostly microwave and lower millimetre wave bands. This limitation is compounded by the considerable numerical and analytical effort necessary to implement the formulation.

2.2.3.12 Generalised Variational Approach

The generalised variational approach [74] incorporates both the variational method and the modal expansion method in order to analyse a patch of arbitrary shape. The aim of the method is to arrive at a network model for a microwave antenna with multiterminals. It is based on an assumption of a thin substrate, and a perfect magnetic wall at the antenna boundaries is assumed. It can be used for almost any arbitrary patch shape, and can handle a multiport patch attachment, these being its two main points of appeal.

Four main steps are followed by this technique. Firstly, assuming an electrically thin substrate, it is assumed that only the quasi TEM propagates. Then, assuming a Newman boundary condition, that is, perfect magnetic walls, a solution to the scalar Helmholtz equation is constructed which expresses E_z as a double integral over the patch surface. The integral in this solution is the product of the Green's function and a function representing the surface current distribution of the patch. Thirdly, the various eigenvalues and eigenmodes involved in the Green's function are computed using a standard variational formulation and the Rayleigh-Ritz method. The accuracy of the eventual solution is affected by the number of the basis functions chosen for each eigenfunction. Finally, the field components can be computed once the Green's function is known. This approach is relatively comprehensive, however, the basic assumptions involved in the method, that is, an electrically thick substrate and perfect magnetic walls, limit its usefulness to mainly microwave frequencies (typically up to around 30 GHz).

2.2.3.13 Dual Integral Equation Approach

This approach provides an analysis based on two assumptions; that there is a zero metallisation thickness and that there is a uniform current on the probe [75]. It then proceeds through four steps. Firstly, taking a case where the patch is absent, thus reducing the problem to a vertically located probe in a dielectric that is encompassed by the ground plane on one side and a free space on the other, the authors derive the z-component of the E-field using a dyadic Green's function formulation in the vector Hankel transform domain. Secondly, a circular patch is put in place (at $z = h$), and the induced current on the patch is computed, assuming a symmetrically located probe. The fields

resulting from this induced current (which are termed conjugate fields) are then derived. Thirdly, suitable boundary conditions are derived, resulting in a pair of vector dual integral equations. The unknown patch current can then be solved from these by using the standard Galerkin's procedure. Finally, once the patch current is known, it is possible to derive the radiation characteristics in a straightforward way. Theoretically, this method should also be applicable to other patch shapes also.

The authors [75] have drawn two significant conclusions regarding this method, these being firstly that for thin substrates, a single mode approximation for the patch current is sufficiently accurate. Secondly, as the substrate thickness approaches zero, the results converge for the case of a magnetic wall resonator model. It would seem to be valid, as the authors conclude, that minimal assumptions and approximations should be made (except for the assumption of a constant current on a probe feed, which becomes more difficult to justify as the frequency increases). The chief drawback of this method is the considerable programming effort required to implement the formulation.

2.3 Conclusion

Some methods and models which have been used to date for analysing microstrip antenna structures have been listed. Each method has its application but also some limitations. Thus there is no method alone which is appropriate for predicting all the fundamental properties of an antenna.

Many techniques used for the analysis of microstrip antennae require the resolution of large systems of linear equations. For large numbers of unknowns, matrix inversion requires a very large memory space and becomes impractical or extremely time consuming.

The classical models generally provide sufficient information. Their main advantages lies in their simplicity, resulting in a relatively small computational effort, and they allow easy synthesis of microstrip antennae.

The TLM and CM have been chosen for application in this thesis. The relevant parts of these methods have been presented. These two models were chosen instead of the more complicated ones because:

- It is an advantage to use simple and general models because only basic computing facilities will be required.

- They have been shown to be quite adequate for design purposes for antenna elements with substrates thinner than approximately $0.13\lambda_d$.

- They use the same field distribution under the patch as the fundamental mode.

- The assumption that most of the energy is stored in the fundamental mode was found to be reasonable because the antenna element has such a narrow bandwidth.

This thesis uses a TLM to calculate the resonant patch length, resonant frequency, far-field radiation patterns and beamwidth for antenna elements with substrates thinner than approximately $0.13\ \lambda_d$. For thicker substrates however, the equations for computing the antenna characteristics have been modified by the addition of empirically derived correction factors or using effective patch dimensions.

The CM has been used for computing the input impedance, efficiency and bandwidth of antenna elements with thin substrates.

Other more general methods involve extensive numerical procedures, resulting in round-off errors, and may also need final experimental adjustment to the theoretical results. They also suffer from a lack of computational efficiency, which in practice can restrict their usefulness due to high computational cost.

Chapter 3

Formulae for the Computation of the Physical Properties of Rectangular Microstrip Antenna Elements with Various Substrate Thicknesses

3.1 Introduction

The basic microstrip antenna element is a resonant patch of metal on the surface of a grounded dielectric slab. The patch is usually printed on a microwave substrate material with thickness h and relative permittivity ε_r. Its physical properties are the resonant length, L, the width, W, and the feed point location, **a**, as shown in Figure 1.1.

Since a microstrip antenna is inhomogeneous and the radiation appears at the edges of the patch, the physical properties are difficult to determine when designing an antenna for a specified frequency and substrate material. It is well known that the antenna performance characteristics depend largely on the physical dimensions of the patch, the diameter and position of the feed probe, the relative permittivity and the thickness of the substrate on which the antenna element is placed. For example: L affects the resonant frequency, the resonant resistance, the bandwidth, the efficiency and the E-plane radiation pattern, W affects the resonant frequency, the bandwidth and the H-plane radiation pattern and the feed point location controls the resonant resistance as will be shown in subsequent chapters. It is also known that a rectangular microstrip antenna

element radiates efficiently when it resonates, which means that the patch length is approximately one-half of the wavelength in the substrate medium. In practice, the fringing capacitance effect associated with the radiating edges causes the effective distance between the radiating edges to be slightly greater than patch physical L, so that the actual resonant length is slightly less than $\lambda_d/2$ for thin substrates and slightly larger than $\lambda_d/2$ for thick substrates, where λ_d is the wavelength in the dielectric substrate.

Although several formulae using different levels of approximation are available in the literature to design the physical properties of rectangular microstrip antenna elements [1 - 5], [9, 18, 21, 32, 99], [120 - 122] there appears to be no reliable general method which gives these properties. The formulae are different, they do not yield similar results, and the ranges of their validity are generally not known. The designed antenna elements using these approximations may not resonate at all for the range of the substrate thicknesses considered in this thesis ($0.0065 \lambda_o \leq h$ and $2.22 \leq \varepsilon_r \leq 10.2$). Above all, the designer needs a practical and reliable method for calculating the physical properties of interest for rectangular microstrip antenna elements with various substrate relative permittivities and thicknesses. The designer has thus been forced to obtain the required physical properties by a trial-and-error technique.

The aim of the work presented in this chapter is to

- carry out a study on the design of physical properties and feeding of antenna elements with various relative permittivity and thickness of substrate materials over a wide frequency band,
- discuss the published formulae on the design of physical properties,
- determine the suitability and threshold of the applicability of these formulae,
- develop formulae that can determine the physical properties of *thin* antennae,
- develop formulae that can calculate the feed point location of these antennae
- derive empirical formulae that can calculate the effective permittivity of their substrate materials,
- develop formulae that can determine the physical properties of *thick* antennae,
- study the effects of the substrate thickness on the patch dimensions.

The methods used to develop the new empirical formulae are described briefly in following sections.

Note that

- antenna elements with substrates thinner than approximately 0.0815 λ_o, which correspond to 0.130 λ_d for $2.22 \leq \varepsilon_r \leq 10.2$ are considered as *thin* as discussed in Chapter 1
- each data point in the figures in this chapter represents a measured or calculated value of an individual antenna element with a set of antenna parameters.

3.2 Review of Formulae for Computing Physical Properties of Rectangular Antenna Elements

The formulae available in the literature for the design of the physical properties of rectangular microstrip antenna elements are discussed and their applicability is determined in the following sections.

3.2.1 Element Width

Patch width is an important consideration for both thin and thick antenna elements. Therefore, when selecting the patch width it must be considered that, due to the excitation of surface waves, a small width results in a large bandwidth, and low antenna efficiency and gain. A large width, however, results in the excitation of high order modes which may distort the radiation pattern, decrease the bandwidth and increase the efficiency. For thin antenna elements the width must be less than $\lambda_d/2$, so that higher order modes are not excited. According to Derneryd [21].

$$W \approx 0.3\lambda_o \tag{3.1}$$

Weinschel [120] suggests that a reasonable dimension for W is approximately:

$$W \approx 0.9\frac{\lambda_o}{\sqrt{\varepsilon_r}} \tag{3.2}$$

Bahl et al [1], Bahl [121] and Schroeder [122] give an empirical approximation for computing the W of those antenna elements which have a substrate thickness less than $0.001\ \lambda_d$:

$$W = \frac{\lambda_o}{2\sqrt{0.5(\varepsilon_r + 1)}} \tag{3.3}$$

Unfortunately, the basis for the derivation of the approximations mentioned above is not given.

3.2.2 Element Length

Microstrip antenna elements rely on some resonance property, and therefore need to occupy a L which is influenced by the dielectric between the patch and the ground plane.

Munson [18] assumes the physical length of a rectangular microstrip antenna element with thin substrates to be slightly less than a half wavelength in the dielectric substrate material:

$$L \approx 0.49\lambda_d \tag{3.4}$$

with

$$\lambda_d = \frac{c_o}{f_r\sqrt{\varepsilon_r}} \tag{3.5}$$

where $c_o = 3x10^8$ m/s is the velocity of electromagnetic waves in free space and f_r is the resonant frequency.

Note, that the exact value of ε_r is critical, and is usually specified and measured by the manufacturer.

Microstrip antennae have an inhomogeneous nature: an electromagnetic field produced by surface charges and currents on the patch conductors extends across at least two different media. These media are the dielectric material on which the antenna is printed and the surrounding space, usually air. The wave velocities in the two media are different, because a quasi-transverse electromagnetic (TEM) wave exist. The phase velocity, v_p, is linked to the effective permittivity, ε_{ew} as follows [1]:

$$v_p = \frac{c_o}{\sqrt{\varepsilon_{ew}}} \tag{3.6}$$

Taking into account the fields in these media through the characteristic impedances of substrate filled, Z_{cw}, and air filled, Z_{ow}, microstrip line of width W, (assuming the thickness of the strip conductor is zero) Wolf et al [123] proposed for v_p the following expression

$$v_p = c_o \frac{Z_{cw}}{Z_{ow}} \tag{3.7}$$

Using equation 3.6 and equation 3.7 an expression has been derived for ε_{ew} for rectangular microstrip antenna elements with various relative permittivity and thicknesses of substrates [83]:

$$\varepsilon_{eW} = \left(\frac{Z_{ow}}{Z_{cw}}\right)^2 \tag{3.8}$$

Z_{cw} can be calculated from equation 2.4 or equation 2.5 and Z_{ow} is determined by setting $\varepsilon_r = 1$ in equation 2.4 or equation 2.5, yielding for $W/h \leq 3.3$:

$$Z_{ow} = \frac{R_o}{2\pi}\left[\ln\left(\frac{4h}{W} + \sqrt{2 + \frac{16h^2}{W^{20}}}\right)\right] \tag{3.9}$$

and for $W/h \geq 3.3$

$$Z_{ow} = \frac{R_o}{2}\left[\frac{W}{2h} + 0.9033 + 0.3184\ln\left(\frac{W}{2h} + 0.94\right)\right]^{-1} \tag{3.10}$$

where $R_o = 120\,\pi\Omega$ is the wave impedance in free space.

It is important to note that equation 3.8 predicts the effective permittivity for antenna elements with various relative permittivity and thicknesses of substrates [83]. Alternatively ε_{ew} can also be calculated from equation 2.10 yielding similar results.

As described above, because part of the region surrounding the patch is air, the resonant length can not be scaled with relative permittivity as $(\varepsilon_r)^{-0.5}$ as an antenna in a homogeneous medium does. James et al [9] gives an approximation for computing the L of those antenna elements which have a substrate thickness less than $0.006\,\lambda_d$:

$$L = \frac{c_o}{2 f_r \sqrt{\varepsilon_{ew}}} \tag{3.11}$$

In effect, the lines of the fringing field do not stop abruptly at the edge of the patch. There is a stray field extending beyond the edges. This can be interpreted as an electrical lengthening, ΔW, of the patch, which implies an amount of stored energy and can be calculated from equation 2.11. The simple transmission line model, along with this line extension can be used to give an approximate length of a rectangular antenna element as
[1, 3, 121]

$$L = \frac{\lambda_o}{2\sqrt{\varepsilon_{ew}}} - 2\Delta W \tag{3.12}$$

For substrate thicknesses less than 0.002 λ_o another simple approximation for the patch resonant length of a rectangular antenna element is given in [5] as

$$L = \frac{\lambda_o}{2\sqrt{\varepsilon_{ew}}} - h \tag{3.13}$$

In this expression the h was assumed to be the same as the ΔW.

3.2.3 The Feed

Another important item in the design of microstrip antennae is the feed structures and their locations. Without adequate attention to the feed, the antenna cannot function properly, despite being designed with care and precision.

Power can be coupled into or out of the antenna element by a variety of methods. Some of the widely used feed types are coaxial probe, microstripline, aperture coupling, and proximity coupling [1 - 5].

The feed of the antenna element must be carefully designed to avoid perturbation of the radiation patterns. In this respect, coaxial feed, also called probe feed, is superior to other types, because it is simpler to model and integrate in the antenna element. The coaxial feed is modelled by attaching a coaxial connector to a suitable point on the ground plane, with the inner conductor

passing through it and the dielectric substrate, to an appropriate point on the metallic patch as shown in Figure 3.1.

Probe fed rectangular antenna elements have been used in this research because:

- input impedances are most accurately measured by a coaxial arrangement,
- the desired impedance characteristic can be obtained by the proper location of the inner conductor,
- the feed line does not cause any radiation loss, and
- the cable can be placed under the ground plane to minimise coupling between the patch and the feed.

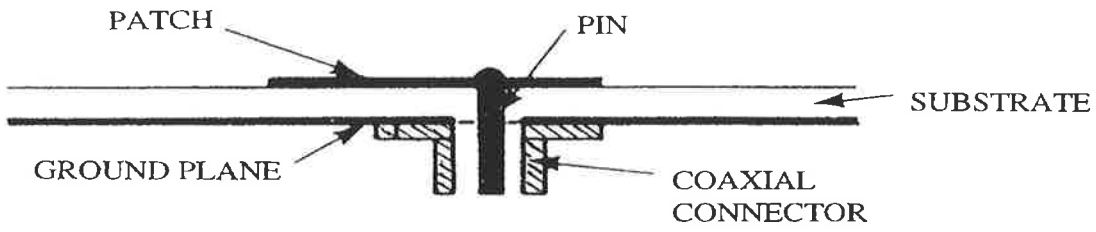

Figure 3.1: Probe coupled microstrip antenna element.

The variation of the input impedance at resonance with the probe position follows that of the cavity field. Further, disadvantages of such a feed include the structure not being completely monolithic, and becoming more difficult and costly to fabricate.

The feed location was chosen to provide a resonant resistance that was close to 50 Ohm.

For completeness some comments on the relative advantages and disadvantages of coaxial probes and other feed models are summarised briefly in Table 3.1.

3.3 Experimental Procedure

3.3.1 Substrates Materials

The antenna elements considered for this thesis were fabricated on five different types of substrate as shown in Table 3.2. The electrical thickness, defined as h/λ_d, of these antenna elements are in the substrate thickness range $0.0065 \leq h/\lambda_d \leq 0.2284$, and the physical thickness is between 0.17 mm and 12.81 mm. They operate over the frequency range 2.980 GHz $\leq f_r \leq$

8.450 GHz. The size of the substrate material was 100 mm square and the ground plane 700 mm square. Note that substrate thicknesses were increased by stacking two or more double sided etched substrate slabs together.

Table 3.1 Microstrip antenna feed techniques [3 - 5]

Techniques	*Advantages*	*Disadvantages*
Coaxial Probe	• Impedance matching by probe location. • Probe location can selectively excite additional modes • Can be used with plated vias for multilayer circuits.	• Impedance is highly inductive when thick substrates are used
Microstripline • **Radiating Edge** • **Nonradiating Edge**	• Monolithic • Good Polarisation • Impedance matching is easier	• Spurious radiation • Must be inset or use transformer to match impedance • Excites cross-pol
Proximity Coupling • **Monolithic**	• No DC contact between feed and radiating patch.	• Direct radiation from coupling region. • Dimensional tolerance.
• **Multilayer**	• Can have large effective thickness for patch substrate and much thinner feed substrate. • Several degrees of freedom available for matching/tuning.	• Multilayer fabrication is required. • Difficult to optimise.
Aperture Coupling]	• Independent choice of substrates for feed and radiators. • No spurious radiation from feed. • No via connectors	• Multilayer fabrication required.

3.3.2 Construction and Testing

The physical properties of thirtythree individual antenna elements have been obtained experimentally by a process of a trial-and-error, because no reliable general rules or formulae exist for predicting them. This experimentation has been performed by varying the relative permittivity and thickness of the substrate, patch length, width and feed point location in order to achieve a minimum return loss and an approximate match to 50 ohm. For each constructed antenna element the return loss and input impedance were measured. Return loss and Smith chart plots are given in Chapters 4 and 5. If the antenna was perfectly matched, and had a minimum return loss, the peak frequency was determined from the return loss plot. Using a micrometer, the patch length, width and feed point location were measured and listed in Tables

3.3 and 3.4. Chapter 4 details the input impedance, and in Chapter 5 the resonant frequency is discussed.

Table 3.2: Substrate materials used in this thesis

	h[mm]	ε_r	Loss tangent tanδ
Duroid substrate	0.17	2.22	0.001
	0.79	2.33	0.001
	1.27	10.2	0.001
	1.57	2.33	0.001
PTFE substrate	0.79	2.50	0.001
	1.50	2.50	0.001
	1.63	2.55	0.002
	4.76	2.55	0.002

The substrate electrical thicknesses of antenna elements listed in Table 3.3 are in the range $0.0065 \leq h/\lambda_d \leq 0.1292$, and the physical thickness is between 0.17 mm and 4.76 mm for $2.22 \leq \varepsilon_r \leq 102$. They operate over the frequency range 3.970 GHz $\leq f_r \leq$ 8.450 GHz. These antenna elements are considered as thin. The substrate electrical thicknesses of antenna elements listed in Table 3.4 are in the range $0.1405 \leq h/\lambda_d \leq 0.2284$, and the physical thickness is between 3.30 mm and 12.81 mm for $\varepsilon_r = 2.55$. They operate over the frequency range 2.980 GHz $\leq f_r \leq$ 8.000 GHz. This class of antenna elements are considered as thick.

3.4 Validations of Available Formulae

The validations of the available design formulae for antenna physical properties are as follows:

Firstly, the experimentally derived patch lengths are plotted as a function of λ_d and compared with $\lambda_d/2$ values of all antenna elements listed in Tables 3.3 and 3.4. A typical plot is shown in Figure 3.2. It is seen the resonant length is slightly less than $\lambda_d/2$ within the substrate thickness threshold of $0.130\lambda_d \geq h$ and slightly larger beyond it.

Secondly, the experimentally obtained electrical lengths, L/λ_d, and electrical widths, W/λ_d, are plotted as a function of electrical thicknesses, h/λ_d, of all antenna elements listed in Tables 3.3 and 3.4. These results are shown in Figure 3.3.

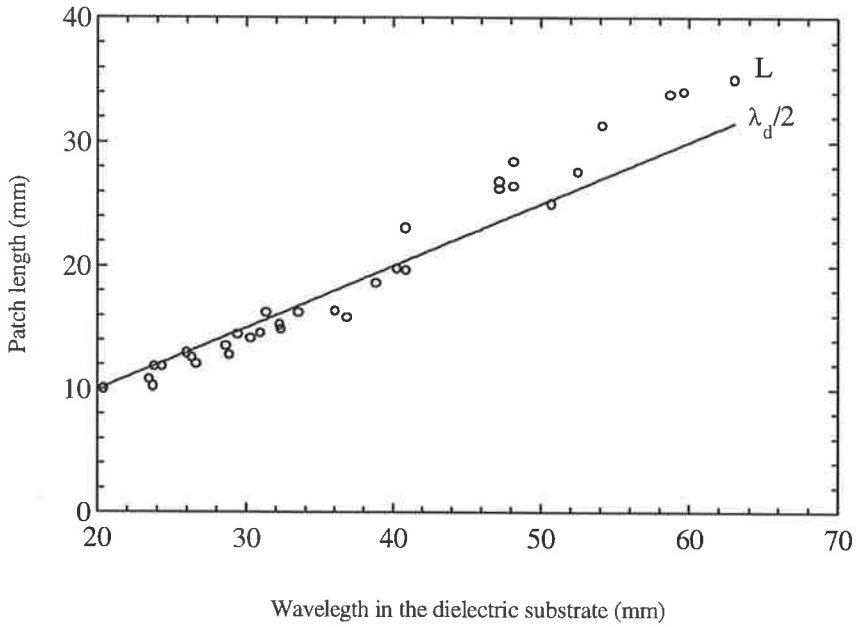

Figure 3.2: Experimentally obtained resonant lengths versus wavelength in the dielectric substrates of all antenna elements listed in Tables 3.3 and 3.4.

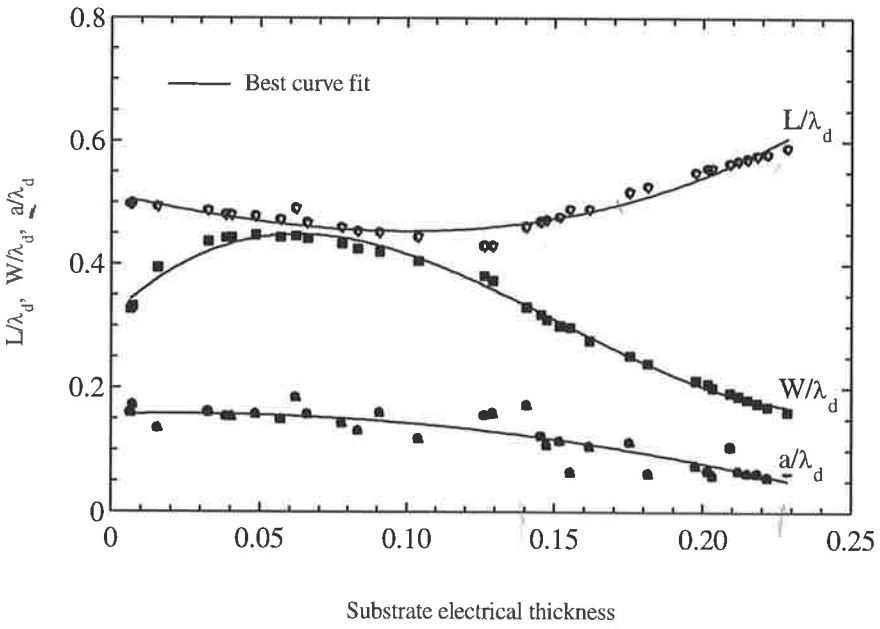

Figure 3.3: Experimentally derived electrical lengths, widths and feed point locations versus electrical thicknesses of all antenna elements listed in Tables 3.3 and 3.4.

It is seen in this figure while the patch electrical lengths decrease slightly up to a threshold value of approximately h = 0.130 λ_d and then increase, the electrical widths the electrical widths increase up to a threshold value of approximately 0.08 λ_d and then decrease.

Thirdly, the experimentally derived patch length results are compared with those obtained from existing formulae from previous research by plotting the ratios of experimentally derived and calculated lengths as a function of substrate electrical thicknesses of all antenna elements listed in Tables 3.3 and 3.4. A typical plot is given in Figure 3.4 It is seen the experimentally derived resonant lengths are identical to those obtained from equation 3.12 and different to those obtained from other formulae for the substrate

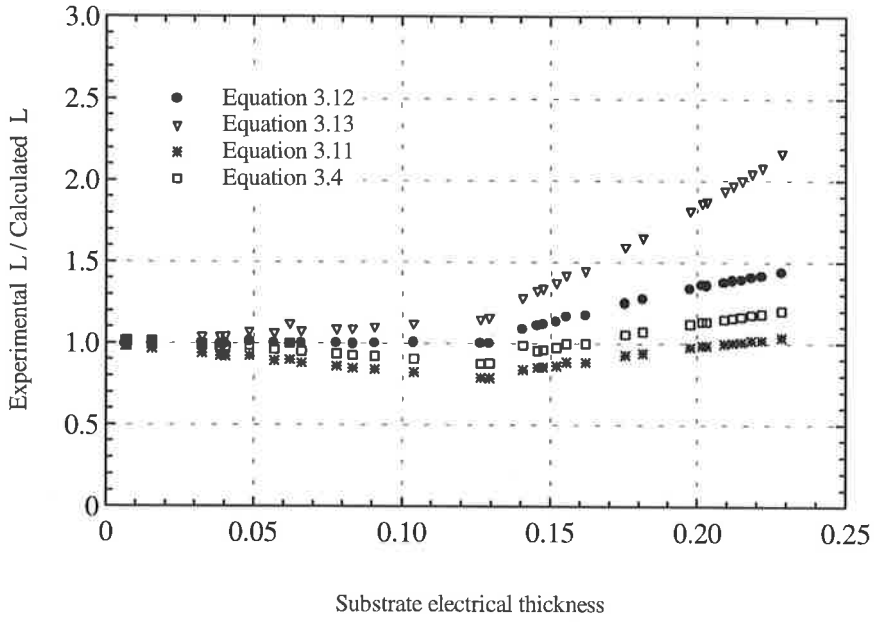

Figure 3. 4: Ratios of experimentally derived element lengths and those obtained from equations 3.4, 3.11, 3.12 and 3.13 versus substrate electrical thicknesses of all antenna elements listed in Tables 3.3 and 3.4.

thickness interval of 130 $\lambda_d \geq$ h. Therefore equation 3.12 can be used to design the resonant lengths of antenna elements with thin substrates at a specified resonant frequency and dielectric substrate material. For thicker substrates, however, these formulae enable the computation of the patch resonant length. Therefore formulae for resonant patch length for thick antenna elements will be empirically derived in the following sections.

Fourthly, because the W of an antenna element can not generally be expressed as a straightforward function of substrate thickness, this relation can be arranged into a design chart by experiment. Use of such a design chart can establish an expression for W that considers the h and ε_r. Therefore, a formula for computing W for antenna elements was devised from the experimental data obtained also from a process of trial- and -error.

The experimentally derived patch widths are compared with those obtained from existing formulae from previous research by plotting the ratios of experimentally derived and calculated widths as a function of substrate electrical thicknesses of all antenna elements listed in Table 3.3 and 3.4 as shown in Figure 3.5. It has been found that antenna elements designed using equations 3.1, 3.2 and 3.3 neither resonated nor attained a minimum return loss or a 50 ohm match. Equations 3.1, 3.2 and 3.3 are therefore not appropriate for designing patch widths for the range of substrate thicknesses considered for this research. It is seen the experimentally derived patch widths are not identical to those obtained from available formulae. Formulae for resonant width for thin and thick antenna elements will be empirically derived in the following sections.

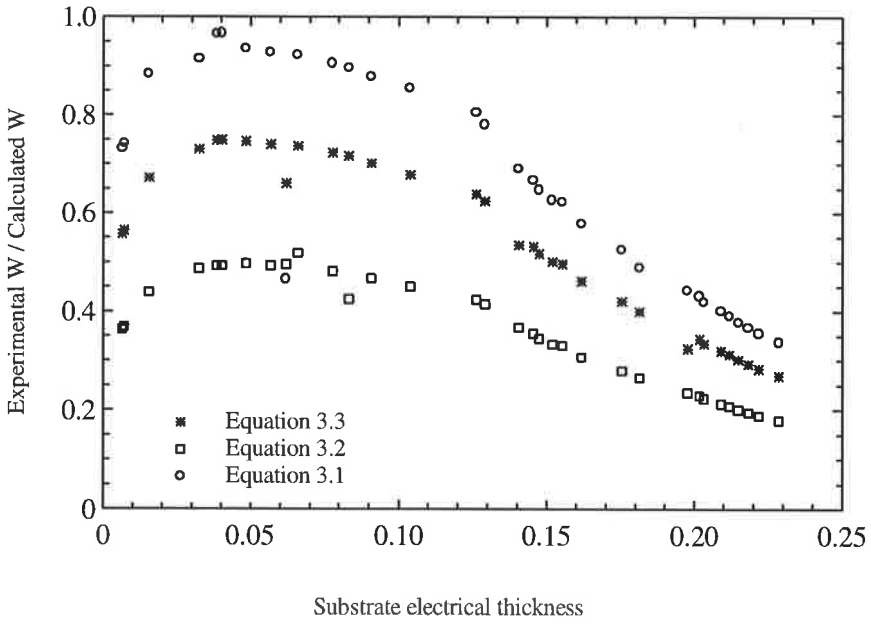

Figure 3.5: Ratios of experimentally derived element widths and those obtained from equations 3.1, 3.2 and 3.3 versus substrate electrical thicknesses of all antenna elements listed in Tables 3.3 and 3.4.

Fifthly, the positioning of the feed probe to obtain a 50 Ω input impedance is also determined by trial because of the lack of a design model for such a feed. Actually, no design data is available on feed location. An approximation for the distance between the coaxial feed probe and the nearest edge of the element which may provide an optimum impedance match is taken as a third of the resonant length for thin antenna elements. However, this approximation enables to determine the feedpoint locations of antenna elements with thicker substrates. Feed point locations as a function of substrate electrical thicknesses of all antenna elements listed in Tables 3.3 and 3.4 are shown in Figure 3.3.

3.5 Physical Properties of Thin Antenna Elements

3.5.1 Element Width

A formula for computing the patch width of rectangular antenna elements has been developed using the experimentally derived W data plotted in Figure 3.6 against substrate electrical thickness. By analysing the dependence of the curve on the relative permittivity and thickness of the substrates and the resonant the following closed-form formula was empirically derived to fit this curve [79, 80].

$$W = \sqrt{h\lambda_d}\left[\ln\left(\frac{\lambda_d}{h}\right) - 1\right] \tag{3.14}$$

This formula allows the designer to predict reliably and quickly the width of a rectangular microstrip antenna element at a specified resonant frequency and dielectric substrate material.

3.5.2 Element Length

The comparative study, using experimental results, confirmed that the formula based on TLM (3.12) best predict the resonant lengths of antenna elements with thin substrate.

3.5.3 Feed Point Location

An alternative empirical approximation can also be used to predict the feed point location [79]

$$a = \frac{L}{2\sqrt{\varepsilon_{eL}}} \tag{3.15}$$

where ε_{eL} is the effective permittivity as a function of the patch length. It can be calculated from (2.10) or (3.8) by replacing W with L. This formula follows the trend of the experimental data plotted in Figure 3.2.

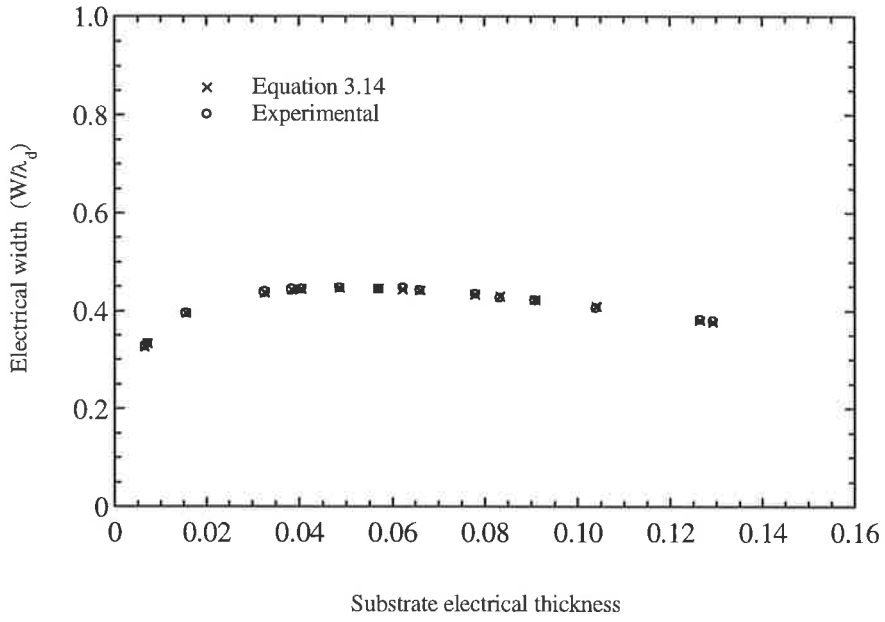

Figure 3.6: Experimentally derived electrical patch widths and those obtained from equation 3.14 versus substrate electrical thicknesses of all antenna elements listed in Table 3.3.

3.6 Physical Properties of Thick Antenna Elements

The equation 3.12 which is based on the TLM as presented in Section 3.2.2 was used successfully to predict the resonant length for a desired resonant frequency of patches with thin substrates. However, it was observed that antenna elements designed using equations 3.4, 3.11 and 3.13 ceased resonating when $h \geq 0.0815\ \lambda_o$. Since no data or formulae exist for calculating the dimensions of antenna elements with thick substrates, the experimental data plotted in

Figure 3.3 have been taken as a basis for developing formulae to calculate the dimensions of such antenna elements.

3.6.1 Element Length

The differences between the L values obtained from equations 3.11 and 3.13 and experimental results of the antenna elements given in Tables 3.2 and 3.3 are shown in Figure 3.2 as a function of wavelength in the dielectric substrate of these elements. This figure also indicates that the resonant lengths of antenna elements with thick substrates are slightly larger then $\lambda_d/2$. A new formula for patch resonant length was derived using Figure 3.7, by analysing the shape and slope of the length curve. By changing the terms within an empirical formula, the outcome was plotted until the length curve fitted that recorded from the experimental data. The resulting formula is [78]:

$$L = \frac{\pi}{\varepsilon_r}\sqrt{h\lambda_d} \tag{3.16}$$

This formula may be used to calculate the length of antenna elements at resonance with thick substrates satisfying the criterion $0.130 \leq \lambda_d$, equivalent to $0.0815 \leq h/\lambda_o$.

3.6.2 Element Width

A formula for patch width was derived using Figure 3.7 focusing on the characteristics of the width curve lying in the interval of $h \geq 0.00815\ \lambda_o$ of Figure 3.3 using the same method as outlined in Sections 3.5.1 and 3.6.1. The resulting formula is:

$$W = \frac{\lambda_d \varepsilon_{eL}}{2\pi}\left[\ln\left(\frac{\lambda_d}{h}\right) - 1\right] \tag{3.17}$$

where ε_{eL} is the effective dielectric constant of a microstrip line of width L. It can be calculated by replacing W by L in equation 2.10 or 3.8. The new formula was used to compute the widths of antenna elements with thick substrates.

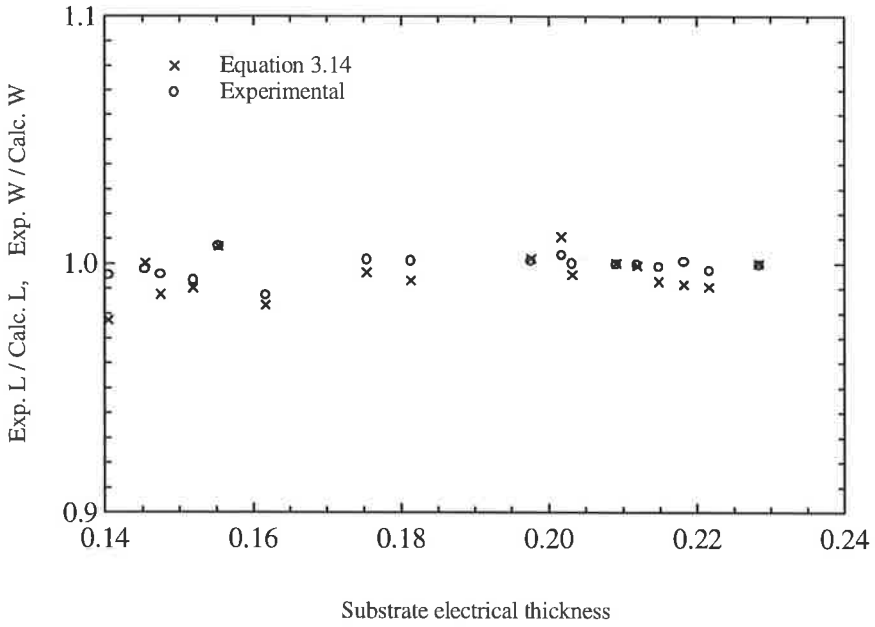

Figure 3.7: Ratios of experimentally derived patch lengths and widths and those obtained from equations 3.16 and 3.17 versus substrate electrical thicknesses of all antenna elements listed in Table 3.4.

Table 3.3 Dimensions and results for antenna elements with *thin substrates*

Patch No	L (mm) Experimental	L (mm) Eq. 3.12	W (mm) Experimental	W (mm) Eq. 3.14	a (mm)	f_r (GHz)	h (mm)	h/λ_d	ε_r
1	12.90	12.98	8.50	8.47	4.15	7.740	0.17	0.0065	2.22
2	11.85	11.89	7.90	7.93	4.10	8.450	0.17	0.0071	2.22
3	25.00	25.08	20.00	20.01	6.83	3.970	0.79	0.0155	2.22
4	11.83	11.83	10.63	10.63	3.90	7.730	0.79	0.0326	2.22
5	10.00	10.09	9.10	9.05	3.75	4.600	1.27	0.0622	10.2
6	18.60	18.64	17.20	17.24	5.94	5.060	1.57	0.0404	2.33
7	19.60	9.68	18.10	18.11	6.27	4.805	1.57	0.0384	2.33
8	13.50	13.51	12.70	12.75	4.25	6.560	1.63	0.0569	2.55
9	16.21	16.00	15.00	14.97	5.28	5.600	1.63	0.0486	2.55
10	14.12	14.12	13.37	13.37	4.75	6.200	2.00	0.0660	2.55
11	12.00	12.00	11.20	11.23	4.25	7.050	2.42	0.0908	2.55
12	14.85	14.85	14.03	14.03	4.60	5.800	2.52	0.0778	2.55
13	16.30	16.36	15.30	15.43	4.70	5.270	3.00	0.0833	2.50
14	12.80	12.75	11.70	11.77	3.40	6.570	3.00	0.1039	2.50
15	10.18	10.16	9.05	9.02	3.70	7.990	3.00	0.1263	2.50
16	15.80	15.77	13.75	13.85	5.82	5.100	4.76	0.1292	2.55

3.6.3 Feed Point Location

For the same reasons as articulated in Section 3.5.3, trial-and-error technique was also used for calculating the feed point locations for thick antenna elements. However, varying the terms within the existing formula did not result in a good fit to the experimental curve shown in Figure 3.3. This figure illustrates the experimentally obtained feed point locations as a function of the substrate electrical thicknesses of antenna elements with various substrate thicknesses. The feed probe must be placed at a suitable point to obtain the best return loss and perfect impedance match (preferably 50 Ω input resistance) [65].

Table 3.4: Dimensions and results for antenna elements with *thick substrates* ($\varepsilon_r = 2.55$)

Patch No	L (mm) Experimental	L (mm) Eq. 3.16	W (mm) Experimental	W (mm) Eq. 3.17	a (mm)	f_r (GHz)	h (mm)	h/λ_d
1	10.80	10.85	7.76	7.77	4.03	8.000	3.30	0.1405
2	12.55	12.64	7.90	7.98	3.00	7.134	4.00	0.1519
3	14.50	14.54	9.87	9.87	3.75	6.070	4.50	0.1454
4	15.20	15.27	10.00	10.13	3.45	5.820	4.76	0.1475
5	14.40	14.59	8.14	8.28	3.10	6.380	4.76	0.1617
6	16.20	16.18	7.90	7.93	3.50	5.990	5.50	0.1754
7	19.70	19.57	12.00	11.92	2.55	4.660	6.26	0.1553
8	23.00	23.01	7.83	7.83	4.25	4.600	8.54	0.2091
9	27.56	27.54	12.56	12.65	3.20	3.580	9.52	0.1814
10	26.20	26.12	9.74	9.64	3.10	3.980	9.52	0.2017
11	26.40	26.38	10.20	10.18	3.55	3.900	9.52	0.1976
12	26.76	26.77	8.83	8.84	3.06	3.980	10.00	0.2119
13	28.35	28.36	7.77	7.77	3.20	3.900	11.00	0.2284
14	31.30	31.40	9.20	9.29	3.00	3.470	12.00	0.2216
15	33.80	33.79	10.30	10.39	3.60	3.200	12.81	0.2182
16	35.00	35.01	12.65	12.71	3.70	2.980	12.81	0.2032
17	34.00	34.05	10.80	10.88	3.70	3.150	12.81	0.2148

3.7 Discussion

The specified, experimentally derived and calculated results are listed in Tables 3.3 and 3.4. The second and third columns of these Tables show respectively the experimentally derived

resonant lengths and those obtained from equations 3.12 and 3.16. The fourth and fifth show respectively the experimentally derived widths and those obtained from equations 3.14 and 3.17. The sixth shows the experimentally derived feed point locations, while the seventh gives the measured resonant frequencies. The physical thicknesses and the electrical thicknesses of the specified substrate materials are listed in the eighth and ninth columns of these tables respectively. And the last column of Table 3.3 shows the relative permittivity of the specified substrate materials.

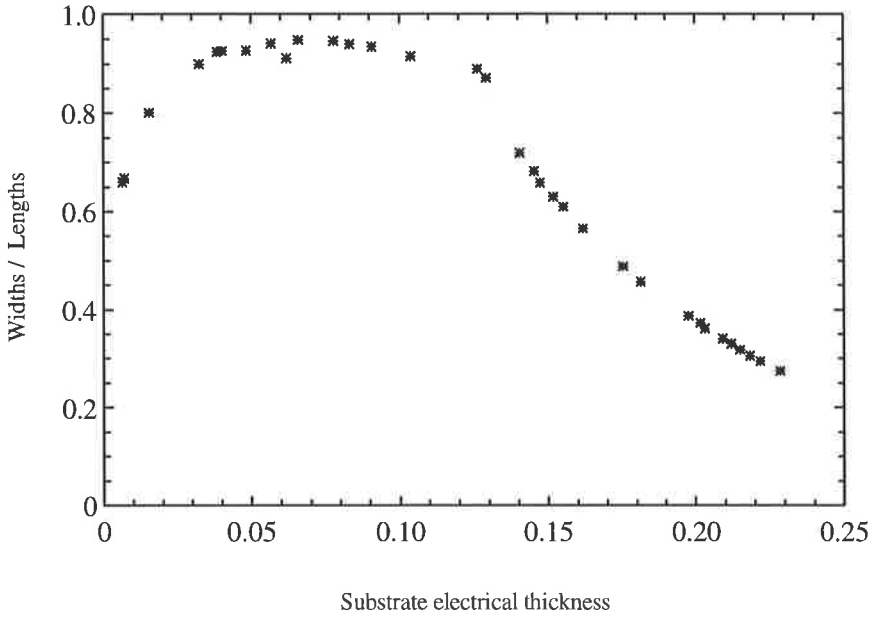

Figure 3.8: Aspect ratios versus substrate electrical thicknesses of all antenna elements listed in Tables 3.3 and 3.4.

The experimentally derived patch lengths are plotted as a function of λ_d and compared with $\lambda_d/2$ values of all antenna elements listed in Tables 3.3 and 3.4 in Figure 3,2. It is seen the resonant length is slightly less than $\lambda_d/2$ within the substrate thickness threshold of $0.130\lambda_d \geq h$ and slightly larger beyond it.

Figure 3.3 illustrates the experimentally obtained data for lengths, widths and feed point locations as a function of the substrate electrical thicknesses for all antenna elements listed in Tables 3.3 and 3.4. Note that the antenna element lengths generally decrease up to approximately the specified substrate thickness threshold, and then increase. The relationship between the increase in

substrate electrical thickness and the increase or decrease in the widths is non-linear. Here an increase in patch length reduces the width, and the width reduction is greater for thicker substrates.

Figure 3.8 illustrates the data for the aspect ration, W/L, as a function of the substrate electrical thicknesses for all antenna elements listed in Tables 3.3 and 3.4. This curve show a non linear behaviour in aspect ratios.

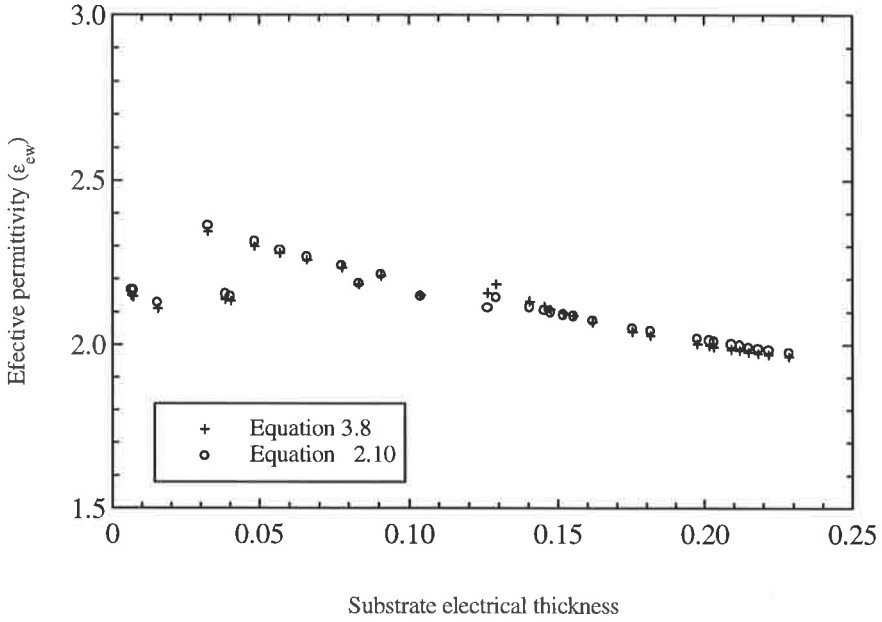

Figure 3.9: Effective permittivities versus substrate electrical thicknesses of all antenna elements listed in Table 3.3 and 3.4.

The ε_{eW} values obtained from equations 2.10 and 3.8 are plotted in Figure 3.9 as a function of the substrate electrical thicknesses of the antenna elements given in Tables 3.3 and 3.4 except that for $\varepsilon_r = 10.2$. Both expressions yield similar results.

3.8 Conclusion

Formulae available in the literature on the design of the physical properties of rectangular microstrip antenna elements have been discussed and their validity assessed. Specifically, it has been demonstrated that the equation based on the TLM (equation 3.12) for computing the resonant lengths for specified frequencies of rectangular microstrip antenna elements, is valid only for elements with substrates thinner than approximately 0.13 λ_d.

It has been found that antenna elements designed using the available formula for calculation of widths failed to resonate when h exceeds 0.002 λ_d. A novel empirical closed-form expression has been derived for computing the widths of antenna elements with thin substrates based on a curve fitting method. The expression (3.14) shows explicitly the dependence of the W on the resonant frequency, the permittivity and thickness of the substrate material.

An expression has been presented that predicts the effective permittivity as a function of patch physical parameters, thickness and constant of the dielectric substrate for rectangular microstrip antenna elements with thin and thick substrates. The technique is adaptable to a wide variety of dielectric materials and is scalable over wide frequency ranges. It is an approach suitable for correcting for relative permittivity effects on the electrical patch dimensions and operational properties.

Using a curve fitting method an approximation was found for estimating feed point locations for antenna elements with thin substrates. This overcomes inadequate design methods for the probe feed.

However, feed point location for antenna elements with thicker substrates should be obtained experimentally, because the lack of formulae for designing them.

All formulae in current use, including the newly devised formulae, fail to accurately predict resonant lengths and widths of rectangular antenna elements with thicker substrates. Therefore, new empirical formulae have been derived using a curve fitting technique, to calculate patch widths and resonant lengths for antenna elements with thick substrate. Although no experimental data is yet available for thick antennae in the research publications to verify formulae 3.16 and 3.17, their correctness is confirmed by the tested performance properties of the antenna elements designed using these formulae.

The formulae derived in this chapter allow rectangular antenna element designers to calculate dimensions for a specified frequency and substrate material. Graphical presentations of the designed dimensions of rectangular microstrip antenna elements with substrates ranging in thickness from 0.0065 λ_d to 0.2284 λ_d have been analysed and discussed.

The contributions described in this chapter are therefore

- The study of the design of physical properties and feeding of antenna elements with various relative permittivity and thickness of substrate materials over a wide frequency band.

- The overview of the published formulae on the design of physical properties.

- The determination of the suitability and threshold of the applicability of these formulae.

- The development of a formula that can determine the physical length of *thin* antenna elements.

- The development of a formula that can calculate the feed point location of *thin* antenna elements.

- The derivation of a formula that can calculate the effective permittivity of antenna elements with *thin* and *thick* substrates.

- The derivation of an empirical formula that can calculate the width of antenna elements with *thin* substrates.

- The derivation of an empirical formula that can calculate the length of antenna elements with *thick* substrates.

- The derivation of an empirical formula that can calculate the width of antenna elements with *thick* substrates.

- The study of the advantages and disadvantages of various feed techniques on *thin* and *thick* substrates.

- The study of the effects of substrate thickness on the patch dimensions.

Chapter 4

The Calculation of the Input Resistance of Rectangular Microstrip Antenna Elements with Various Substrate Thicknesses

4.1 Introduction

The input impedance of an antenna directly affects the efficiency of energy transfer to or from the antenna. It varies according to the antenna properties such as the excitation frequency, the permittivity and thickness of the substrate, patch length and width, and the location of the feed point. Owing to its effects on the efficiency of energy transfer, it should be determined accurately in order to provide a good match between the patch and the feed.

Several analytical and theoretical methods varying in accuracy and computational effort are available in the literature for the calculation of the input impedance for rectangular microstrip antenna elements with substrates ranging in electrical thickness from 0.005 λ_d to 0.166 λ_d [1-16], [30-34], [39, 42, 53], [124-131] where λ_d is the wavelength in the dielectric substrate. The maximum electrical thickness of 0.166 λ_d given above was obtained using a 3.175 mm thick substrate with dielectric constant of 2.33 measured at 10.25 GHz [130]. In this case the electrical thickness is large because the frequency is large, but the physical thickness is small compared with other antennae elements used in this thesis. A summary of the methods is given in

Chapter 2. The most of these methods involve complex analysis of the physical phenomena, often require considerable computation time and do not easily yield the equivalent circuit. As far as it is known, none of the models described in the literature have successfully computed the resonant input resistance of antenna elements with thick substrates, except for the isolated example above. Basically, no design data exists on input impedance in the higher frequency ranges and for antenna elements with electrically thicker substrates. The choice of method to calculate the resonant input resistance is a practical concern, because the existing methods do not give consistent results [125] and are computationally demanding. This indicates that further studies concerning the influences of various parameters and also losses on the resonant input resistance of antenna elements with various thicknesses of the dielectric substrate are still necessary.

As briefly outlined in Chapter 3 the antenna element can be considered as open circuit termination, whereby the incident Transverse Electromagnetic (TEM) wave in the line is not only reflected and radiated at the termination, but generates surface waves in the substrate which must be considered in the design formulae. James et al [133] proposed that the surface wave excitation is not important and can be neglected in thin antennae: that is if $h/\lambda_o > 0.09$ for $\varepsilon_r \approx 2.3$ and $h/\lambda_o > 0.03$ for $\varepsilon_r \approx 10$, where λ_o is the free space wavelength, ε_r the relative permittivity and h the thickness of the substrate material. Note that the antenna elements which are considered as thin in this thesis, are within this range. But as the substrate becomes thicker, more surface wave modes can exist, and more power can be coupled into them. Therefore, the surface wave power must be taken into account when designing antenna elements with thick substrates.

In addition to the losses due to surface waves, microstrip antennae suffer losses due to radiated power, as well as heating of the conductor and the substrate itself. A detailed discussion of these losses is beyond the scope of this chapter. Only directly relevant formulae are considered for the calculation of the resonant input resistance with thick substrates.

This chapter presents three efficient methods for the calculation of the resonant input resistance of rectangular microstrip antenna elements. The *first method* is based on a refinement of the cavity model [34, 131] considering the antenna element in the fundamental modes and is modelled by a simple resonant parallel RLC circuit in series with conductance X_L, which represents the feed probe as shown in Figure 2.2. The RLC element values are related to the physical parameters, such as patch length, width, feed point location, permittivity and thickness of the substrate. Due to the resonant nature of the investigated antenna element, its resonant input resistance is related to the quality factors associated with the system losses. This technique has been successfully used to calculate the resonant input resistance of rectangular antenna elements with thin substrates [131].

A *second method* based on the improved cavity model has been developed for computing the resonant input resistance for antenna elements with thick substrates by considering the antenna in the fundamental

mode, modelled by a simple resonant parallel RLC circuit. It takes into account the resistance due to power loss in surface wave, R_s, the radiation resistance of the patch, R_r, and the resistances due to losses in the conductor, R_c, and dielectric, R_d [132].

A *third method* is an alternative formula for computing the resonant input resistance of antenna elements with thick substrate derived empirically using experimentally derived input resistances data [132].

The development of the formulae is shown in the following sections.

4.2 The Input Impedance of Probe-Fed Antenna Elements

A formula is given for computing the input impedance of a rectangular antenna element excited by coaxial probe using the cavity model and the equivalent resonant circuit [32, 34, 107]. In order to consider the antenna element in the fundamental mode, and to model the frequency dependence of the input impedance, a simple parallel RLC lossy resonant circuit shown in Figure 2.2 has been used. The formula shows explicitly the dependence of the input impedance on the physical parameters, the quality factors associated with antenna losses including radiation from walls, losses in dielectric, and losses in patch conductor. The feed probe, as outlined briefly in Chapter 3, carries the energy from a coaxial line to the antenna element, behaving like a simple inductive reactance in series with the parallel resonant circuit of the antenna element. This causes a clockwise rotation on the Smith chart of the input impedance, as seen at the feed point.

Long et al [12, 108] gives the input impedance in terms of the loaded quality factor, and the inductive reactance of the probe as:

$$Z_{in}(f) = \frac{R_{in}}{X} + jX_L \tag{4.1}$$

with

$$X = 1 - jQ_T\left(\frac{f}{f_r} - \frac{f_r}{f}\right) \tag{4.2}$$

where R_{in} is the input resistance at resonance. Substituting equation 4.2 into 4.1 and separating real and the imaginary parts, one obtains for the input impedance:

$$Z_{in} = R_{in}\left[1+Q_T^2\left(\frac{f}{f_r}-\frac{f_r}{f}\right)\right]^{-2} + j\left\{X_L + R_{in}Q_T\left(\frac{f}{f_r}-\frac{f_r}{f}\right)\left[1+Q_T^2\left(\frac{f}{f_r}-\frac{f_r}{f}\right)\right]^{-2}\right\} \tag{4.3}$$

where f_r is the resonant frequency and f is any frequency around f_r.

The resonant input resistance at a distance "a" from the nearest edge of the patch, which is the same as the resonant resistance of the parallel RLC circuit, assuming perfect standing waves under the patch, is given by [1, 32, 131]:

$$R_{in} = \frac{Q_T}{\omega C_{10}} \tag{4.4}$$

where C_{10} is the capacitance of the TM_{10} mode [28], which can be calculated from equation 2.58 and ω is the radian frequency at resonance.

$$\omega = 2\pi f_r \tag{4.5}$$

The total quality factor associated with antenna element losses is Q_T which includes radiation from the edges, Q_r, the loss due to heating in the conducting element, and the ground plane, Q_c, and the loss due to heating within the dielectric medium, Q_d. The Q_T can be calculated from equation 2.53, Q_d from 2.55 and Q_r was derived from a closed resonator model and the transmission line model as in equation 2.56. In addition to the radiation, dielectric and copper losses, which are represented in equation of Q_T, the cavity suffers losses through surface waves. These waves are an intrinsic feature of the microstrip antennae due to the discontinuity between the dielectric constant of the substrate and that of the semi-infinite medium above the antenna (usually air). For antenna elements satisfying the substrate thickness criteria $h < 0.0815\ \lambda_o$ surface wave excitation is generally not important. For thicker substrates surface waves may have a detrimental effect on microstrip antenna performance, hence they must be considered for the calculations. Note that, the effects of surface waves have not been considered in the calculation of resonant input resistance for thin antenna elements.

The Q_c for copper is calculated from the equation given by [134 - 135]

$$Q_c = 7.86\, h(mm)\, \frac{Z_{ow}}{P_w}\, \sqrt{f_r(GHz)} \tag{4.6}$$

Where Z_{ow} is the impedance of an air filled ($\varepsilon_r = 1$) microstrip line of width W and thickness h. It can be calculated from equations 3.9 or 3.10. The term P_w is given by James et al [134] as for W/h>2.

$$P_w = \frac{P_{w1}}{P_{w2}^2} \tag{4.7}$$

with

$$P_{w1} = 2\pi\left[\frac{W}{h} + \frac{W}{\pi h}\left(0.94 + \frac{W}{2h}\right)^{-1}\right]\left[1 + \frac{h}{W}\right] \tag{4.8}$$

and

$$P_{w2} = \left[\frac{W}{h} + \frac{2}{\pi}\ln\left[2e\pi\left(\frac{W}{2h} + 0.94\right)\right]\right] \tag{4.9}$$

and for W/h<2

$$P_w = \left[1 - \left(\frac{W}{4h}\right)^2\right]\left[1 + \frac{h}{W}\right] \tag{4.10}$$

4.3 The Resonant Input Resistance

Practical formulae based on the cavity model and the equivalent resonant circuits have been developed for computing input resistance at resonance of antenna elements with both thin and thick substrates. A physical explanation of the variation of the input impedance with feed point and the dependence of resonant resistance on the substrate thickness are also delineated.

4.3.1 The Determination of the Resonant Input Resistance for Antenna Elements with Thin Substrates

In this section a formula based on the cavity model and the equivalent resonant circuit has been developed to calculate the resonance input resistance of probe-fed rectangular microstrip antenna elements with substrates satisfying the criteria $h \leq 0.0815\ \lambda_o$ for $2.22 \leq \varepsilon_r \leq 10.2$.

Following [81, 82, 84, 131] equations 2.58, and 4.5 are substituted into 4.4 to obtain a equation for the resonant input resistance

$$R_{in} = \frac{Q_T}{\pi\varepsilon_o\varepsilon_r f_r}\frac{h}{WL}\cos^2\left(\frac{a\pi}{L}\right) \tag{4.11}$$

The Smith chart or magnitude of resistance and reactance on cartesian coordinates of each antenna element listed in Table 4.1 was plotted as a function of frequency as were those shown for example in Figures 4.2 - 4.8. The input resistance was determined for each antenna element at centre (resonant) frequency. The determined results are listed in the second column of Table 4.1, which is a continuation of Table 3.3.

Equation 4.11 was used to calculate these resonant input resistances of all antenna elements listed in Table 4.1.

For thin substrates, the losses associated with the surface waves are negligibly small in comparison with the radiation loss. Hence, these losses have not been taken into consideration.

The 50 Ohm input resistance point may be obtained by varying the distance from the radiating edge of the antenna element to the feed location, a, as shown in Figure 4.8. Note that the resistance of the antenna element goes essentially to zero at the center of the element.

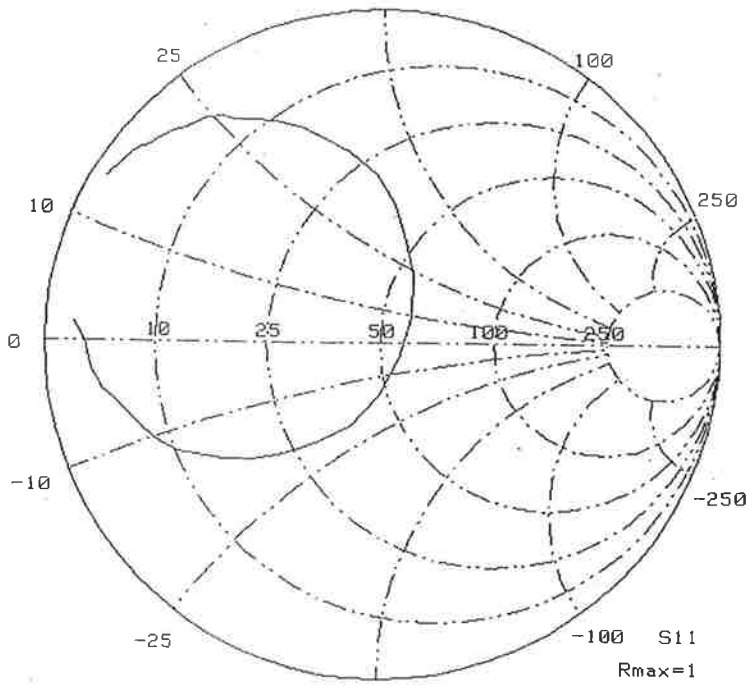

Figure 4.1: Smith chart plot of the impedance of antenna element number 1 in Table 4.1.

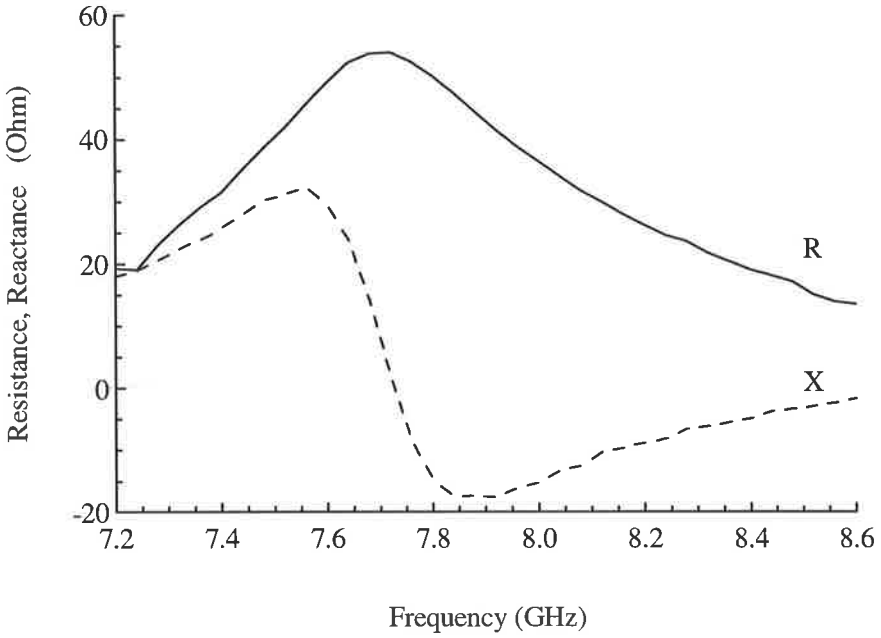

Figure 4.2: Measured variation of resistance and reactance with frequency of antenna element number 4 in Table 4.1.

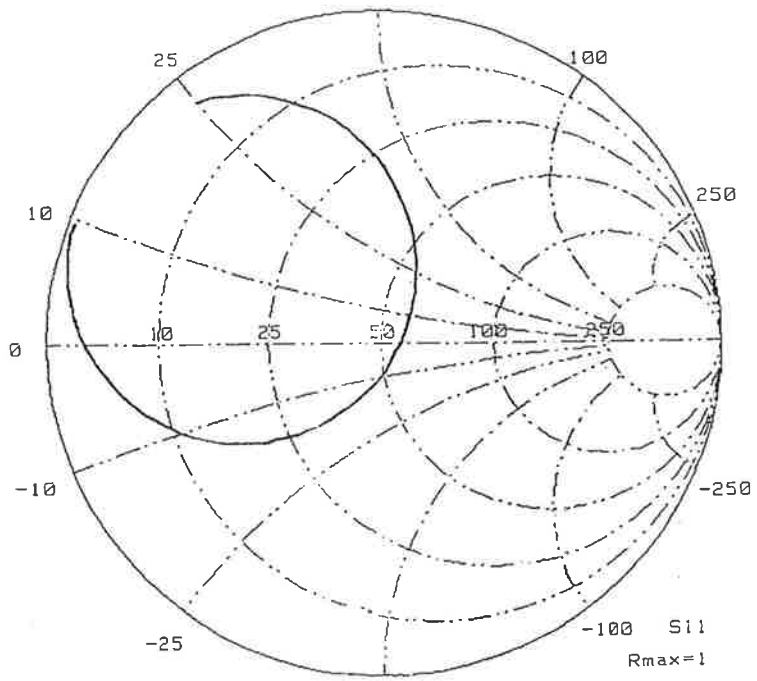

Figure 4.3: Smith chart plot of the impedance of antenna element number 5 in Table 4.1.

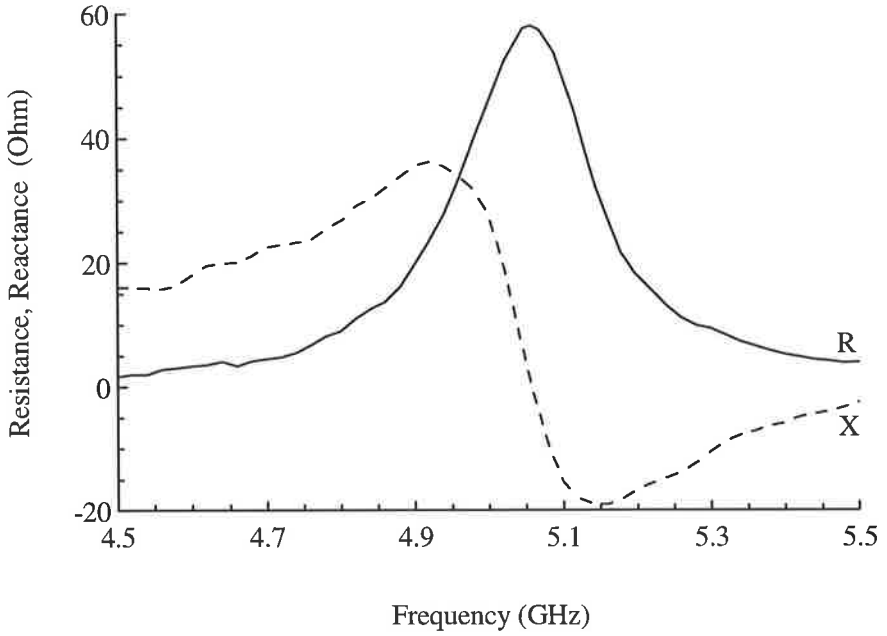

Figure 4.4: Measured variation of resistance and reactance with frequency in an antenna element number 6 in Table 4.1.

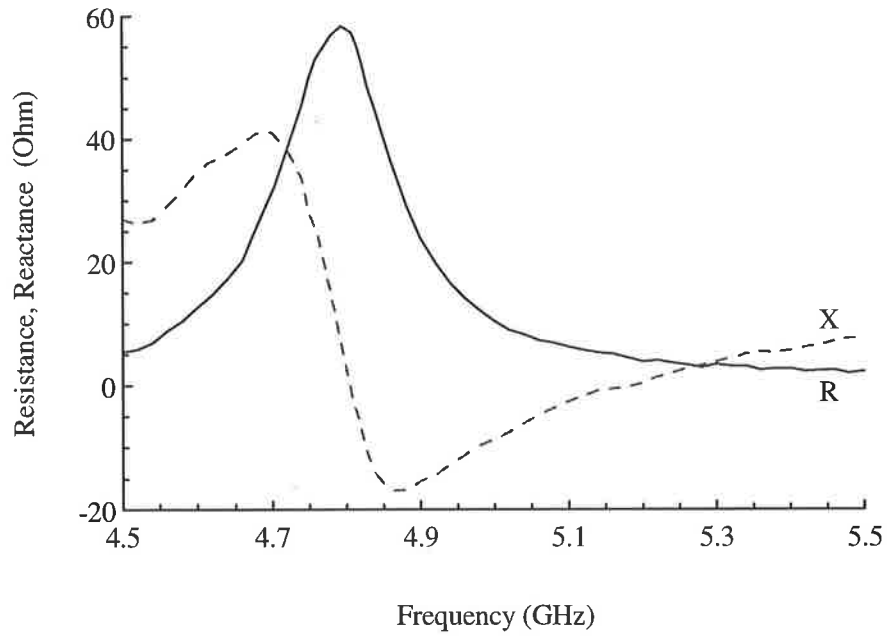

Figure 4.5: Measured variation of resistance and reactance with frequency in an antenna element number 7 in Table 4.1.

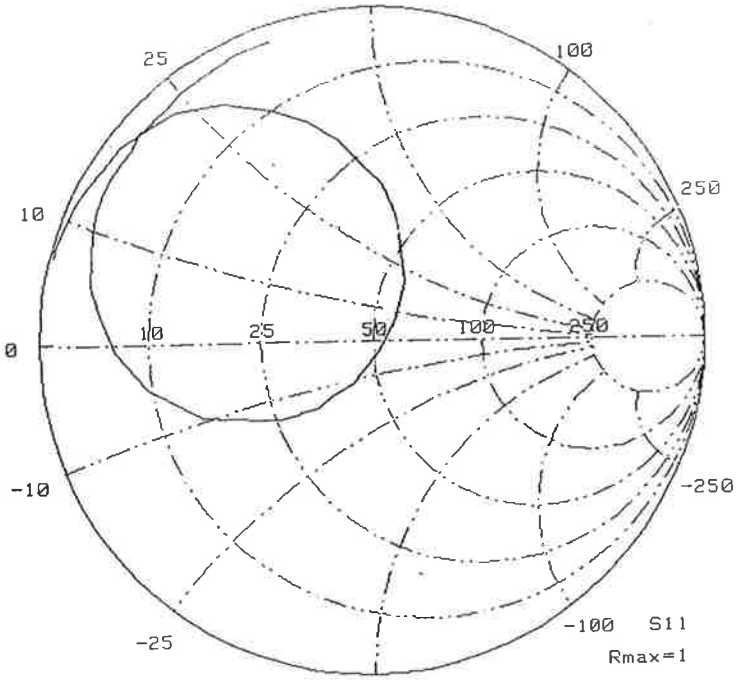

Figure 4.6: Smith chart plot of the impedance of antenna element number 9 in Table 4.1.

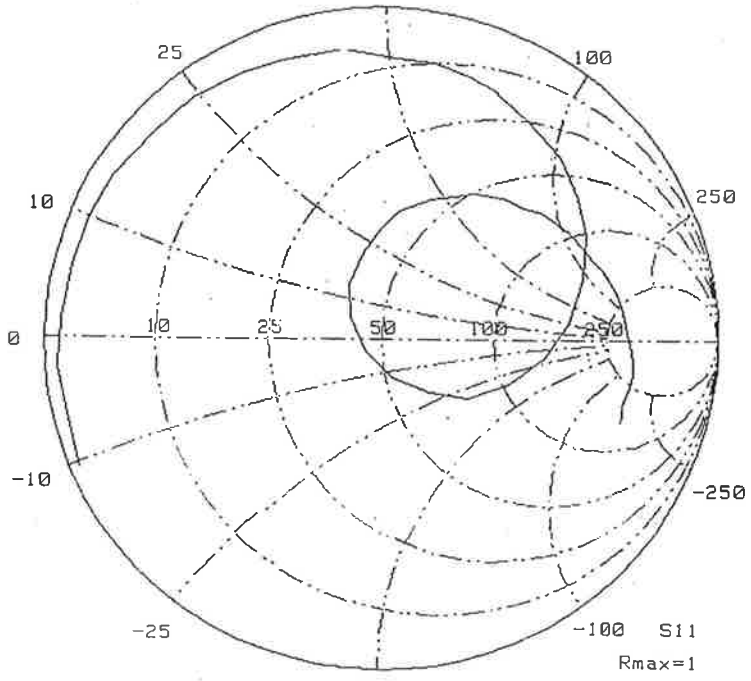

Figure 4.7: Smith chart plot of the impedance of antenna element number 16 in Table 4.1.

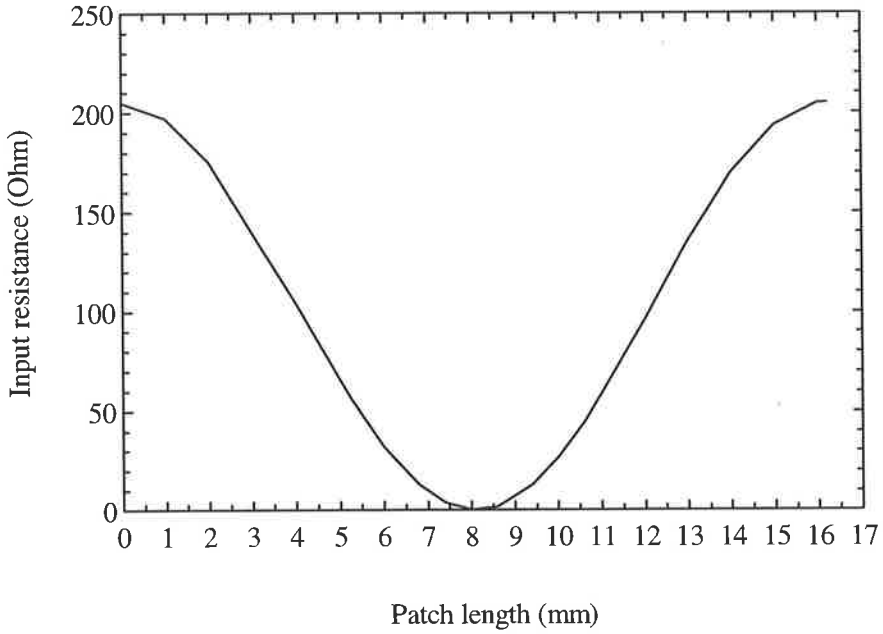

Figure 4.8: The theoretical variation of resonant resistance as a function of feed point on the microstrip antenna element number 9 Table 4.1.

Table 4.1 Measured and calculated input resistances at feeds of antenna elements with *thin substrates*, continuation of Table 3.3

Patch No	Measured R_{in} (Ω)	Present Method R_{in} (Ω)	Error δR_{in} (%)	f_r (GHz)	h (mm)	h/λ_d	ε_r
1	58	58.5	0.86	7.740	0.17	0.0065	2.22
2	44	45.3	2.95	8.450	0.17	0.0071	2.22
3	89	90.2	1.34	3.970	0.79	0.0155	2.22
4	54	53.6	-0.74	7.730	0.79	0.0326	2.55
5	56	55.6	-0.71	4.600	1.27	0.0622	10.2
6	58	58.7	1.20	5.060	1.57	0.0404	2.33
7	58	58.4	0.68	4.805	1.57	0.0384	2.33
8	64	63.9	-0.15	6.560	1.63	0.0569	2.55
9	53	53.8	1.50	5.600	1.63	0.0486	2.55
10	52	51.9	-0.19	6.200	2.00	0.0660	2.55
11	46	45.4	-1.30	7.050	2.42	0.0908	2.55
12	70	70.3	0.42	5.800	2.52	0.0778	2.55
13	86	86.9	1.04	5.270	3.00	0.0833	2.50
14	110	109.5	-0.45	6.270	3.00	0.1039	2.50
15	46	45.8	-0.43	7.990	3.00	0.1263	2.50
16	44	43.8	-0.45	5.100	4.76	0.1292	2.55

4.3.2 The Determination of the Resonant Input Resistance for Antenna Elements with Thick Substrates

As far as it is known, the methods published in the literature for calculating the resonant input resistance do not take into account thick substrates and also surface waves effects. In practice, it is essential to characterise the rectangular microstrip antennae with thick substrates by considering the presence of the surface waves.

A new formula based on the cavity model and the equivalent lossy resonant circuit, as shown in Figure 2.2 has been developed to calculate the resonant input resistance of probe fed rectangular antenna elements with substrates thickness satisfying the criteria $h \geq 0.00815\ \lambda_o$. The antenna elements were considered in their fundamental mode and assumed infinite ground plane. The resonant input resistances of such antennae can be calculated from [85, 132]

$$R_{in} = R_T = R_c + R_d + R_r + R_s \tag{4.12}$$

where R_c is calculated from [1, 28]

$$R_c = 0.00027 \frac{L}{W} Q_r^2 \sqrt{f(GHz)} \tag{4.13}$$

and R_d is given as [1, 28]

$$R_d = 30 \frac{\tan\delta}{\varepsilon_r} \frac{h\lambda_o}{WL} Q_r^2 \tag{4.14}$$

The influence of the fringing fields at the edges of the antenna element with thick substrates is taken into account by replacing the capacitance C_{10} in equation 4.4 by a total capacitance, C_T, so that equation 4.4 can be written as

$$R_r = \frac{Q_r}{2\pi f_r C_T} \tag{4.15}$$

The total static capacitance of the patch in the presence of dielectric substrate can be obtained from [123] as

$$C_T = C_b + 2(C_1 + C_2) \tag{4.16}$$

where C_b is the static capacitance due to the main field just below the patch. This can be calculated from [28, 123, 136]

$$C_b = \varepsilon_o \varepsilon_r \frac{WL}{h} \tag{4.17}$$

where $\varepsilon_o = 8.854\ 10^{-12}$F/m is the permittivity of free space, and C_1 and C_2 represent the static edge fringe capacitances along the patch length and width, respectively. The last two terms of equation 4.16 account for two edge-fringe capacitances along the length sides and two edge-fringe capacitances along the width sides of the patch. Then C_1 may be given by [123]:

$$C_1 = \frac{L}{2}\left[\frac{1}{v_{pw} Z_{cw}}\right] - \frac{1}{2} C_b \tag{4.18}$$

where v_{pw} is the phase velocity of a quasi-TEM mode on a strip line of width W, and can be calculated from equation 3.6. Z_{cw} is the characteristic impedance of a substrate filled strip line of width W. This can be calculated form equation 2.4 or 2.5 depending on the ratio of W/h. Z_{ow} is the characteristic impedance of an air filled ($\varepsilon_r = 1$)strip line of width W, and is obtained from equation 3.9 or 3.10.

Similarly C_2 is given by

$$C_2 = \frac{W}{2}\left[\frac{1}{v_{pL} Z_{cL}}\right] - \frac{1}{2} C_b \tag{4.19}$$

where v_{pL} is the phase velocity of a quasi-TEM mode on a microstrip line of length L [9].

$$v_{pL} = c_o \frac{Z_{cL}}{Z_{oL}} \tag{4.20}$$

and Z_{cL} is the characteristic impedance of a substrate filled microstrip line of length L, and is obtained from equation 3.9 or 3.10 by replacing W by L. Z_{oL} is the characteristic impedance of an

air filled microstrip line of length L, and is calculated from equation 3.9 or 3.10 by replacing W by L and setting $\varepsilon_r = 1$.

The final equation for C_T considered for the computation of the radiation resistance of rectangular antenna elements with thick substrates is obtained by substituting equations 4.18 - 4.20 into 4.16 and by incorporating the effective patch width, W_{ef}, and length, L_{ef}, to take into account the influence of the fringing fields at the edges, and of the dielectric inhomogeneity of the antenna element. The resulting equation is [132]

$$C_T = L_{ef}\frac{Z_{ow}}{c_o Z_{cw}^2} + W_{ef}\frac{Z_{oL}}{c_o Z_{cL}^2} - C_b \tag{4.21}$$

where L_{ef} can be calculated from the following relation [137]:

$$L_{ef} = L + \left(\frac{W_{eq} - W}{2}\right)\left(\frac{\varepsilon_e(W) + 0.300}{\varepsilon_e(W) - 0.258}\right) \tag{4.22}$$

where W_{eq} is the equivalent patch width calculated from the planar waveguide model [9]:

$$W_{eq} = \frac{R_o h}{Z_{cw}\sqrt{\varepsilon_{ew}}} \tag{4.23}$$

Here W_{ef} can be calculated from equation 4.22 by replacing L with W and L_{eq} from 4.23 by replacing W with L.

The existence of a dielectric substrate over a conducting ground plane in a microstrip antenna element can cause the excitation of surface waves along the air-dielectric interface. Such waves propagate without attenuation in a direction parallel to the interface while, in the normal direction, they decay exponentially, without propagation. Fortunately these waves radiate some of their energy as they reach the microstrip discontinuity, and the electromagnetic fields from this radiation add to the space wave fields to contribute to the total radiation fields from the microstrip structure.

The resistance due to surface waves excitation can be derived from the ratio of the power lost to surface waves, P_s, and radiation, P_r, given by James et al [85, 132-134]:

$$S_L = \frac{P_s}{P_r} = \frac{G_s}{G_r} = \frac{\cos^2(k_1 h)\varepsilon_r k_1^2}{\cos^2(k_1 h)\varepsilon_r k_2^2 + k_1^2 k_2 h} \tag{4.24}$$

where k_1 and k_2 are surface wave propagation coefficients determined from [138]

$$\tan(k_1 h) = \varepsilon_r \frac{k_2}{k_1} \tag{4.25}$$

$$k_1^2 + k_2^2 = k_o^2(\varepsilon_r - 1) \tag{4.26}$$

where $k_o = 2\pi f_r / c_o$, is the free space wave number.

When $h/\lambda_o \ll 1$, k_1 can be found from

$$k_1 = \sqrt{\frac{-\varepsilon_r^2 + \varepsilon_r\sqrt{\varepsilon_r^2 + 4k_o^2 h^2(\varepsilon_r - 1)}}{2h^2}} \tag{4.27}$$

which is accurate provided that

$$\tan(k_1 h) \approx k_1 h + \frac{1}{3}(k_1 h)^3 + \cdots \tag{4.28}$$

Combining equations 4.25 and 4.28 one obtains

$$k_2 \approx \frac{k_1}{\varepsilon_r}\left[k_1 h + \frac{1}{3}(k_1 h)^3\right] \tag{4.29}$$

Inverting equation 4.24 and solving for the equivalent resistance of the surface waves, R_s, gives

$$R_s = R_r\left[\frac{k_2^2}{k_1^2} + \frac{k_2 h}{\varepsilon_r \cos^2(k_1 h)}\right] \tag{4.30}$$

Substitution of equation 4.29 into 4.30 yields

$$R_s \approx T_1 R_r \tag{4.31}$$

with

$$T_1 = \left(\frac{k_1 h}{\varepsilon_r}\right)^2 \left[\left(1+\frac{1}{3}k_1^2 h^2\right)^2 + \left(1+\frac{1}{3}k_1^2 h^2\right)\cos^{-2}(k_1 h)\right] \tag{4.32}$$

The resulting equation for the R_T can be given by substituting equation 4.31 into equation 4.12 as

$$R_T = R_c + R_d + R_r(1+T_1) \tag{4.33}$$

The Smith chart of each antenna element listed in Table 4.2 was plotted as a function of frequency as were those shown for example in Figures 4.9 - 4.13. The input resistance was determined for each antenna element at centre frequency (resonant frequency). The determined results are listed in the second column of Table 4.2.

The ratios of the results obtained from equation 4.33 and measured results are plotted as a function of substrate electrical thicknesses of all antenna elements listed in Table 4.2 in Figure 4.14. Note that each point in the figures represents a measured or calculated value of an individual antenna element. Equation 4.33 is found to yield resonant input resistances of antenna elements with substrate thickness within the range of $0.14\ \lambda_d \le h \le 0.2\ \lambda_d$ with good accuracy, however it becomes increasingly inaccurate as the substrate thickness increases. One can obtain a much better estimate of the input resistance if one replaces the relative permittivity of the substrate by dynamic permittivity in equations 4.24 - 4.32. For this case the resulting equation for R_T can be given as

$$R_T = R_c + R_d + R_r(1+T_2) \tag{4.34}$$

with

$$T_2 = \left(\frac{k_{1e} h}{\varepsilon_{dyn}}\right)^2 \left[\left(1+\frac{1}{3}k_{1e}^2 h^2\right)^2 + \left(1+\frac{1}{3}k_{1e}^2 h^2\right)\cos^{-2}(k_{1e} h)\right] \tag{4.35}$$

and

$$k_{le} = \sqrt{\frac{-\varepsilon_{dyn}^2 + \varepsilon_{dyn}\sqrt{\varepsilon_{dyn}^2 + 4k_o^2 h^2 (\varepsilon_{dyn} - 1)}}{2h^2}} \tag{4.36}$$

where ε_{dyn} is the dynamic permittivity given by [123]

$$\varepsilon_{dyn} = \frac{C_T}{C_T(\varepsilon = 1)} \tag{4.37}$$

C (ε_r =1) can be calculated from equation 4.21 by setting $\varepsilon_r = 1$.

The ratios of the results obtained from equation 4.34 and measured results are plotted as a function of substrate electrical thicknesses of all antenna elements listed in Table 4.2 in Figure 4.14. It is evident from these results that equation 4.34 is suitable for the calculation of the resonant input resistances for antenna elements with $h \geq 0.0815\ \lambda_o$ (or $h \geq 0.13\lambda_d$).

4.4 Empirical Formula for Resonant Input Resistance of Thick Antenna Elements

A new empirical formula for computing the resonant input resistance has been developed using the measured resistances data given in second column of Table 4.2. These data are plotted as a function of substrate electrical thicknesses in Figure 4.14. After analysing the dependence of the curve on substrate and the patch parameters a formula was derived to fit this curve. The following new closed-form formula was obtained for the resonant input resistance for the antenna elements [132]

$$R_{in} = R_o \frac{L_{ef}}{\lambda_o\left(\varepsilon_{eL} - \frac{1}{\pi}\varepsilon_{edL}\right)} \frac{1 - \frac{\sin[2k_o(a + \Delta L)]}{2k_o(a + \Delta L)}}{\{1 - \cos[2k_o(a + \Delta L)]\}} \tag{4.38}$$

where ε_{edL} is the effective dynamic permittivity as a function of L given by Mosig et al. [12] as

$$\varepsilon_{edL} = \left(\frac{\lambda_o}{2L}\right)^2 = \left(\frac{c_o}{2f_r L}\right)^2 \tag{4.39}$$

where ΔL is the line extension as a function of patch length and can be calculated from equation 2.11 by replacing W with L.

The results obtained from equation 4.38 agree with results obtained from 4.34 and the measured results as can be seen in the fifth column of Table 4.2.

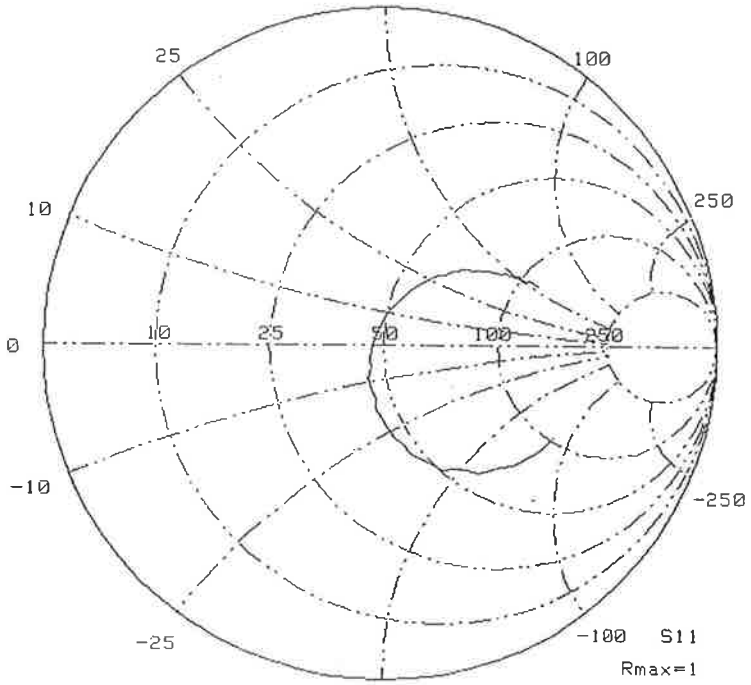

Figure 4.9: Smith chart plot of the impedance of antenna element number 2 in Table 4.2.

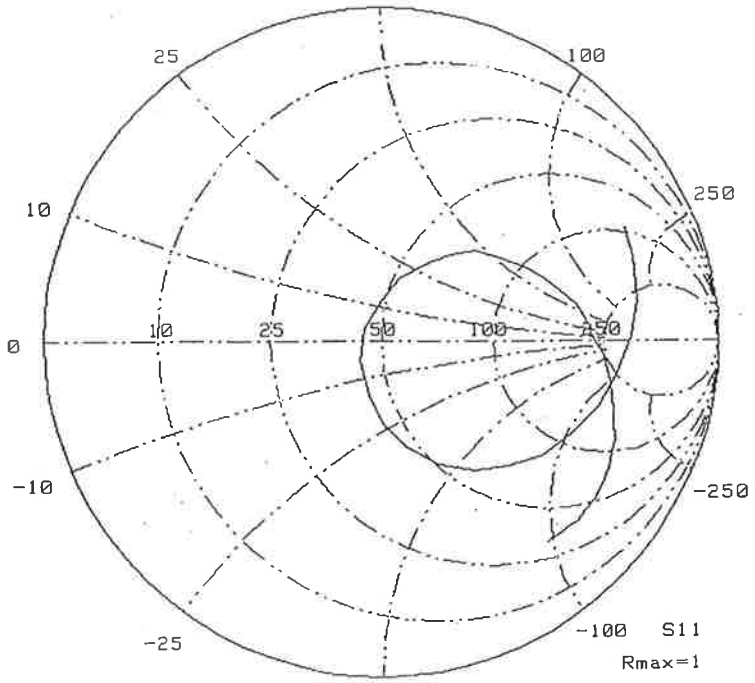

Figure 4.10: Smith chart plot of the impedance of antenna element number 7 in Table 4.2.

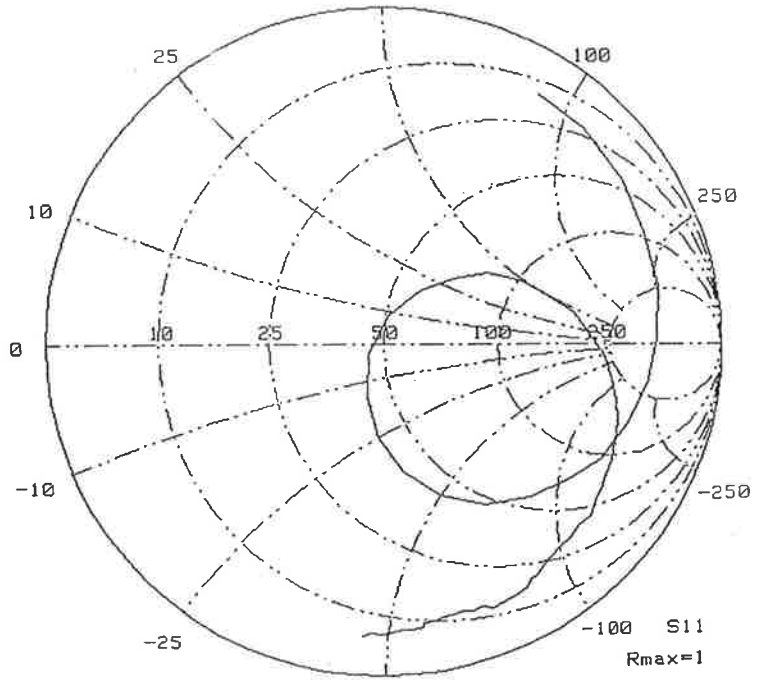

Figure 4.11: Smith chart plot of the impedance of antenna element number 9 in Table 4.2.

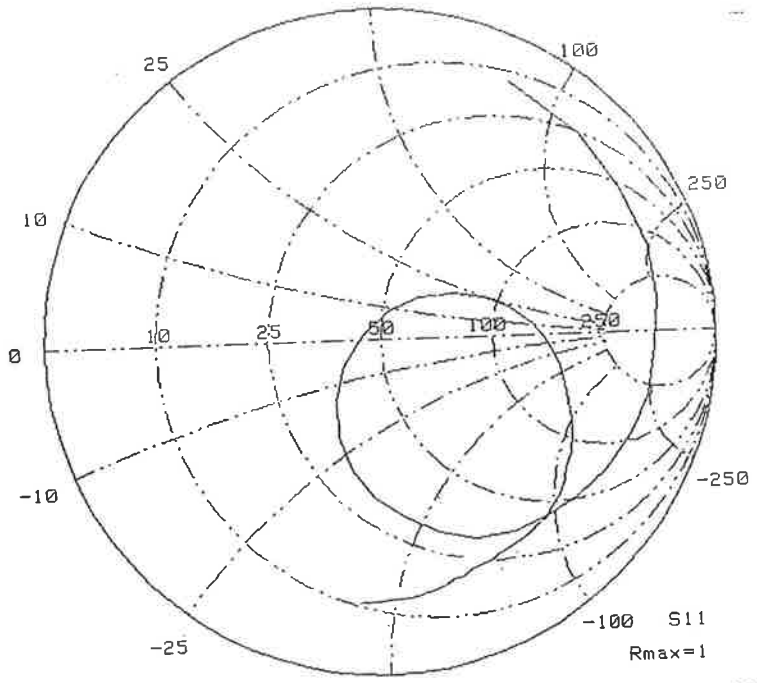

Figure 4.12: Smith chart plot of the impedance of antenna element number 12 in Table 4.2.

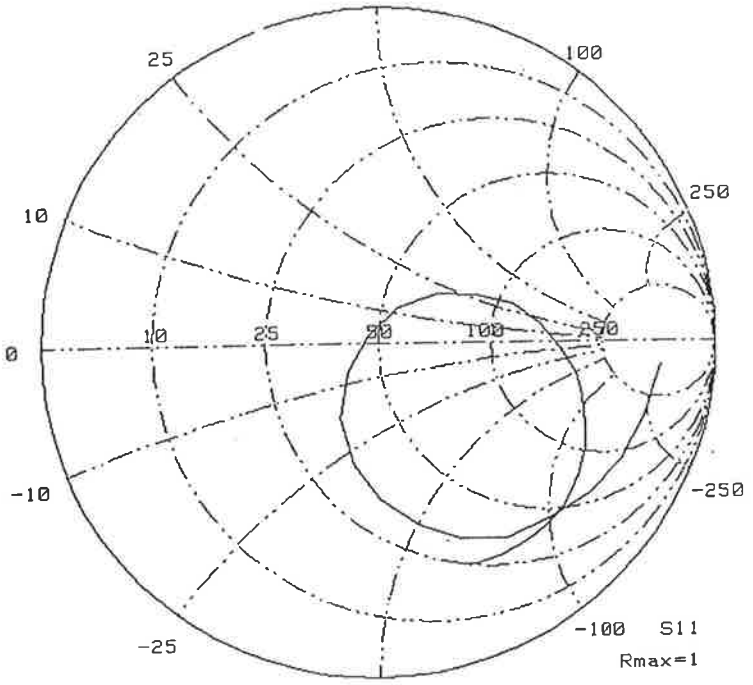

Figure 4.13: Smith chart plot of the impedance of antenna element number 15 in Table 4.2

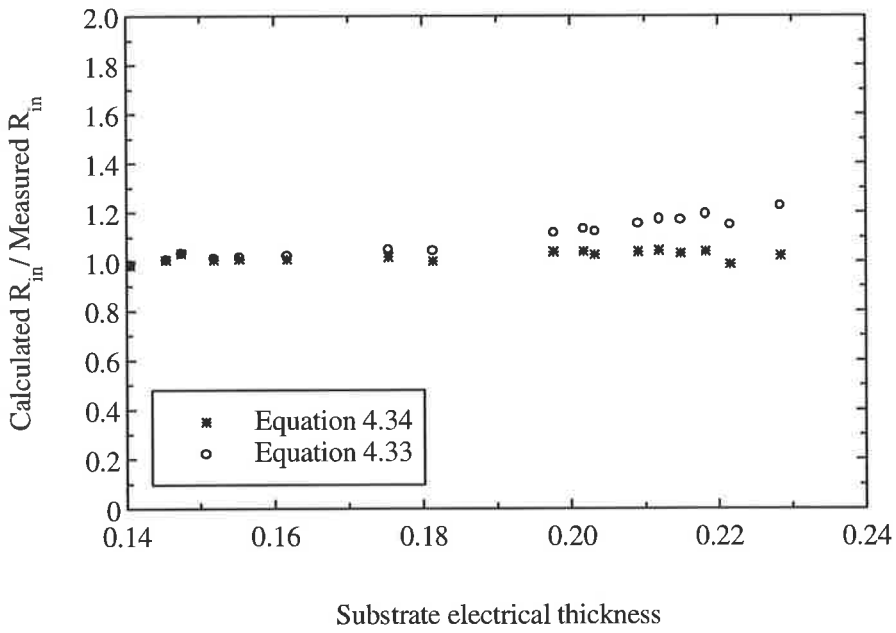

Figure 4.14: Ratios of results obtained form equations 4.33 and 4.34 and measured results respectively versus substrate electrical thicknesses of all antenna elements listed in Table 4.2.

Table 4.2 Measured and calculated input impedances at feeds for antenna elements with *thick substrates*, continuation of Table 3.4.

Patch No	measured R_{in} (Ω)	R_{in} (Ω) Eq. 4.34	Error δR_{in}(%) Eq. 4.34	R_{in} (Ω) Eq. 4.38	f_r (GHz)	h (mm)	h/λ_d
1	47	46.6	-0.8	49.5	8.000	3.30	0.1405
2	46	46.4	0.8	46.7	7.134	4.00	0.1519
3	46	46.4	0.8	48.5	6.070	4.50	0.1454
4	45	46.5	3.3	46.4	5.820	4.76	0.1475
5	46	46.4	0.8	46.5	6.380	4.76	0.1617
6	45	45.7	1.5	46.6	5.990	5.50	0.1754
7	44	45.5	3.4	44.6	4.660	6.26	0.1553
8	46	47.3	2.8	47.7	4.600	8.54	0.2091
9	46	46.0	-0.0	45.0	3.580	9.52	0.1814
10	45	46.5	3.3	45.9	3.980	9.52	0.2017
11	45	46.5	3.3	46.0	3.900	9.52	0.1976
12	46	47.4	3.0	46.4	3.980	10.00	0.2119
13	49	49.3	0.6	47.2	3.900	11.00	0.2284
14	50	48.7	-2.6	46.5	3.470	12.00	0.2216
15	47	48.2	2.5	46.5	3.200	12.81	0.2182
16	46	46.9	1.9	45.8	2.980	12.81	0.2032
17	47	47.9	1.9	46.4	3.150	12.81	0.2148

4.5 Results and Discussions

In this section, numerical results using the method described above are presented and compared with measured input resistances of rectangular antenna elements whose dimensions, feed point locations, substrate thicknesses, permittivity of substrate materials and resonant frequencies are given in Tables 3.3 and 3.4. The antenna elements were fabricated on microwave substrates given in Table 3.2. The input impedances measurements were performed by a HP-8410 network analyser system.

The input impedance ($Z_{in} = R_{in} + jX_{in}$) of each antenna element given in Tables 3.3 and 3.4 was plotted on a Smith chart or magnitude of resistance and reactance on Cartesian coordinates as a function of frequency. The input resistance was then determined for each test antenna element at the first real-axis crossing frequency, at which the reactance (imaginary part) of the input impedance is zero. The measured R_{in} results are listed in the second columns and calculated using equations 4.11

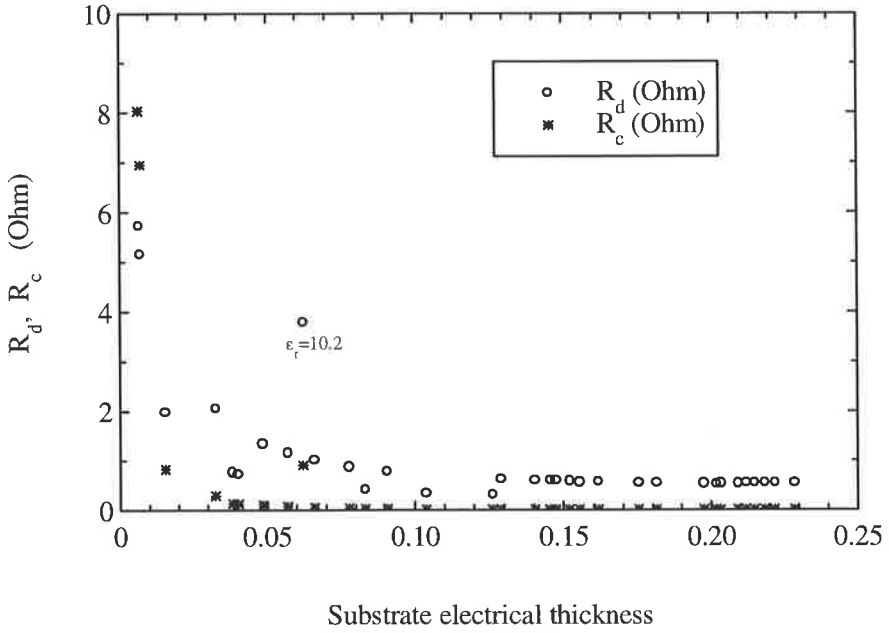

Figure 4.15: Computed equivalence resistances of dielectric and conductor losses versus substrate electrical thicknesses of all antenna elements listed in Tables 4.1 and 4.2.

and 4.34 in the third columns of Tables 4.1 and 4.2 respectively. These tables respectively are a continuation of Tables 3.3 and 3.4 in Chapter 3. The results obtained from the empirical formula are listed in the fifth column of Table 4.2.

A comparison was made by determining the percentage difference δR_{in} between measured R_{in} values and those obtained by above present methods using the following formula

$$\delta R_{in}(\%) = 100\left(1-\frac{R_{inC}}{R_{inM}}\right) \qquad (4.40)$$

Where R_{inC} is the calculated and R_{inM} the measured resonant input resistances. The δR_{in} results are listed in the fourth columns of Table 4.1 and 4.2.

As is evident from the close agreements between the measured and calculated results in Table 4.1, equation 4.11 predicts the resonant input resistances of antenna elements with thin substrates with good accuracy. This equation gives resonant input resistances within ±2.95 percent of the measured values, but the average discrepancy is ±0.9 percent. This is well within the average tolerances of the substrates material parameters.

A comparative study, using measured results given in Table 4.2, confirmed that the derived equation 4.34 predicts R_{in} for antenna elements with thick substrates with accuracy better than ±3.4

percent. Note that the average discrepancy is ±2.0 percent. These small discrepancies can be due to a variety of factors, the tolerances associated with the thickness and permittivity of the substrate material, the error in the fabrication process, the actual patch dimensions not being the same as the designed dimensions, and the tolerance of the network analyser system. Even the best calibration process cannot provide accurate results when transitions and connectors are badly mismatched or lossy.

Figures 4.1 - 4.7 show the measured input impedance loci for the selected examples of thin antenna elements of which physical parameters are given in Table 3.3. The corresponding data for measured resistances are given in the second column of Table 4.1.

Figures 4.9 - 4.13 show the measured input impedance loci for the selected examples of thick antenna elements of which physical parameters are given in Table 3.4. The corresponding data for measured resistances are given in the second column of Table 4.2.

The input impedance loci steadily shift toward the capacitive region of the Smith chart as the thickness of the substrate increases, as is clearly observed in Figures 4.9 - 4.13. This is due to the fact that for a large substrate thickness the probe inductance and C_T constitute a significant part of the overall antenna element input impedance.

The dependence of equivalence resistances of dielectric, R_d, and conductor losses, R_c, on substrate electrical thickness of all antenna elements listed in Tables 4.1 and 4.2 is depicted in Figure 4.15. Both the R_d, and the R_c in this figure decreases rapidly with substrate except for antenna number 6 in Table 4.1 (with $\varepsilon_r = 10.2$).

Figure 4.16 depicts the computed equivalence resistances of radiation as well as the surface wave resistances as a function of substrate electrical thicknesses of all antenna elements listed in Tables 4.1 and 4.2. This figure indicates that the increase of substrate thickness affects not only the equivalent resistance of the surface waves but also the radiation resistance. Furthermore, the substrate thickness has a slight increase effect on the surface wave resistance and a decrease effect on radiation resistance, which affect the efficiency and bandwidth of these antennae as outlined in Chapter 6.

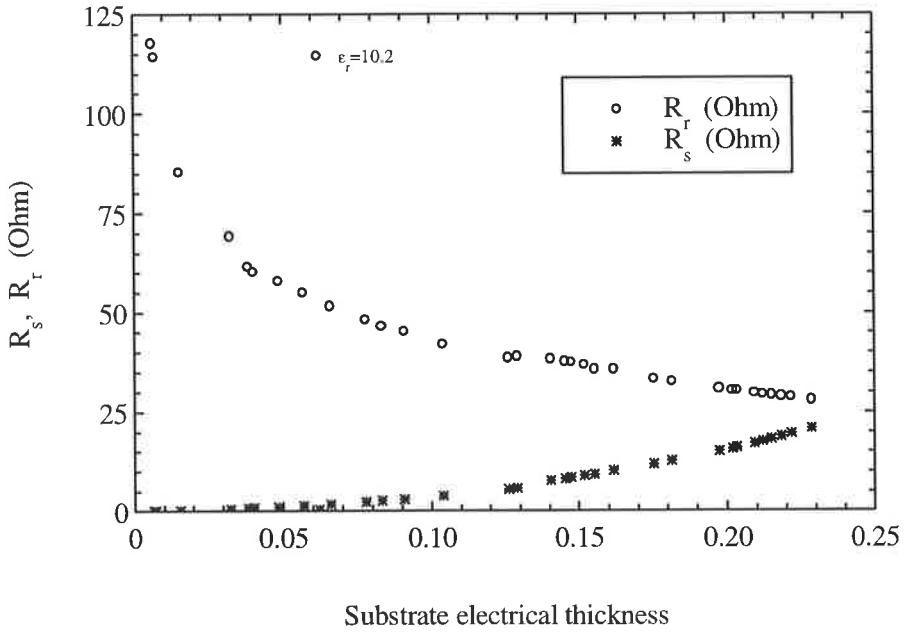

Figure 4.16: Computed equivalence resistances of radiation and surface wave versus substrate electrical thicknesses of all antenna elements listed in Tables 4.1 and 4.2.

4.6 Conclusion

Three methods of calculation of resonant input resistance for rectangular antenna elements with various substrate thicknesses and permittivities have been developed and implemented.

- The *first method* is based on the refinement of the cavity model considering the antenna in the fundamental modes and is modelled by a simple resonant parallel RLC circuit in series with feed probe conductance. It takes into account the physical properties of the antenna and the quality factors associated with the antenna losses. This technique has been successfully used tho calculate the resonant input resistance of antenna elements with thin substrates.

- The *second method* is based on the modified cavity model considering the antenna once again in the fundamental modes and is modelled by a simple resonant parallel RLC circuit in series with feed probe conductance. It takes into account the effective properties of the antenna, the substrate dynamic permittivity, the resistance due to power loss in the surface wave, the radiation resistance and the resistances due to losses in the conductor and dielectric. This technique has

been successfully used tho calculate the resonant input resistance of antenna elements with thick substrates.

- The *third method* is an alternative formula for computing the resonant input resistances of antenna elements with thick substrates, it has been developed using the measured resistance data.

Among the important contributions of the work described in this chapter are:

- A discussion of resonant resistance of rectangular antenna elements with various substrate thicknesses.

- The theoretical development enables rapid computation of input resistance of a probe fed rectangular antenna elements with various substrate thicknesses.

- The development of an accurate and computationally efficient method for the calculation of resonant input resistance of *thin* antenna elements.

- The development of an accurate and computationally efficient method for the calculation of resonant input resistance of *thick* antenna elements.

- The development of an alternative empirical formula for the calculation of resonant input resistance of *thick* antenna elements.

- Experimental measurements are used to test and verify the methods that are developed.

- The effect of the substrate thickness on the input resistance, the dielectric, conductor, radiation and surface wave resistances is delineated.

Note that the equations developed in this chapter allow accurate input resistance prediction for antenna elements on substrates considerably thicker than is possible with those reported in the literature. This is evident from the good agreement between the computed and measured results of input resistance. The equations also provide excellent results for different values of ε_r.

Chapter 5

The Resonant Frequency of Rectangular Microstrip Antenna Elements with Various Substrate Thicknesses

5.1 Introduction

The resonant frequency of microstrip antenna elements must be determined accurately as they have narrow bandwidth and can only operate effectively in the vicinity of the resonant frequency.

Factors for determining the frequency at which resonance occurs include:

- The voltage standing wave ratio (VSWR), referred to the input terminals of the antenna, is at a minimum. This corresponds to a minimum in the magnitude of the reflection coefficient.
- The input impedance, referred to the input terminals, is real ($Z_{in} = R_{in}$), which means the input impedance has no reactive part. Generally, this point is very close to the frequency where the resistance reaches a maximum. Therefore the resonant frequency may also be defined as the point at which the resistance reaches a maximum, independent of the value of reactance.

This chapter is primarily concerned with antenna elements that are matched to their feeds. In this case, the frequency at which the input impedance is real, is equal to the frequency at which the VSWR is at a minimum.

Several analysis techniques have been proposed to determine performance properties of microstrip antenna elements [1 - 20]. These methods have different levels of complexity and require vastly different computational efforts and can generally be divided in three groups: simple classical analysis techniques, full-wave analysis and other numerical techniques. Basically, there is no clear-cut rule as to which one of these is the best to use, the first guideline would be the thickness of the substrate.

As discussed in Chapter 2 exact mathematical formulations in full wave and some other analysis techniques

- involve extensive numerical procedures, resulting in round-off errors and may also need final experimental adjustments to the theoretical results,
- have low level of user confidence when experimental validation is absent,
- are very time-consuming computationally, due to numerical integrations of
- Sommerfeld-type integrals, in either space domain or spectral domain,
- are not easily included in a computer-aided-design system (CAD),
- have high computational cost.

Based on this observation and also details given in Chapter 2 regarding the analysis techniques, classical analysis techniques are used in this chapter, because these can give

- a good understanding of the physical mechanisms that reign these antennae,
- a good intuitive explanation of antenna radiation properties,
- a deep insight into the operation of microstrip antennae,
- are simple and entail less computation,
- are adequate for most engineering purposes.

In this chapter,

- formulae based on the TLM, CM and magnetic wall models, MWM, to determine the resonant frequencies of rectangular microstrip antenna elements have been studied and their validity assessed. Their variations were experimentally verified by analysing a set of new designed antenna elements with substrates satisfying the criteria $h \leq 0.0815\ \lambda_o$ ($0.17\ mm \leq h \leq 4.76\ mm$)

for $2.22 \leq \varepsilon_r \leq 10.2$, where λ_o is the free space wavelength, h the thickness and ε_r the relative permittivity of the dielectric substrate [87].

- three closed-form expressions are presented for computing the resonant frequencies of antenna elements with thicker substrates. They are derived by modifying the TLM, and the CM and by the curve fitting method. The results of these expressions are compared to the resonant frequencies obtained from the return loss plots of antenna elements with substrates satisfying the thickness criterion $h \geq 0.0815\ \lambda_o$, (3.30 mm $\leq h \leq$. 12.81 mm) for $\varepsilon_r = 2.55$ [86, 88].

5.2 Measurement

The configuration of a probe fed rectangular microstrip antenna element is shown in Figure 1.1. The return loss of each antenna element listed in Tables 5.1 and 5.2 was plotted as a function of frequency as were those shown for example in Figures 5.1 - 5.10. The resonant frequency was determined for each antenna element at minimum VSWR. The measured resonant frequency results are listed in the second column of each of these Tables.

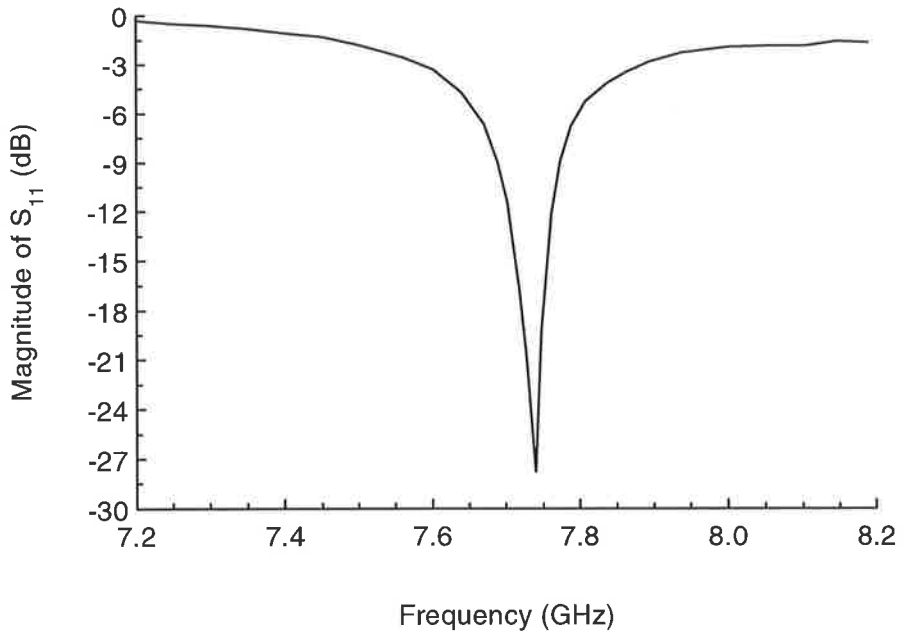

Figure 5.1: Measured return loss as a function of frequency for antenna element number 1 in Tables 3.3 and 5.1

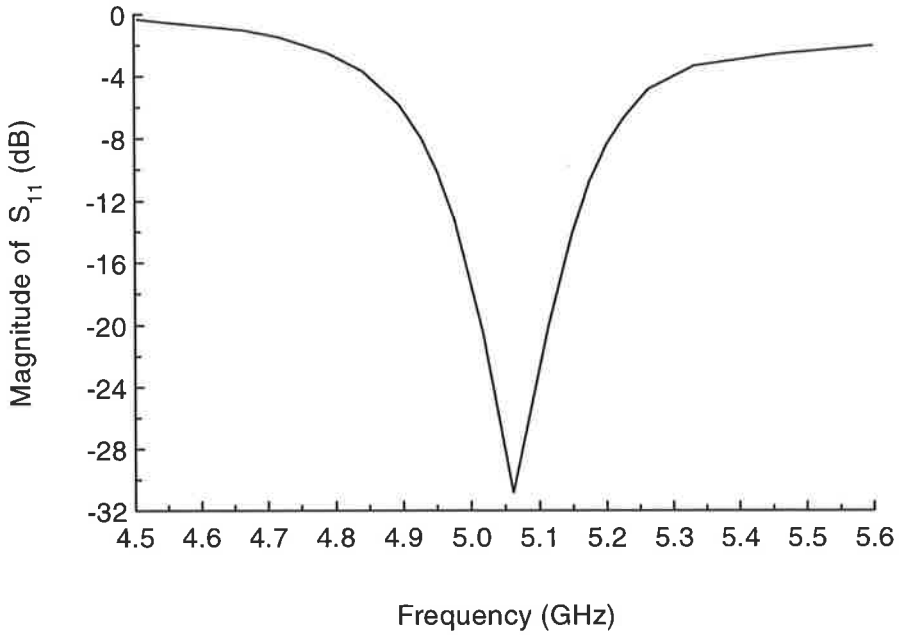

Figure 5.2: Measured return loss as a function of frequency for antenna element number 6 in Tables 3.3 and 5.1.

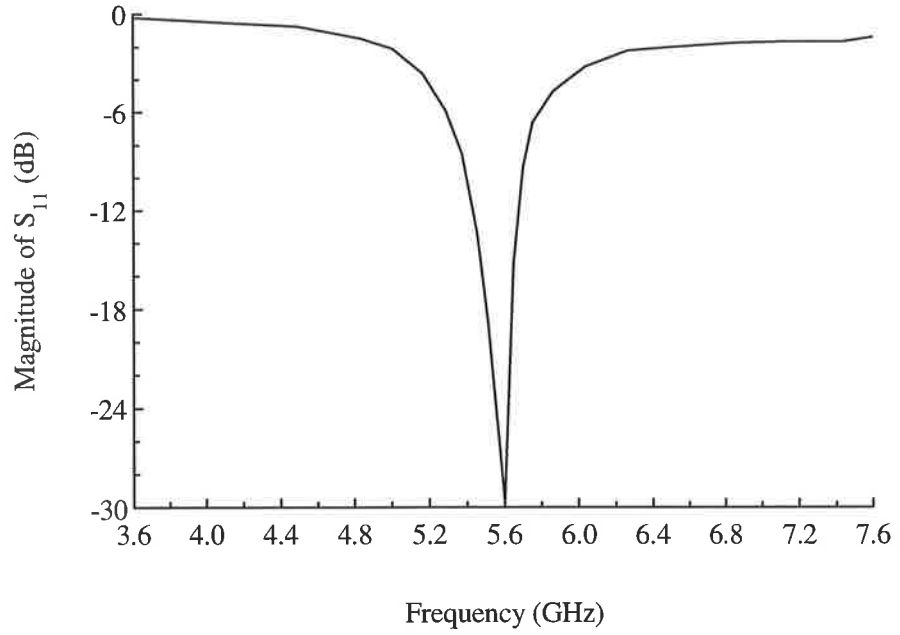

Figure 5.3: Measured return loss as a function of frequency for antenna element number 9 in Tables 3.3 and 5.1

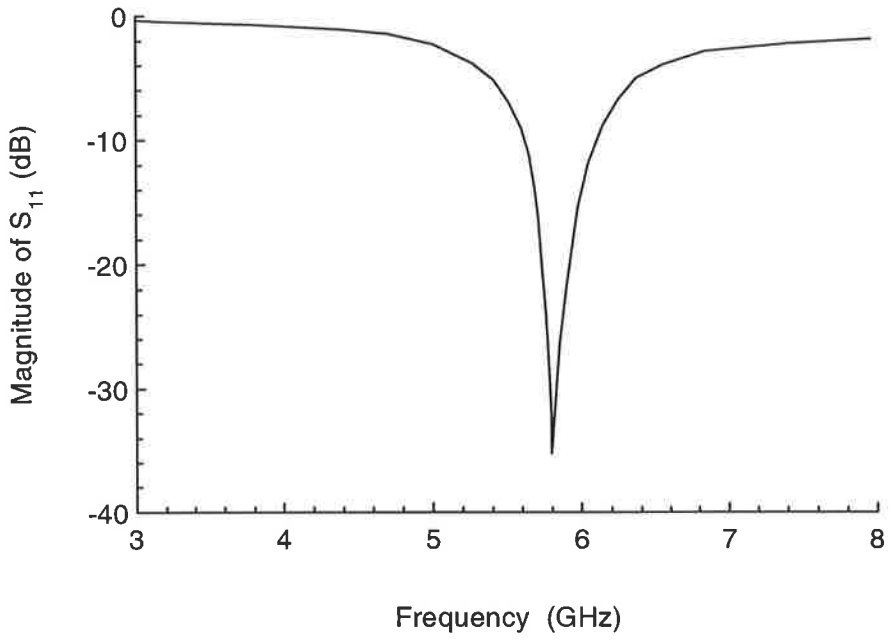

Figure 5.4: Measured return loss as a function of frequency for antenna element number 12 in Tables 3.3 and 5.1

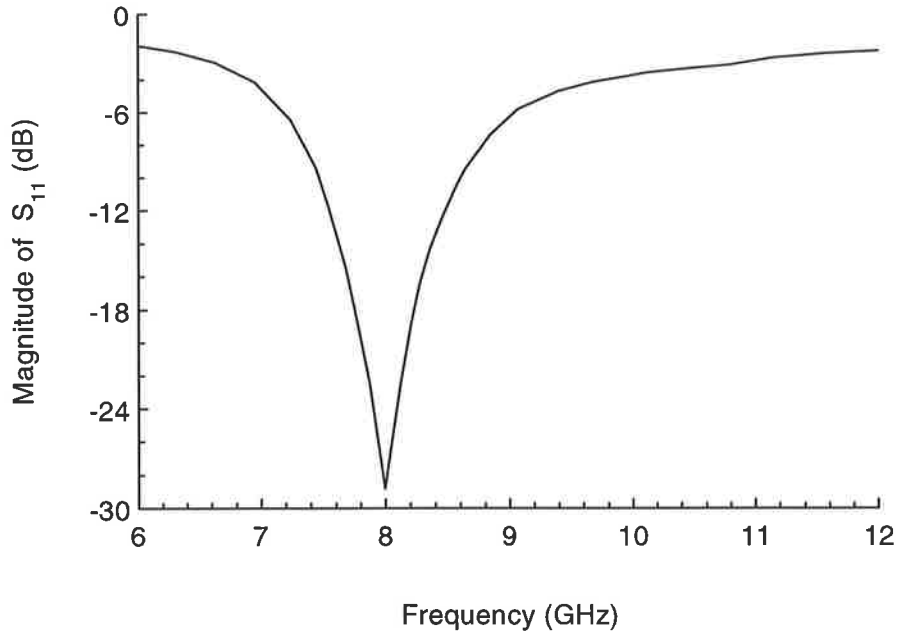

Figure 5.5: Measured return loss as a function of frequency for antenna element number 15 in Tables 3.3 and 5.1.

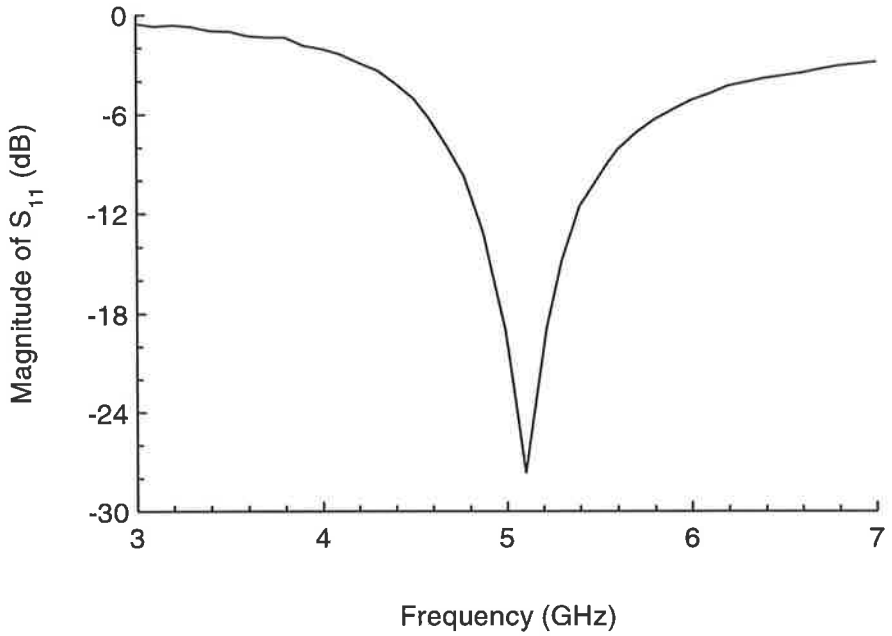

Figure 5.6: Measured return loss as a function of frequency for antenna element number 16 in Tables 3.3 and 5.1

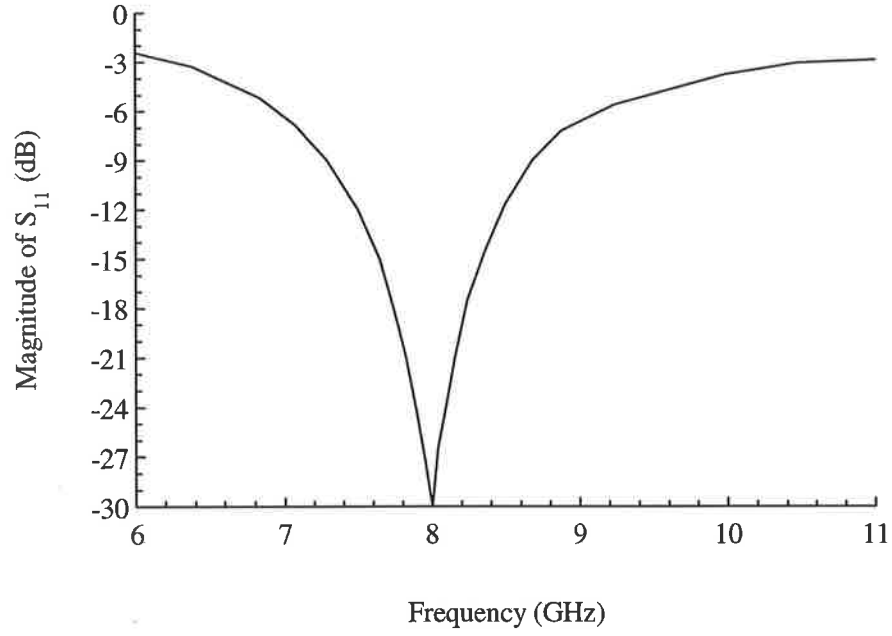

Figure 5.7: Measured return loss as a function of frequency for antenna element number 1 in Tables 3.4 and 5.2

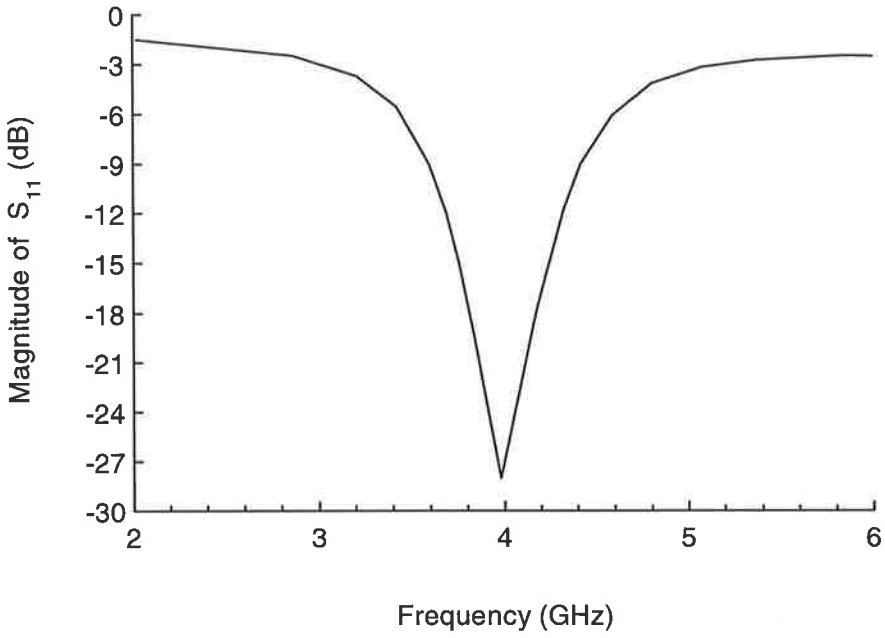

Figure 5.8: Measured return loss as a function of frequency for antenna element number 10 in Tables 3.4 and 5.2

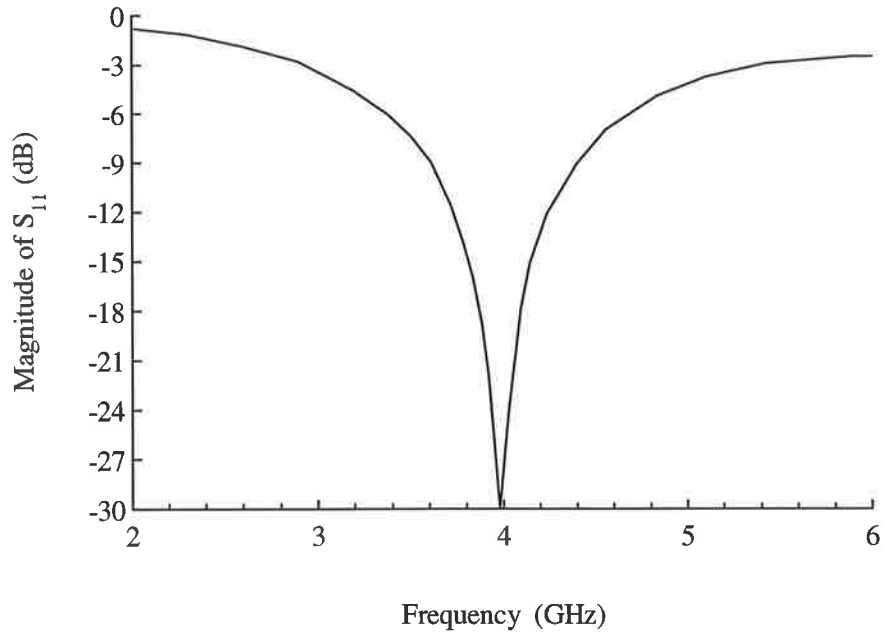

Figure 5.9: Measured return loss as a function of frequency for antenna element number 12 in Tables 3.4 and 5.2.

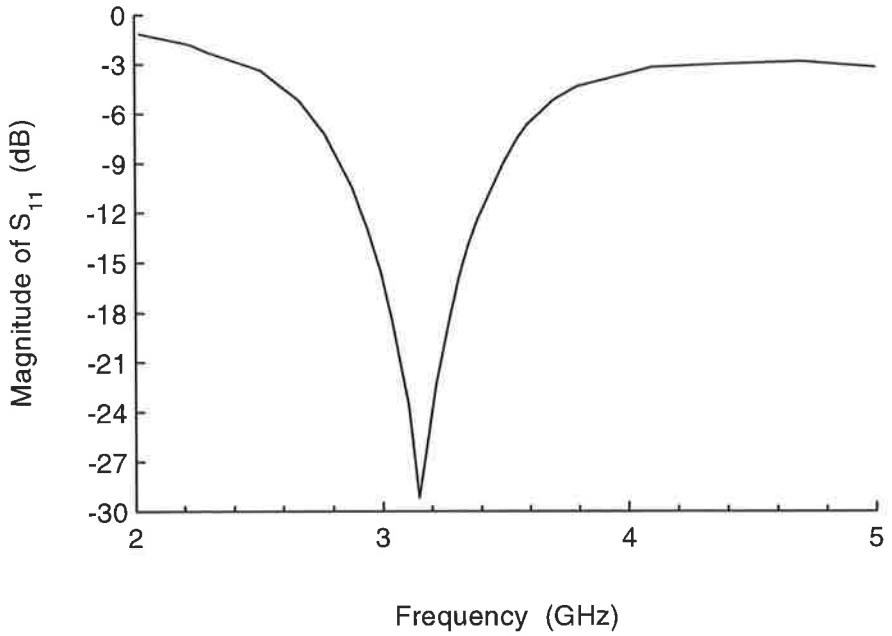

Figure 5.10: Measured return loss as a function of frequency for antenna element number 17 in Tables 3.4 and 5.2

5.3 Formulae for the Resonant Frequency of Thin Antenna Elements

The transmission line [1, 18, 19, 139], the cavity [3, 27, 30, 34, 106, 107] and the magnetic wall models [3, 9] have been used for calculating the resonant frequencies of antenna elements with thin substrates and their variations compared with measurements.

The basic formulae for computing the resonant frequencies are given in the following sections.

5.3.1 Formulae Based on the Transmission Line Model

To calculate the resonant frequency of a rectangular microstrip antenna element, the antenna is regarded as two parallel radiating slots [19] with dimensions element width, W, and substrate thickness, h, having constant field aperture distributions and separated by the length, L, of approximately half the wavelength in the dielectric substrate.

As outlined in Chapters 2 and 3 the electric field at the open end of the patch are distorted by an abrupt termination at the edges, resulting in fringing electric fields. This fringing effect is incorporated into the formula for the resonant frequency.

A formula which calculates the resonant frequencies of rectangular antenna elements with thin substrates was given by Bahl et al [1], Bahl [121 and Derneryd [139] using the approximation given in equation 2.19

$$f_r = \frac{c_o}{2(L + 2\Delta W)\sqrt{\varepsilon_{ew}}} \tag{5.1}$$

where c_o is the velocity of electromagnetic waves in free space and ε_{ew} the effective dielectric constant as obtained from equation 2.10 or equation 3.8. The term ΔW is the line extension and obtained from equation 2.11.

The values resonant frequencies calculated from equation 5.1 agree well with measured values as can be seen in the second and third columns of Table 5.1. Figure 5.11 plots all percentage differences between the calculated and measured results, δf_r, listed in the fourth column of this table as a function of substrate electrical thicknesses of these antenna elements. This formula gives resonant frequencies within ±1.16 % of the measured values, but the average δf_r is ± 0.29%. This is well within the average tolerances of the substrate material of all the antenna elements given in this table. The δf_r results are calculated from the following formula

$$\delta f_r = \left(1 - \frac{f_{rC}}{f_{rM}}\right) 100\% \tag{5.2}$$

where f_{rC} is the calculated and f_{rM} the measured resonant frequencies.

The resonant frequency depends strongly on the patch dimensions, the thickness and the relative permittivity of the substrate material and, also on the edge extension.

5.3.2 Formulae Based on the Cavity Model

The resonant frequency of a rectangular microstrip antenna element may be given by the same formula as for cutoff in the waveguide by considering the region between the patch and the ground

plane as a cavity bounded by dielectric walls on the top and bottom and by a magnetic wall along the side. In other words the resonant frequencies, or modes, are proportional to the patch dimensions. The resonant frequencies, f_{mn}, of a rectangular antenna element of L and W, both comparable to $\lambda_d/2$, where λ_d is the wave length in the dielectric material, are given by assuming that only TM_{mn} modes exist [3, 34, 123]

$$f_{mn} = k_{mn} \frac{c_o}{2\pi\sqrt{\varepsilon_r}} \tag{5.3}$$

where m and n are the mode indicates in the x and y directions respectively, and k_{mn} are resonant wave numbers of the modes.

$$k_{mn} = \sqrt{\left(\frac{m\pi}{L}\right)^2 + \left(\frac{n\pi}{W}\right)^2} \tag{5.4}$$

m, n = 0, 1, 2, 3...

Equation 5.3 is based on the assumption of a perfect magnetic wall surrounding the cavity and it does not take into account the inhomogeneous structure and fringing fields of the antenna.
To calculate the resonant frequencies of rectangular microstrip antenna elements with thin substrates driven at their fundamental TM_{10} modes, equation 5.3 can be written as [17, 140]

$$f_{10} = \frac{c_o}{2L\sqrt{\varepsilon_r}} \tag{5.5}$$

The resonant frequencies obtained from this equation are compared with measured results, as shown in the fifth column of Table 5.1. The results are within 4.4% of the measurements for antenna elements with substrates thinner than approximately 0.04 λ_d and within 16.6 % for thicker antenna elements.

Pozar [14] has written a program called MSAnt which allows the user to analyse a given rectangular microstrip antenna element in terms of its resonant frequency, resonant resistance, bandwidth, and radiation patterns. The program uses a version of the cavity model introduced by Carver et al [32]. The resonant frequency used in MSAnt is found from the complex eigenvalue of the perturbed mode. Using this program the resonant frequencies were calculated for all antenna elements listed in Table 5.1. The percentage differences are given in the sixth column of this table and plotted as a function of substrate electrical thicknesses of these antennae elements in Figure 5.11. The results are within 3.4% of the measurements for antenna elements with substrates thinner than 0.04 λ_d and within 6.5% for thicker antenna elements.

5.3.3 Formulae Based on the Magnetic Wall Model

A formula for the resonant frequency was derived by James et al [9] by modelling the antenna element as a resonator with magnetic conductor walls at the periphery

$$f_{r1} = f_{10} \frac{\varepsilon_r}{(\Delta + 1)\sqrt{\varepsilon_{ew}\varepsilon_{eL}}} \tag{5.6}$$

with

$$\Delta = \frac{h}{L}\left\{\frac{0.164(\varepsilon_r + 1)}{\varepsilon_r^2} + 0.882 + \frac{(\varepsilon_r + 1)}{\pi\varepsilon_r}\left[0.758 + \ln\left(\frac{L}{h} + 1\right)\right]\right\} \tag{5.7}$$

Using equation 5.6 the resonant frequencies were calculated for all antenna elements listed in Table 5.1 and compared with measured results. The percentage differences are shown in the seventh column of this table and plotted as a function of substrate electrical thicknesses of these antenna elements in Figure 5.11. The calculated results are within 4% of the measurements for antenna elements with substrates thinner than 0.066 λ_d and within 8.5 % for thicker antenna elements.

Equations 5.3, 5.6 and the MSAant program are found to yield resonant frequencies of antenna elements with substrates respectively thinner than approximately 0.04 λ_d and 0.066 λ_o with reasonable accuracy. However, they became increasingly inaccurate as the substrate thicknesses increase, as shown in Table 5.1, columns four, five and six. Figure 5.9 plots all δf_r results listed in columns 4, 5, 6 and 7 of Table 5.1 as a function of substrate electrical thicknesses of these antenna elements. It is evident from these results that equation 5.1 is the most suitable formula for the calculation of the resonant frequencies for antenna elements with $h \leq 0.0815\ \lambda_d$.

5.4 Formulae for the Resonant Frequency of Thick Antenna Elements

The resonant frequencies of all antenna elements listed in Table 5.2 have been calculated using the same methods discussed in Section 5.3. Their variations are compared with measurements

Table 5.1 Measured and calculated resonant frequencies of antenna elements with thin substrates, continuation of Tables 3.3 and 4.1

Patch No	Measured f_r (GHz)	Calculated f_r (GHz) Eq. 5.1	Error δf_r (%) Eq. 5.1	Error δf_r (%) Eq. 5.5	Error δf_r (%) MSAnt) [14]	Error δf_r (%) Eq. 5.6	h (mm)	h/λ_d
1	7.740	7.791	0.65	0.82	-1.53	-0.03	0.17	0.0065
2	8.450	8.478	0.33	0.42	-1.90	-0.40	0.17	0.0071
3	3.970	3.982	0.32	1.43	-2.31	-0.95	0.79	0.0155
4	7.730	7.732	0.03	2.72	-3.40	-1.99	0.79	0.0326
5	4.600	4.640	0.86	2.10	-6.08	-3.23	1.27	0.0622
6	5.060	5.069	0.17	4.41	-3.16	-2.41	1.57	0.0404
7	4.805	4.823	0.37	4.34	-2.98	-2.10	1.57	0.0384
8	6.560	6.566	0.09	6.06	-3.93	-3.29	1.63	0.0569
9	5.600	5.601	-1.16	3.47	-3.78	-4.00	1.63	0.0486
10	6.200	6.200	0.00	7.29	-4.20	-3.91	2.00	0.0660
11	7.050	7.052	0.02	11.03	-4.92	-5.53	2.42	0.0908
12	5.800	5.801	0.00	9.06	-4.51	-4.65	2.52	0.0778
13	5.270	5.286	0.30	10.46	-4.36	-4.80	3.00	0.0833
14	6.570	6.549	-0.32	12.80	-5.63	-6.78	3.00	0.1039
15	7.990	7.981	-0.11	16.63	-6.09	-8.28	3.00	0.1263
16	5.100	5.091	-0.17	16.57	-6.49	-8.54	4.76	0.1292

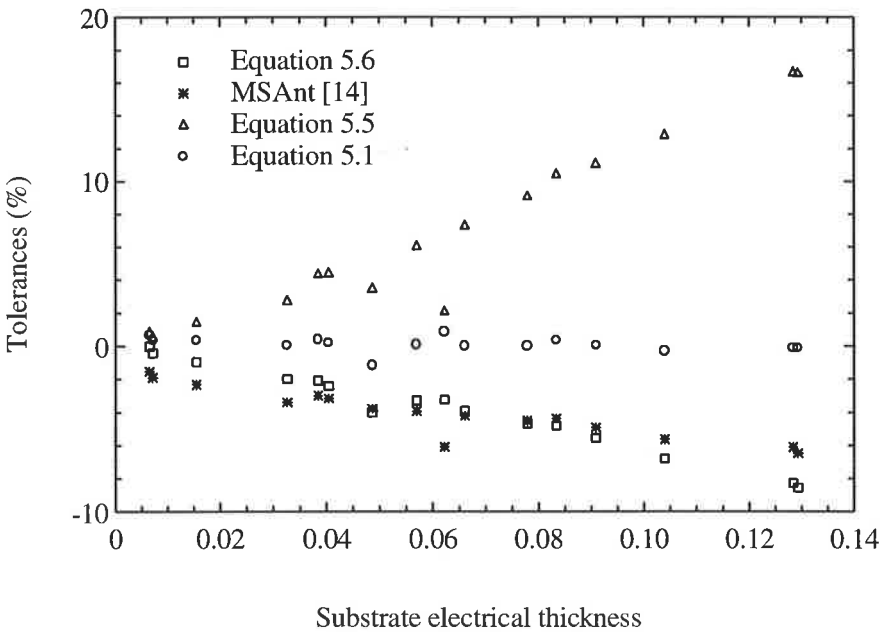

Figure 5.11: Differences between resonant frequencies obtained from equation 5.1, 5.5, 5.6, and MSAnt and measured results versus substrate electrical thicknesses of all antenna elements listed in Table 5.1.

by plotting their percentage errors as a function of substrate electrical thicknesses of these antenna elements as shown in Figure 5.12. As is evident from the large discrepancies between the measured and calculated results the methods are not valid for thicker substrates [88]. Comparison with experimental results shows that equation 5.1 gives error in resonant frequency as high as 24% for antenna elements with substrates in the range of $h \geq 0.0815\ \lambda_o$. Because of the limitation of the two classical analytical models to thin substrate and the involvement of extensive numerical procedures in exact mathematical formulations in the rigorous methods, for computing the resonant frequencies of thicker antenna elements, modifications have been carried out to the classical analytical models. In addition, the lengthy formulations of rigorous methods can also result in round-off errors, and the theoretical result may need final experimental adjustment.

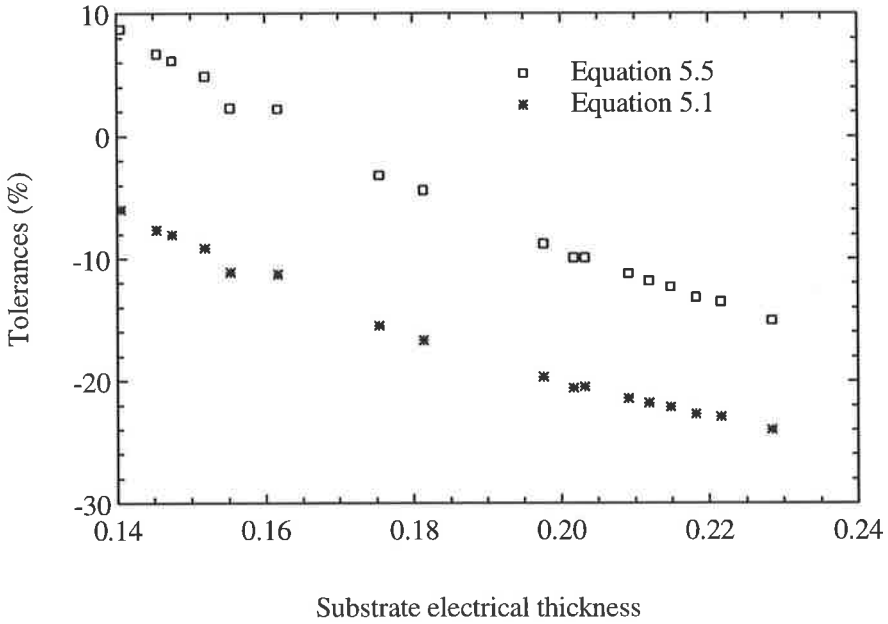

Figure 5. 12 Differences between resonant frequencies obtained from equation 5.1 and 5.5 versus substrate electrical thicknesses of all antenna elements listed in Table 5.2.

5.4.1 Formulae Based on the Transmission line model

Since the TLM and the CM fail to yield an explicit expression for the resonant frequency for this range of substrate thickness, so a correction factor, α, was established by curve fitting. The rationale behind the derivation of α follows. The ratios of the measured results and those obtained

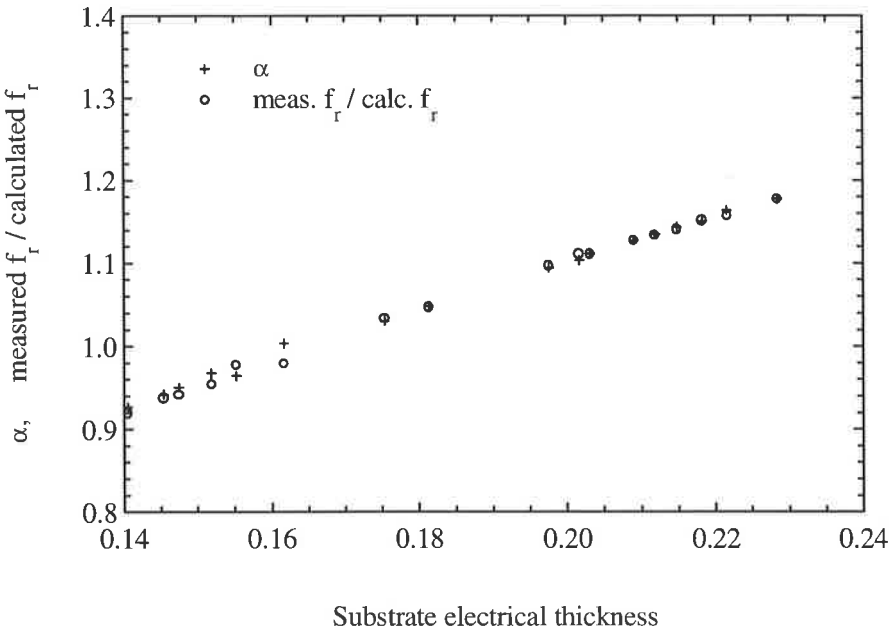

Figure 5.13: Ratios of measured resonant frequency to those obtained from equation 5.1 and the empirically derived correction factors versus substrate electrical thicknesses of all antenna elements listed in Table 5.2.

from equation 5.1 are plotted against the ratios of substrate physical thickness and patch physical length in Figure 5.13. The details for these antenna elements are given in Table 5.2. Note that each data point in the figures represents a measured or calculated value of an individual antenna element. After analysing the dependence of the curve on the substrate and patch parameters a correction factor, α, was derived to fit this curve. The following correction term was obtained [88]

$$\alpha = \frac{h}{L_{ef}}\pi\sqrt{\varepsilon_r} \tag{5.8}$$

where L_{ef} is the effective patch length. According to Garg et al. [137]

$$L_{ef} = L + \left(\frac{W_{eq} - W}{2}\right)\left(\frac{\varepsilon_{ew} + 0.300}{\varepsilon_{ew} - 0.258}\right) \tag{5.9}$$

W_{eq} is the equivalent patch width calculated from the planar waveguide model [9]:

$$W_{eq} = \frac{h\ R_o}{Z_{cw}\sqrt{\varepsilon_{ew}}} \tag{5.10}$$

where $R_o = 120\pi\ \Omega$ is the vacuum resistance and Z_{cw} is the characteristic impedance of a microstrip line determined by the ε_r, h and W of the line. Equations 5.11 and 5.12 describing the characteristic impedance given previously as equations 2.4 and 2.5 are reproduced here for convenience [102], for $W/h \leq 3.3$

$$Z_{cw} = \frac{R_o}{\pi\sqrt{2(\varepsilon_r+1)}}\left[\ln\left(\frac{4h}{W}+\sqrt{\frac{16h^2}{W^2}+2}\right)-\frac{(\varepsilon_r-1)}{(\varepsilon_r+1)}\left(0.2258+\frac{0.1208}{\varepsilon_r}\right)\right] \tag{5.11}$$

and for $W/h \geq 3.3$

$$Z_{cw} = \frac{R_o}{2\sqrt{\varepsilon_r}}\left\{\frac{W}{2h}+0.4413+\frac{0.0823(\varepsilon_r-1)}{\varepsilon_r^2}+\frac{(\varepsilon_r+1)}{\varepsilon_r}\left[0.231+0.1592\ln\left(\frac{W}{2h}+0.94\right)\right]\right\}^{-1} \tag{5.12}$$

A new closed-form expression for the resonant frequency of a rectangular microstrip antenna elements with substrates satisfying the criteria $h \geq 0.0815\ \lambda_o$ and 3.3 mm $\leq h \leq$ 12.81 mm was obtained by including equation 5.8 in 5.1 [88]:

$$f_r = \alpha\ \frac{c_o}{2(L+2\Delta W)\sqrt{\varepsilon_{ew}}} \tag{5.13}$$

The δf_r values are given in the third column of Table 5.2.

5.4.2 Formulae Based on the Cavity Model

Using equation 5.5 the resonant frequencies were calculated for all antenna elements listed Table 5.2. The percentage differences between the measured results and those obtained from this equation are plotted in Figure 5.11 as a function of substrate electrical thicknesses of these antennae. As is seen, the results are within 15% of the measurements.

Since a perfect magnetic wall does not exist for a practical microstrip antenna, the computed resonant frequencies using the cavity model should be corrected in some way. To do this, the ratios of measured the resonant frequencies and those obtained from equation 5.5 were plotted as a

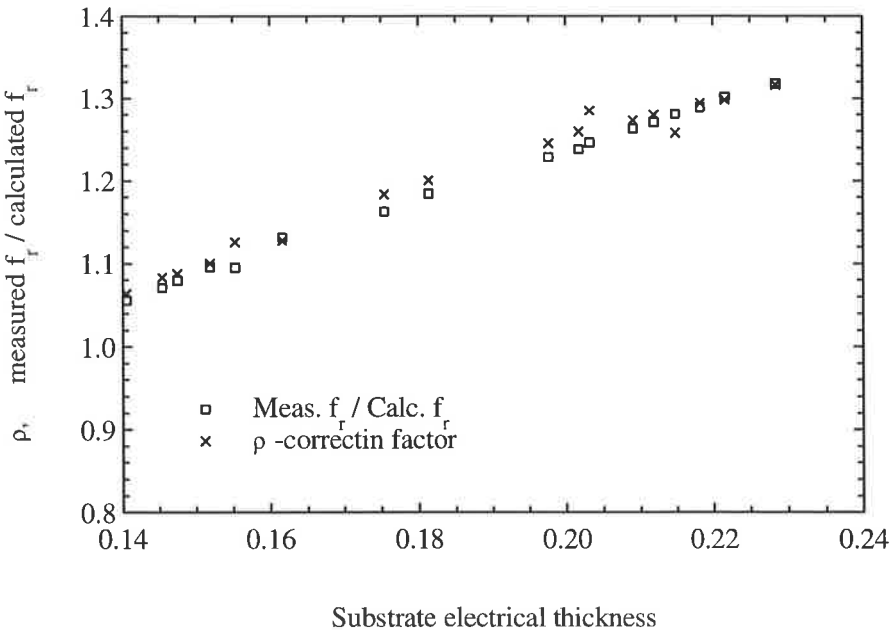

Figure 5.14: Ratios of measured resonant frequency to those obtained from equation 5.5 and the empirically derived correction factors versus substrate electrical thicknesses of all antenna elements listed in Table 5.2.

function of ratios of substrate physical thicknesses and patch physical length of all antenna elements listed in Table 5.2 as is seen in Figure 5.14.

A correction factor, ρ, was devised using Figure 5.14 focusing on the parameters of the antennas using the same method as outlined in Section 5.4.1. The following correction term was obtained

$$\rho = 2\frac{h}{L}\left(\frac{\pi}{\varepsilon_r}\right)^2 \tag{5.14}$$

A new closed-form expression for the resonant frequency of a rectangular microstrip antenna elements with substrates satisfying the criteria $h \geq 0.0815\ \lambda_o$ and 3.3 mm $\leq h \leq$ 12.81 mm was obtained by including expression 5.14 in 5.5:

$$f_r = \rho\ f_{10} = c_o \frac{h}{\sqrt{\varepsilon_r}}\left(\frac{\pi}{L\varepsilon_r}\right)^2 \tag{5.15}$$

The differences between the calculated and measured results are given in the fourth column of Table 5.2.

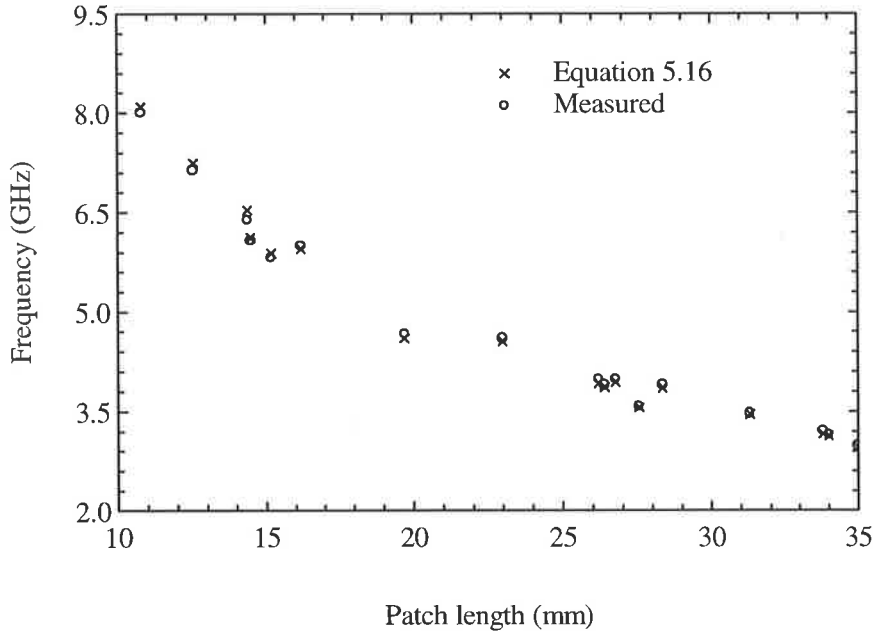

Figure 5.15: Measured resonant frequencies and those obtained from equation 5.16 versus lengths of all antenna elements listed in Table 5.2.

5.4.3 Formula Based on Curve Fitting Technique

A new closed-form expression for computing the resonant frequencies has been developed using the measured resonant frequencies data given in the second column of Table 5.2. These data are plotted as a function of patch physical lengths in Figure 5.13. After analysing the dependence of the curve on substrate and patch parameters an expression was derived to fit this curve. The following new closed-form expression was obtained for the resonant frequency of rectangular microstrip antenna elements with thick substrates [86, 88].

$$f_r = c_o \frac{h}{L^2} \varepsilon_{eL} \frac{2 \ln 2}{\pi} \tag{5.16}$$

where ε_{eL} is the effective permittivity as a function of the patch length. It can be calculated from equation 2.10 or equation 3.8 by replacing W with L. The resonant frequency results obtained from equation 5.16 agree with results obtained from equations 5.13, 5.15 and the measured results as can be seen in the third, fourth and the fifth columns of Table 5.2.

5.5 Discussion of Results

The return loss of each antenna element given in Tables 3.3 and 3.4 was plotted as function of frequency like those shown in Figures 5.1 - 5.10. The resonant frequency was determined for each antenna element at VSWR minimum. The measured f_r results are listed in the second columns and calculated using the above methods in the third columns of Tables 5.1 and 5.2. These tables respectively are a continuation of Tables 3.3 and 3.4 in Chapter 3 and also 4.1 and 4.2 in Chapter 4. A comparison was made by determining the percentage difference δf_r between measured f_r values and those obtained by the methods described above of rectangular antenna elements whose dimensions, feed point locations, thicknesses and relative permittivity of the substrate materials are given in Tables 3.1, 3.3 and 3.4.

As is evident from the close agreement between the measured and calculated results in the third column of Table 5.1 and in Figures 5.11 and 5.16, the equation 5.1 predicts the resonant frequencies of antenna elements satisfying the criteria $h \leq 0.0815\ \lambda_o$ ($h \leq 0.13\ \lambda_d$) for $2.22 \leq \varepsilon_r \leq 10.2$, with very good accuracy while equation 5.5 fails to calculate f_r satisfactorily. As shown in the fourth column of Table 5.1 equation 5.1 gives f_r within ±1.16% of the measured values, but the average discrepancy is ±0.29 %. This is well within the average tolerances of the substrate material parameters. However, comparison with experimental results shows that equation 5.1 gives error in resonant frequency as high as 24% for antenna elements with thicker substrates, as shown in the seventh column of Table 5.2 and Figure 5.16.

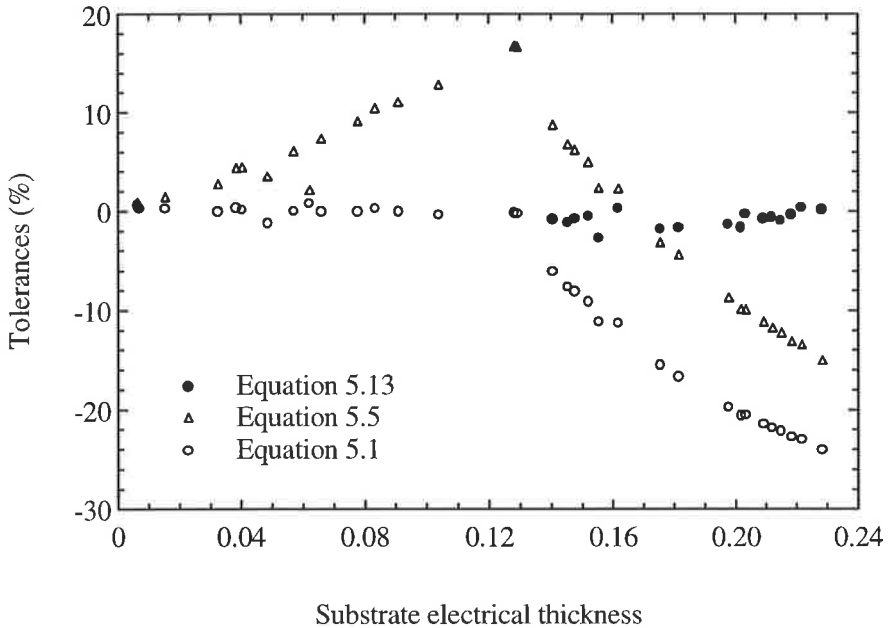

Figure 5.16: Differences between resonant frequencies obtained from equation 5.1, 5.5 and 5.13 versus substrate electrical thicknesses of all antenna elements listed in Tables 5.1 and 5.2.

Table 5.2 Measured and calculated resonant frequencies for antenna elements with thick substrates, continuation of Tables 3.4 and 4.2.

Patch No	Measured f_r (GHz)	Present Method f_r (GHz) Eq. 5.13	Modified TLM Errors δf_r (%) Eq. 5.13	Modified CM Errors δf_r (%) Eq. 5.15	Empirical Errors δf_r (%) Eq. 5.16	TLM Errors δf_r (%) Eq. 5.1	CM Errors δf_r (%) Eq. 5.5	h (mm)	h/λ_d
1	8.000	7.973	-0.76	-0.83	1.11	-6.01	8.71	3.30	0.1405
2	7.134	7.156	-0.42	1.51	1.50	-9.11	4.90	4.00	0.1519
3	6.070	6.031	-1.12	0.54	0.70	-7.63	6.72	4.50	0.1454
4	5.820	5.806	-0.73	0.94	1.04	-8.04	6.18	4.76	0.1475
5	6.380	6.469	0.36	2.60	2.33	-15.49	2.24	4.76	0.1617
6	5.990	5.906	-1.76	-0.23	-0.67	-15.47	-3.20	5.50	0.1754
7	4.660	4.546	-2.68	-1.28	-1.28	-11.12	2.32	6.26	0.1553
8	4.600	4.549	-0.78	0.06	-0.96	-20.64	-11.21	8.54	0.2091
9	3.580	3.532	-1.62	0.16	-0.73	-20.97	-4.79	9.52	0.1814
10	3.980	3.908	-1.68	-0.62	-1.50	-20.54	-9.91	9.52	0.2017
11	3.900	3.849	-1.33	-0.13	-0.94	-19.67	-8.76	9.52	0.1976
12	3.980	3.935	-0.67	0.05	-1.00	-21.81	-11.80	10.00	0.2119
13	3.900	3.857	0.10	0.07	-1.23	-24.00	-15.04	11.00	0.2284
14	3.470	3.452	0.31	0.66	-0.57	-22.92	-13.51	12.00	0.2216
15	3.200	3.160	-0.40	-0.09	-1.25	-22.69	-13.15	12.81	0.2182
16	2.980	2.947	-0.93	0.06	-0.87	-20.47	-9.93	12.81	0.2032
17	3.150	3.123	-0.28	0.31	-0.79	-22.11	-12.29	12.81	0.2148

Figure 5.16 shows the percentage tolerances between the measured resonant frequencies and those obtained from equations 5.1, 5.5 and 5.13 as function of substrate electrical thicknesses of all antenna elements given in Tables 5.1 and 5.2.

As is evident from the close agreement between the measured and calculated results in the third column of Table 5.2 and in Figure 5.16, the equation 5.13 predicts the resonant frequencies of antenna elements satisfying the criteria $h \geq 0.0815\ \lambda_o$ ($h \geq 0.13\ \lambda_d$) with good accuracy. As shown in the fourth column of Table 5.2 equation 5.13 gives f_r within ±2.68 % of the measured values, but the average discrepancy is ±0.9 %. Furthermore, as shown in the fifth and sixth columns of Table 5.2, the average tolerances of equations 5.15 and 5.16 are respectively ± 0.6 % and ± 1 %. These small discrepancies can be due to a variety of factors eg. the tolerances associated with the thickness

and permittivity of the substrate material, the error in the fabrication process, the actual patch dimensions not being the same as the designed dimensions, and the tolerance of the network analyser system. Even the best calibration process cannot provide accurate results when transitions and connectors are badly mismatched or lossy.

5.6 Conclusion

This chapter has verified the applicability of the TLM, CM and the MWM analysis techniques for calculating the resonant frequencies of rectangular microstrip antenna elements with various substrate thicknesses and permittivities. Specifically, it also has demonstrated that the formula based on the TLM for computing the resonant frequencies confines itself to elements with substrates in the thickness range of $h \leq 0.0815\ \lambda_o$. The average difference between the results obtained by TLM and the measured results is ± 0.29 % for antenna elements in this substrate thickness range, Table 5.1, however, it has been found that the applicability of the formula based on the CM is limited to substrate thickness less than approximately $0.04\ \lambda_d$ and the magnetic wall less than $0.066\ \lambda_d$.

The inadequate performance in calculating the resonant frequencies of antenna elements with thicker substrates prompted the introduction of a correction factor to the equation 5.1 or 5.5 derived using a curve fitting technique.

Three new closed-form expressions for calculating the resonant frequency of a rectangular microstrip antenna elements with substrates satisfying the criterion $h \geq 0.0815\ \lambda_o$ and $3.3\ \text{mm} \leq h \leq 12.81\ \text{mm}$ for $\varepsilon_r = 2.55$ have been proposed. They are derived by modifying the TLM, the CM, and by the curve fitting method. The correction factors were derived by means of a curve-fitting method. The accuracy of the proposed expressions have been established by comparing calculated results with measurements for all antenna elements listed in Table 5.2.

The contributions described in this chapter are therefore:

- A discussion of resonant frequency of rectangular antenna elements with various substrate thicknesses and relative permittivities.

- The establishment of threshold of the applicability of the expressions based on the TLM, the CM, and MWM analysis techniques.

- The development of fast and efficient method for computing the resonant frequencies of thin antenna elements.

- The development of three new closed-form expressions for efficiently computing the resonant frequencies of thick antenna elements. These expressions allow accurate resonant frequency prediction for elements considerably thicker than those reported elsewhere.

- The use experimental measurements to test and verify the expressions that are developed.

Chapter 6

The Bandwidth of Rectangular Microstrip Antenna Elements with Various Substrate Thicknesses

6.1 Introduction

The desirable features of classical microstrip antennae are discussed in Chapter 1, as is the fact that narrow intrinsic bandwidth is perhaps the most serious of their limitations. This arises from the fact that the region under the patch is basically a thin resonant cavity with a high quality factor. Despite the benefits and the drawbacks of classical microstrip antennae, they are useful in many applications in civilian and military systems. In fact, small bandwidth, sometimes can be considered as a benefit in some applications. While small bandwidth is useful in some applications where the antenna itself acts as a filter for unwanted frequency components, in many applications, such as in electronic intelligence (including signal intelligence and communication intelligence), electronic support measures, radar, and electronic warfare, an imperative is that the systems have a large bandwidth.

The design of microstrip antenna elements having wide bandwidth is an area of major interest in microstrip antenna technology, particularly in the fields of electronic warfare, communications systems and wideband radars. Over the years, many techniques have been

suggested and implemented to improve the impedance bandwidth of microstrip antennae. Some techniques include:

- physical shaping or alteration of the patch by the use of notches or stubs [2, 3],
- short circuiting of the antenna [141],
- using low-dielectric materials [142] (eg., hard foam with $\varepsilon_r = 1.05$),
- matching structure [143 - 144],
- using a parasitic element both horizontally [145] and vertically [146],
- stacking of elements [2, 9, 148],
- the loading of the patch with diodes [2, 149],
- log-periodic arrays [2, 9],
- microstrip spiral antennae [150],
- using miniaturised microstrip antenna elements [81, 84, 95 - 97],
- using thick patch conductor [151],
- using thicker substrates [86, 89, 90, 92, 94].

This chapter considers the use of thin and thick substrate materials of various relative permittivity for possible impedance bandwidth improvement [89, 90]. However, microstrip antennae with thick substrates excite surface waves which propagate along the air-dielectric interface. This can produce undesirable effects on the radiation pattern (see Chapter 7) as well as reducing the radiation efficiency and also the bandwidth of the antenna as will be shown in the following sections.

Classical microstrip antenna elements have been analysed by many authors and several methods [1, 2, 9, 14, 22, 32, 34, 37, 45, 53, 63, 106, 132, 134, 152] have been developed to determine their bandwidth for given physical properties. Some of these methods include: the transmission line model, TLM, [1, 2, 9, 132], cavity model, CM, [2, 9, 34], the electric surface current model [63] and the moment method [53]. Many of these methods show good quantitative agreement for cases given in the literature but the ranges of validity are generally not known, and computed results using these methods may not be sufficiently accurate for many practical values of dielectric constant and substrate thickness [89, 90].

This chapter

- carries out a study on bandwidth for rectangular microstrip antenna elements,

- accomplishes experiments for bandwidth of antenna elements with various substrate thicknesses and relative permittivity,
- discusses formulae based on TLM and CM for computing the bandwidth of these antennae,
- determines the threshold of the applicability of these formulae,
- develops formulae that can determine the bandwidth of these antennae,
- combines several formulae based on the cavity model and the transmission line model to produce closed-form expressions for calculating the bandwidth of probe-fed rectangular microstrip antenna elements with substrates satisfying the criteria $h \leq 0.0815\ \lambda_o$ for $2.22 \leq \varepsilon_r \leq 10.2$, where h is the thickness and ε_r the relative permittivity of the substrate and λ_o is the free space wavelength. The formula takes into account the effects of radiation, conductor and dielectric losses, with their quality factors. It also provides insight into the fundamental influence of the substrate materials and antenna dimensions on bandwidth. The results obtained from this technique confirm those calculated from the MSAnt program of Pozar [14], and measured results. However, there is a dearth of both measured and analytical BW data for antenna elements with thicker substrates in the literature. As far as its known, at present, BW can not be calculated satisfactorily by using existing formulae for such antenna elements.
- develops a novel closed-form expression based on the TLM, the CM and the exact Green's function for a grounded dielectric slab, for computing the bandwidth of rectangular microstrip antenna elements with thick substrates. This takes into account the power radiated in the space waves and the power radiated in surface waves and an empirically derived correction factor. The antenna elements investigated here vary in electrical thickness, defined as h/λ_d, from 0.1405 to 0.2284, and in physical thickness from 3.30 mm to 12.81 mm, and operate over the frequency range 2.980 GHz to 8.000 GHz. The BW values obtained from the return loss plots are compared with those calculated using the equations introduced in this paper and with results obtained from Pozar's computer program, MSAnt.

Note that each data point in the figures presented in this chapter represent a measured or calculated value of an individual antenna element.

6.2 Bandwidth Definitions

The bandwidth of an antenna is difficult to define in general terms, since the operating specifications of an antenna may involve a variety of parameters, so it is important to specify the

criteria being used when antenna bandwidth is quoted. According to ref [153] the bandwidth is "the frequencies range within which the performance of the antenna, with respect to some characteristic, conforms to a specific standard". In the case of the microstrip antenna, which is basically a strongly resonant device, the definitions of bandwidth are listed below [5]:

- *Polarisation or Axial Ratio Bandwidth:*

  The polarisation properties (linear or circular) of an antenna are usually preferred to be fixed with frequency. Specifying a maximum cross-polarisation or axial ratio level can be used to find this bandwidth.

- *Pattern Bandwidth:*

  The bandwidth, sidelobe level, and gain of an antenna all vary with frequency. If any of these quantities is specified as a maximum or minimum, the operating frequency range can be determined.

- *Impedance Bandwidth:*

  The impedance variation with frequency of the antenna element results in a limitation of the frequency range over which the element can be matched to its feed line. Impedance bandwidth is usually specified in terms of a return loss or maximum Standing Wave Ratio (SWR) over a frequency range. Conversation of bandwidth from one SWR level to another is discussed in Section 6.4. Note that, for single microstrip antenna elements, the impedance bandwidth is generally the limiting factor; the antenna directivity and patterns generally vary little with frequency

6.3 Determination of the Bandwidth from Measured Results

The return loss of each antenna element listed in Tables 6.1 and 6.2 was measured to determine the resonant frequency and fractional BW, as illustrated in Figures 5.1 - 5.10 If the antenna impedance is matched to the transmission line at resonance, the mismatch off resonance is related to the voltage standing wave ratio, VSWR. The value of VSWR which can be tolerated then defines the bandwidth of the antenna element.

A return loss of 30 dB or better was used as the criterion for acceptable impedance matching at resonance, and the fractional bandwidth [132, 154] was obtained as the frequency difference between points either side of resonance where the loss is 9 dB, equivalent to a VSWR = 2.1

$$BW = \frac{f_2 - f_1}{f_r} 100\% \qquad (6.1)$$

Here f_r is the centre of the operating frequency range, f_1 is the lowest operating frequency and f_2 the highest operating frequency. Note that this relationship is only valid whilst the patch behaves essentially as a simple tuned RLC circuit like that shown in Figure 2.2. Equation 6.1 has been applied to all antenna elements listed in Tables 6.1 and 6.2. The obtained results are than plotted as a function of substrate electrical thicknesses of these antenna elements in Figure 6.1.

6.4 Calculation of Impedance Bandwidth for Thin Antenna Elements

Consider a probe-fed rectangular microstrip antenna element of resonant length L, width W, and feed point location **a** over a ground plane with a substrate of thickness h, a relative permittivity ε_r and loss tangent tanδ, as shown in Figure 1.1.

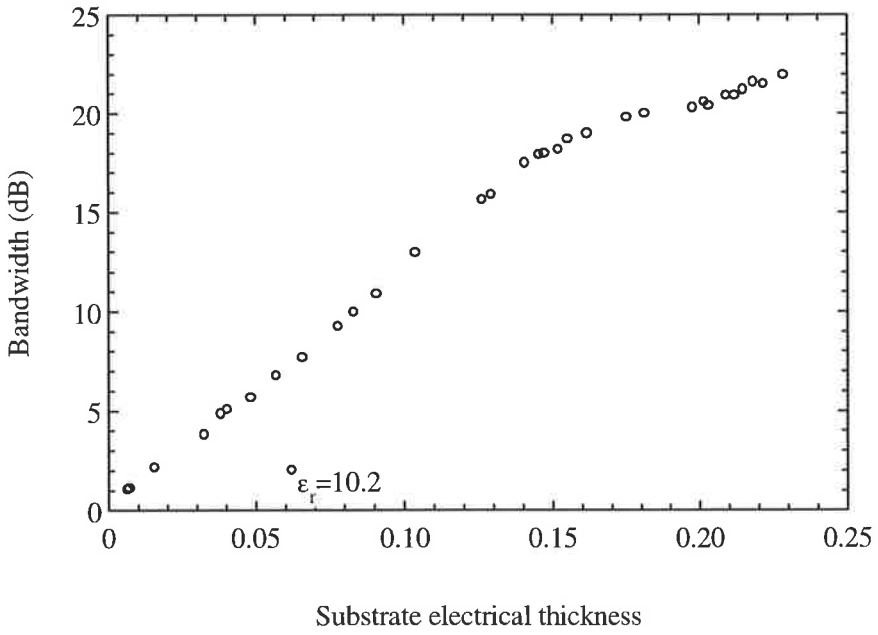

Figure 6.1: Measured bandwidth versus substrate electrical thicknesses of all antenna elements listed in Tables 6.1 and 6.2.

Generally, the operating frequency range of the basic microstrip antenna element with thin substrate is limited by its narrow impedance bandwidth. The equivalent circuit of a probe-fed microstrip antenna element appears as a parallel RLC resonator with a high quality factor, because of the thin substrate. Therefore, at resonance the microstrip antenna element may be assigned a quality factor, Q_T, to describe its bandwidth. The Q_T factor is the total of all quality factors associated with antenna losses, which include power dissipated within the patch due to lossy metal conductors, Q_c, and substrate, Q_d, and power lost due to radiation, Q_r. For rectangular antenna elements displaying a parallel RLC-type resonance response, the BW can be based on the impedance characteristics [1, 2, 5, 30, 32, 89, 90, 106] and expressed as

$$BW = \frac{(S-1)}{Q_T\sqrt{S}}100\% \tag{6.2}$$

where S is the maximum allowable VSWR (>1) within the band of operation.

The total quality factor of the antenna element is given by Carver et al [32] as:

$$Q_T = \left(\frac{1}{Q_r} + \frac{1}{Q_c} + \frac{1}{Q_d}\right)^{-1} \tag{6.3}$$

The quality factor associated with the radiation was derived using a closed resonator model by Vandesande et al [22] as:

$$Q_r = \frac{c_o}{4hf_r}\sqrt{\varepsilon_{ew}} \tag{6.4}$$

where c_o is the speed of light in vacuum and ε_{ew} the effective permittivity can be calculated from equation 2.10 or 3.8. Q_d is determined by the dielectric loss tangent of the substrate and is given by

$$Q_d = \tan^{-1}\delta \tag{6.5}$$

Q_c for copper can be calculated from the formula given by Knoppik [135]:

$$Q_c = 0.7866\ \ h\frac{Z_{cw}}{P_w}\sqrt{f_r(GHz)} \tag{6.6}$$

P_W is given by [134]

$$P_W = \frac{2\pi\left[\frac{W}{h} + \frac{W}{\pi h}\left(0.94 + \frac{W}{2h}\right)^{-1}\right]\left(1 + \frac{h}{W}\right)}{\left(\frac{W^2}{h} + \frac{2}{\pi}\ln\left[2e\pi\left(0.94 + \frac{W}{2h}\right)\right]\right)^2} \tag{6.7}$$

for W/h>2, where e = exp(1), and

$$P_W = \left[1-\left(\frac{W}{4h}\right)^2\right]\left[1+\frac{h}{W}\right] \tag{6.8}$$

for W/h<2.

Here Z_{cw} is the characteristic impedance of a substrate filled strip line with strip line thickness t = 0, as a function of ε_r, h and W. According to Owens [102] this is given by:

$$Z_{cw} = \frac{R_o}{\pi\sqrt{2(\varepsilon_r+1)}}\left[\ln\left(\frac{4h}{W}+\sqrt{\frac{16h^2}{W^2}+2}\right)-\frac{(\varepsilon_r-1)}{(\varepsilon_r+1)}\left(0.2258+\frac{0.1208}{\varepsilon_r}\right)\right] \tag{6.9}$$

for $W/h \leq 3.3$, and

$$Z_{cw} = \frac{R_o}{2\sqrt{\varepsilon_r}}\left[\frac{W}{2h}+0.4413+\frac{0.0823(\varepsilon_r-1)}{\varepsilon_r^{\,2}}+\frac{\varepsilon_r+1}{\varepsilon_r}\left[0.231+0.1592\ln\left(\frac{W}{2h}+0.94\right)\right]\right]^{-1} \tag{6.10}$$

for $W/h \geq 3.3$

where $R_o = 120\,\pi\Omega$ is the vacuum resistance. Z_{ow} is the characteristic impedance of an air filled stripline derived from the characteristic impedance of a substrate filled strip line of width W. Now setting $\varepsilon_r = 1$, one obtains for $W/h \leq 3.3$

$$Z_{ow} = \frac{R_o}{2\pi}\left[\ln\left(\frac{4h}{W}+\sqrt{\frac{16h^2}{W^2}+2}\right)\right] \tag{6.11}$$

and for W/h ≥ 3.3

$$Z_{ow} = \frac{R_o}{2}\left[\frac{W}{2h} + 0.9034 + \frac{1}{\pi}\ln\left(\frac{W}{2h} + 0.94\right)\right]^{-1} \qquad (6.12)$$

The surface wave power loss, however, constitutes only a very small proportion of the total power loss for antenna elements with substrates thinner than approximately 0.00815 λ_o, and therefore is not included in the calculation.

Equations 6.2 to 6.12 were used to calculate the bandwidth of all antenna elements listed in Tables 6.1 and 6.2. Note that Table 6.1 is a continuation of Tables 3.3, 4.1 and 5.1 and Table 6.2 of Tables .3.4, 4.2 and 5.2. To check the accuracy of equations 6.2 to 6.12, the bandwidth of all antenna elements given in Tables 6.1 and 6.2 are plotted as a function of their substrate electrical thicknesses together with those results obtained from the MSAnt program and measured results in Figure 6.2.

Note from this figure that equations 6.2 to 6.12 and the MSAnt program are found to yield bandwidths of antenna elements with substrates respectively thinner than approximately 0.13 λ_d and 0.1 λ_d with good accuracy, however, they became increasingly inaccurate as the substrate thicknesses increased. Thus, a formula for the calculating the bandwidth of antenna elements with thicker substrates will now be proposed in the following section.

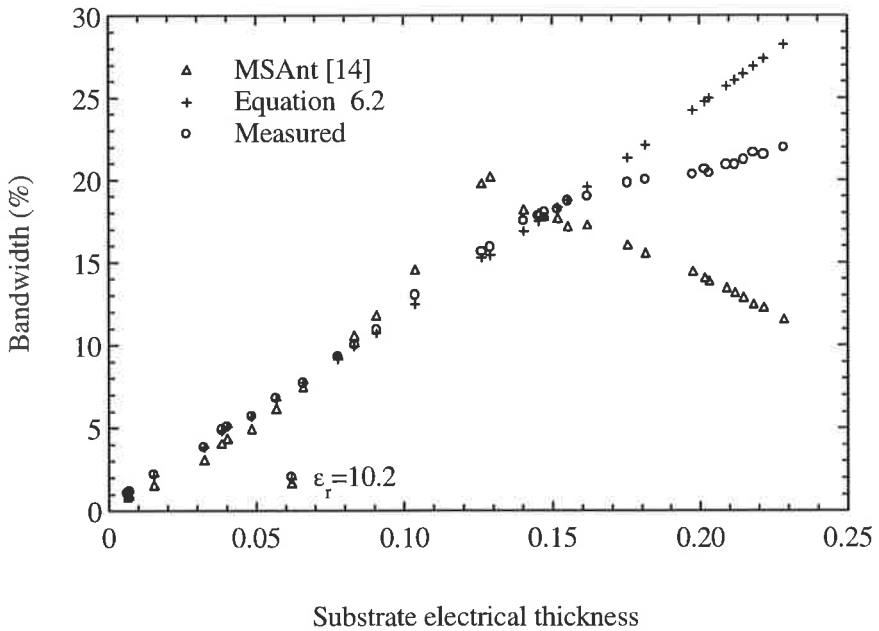

Figure 6.2: Measured bandwidth results and those results obtained from equation 6.2 and MSAnt program versus substrate electrical thicknesses of all antenna elements listed in Tables 6.1 and 6.2.

Table 6.1 Measured and calculated bandwidth and efficiencies of antenna elements with *thin substrates* (it is a continuation of Tables 3.3, 4.1 and 5.1).

Patch No	Measured BW (%)	Present Method BW(%) Eq. 6.2	Calculated BW(%) MSAnt [14]	Calculated η [%]	h/λ_d	h (mm)	ε_r
1	1.07	1.08	0.80	98.32	0.0065	0.17	2.22
2	1.15	1.15	0.90	98.17	0.0071	0.17	2.22
3	2.20	2.11	1.50	96.08	0.0155	0.79	2.22
4	3.85	3.84	3.00	90.81	0.0326	0.79	2.22
5	2.05	1.94	1.60	81.06	0.0622	1.27	10.20
6	5.10	5.09	4.30	89.83	0.0404	1.57	2.33
7	4.90	4.83	4.00	90.30	0.0384	1.57	2.33
8	6.80	6.67	6.10	84.96	0.0569	1.63	2.55
9	5.70	5.69	4.90	86.87	0.0486	1.63	2.55
10	7.70	7.74	7.40	82.97	0.0660	2.00	2.55
11	10.90	10.71	11.70	77.97	0.0908	2.42	2.55
12	9.30	9.14	9.30	80.51	0.0778	2.52	2.55
13	10.00	9.92	10.50	99.75	0.0833	3.00	2.50
14	13.00	12.46	14.50	75.96	0.1039	3.00	2.50
15	15.60	15.26	19.70	72.21	0.1263	3.00	2.50
16	15.90	15.41	20.10	71.33	0.1292	4.76	2.55

6.5 Calculation of Bandwidth for Thick Antenna Elements

In this case the BW can also be calculated from equations 6.2 to 6.12 in which Q_T is calculated from [1]

$$Q_T = \frac{Q_r}{\eta} \tag{6.13}$$

where Q_r, is the quality factor associated with the radiation is given for this case as a function of the relative permittivity of the substrate as

$$Q_r = \frac{\lambda_o}{4}\frac{\sqrt{\varepsilon_r}}{h} \tag{6.14}$$

and η is the radiation (space wave) efficiency as defined by Pozar [155]

$$\eta = \frac{P_r}{P_r + P_s} 100\% \tag{6.15}$$

where P_r is the power radiated in the space waves (direct main beam power) is given by

$$P_r \approx \frac{R_o k_o^2 (k_o h)^2}{3\pi} \left(1 - \frac{1}{\varepsilon_r} + \frac{2}{5\varepsilon_r^2}\right) \tag{6.16}$$

and P_s is the power radiated in surface waves is given by

$$P_s \approx \frac{R_o k_o^2}{4} \frac{(\varepsilon_r - 1)^3 (k_o h)^3}{\varepsilon_r^3} \tag{6.17}$$

where $k_o = 2\pi/\lambda_o$ is the free space wavelength. In addition, ignoring the dielectric loss, $P_r + P_s$ is the total power delivered to the microstrip antenna element.

An expression for bandwidth as a function of efficiency can be found by combining equations 6.2 and 6.13:

$$BW(\%) = \frac{(S-1)}{\sqrt{S}} \frac{\eta}{Q_r} \tag{6.18}$$

To check the accuracy of equation 6.18, the bandwidths of all antenna elements given in Tables 6.1 and 6.2 have been calculated and plotted as a function of their substrate electrical thicknesses together with those obtained from equation 6.2 and measured results in Figure 6.3. As is evident from the close agreement between the measured and calculated results equation 6.18 calculates the bandwidth of antenna elements with substrates in the range of $h \geq 0.06\lambda_d$ with good accuracy. As can be also seen, neither the equation 6.2 nor that of 6.18 yield an explicit expression for the bandwidth of antennae elements for the substrate thickness range $h \geq 0.13\lambda_d$, so a correction factor for equation 6.18 was established by curve-fitting. The rationale behind the derivation of the correction factor P follows. The ratios of the measured bandwidth results and those obtained from equation 6.18 are plotted as a function of substrate electrical thickness in Figure 6.6.

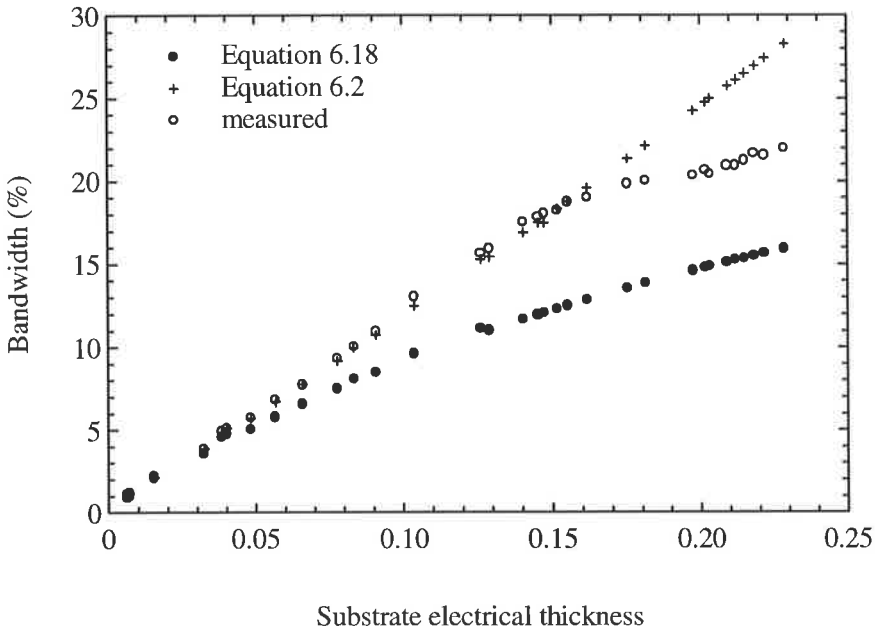

Figure 6.3: Measured bandwidth results and those results obtained from equations 6.2 and 6.18 versus substrate electrical thicknesses of all antenna elements listed in Tables 6.1 and 6.2.

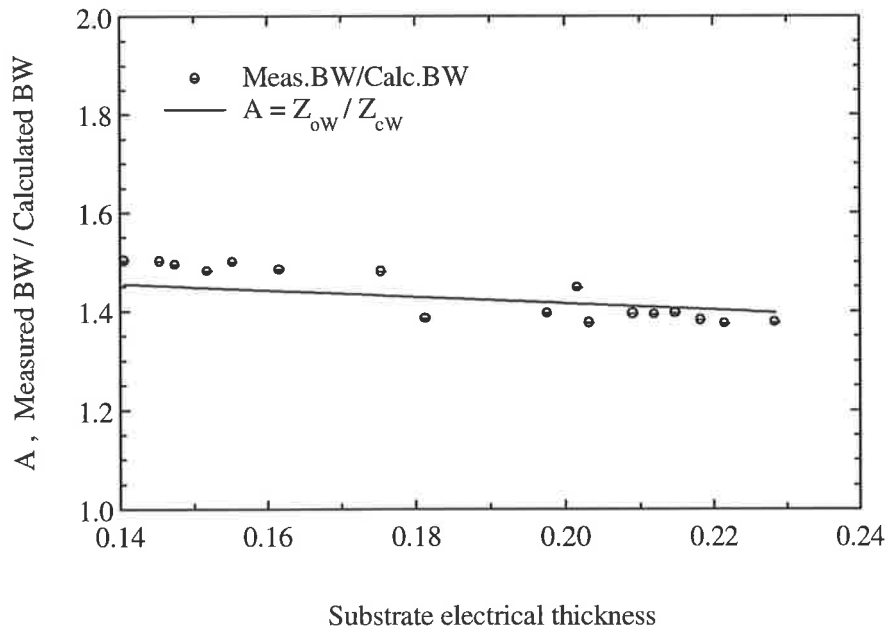

Figure 6.4: Design chart to determine the correction factor A for all antenna elements listed in Table 6.2.

The details for these antenna elements are given in Table 6.2. After analysing the dependence of the curves on the patch and substrate parameters, a correction factor was derived to fit the measured results. The following correction factor, P, was obtained

$$P = \frac{Z_{oW}}{Z_{cW}} \tag{6.19}$$

where Z_{cw} can be calculated from equation 6.9 or 6.10 and Z_{ow} is calculated from equation 6.11 or 6.12.

A new closed-form expression for the bandwidth for an antenna with VSWR < S is then derived by substituting equations 6.13 and 6.19 into 6.18:

$$BW(\&\%) = \frac{\eta}{Q_r}\frac{(S-1)}{\sqrt{S}}P \tag{6.20}$$

Equation 6.20 was used to calculate the bandwidth of all antenna elements listed in Table 6.2. The second and third columns of this table compare measured results with those calculated using this formula. Results obtained from the new formulas conform well with measured results for antenna elements with thick substrates.

6.6 Results and Discussion

The microstrip antenna elements investigated are rectangular patches with geometry as illustrated in Figure 1.1. They are fabricated on PTFE (polytetrafluoroethylene) woven glass laminate material (ε_r = 2.50 and 2.55) and on duroid microwave substrate which is made of a glass microfiber reinforced PTFE composite (ε_r = 2.22, 2.33 and 10.2). These substrate materials are summarised in Table 3.1. The inner conductor of the standard 50 ohm coaxial feed was extended to form the probe through the substrate to all antenna elements tested. Antenna elements with substrate thicknesses in the range of $h \leq 0.13\ \lambda_d$ (or $h \leq 0.0815\ \lambda_d$) are listed in Table 6.1 and are considered to be thin antennae, otherwise thick. Thick antenna elements are listed in Table 6.2.

Table 6.1 gives the measured bandwidth (column two) for VSWR = 2.1 of these antennae and the output values from equations 6.2 to 6.12 (column three) as calculated over a representative range of antenna dimensions shown in Table 3.3. The fourth and fifth columns of Table 6.1

Table 6.2 Measured and calculated bandwidth and efficiencies of antenna elements with thick substrates (it is a continuation of Tables 3.4, 4.2 and 5.2)

Patch No	Measured BW (%)	Present Method BW (%) Eqn. 6.20	Calculated BW(%) MSAnt	Calculated η (%)	h/λ_d	h (mm)
1	17.50	17.00	18.10	69.60	0.1405	3.30
2	18.20	17.77	17.60	67.90	0.1519	4.00
3	17.90	17.34	17.90	68.85	0.1454	4.50
4	18.00	17.47	17.70	68.60	0.1475	4.76
5	19.00	18.42	17.20	66.50	0.1617	4.76
6	20.00	19.29	16.00	64.70	0.1754	5.50
7	18.70	18.01	17.10	67.40	0.1553	6.26
8	20.90	21.26	13.40	60.60	0.2091	8.45
9	20.00	19.66	15.50	63.90	0.1814	9.52
10	20.60	20.85	14.00	61.45	0.2017	9.52
11	20.30	20.61	14.40	61.90	0.1976	9.52
12	20.90	21.40	13.10	60.30	0.2119	10.00
13	21.96	22.26	11.50	58.50	0.2284	11.00
14	21.50	21.91	12.20	59.20	0.2216	12.00
15	21.60	21.73	12.40	59.60	0.2182	12.81
16	20.40	20.92	13.80	61.30	0.2032	12.81
17	21.20	21.55	12.80	59.95	0.2148	12.81

show respectively the bandwidth obtained from MSAnt program and the calculated radiation efficiencies for these antenna elements. Table 6.2 however, gives the measured bandwidth (column two) and the output values from equations 6.20 (column three) as calculated over a representative range of antenna dimensions shown in Table 3.4. The fourth and fifth columns of Table 6.2 show respectively the bandwidth obtained from MSAnt program and the calculated radiation efficiencies for these antenna elements.

Although it is commonly assumed that the bandwidth increases with substrate thickness and decreases as the value of the permittivity of the substrate increases, study of Figure 6.1 shows that the BW dependence on these parameters is quite complicated. The BW increases rapidly, except for antenna number 5 of Table 6.1, because its ε_r =10.2, so that bandwidth of 1.07 % - 17.8% can be obtained for substrate thicknesses in the range of 0.0065 λ_d to 0.15λ_d. Beyond this substrate thickness threshold it increases moderately, so that bandwidth of 18% - 22.2% is obtained.

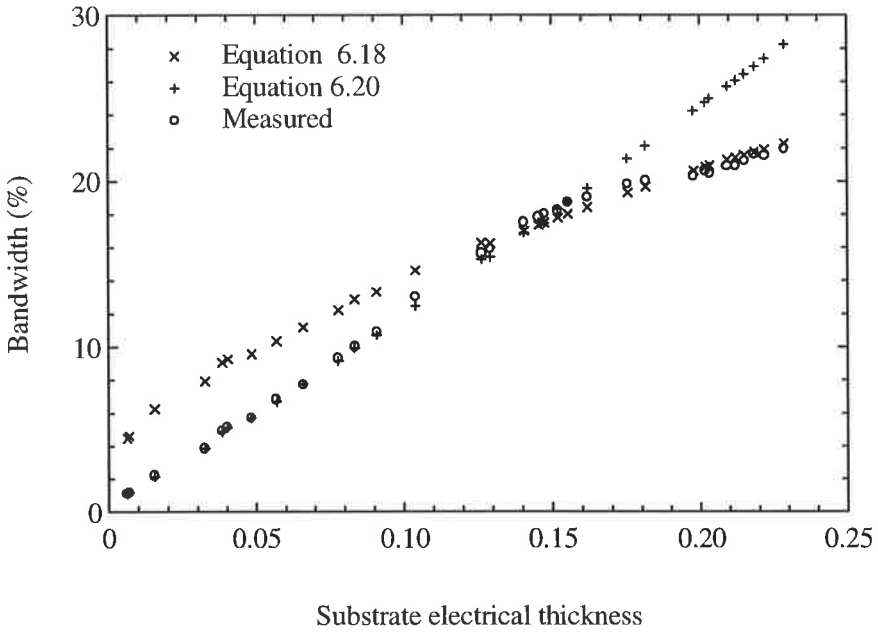

Figure 6.5: Measured bandwidth results and those results obtained from equations 6.18, and 6.20 versus substrate electrical thicknesses of all antenna elements listed in Tables 6.1 and 6.2.

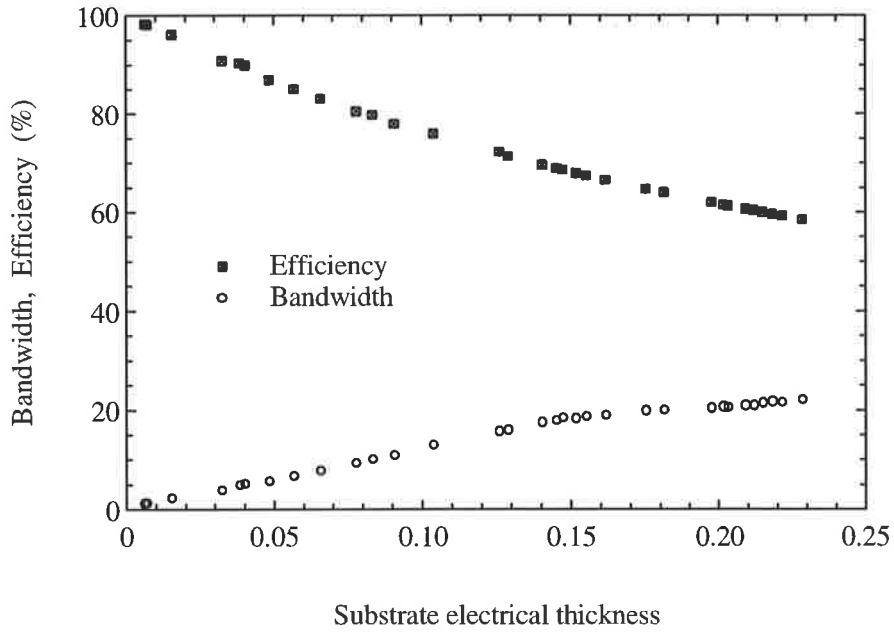

Figure 6.6: Measured bandwidth and calculated efficiencies versus substrate electrical thicknesses of all antenna elements listed in Tables 6.1 and 6.2.

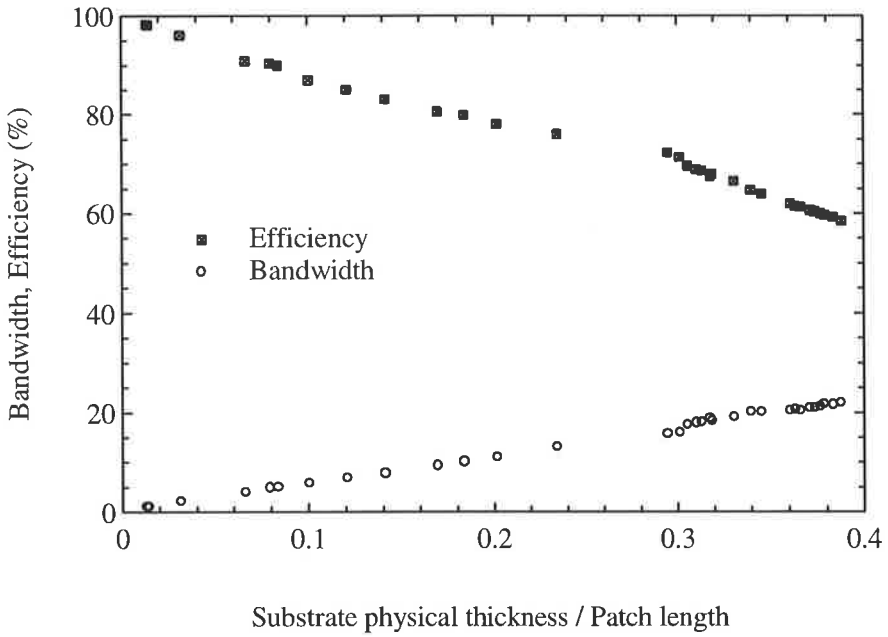

Figure 6.7: Measured bandwidth and calculated efficiencies versus substrate physical thickness and patch length ratios of all antenna elements listed in Tables 6.1 and 6.2

Figure 6.5 shows the graphical representation of the bandwidth obtained from equations 6.2 and 6.20 as well as measured results as a function of substrate electrical thicknesses of all antenna elements listed in Tables 6.1 and 6.2. Note from this figure that the bandwidth results obtained from equation 6.2 agree well with measured results for antenna elements with substrate thicknesses only when $h \leq 0.0815\ \lambda_o$. Beyond this substrate thickness threshold, however, equation 6.2 fails to accurately predict the bandwidth due to the omission of the surface wave contribution. For this case, the bandwidth can be calculated with a considerable accuracy using equation 6.20.

As substrate thickness increases the TM_o surface mode becomes stronger, reducing the efficiency and also BW, as can be seen in Figure 6.6. In this figure bandwidth and radiation efficiencies are plotted as a function of substrate electrical thicknesses of all antenna elements listed in Tables 6.1 and 6.2. Note that η decreases with increasing substrate thicknesses. For example, a 98.3% efficiency was calculated for an $0.0065\lambda_d$ thick antenna element, but only a 58.5% efficiency with a $0.2284\ \lambda_d$ thick antenna was calculated.

Figure 6.7 shows the graphical representation of the calculated efficiencies and measured bandwidth as a function of substrate physical thickness to patch length ratios (h/L ratios) of all antenna elements listed in Tables 6.1 and 6.2. Note that this figure yields similar characteristics as Figure 6.6

6.7 Conclusion

A study of the bandwidth of rectangular microstrip antenna elements with various substrate thicknesses and relative permittivities has been presented. The study includes

- a technique based on the cavity model and the transmission line model have been given for incorporating the various loss mechanisms including dielectric conductor and radiation losses, into the equations for the calculation of bandwidth of probe fed rectangular microstrip antenna elements with substrates ranging in thickness from 0.0065 λ_d to 0.1292 λ_d (0.17 mm $\leq h \leq$ 4.76 mm) and operating over the frequency range 3.545 GHz to 8.450 GHz. The results obtained from this technique are confirmed with those calculated from the MSAnt program and measured results for all antenna elements given in Table 6.1. This research has also revealed that increased substrate thickness produces increased bandwidth. For example, a 1.07% bandwidth was measured for VSWR = 2.1 at 7.740 GHz with a 0.0065 λ_d (0.17 mm) substrate thickness, but a 15.90% bandwidth was achieved at 5.100 GHz with a 0.1292 λ_d (4.76 mm) substrate thickness. It has also been demonstrated that electrically thin antenna elements are between 98.30 % and 71.30 % efficient. It has been shown that the method given here gives results in good agreement with measurements.

- A novel closed-form expression based on the modified cavity model and the exact Green's function for a grounded dielectric slab has been developed for computing the BW of probe fed rectangular microstrip antenna elements wit thick substrates taking into account both the power radiated in the space waves and the power radiated in surface waves. The correction factor was derived by means of a curve-fitting technique taking the inhomogeneus nature of microstrip antennae into account. Substrate thicknesses of the investigated antenna elements range $h \geq 0.13\ \lambda_d$ (3.3 mm $\leq h \leq$ 12.81 mm) for $\varepsilon_r = 2.55$ and operating frequencies range from 2.980 GHz to 8.000 GHz. The accuracy of the proposed expression has been established by comparing calculated results with experimental measurements of BW for all elements listed in Table 6.2. It has been shown that the method given here gives results in good agreement with measurements.

This work has also revealed that increased substrate thickness produces a moderate increment in bandwidth only. For example, a 17.50 % BW was measured for VSWR = 2.1 at 8.000 GHz with a 0.1405 λ_d (3.30 mm) thick antenna, but only a 21.20 % BW at 3.150 GHz

with a 0.2148 λ_d (12.81 mm) thick antenna was achieved. It has also been demonstrated that electrically thick antenna elements are between 69.60 % and 58.50 % efficient. Comparison with measured bandwidth serve to confirm the accuracy of the computed results.

Among the important contributions of the work described in this chapter are:

- The bandwidth issue in general of microstrip antenna elements is discussed.
- Some of the more useful practical techniques for microstrip antenna bandwidth enhancement are reviewed.
- The development of an accurate and computationally efficient method for the calculation of the bandwidth of *thin* antenna elements.
- The development of an accurate and computationally efficient algorithm for the calculation of the bandwidth of *thick* antenna elements.
- Experimental measurements are used to test and verify the techniques that are developed.
- The effect of the substrate thickness on the bandwidth and efficiency is described.

Chapter 7

The Far-Field Radiation Patterns of Rectangular Microstrip Antenna Elements with Various Substrate Thicknesses

7.1 Introduction

In the close proximity of an antenna, the radiation fields exhibit complex characteristics, since reactive components are present in addition to the radiated field. The reactive components vanish and only the radiated field remains in the far field region when moving far enough away from the antenna. The distance R between the calibrated reference antenna and the antenna under test must satisfy the condition $R \geq 2D^2 / \lambda_o$, where D is the largest dimension of the antenna and λ_o is the free space wavelength. In addition, the reactive field may be considered to be that region immediately surrounding the antennae, and the radiating field is that region, beyond the reactive field, in which the radiation pattern is dependent upon R [3]. All antenna elements considered for this chapter are linearly polarised and the E- and H-plane radiation patterns are measured in the far field region. Note that, the E-plane is the plane containing the electric field vector and the direction of maximum radiation and the H-plane is the plane containing the magnetic field vector and the direction of maximum radiation.

Radiation from a microstrip antenna occurs mainly from the fringing fields between the edge of the patch conductor and the ground plane, Figure 7.1. The fields at the edges can be resolved into normal and tangential components with respect to the ground plane. The tangential components

(those parallel to the ground plane) are in phase, and are combined to give a maximum radiated field normal to the ground plane.

Several analysis techniques have been proposed for the determination of the far-field radiation patterns of microstrip antenna elements [1 - 16, 63, 64, 156]. Many of these analysis techniques employ approximations which are valid only for thin substrates. Other more general approaches suffer from a lack of computational efficiency, which is in practice can restrict their usefulness due to high computational time and costs.

Based on this observation, this chapter investigates formulae based on the two-slot model, TSM, the cavity model, CM, and the electric surface current model, ESCM, methods for calculating the far field radiation patterns in both the E- and the H-plane respectively. This is because of their applicability to the pattern analysis of rectangular microstrip antenna elements and their procedural simplicity for computing the radiation patterns. Their respective regions of validity in theory and applicability for a given antenna element have also been established by comparing the measured results with those obtained from these models. For antenna elements with substrates in the range of $h \leq 0.0815\ \lambda_o$ the TSM and CM have been verified and successfully used to calculate the far radiation patterns in the field E- and H-plane, where h is the substrate thickness. However, as far as it is known, there is no method available in the literature which calculate the E-plane radiation pattern for antenna elements with thicker substrates. In reality, there is also no experimental work that has been carried out on antenna elements with substrate ranges considered in this chapter. In addition, this chapter will not review previous work on radiation patterns, the formulae that can be relied upon to give a stated degree of design precision are given only. The formulae used to calculate the radiation patterns and their modification are discussed briefly in the following sections. Furthermore, the far field radiation patterns in the E- and H-plane are measured and compared with results obtained from TSM, CM and ESCM for antenna elements with substrates thickness in the range of $0.0071\ \lambda_d \leq h \leq 0.2148\ \lambda_d$, and physical thickness $0.17\ \text{mm} \leq h \leq 12.81\ \text{mm}$, where λ_d is the wavelength in the dielectric substrate. They operate over the frequency range $2.980\ \text{GHz} \leq f_r \leq 8.450\ \text{GHz}$.

In this investigation the (1, 0) mode has been used, because in this mode the magnetic currents on the two opposite radiating edges are constant. The magnetic currents on the remaining two edges suffer a phase reversal and hence the fields radiated by them largely cancel. The pattern this mode produces is linearly polarised and has a broadside maximum.

The aim of the work presented in this chapter is to

- carry out a study on far-field radiation patterns in both the E- and the H-plane,
- discuss formulae based on the TSM, the CM and the ESCM models for computing these patterns for rectangular microstrip antenna elements,
- determine the suitability and threshold of the applicability of these formulae,
- develop formulae that can determine the patterns for antenna elements with various substrate thicknesses,
- conduct experiments for radiation patterns,
- verify the calculated results by comparison with experimental measurements,
- study the 3 dB beamwidths of these antenna elements,
- identify the fundamental effects associated with the dielectric substrate,
- study the effect of the edges of the ground plane to the radiation patterns.

For computing the E-plane radiation pattern for antenna elements with substrates in the range of $h \geq 0.0815\ \lambda_o$, the equation based on the TSM used for thin antennae was modified by adding the line extension to patch resonant length. This is because the lines of the fringing field do not stop abruptly at the edges of the patch. There is a stray field extending beyond the patch edges which can be interpreted as an electrical lengthening of the patch, which implies an amount of stored energy.

7.2 Experimental Procedures

Radiation pattern measurement requires two antennae: one to transmit the signal., the other to receive it. The antenna under test acts as receiving antenna and is mounted on a large 183 cm diameter circular aluminium ground plane in a 3 x 3 x 8.1 m microwave anechoic chamber lined on all faces with 0.46 metre high microwave absorbing carbon impregnated foam pyramids.

All of the antenna elements considered for this research are fed by a standard 50 ohm coaxial line. The APC-7 connector was attached to the back side of the printed circuit board, with its central conductor passing through the ground plane and the dielectric substrate and connecting to a suitable position on the patch. The dimensions of the APC-7 connector are: inner radius is 1.520 mm, outer radius is 3.500 mm. Moreover, a standard gain horn antenna with known electrical

characteristics was used as a transmitting antenna (reference antenna). This was mounted on a fixed pillar situated at the opposite end of the chamber, at a height equal to that of the test microstrip antenna element. The distance between the antenna element under test and transmitting antenna was 6 metres.

The test path of the automatic microwave network analyser system was then used to measure both the E- and the H-plane radiation patterns at the polar coordinates of the microstrip test antenna element. This was carried out by determining the magnitude of the scattering transfer coefficient S_{21} for the free space path loss between the receiving test antenna element and the transmitting horn. In addition, the dimension of the substrate material, on which the patch is printed, was 100 by 100 mm large. Absorbing material is placed around the perimeter of the ground plane to reduce diffraction from the edge. This inhibits measurements at angles greater than approximately 80 degrees off the z-axis; however, it extends the angular range over which measurements can be adequately made with a finite ground plane size.

The accurate measurement of far-field radiation patterns in the E- and H-plane involves the consideration of a number of factors, such as the physical and effective dimensions of the antenna element, its feed point location, operational frequency and the environment in which it is operated (eg. ground plane). In addition the feeding and construction discontinuities can cause asymmetry in the radiation patterns.

7.3 The Calculation of Radiation Patterns

The configuration of a probe fed rectangular microstrip antenna element is shown in Figure 1.1. The TSM, the CM and the ESCM methods have been used for calculating the far field radiation patterns in the E- and H-plane and their variations compared with measurements.

The basic formulae for computing these patterns are given in the following sections.

7.3.1 Formulae Based on the Two-Slot Model Method

Generally, the fringing fields which give rise to the slot model for patch antenna radiation, occur around the four sides of the patch. The fringing fields at the top and bottom of a patch (patch

length walls) are depicted in Figure 7.1. These fields represent the preferred sources of radiation for the antenna, which is vertically polarised. The fields along the side walls (patch width walls) radiate horizontally polarised power and cannot be avoided. Based on this observation, the antenna element can be regarded as an antenna system equivalent to the two-slot model shown in Figure 7.1. The E-plane pattern (x-z plane) is determined by multiplying the radiated field of a single slot by an array factor corresponding to the arrangement of two slot array. The total radiation field in the E-plane of rectangular microstrip antenna element operating in the TM_{10} mode is given by [6] as

$$E_\theta(\theta)\Big|_{\phi=0} = -jV_o W k_o \left(\frac{e^{-jk_o R}}{4\pi R}\right) F_E(\theta) \tag{7.1}$$

where

$$F_E(\theta) = \sin\left(\frac{k_o h}{2}\sin\theta\right)\left(\frac{k_o h}{2}\sin\theta\right)^{-1}\cos\left(\frac{k_o L}{2}\sin\theta\right) \tag{6.2}$$

For the H-plane (y-z plane),

$$E_\phi(\theta)\Big|_{\frac{\pi}{2}} = -jV_o W k_o \left(\frac{e^{-jk_o R}}{4\pi R}\right) F_H(\theta) \tag{6.3}$$

where

$$F_H(\theta) = \sin\left(\frac{k_o W}{2}\sin\theta\right)\left(\frac{k_o W}{2}\sin\theta\right)^{-1}\cos\theta \tag{6.4}$$

where k_o is the propagation constant in free space, W and L are the patch width and length, V_o the voltage across the slot, θ and ϕ are the spherical coordinates defined in Figure 7.1.

7.3.2 Formulae based on the Cavity Model

As briefly described in Chapter 2 this model treats the region between two parallel conductor planes, consisting of a patch conductor and ground plane, as a cavity bounded by the electric walls and a magnetic wall along the periphery of the patch. The fields in the antenna element are assumed to be those of this cavity [28].

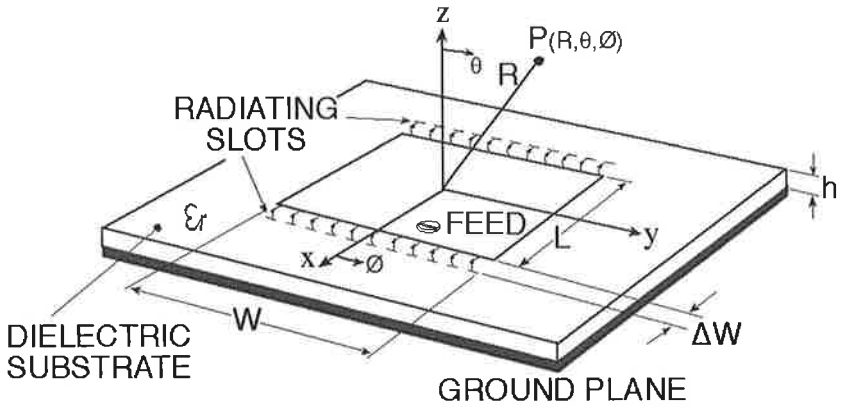

Figure 7.1: Rectangular antenna element represented as two slot radiating slots with dimensional parameters.

This cavity will support quasi-discrete TM_{mn} modes transverse to z, where m and n are the mode numbers associated with the y and x directions respectively. The radiating mode of interest is the TM_{10} mode, obtained for $L = \lambda_d/2$. The radiation patterns in the E- and H-planes can be derived from equations 2.60 and 2.64 respectively.

For the E-plane

$$F_{\phi}(\theta,90^{0}) = \cos\left(\frac{k_o h}{2}\cos\theta\right)\cos\left(\frac{k_o L_e}{2}\sin\theta\right) \tag{7.5}$$

and for the H-plane

$$F_{\theta}(\theta,0^{\circ}) = \cos\left(\frac{k_o h}{2}\cos\theta\right)\frac{\sin\left(\frac{k_o W_e}{2}\sin\theta\right)}{\left(\frac{k_o W_e}{2}\sin\theta\right)}\cos\theta \tag{7.6}$$

where W_e and L_e are the effective dimensions, taking into account the fringing fields at the edge of the patch. In the case of the TM_{10} mode, W_e and L_e may be approximated as follows [6]

$$L_e = L[1+\delta(L)]\frac{\sqrt{\varepsilon_{eL}\varepsilon_{ew}}}{\varepsilon_r} \tag{7.7}$$

and

$$W_e = W \tag{7.8}$$

with

$$\delta(L) = \frac{h}{L}\left\{0.882 + \frac{0.164(\varepsilon_r - 1)}{\varepsilon_r^2} + \frac{\varepsilon_r + 1}{\pi\varepsilon_r}\left[0.758 + \ln\left(\frac{L}{h} + 1.88\right)\right]\right\} \tag{7.9}$$

where ε_{eL} is the effective relative permittivity as a function of the patch resonant length, and can be calculated from 2.10 or 3.8 by replacing W with L.

Of interest is that equations 7.5 and 7.6 correspond to equations 2.22 and 2.24, derived by the transmission line model, TLM, method, when the h is assumed to be zero.

7.3.3 Formulae Based on the Electric Surface Current Model

The antenna element is replaced by as assumed surface current distribution, and the fields are solved taking into account the presence of the dielectric layer. Calculation takes place in the Fourier domain. The far field, calculated asymptotically from this solution, is used to get the radiation patterns of the antenna element.

The radiation pattern in the E-plane is functionally expressed as [63, 64]

$$F_E(\theta, \phi = 0) = \varepsilon_{ew}\left[1 + \varepsilon_r \cot^2\left(k_o h\sqrt{\varepsilon_r}\right)\right]\frac{\cos^2\left(\frac{\pi \sin\theta}{2\sqrt{\varepsilon_{ew}}}\right)}{\left(\sin^2\theta - \varepsilon_{ew}\right)^2} \cdot \frac{\cos^2\left(\varepsilon_r - \sin^2\theta\right)}{\left(\varepsilon_r - \sin^2\theta\right) + \varepsilon_r^2 \cos^2\theta \cot^2\left(k_o h\sqrt{\varepsilon_r - \sin^2\theta}\right)} \tag{7.10}$$

and for the H-plane

$$F_H\left(\theta,\phi=\frac{\pi}{2}\right)=\left[1+\varepsilon_r\cot^2\left(k_o h\sqrt{\varepsilon_r}\right)\right]\sin c^2\left(\frac{Wk_o\sin\theta\sin\phi}{2}\right)$$
$$\cdot\frac{\cos^2\theta}{\left(\varepsilon_r-\sin^2\theta\right)\cot^2\left(k_o h\sqrt{\varepsilon_r-\sin^2\theta}\right)+\cos^2\theta} \qquad (7.11)$$

The brief derivation of equations 7.10 and 7.11 follows that of [63, 64] and is given in Appendix A.

7.4 The Radiation Patterns for Thin Antenna Elements

The radiation pattern in the E-plane of rectangular microstrip antenna elements with substrates in the range of $h \leq 0.0815\ \lambda_o$ can be calculated by equation 7.2, or 7.5, because all three equations yield similar results. The results obtained from these formulae agree well with measured results at desired frequency range values as can be seen in Figures 7.2 - 7.6. However, the agreement between the measured radiation pattern in the E-plane results and those obtained from equation 7.10 has been found not to be promising.

As the substrate electrical thickness increases the formulae for calculation of E-plane radiation patterns equations 7.2 and 7.5 begin to lose accuracy and also applicability, as will be shown in Section 7.5. Thus, a formula for calculating radiation patterns in the E-plane for antenna elements with any substrate thickness and frequency will now be proposed.

As is evident from the close agreement between the measured and calculated patterns in the H-plane shown in Figures 7.7 - 7.10 the formulae based on the TSM and the CM calculate these patterns for antenna elements with substrates in the range of $h \leq 0.0815\ \lambda_o$ with good accuracy. Similar to the E-plane case, the agreement between the measured radiation pattern in the H-plane results and those obtained from equation 7.11 is once again not promising.

Note that the results for the radiation pattern in the E- and H- plane obtained from equations 7.2 and 7.4 are similar to the results obtained from 7.5 and 7.6 respectively.

7.5 The Radiation Pattern for Thick Antenna Elements

For this case the antenna element is assumed to be an open circuit microstrip line, as outlined in Section 2.2.1.1. The electric fields at the open end of a microstrip line are distorted by an abrupt termination at the edges, resulting in fringing electric fields which leak out into the dielectric surrounding the conductor pattern and also out into the air region and around the substrate. Since the patch is modelled as a transmission line of length L, an electrical lengthening of ΔL will occur, due to this open-end effect, at both patch ends. This forms the slots, as shown in Figure 7.1. To improve the accuracy of equation 7.2 the line extension has been taken into account by replacing the physical patch length by $(L + 2\Delta L)$. The resulting formula for the radiation pattern in the E-plane (x-z plane) of rectangular antenna elements with thick substrates can be given as

$$F_T(\theta) = \frac{\sin\left(\frac{k_o h}{2}\sin\theta\right)}{\frac{k_o h}{2}\sin\theta}\cos\left[\frac{k_o(L+2\Delta L)}{2}\sin\theta\right] \tag{7.12}$$

where ΔL is the edge extension as a function of patch length, and can be calculated from equation 2.11 by replacing W with L as follows

$$\Delta L = 0.412\ h\frac{(\varepsilon_{eL}+0.300)}{(\varepsilon_{eL}-0.258)}\left(\frac{L}{h}+0.264\right)\left(\frac{L}{h}+0.813\right)^{-1} \tag{7.13}$$

It has been found that formulae based on the TSM (equation 7.4) and the CM (equation 7.6) for calculating the H-plane patterns are valid for rectangular microstrip antenna elements with substrates of any thickness, as will be shown in the following section.

7.6 Results and Discussion

Far field radiation patterns were measured for angles from -90° to 90° in both the E-and H-plane for all antenna elements given in Tables 3.3 and 3.4. These antenna elements were fabricated on substrate materials given in Table 3.1. However, patterns in the E- and H-plane of only five thin and five thick antenna elements have been selected for this chapter. These provide sufficient

validation for the proposed methods. Numerical results obtained from the methods described above are compared with these pattern measurements.

The radiation patterns of rectangular microstrip antenna elements are hemispherical, but both the E-and H-plane patterns have a null in the horizontal plane ± 90°. Evidently any E-plane radiation pattern in this plane occurs in the form of surface waves. All radiation patterns for both the E- and H-planes were measured and calculated at resonant frequency.

Figures 7.2 - 7.6 show the selected measured E-plane radiation patterns of thin antenna element numbers 2, 4, 8, 12 and 14 of Table 3.3 compared with results obtained from equations 7.5 and 7.10. The patterns obtained by equation 7.5 agree very well with measured values at desired angular regions below ± 60° on the E-plane, while equation 7.10 fails to predict these patterns satisfactorily.

Note that diffraction from the edges of the ground plane has a profound effect on these antenna patterns above ± 60°. In the main beam region, the ideal patch pattern is modulated by diffracted fields.

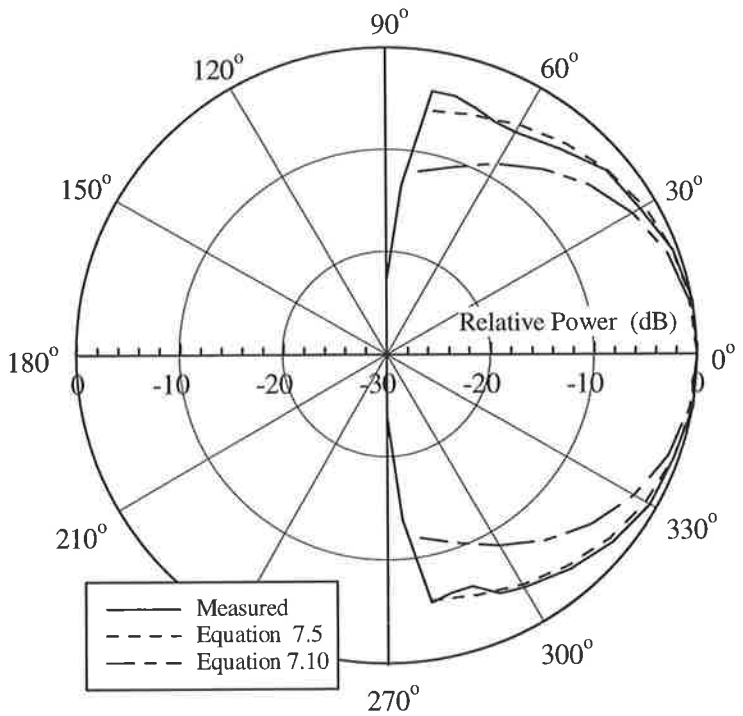

Figure 7.2: Measured far-field radiation pattern in the E-plane at 8.450 GHz for antenna element number 2 in Table 3.3 compared with results obtained from equation 7.5 and 7.10.

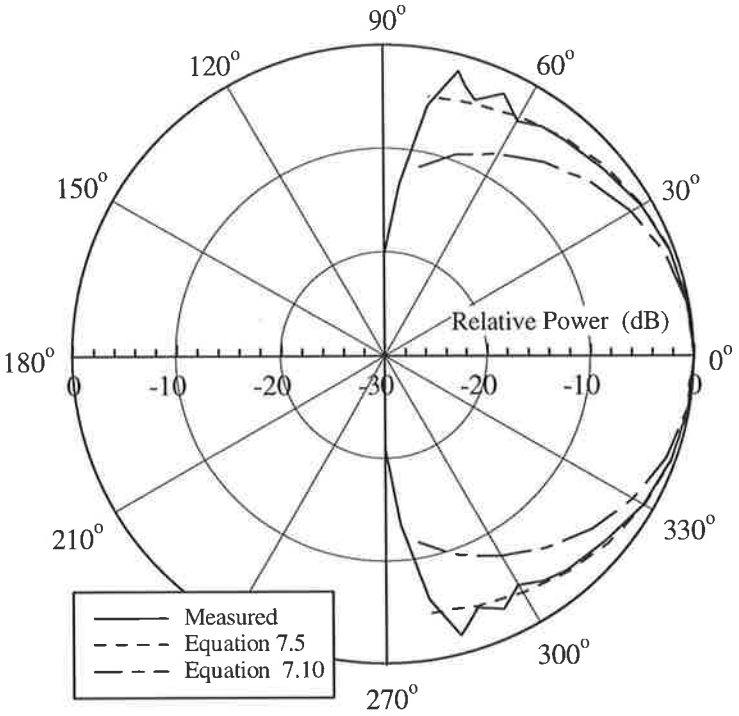

Figure 7.3: Measured far-field radiation pattern in the E-plane at 7.730 GHz for antenna element number 4 in Table 3.3 compared with results obtained from equation 7.5 and 7.10.

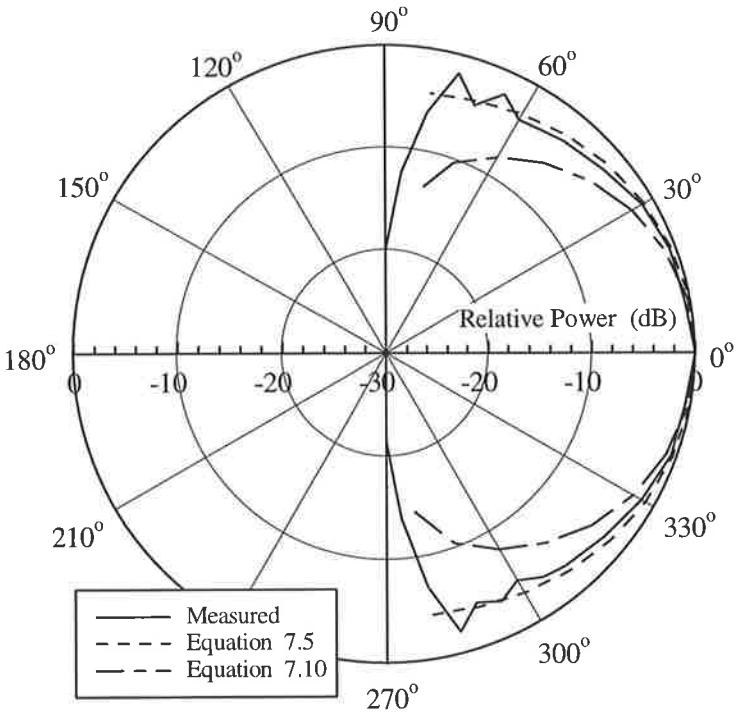

Figure 7.4: Measured far-field radiation pattern in the E-plane at 6.560 GHz for antenna element number 8 in Table 3.3 compared with results obtained from equation 7.5 and 7.10.

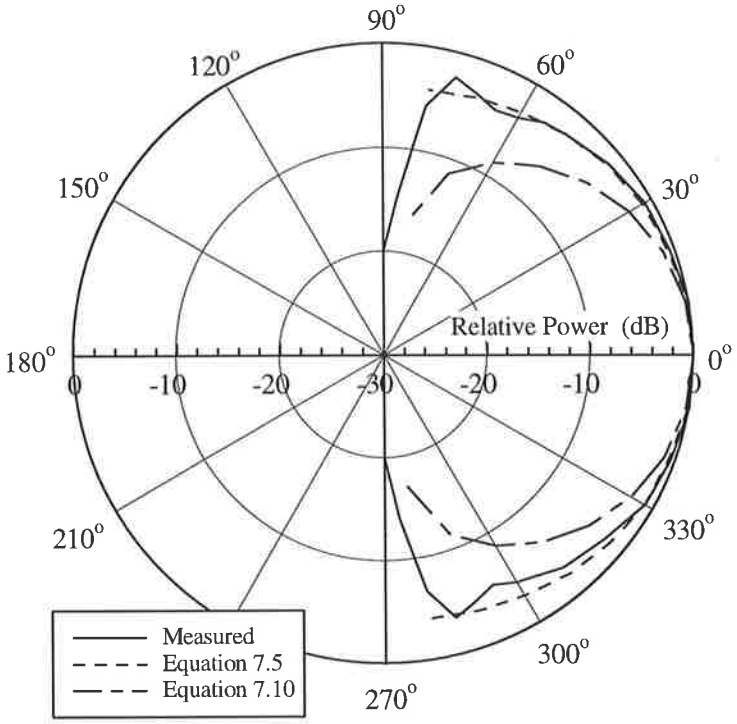

Figure 7.5.: Measured far-field radiation pattern in the E-plane at 5.800 GHz for antenna element number 12 in Table 3.3 compared with results obtained from equation 7.5 and 7.10.

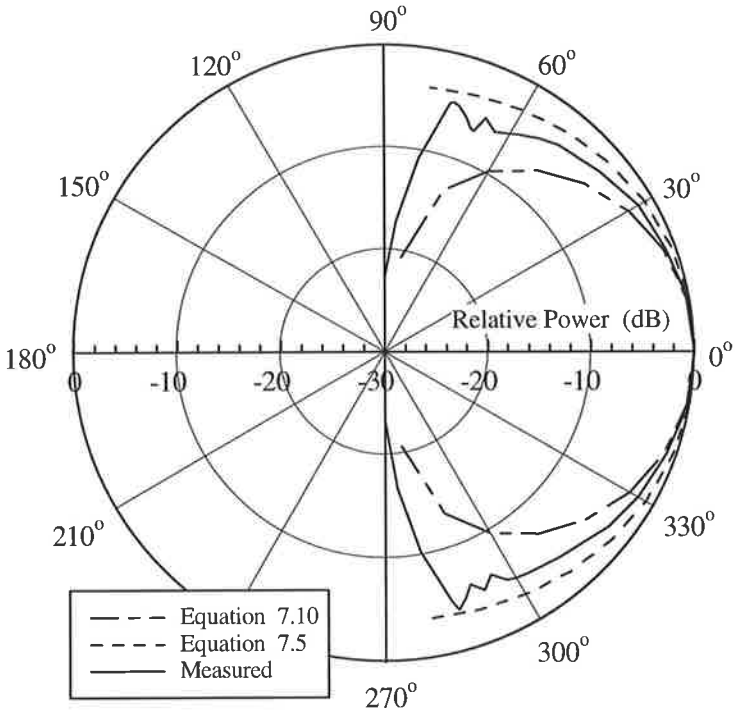

Figure 7.6: Measured far-field radiation pattern in the E-plane at 6.570 GHz for antenna element number 14 in Table 3.3 compared with results obtained from equation 7.5 and 7.10.

Figures 7.7 - 7.10 show the selected measured H-plane radiation patterns of thin antenna element numbers 2, 4, 9 and 14 of Table 3.3 compared with results obtained from equations 7.6 and 7.11. The patterns obtained by equation 7.6 coincide well with measured values while equation 7.11 fails to accurately calculate them.

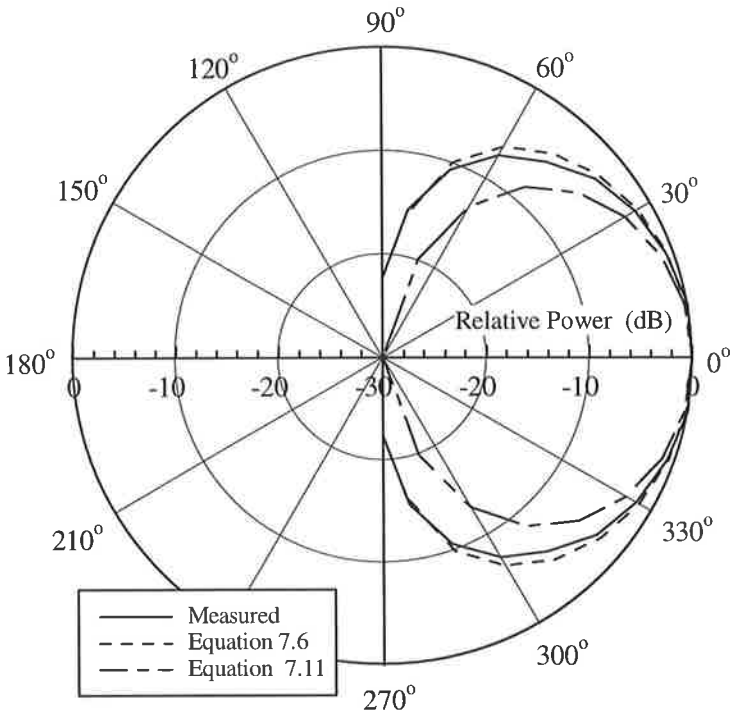

Figure 7.7: Measured far-field radiation pattern in the H-plane at 8.450 GHz for antenna element number 2 in Table 3.3 compared with results obtained from equation 7.6 and 7.11.

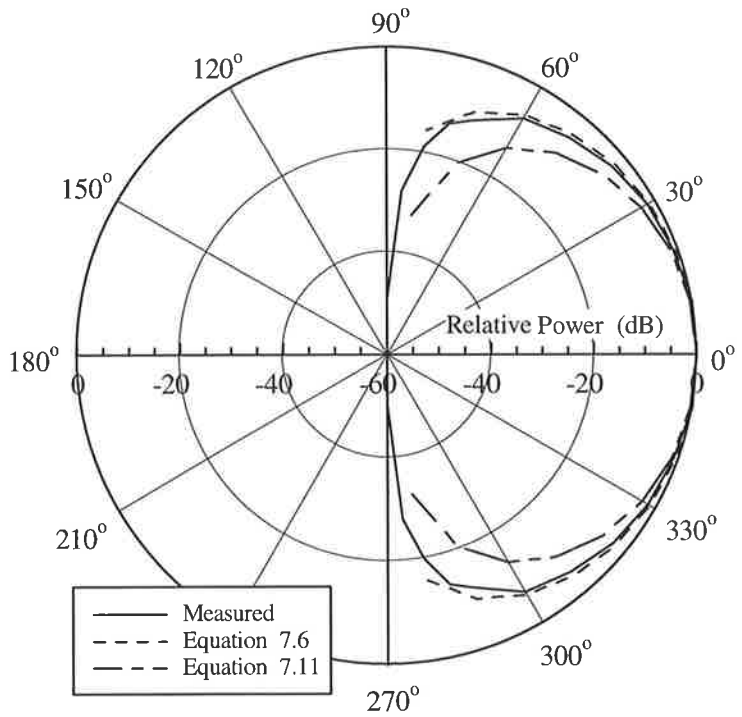

Figure 7.8: Measured far-field radiation pattern in the H-plane at 7.730 GHz for antenna element number 4 in Table 3.3 compared with results obtained from equation 7.6 and 7.11.

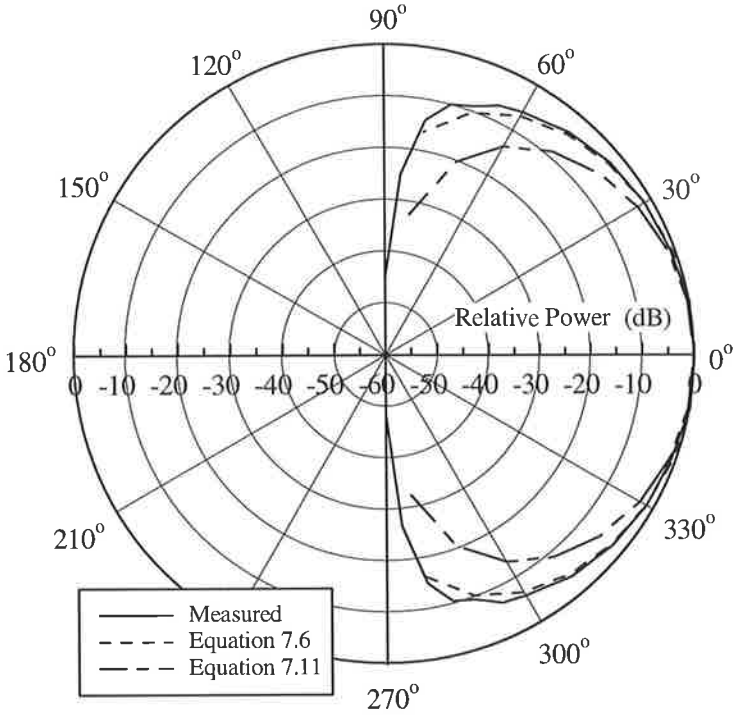

Figure 7.9: Measured far-field radiation pattern in the H-plane for at 5.600 GHz for antenna element number 9 in Table 3.3 compared with results obtained from equation 7.6 and 7.11.

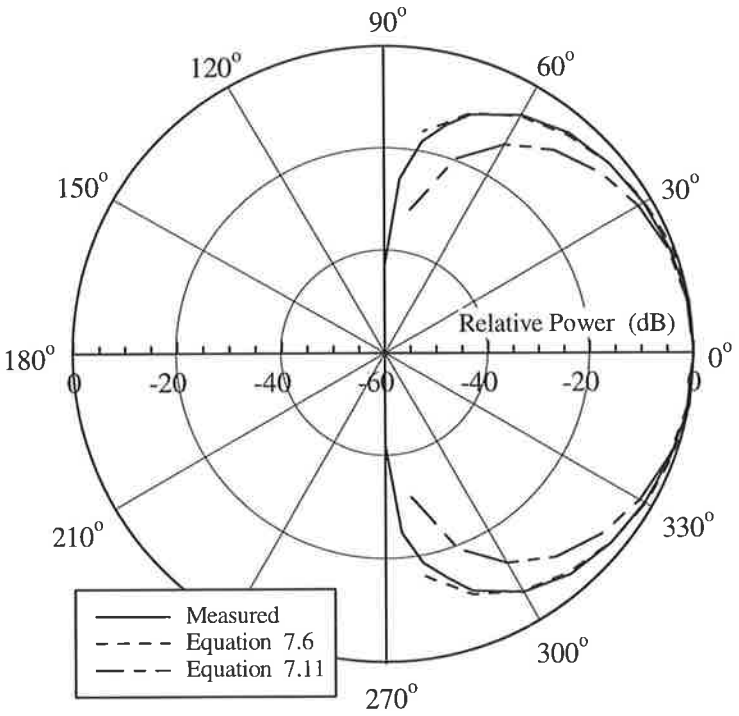

Figure 7.10: Measured far-field radiation pattern in the H-plane at 6.570 GHz for antenna element number 14 in Table 3.3 compared with results obtained from equation 7.6 and 7.11.

Figures 7.11 - 7.15 show the selected measured E-plane radiation patterns of thick antenna element numbers 4, 7, 8, 9 and 17 of Table 3.4 compared with results obtained from equations 7.5, 7.10 and modified equation 7.12. The patterns obtained by the modified equation 7.12 coincide very well with measured values at desired angular regions below ± 60° on the E-plane. But the results obtained from equations 7.5 and 7.10 are not valid for antenna elements with thick substrates.

The E-plane radiation patterns vary significantly with substrate thickness as is shown in these figures. They are also slightly affected by the surface waves and the edges of the ground plane. Since the substrate is thick, the E-plane patterns exhibit variations that could be caused by surface wave and diffraction at the substrate edges.

Figures 7.16 - 7.19 show the selected measured H-plane radiation patterns of thick antenna element numbers 4, 7, 11 and 17 of Table 3.4 compared with results obtained from equations 7.6 and 7.11. The patterns obtained by equation 7.6 coincide very well with measured values, while equation 7.11 fails to calculate these pattern accurately.

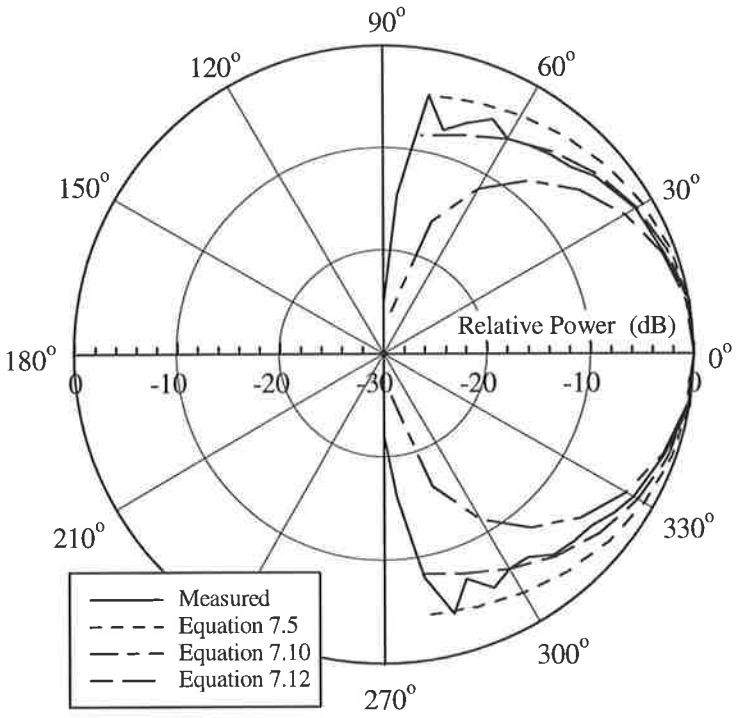

Figure 7.11: Measured far-field radiation pattern in the E-plane at 5.820 GHz for antenna element number 4 in Table 3.4 compared with results obtained from equation 7.5, 7.10 and 7.12.

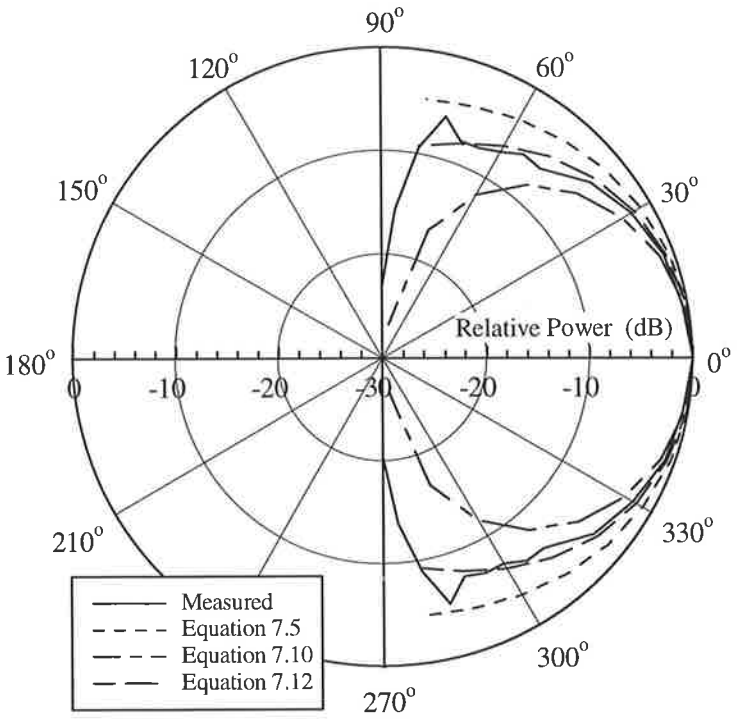

Figure 7.12: Measured far-field radiation pattern in the E-plane at 4.660 GHz for antenna element number 7 in Table 3.4 compared with results obtained from equation 7.5, 7.10 and 7.12.

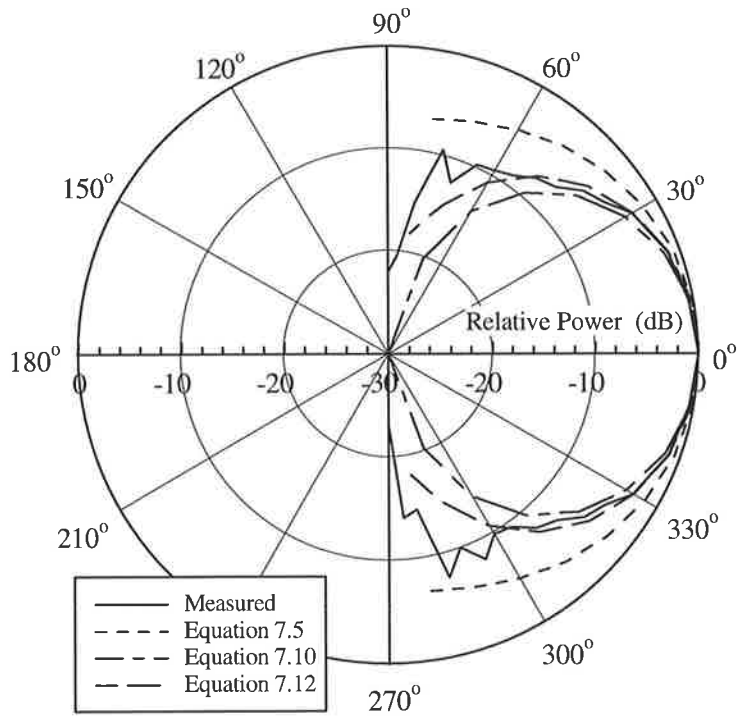

Figure 7.13: Measured far-field radiation pattern in the E-plane at 4.600 GHz for antenna element number 8 in Table 3.4 compared with results obtained from equation 7.5, 7.10 and 7.12.

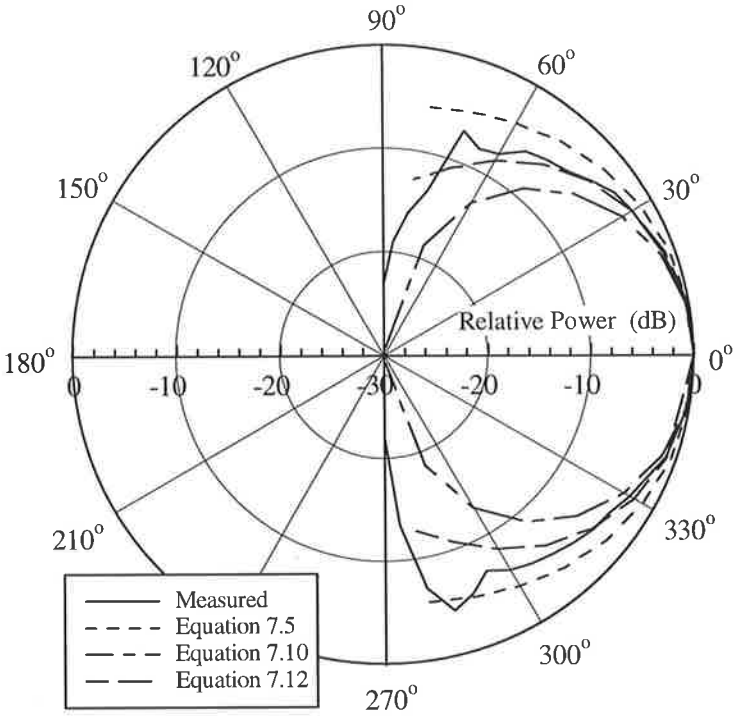

Figure 7.14: Measured far-field radiation pattern in the E-plane at 3.580 GHz for antenna element number 9 in Table 3.4 compared with results obtained from equation 7.5, 7.10 and 7.12.

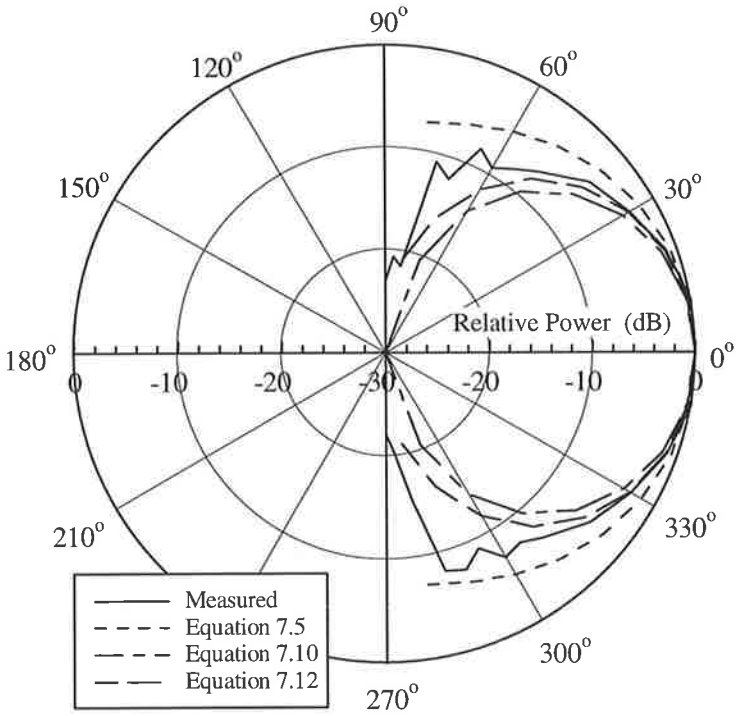

Figure 7.15: Measured far-field radiation pattern in the E-plane at 3.150 GHz for antenna element number 17 in Table 3.4 compared with results obtained from equation 7.5, 7.10 and 7.12.

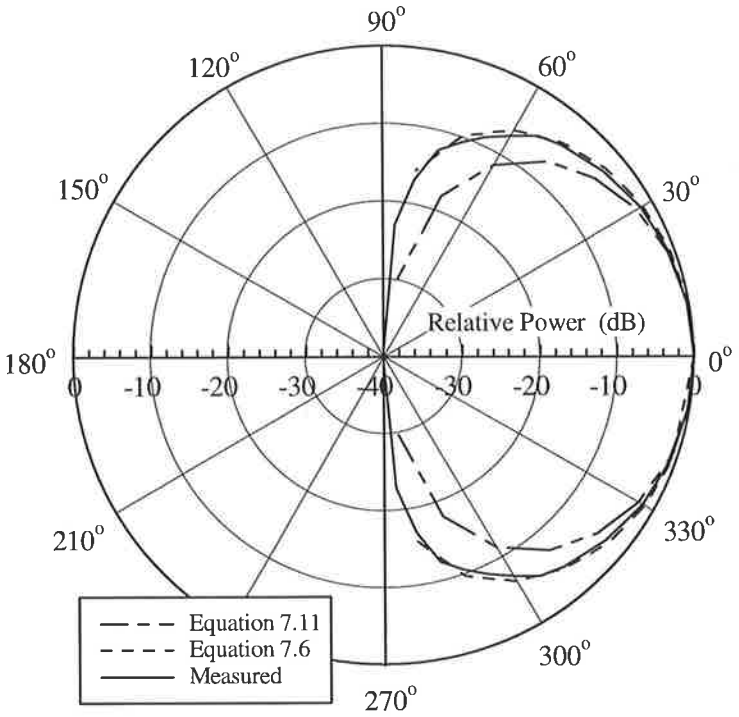

Figure 7.16: Measured far-field radiation pattern in the H-plane at 5.820 GHz for antenna element number 4 in Table 3.4 compared with results obtained from equation 7.6 and 7.11.

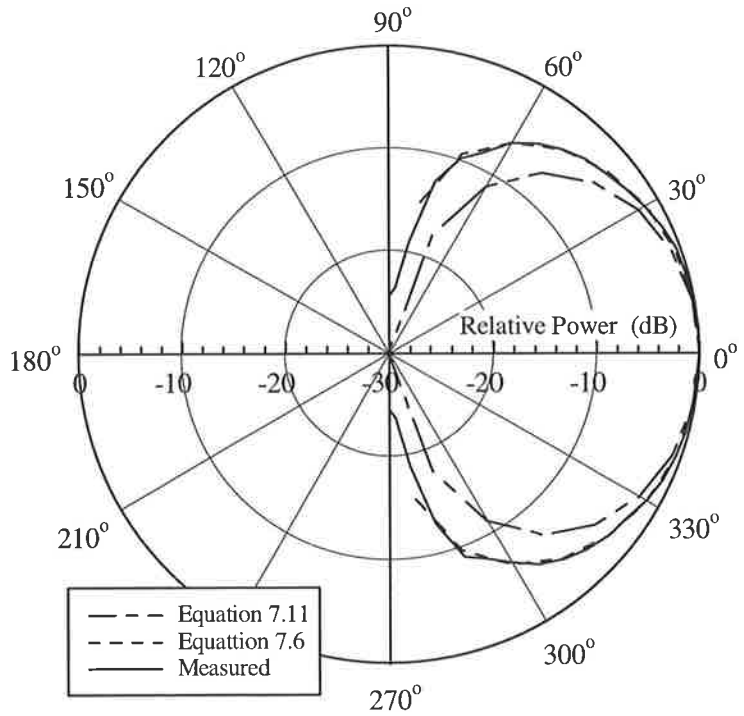

Figure 7.17: Measured far-field radiation pattern in the H-plane at 4.660 GHz for antenna element number 7 in Table 3.4 compared with results obtained from equation 7.6 and 7.11.

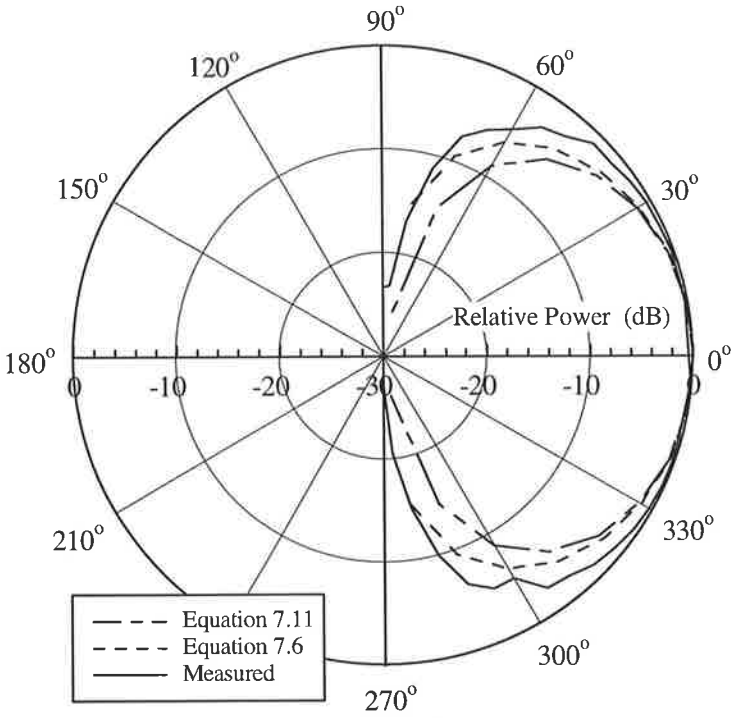

Figure 7.18: Measured far-field radiation pattern in the H-plane at 3.900 GHz for antenna element number 11 in Table 3.4 compared with results obtained from equation 7.6 and 7.11.

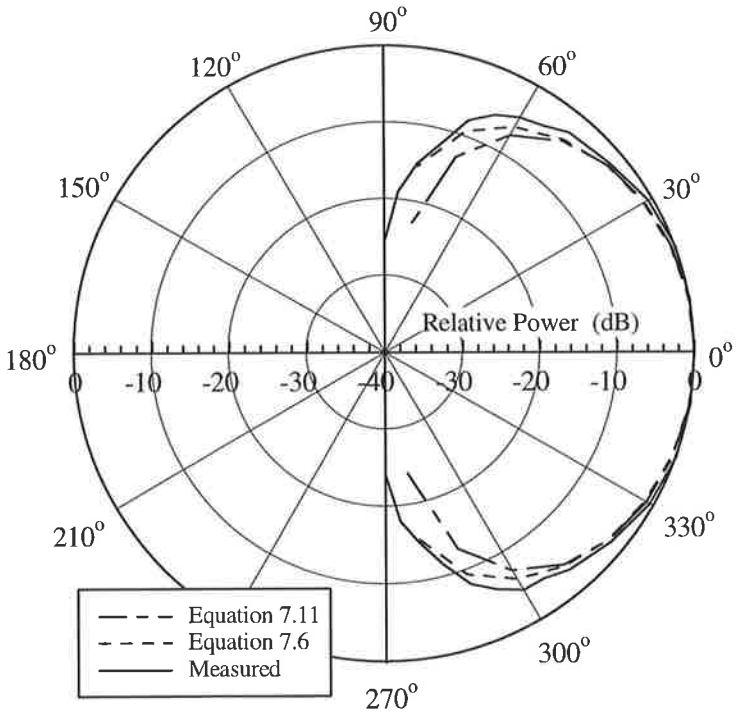

Figure 7.19: Measured far-field radiation pattern in the H-plane at 3.150 GHz for antenna element number 17 in Table 3.4 compared with the results obtained from equation 7.6 and 7.11.

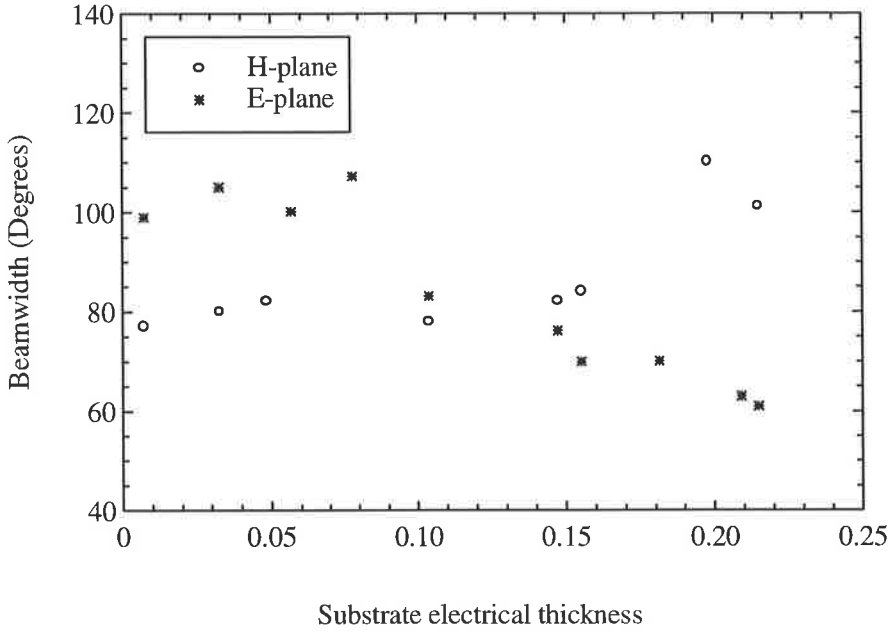

Figure 7.20: Beamwidths in the E- and H-planes versus substrate electrical thicknesses of all antenna elements considered for this chapter.

The dependence of half-power beamwidths in E- and H-plane of all antenna elements considered for this chapter on substrate electrical thicknesses is depicted in Figure 7.20.

Note that the E-plane beamwidth decrease with increasing substrate thicknesses, while the H-plane slightly increase.

In summary,

- the agreement between the calculated and measured result for patterns in the E-plane is very good, except for the noticeable effects of the diffraction at large angles from the z-axis due to the imperfect ground plane used in the measurements,
- the E-plane patterns of thick antenna elements exhibit variations below $\pm$ 60° that could be caused by surface wave and diffraction at the ground plane edges,
- the agreement between the calculated and measured result for patterns in the H-plane is also good,
- despite the use of a very thick substrate, the microstrip antenna element exhibited satisfactory and nearly symmetrical E- and H-plane radiation patterns.

7.7 Conclusion

A study of the far field radiation patterns in both the E- and the H-plane for antenna elements with substrates ranging in thickness from 0.0065 λ_d to 0.2284 λ_d and physical thickness from 0.17 mm to 12.81 mm, and operating over the frequency range 2.980 GHz to 8.450 GHz, has been carried out.

This chapter has verified the applicability of the TSM, the CM and the ESCM methods for computing the far field radiation patterns in both the E- the and H-plane of rectangular microstrip antenna elements. It has also demonstrated that the formulae based on the TSM and the CM are found to yield the radiation patterns in the E-plane of antenna elements with substrates in the order of $h \leq 0.0815\lambda_o$ with good accuracy, but they become increasingly inaccurate as the substrate thickness is increased. It has also been demonstrated that the applicability of the formulae based on the TSM and the CM for predicting the radiation patterns in the H-plane are not restricted to a certain material and substrate thicknesses. They are valid for all antenna elements introduced in this thesis.

The inadequate performance of the formulae based on the TSM, the CM and the ESCM for predicting the radiation patterns in the E-plane of antenna elements with thicker substrates prompt the necessity of modification of the formulae based eg on the TSM to fit the measured results. This has been done by taking into account the line extension. The modified equation 7.12 gives the radiation patterns in the E-plane for substrates in the range of $h \geq 0.0815\ \lambda_o$ correctly, as is evident from the close agreement between the calculated and measured results. Measurements confirmed the calculated results for all cases.

The effect of substrate thickness and the aspect ratio on the far-field radiation patterns for rectangular microstrip antenna elements has been shown to be quite significant. The characteristic of the pattern is changed for a different thickness of the substrate.

The relationship between half power beamwidth in the E- and H-plane and the substrate thicknesses has also been successfully investigated.

Chapter 8

Novel Broad-Band Miniaturised Rectangular Microstrip Antenna Elements

8.1 Introduction

The many desirable features of classical microstrip antennae are well known, as is the fact that narrow intrinsic bandwidth is perhaps the most serious of their limitations. This arises from the fact that the region under the patch is basically a thin resonant cavity with a high quality factor. The bandwidth that can be obtained with a single antenna element operating at the lowest mode is from less than 2% to 6% for thin substrates satisfying the criteria $h \leq 0.06\ \lambda_d$ for $2.22 \leq \varepsilon_r \leq 10.2$ and for VSWR of 2:1, as the results of Chapter 6 and [5, 89, 90] indicate. where λ_d denotes the wavelength in the dielectric substrate material at resonance, ε_r is the relative permittivity of the substrate and VSWR is the voltage standing wave ratio.

In electronic warfare, wideband radar and communication systems applications, the antenna must meet particularly demanding specifications. Physically, it must be low profile, light weight, able to withstand thermal stress and be extremely rugged. Moreover, it should neither protrude inwardly to disrupt the mechanical structure, nor disturb the aerodynamic flow across the skin of the platform. The electrical characteristics of the antenna must include high efficiency and wide frequency bandwidth, together with low side-lobes.

In recent years much research has been carried out on methods for impedance bandwidth enhancement, since the narrow bandwidth of the basic element is usually the dominant characteristic that may limit its application. Because of the low-profile geometry, the basic microstrip antenna element does not make very effective use of the entire volume of its enclosing sphere. Therefore, some of the available enhanced bandwidth design methods can be interpreted as either increasing the enclosing volume, eg., by using adjacent parasitic elements or as employing the enclosing spherical volume more effectively eg., by stacking patches. Note that the narrow bandwidth of the basic microstrip antenna element is not caused by the size of its enclosing volume, but by the thin grounded substrate. As a result, improved impedance bandwidth can only be achieved with

- larger size which leads to a larger enclosing sphere,
- greater complexity by making more effective use of the enclosing volume, or
- the introduction of loss which reduces the radiation efficiency.

Some of the methods for impedance bandwidth enhancement include [2, 5]:

- using a passive coplanar matching network [157, 158]
- by combining a patch radiator and an FET amplifier with an optically fed photodiode [159],
- by inclusion of transistors in the matching network to combine amplification with the matching function [160],
- with a circular or linear very narrow gap in the patch conductor around the feed point of a patch fed with a coax probe [161] (fabrication of the gap is problematic),
- using a two layer proximity-coupled design [162],
- using a stacked patch configuration [148, 163] with bottom patch fed a coaxial probe or microstrip feed line [164, 165] or aperture coupling [166],
- using the coplanar arrangement of a fed element with one or more parasitic patches 167, 168],
- by adding a 6 dB attenuator in series with a microstrip antenna [5],
- using a substrate with low unloaded quality factor, Q, [169] and
- using thick substrates [89, 90, 125, 132].

Note,

- if the substrate is not very thin, some consideration may have to be given to spurious radiation from the matching and tuning network,
- the network must be as close as possible to the radiating element in order to achieve best results of bandwidth.

The wider bandwidth is usually accomplished by using a thick substrate with low permittivity; yet there is a limit on the maximum useable substrate thickness such that surface waves will not be radiated. Here increasing the substrate thickness increases the excitation of surface waves, resulting in lowered efficiency and also bandwidth [90]. The design of the antennae is complicated by the added matching structures, diodes, shorting pins and their associated biasing structures. When a frequency greater than 10 GHz is used, the size of antenna elements becomes small, hence it is not possible to accommodate the diodes underneath each element. The stacked antennae, however, are thicker than those of single element and the low profile characteristics of such antennae is slightly compromised.

This Chapter introduces a novel broad-band miniaturised rectangular microstrip antenna element (or microstrip block antenna element) [81, 95-97] which consists of a metal patch on one side of a dielectric sheet in which the dielectric substrate is restricted to the same size as the metal patch, and a ground plane on the other side as shown in Figure 8.1. It is fed by a coaxial line from the back through the ground plane. It also reports on a simple and accurate design procedure based on the transmission line model and the cavity model for this antenna and presents the experimental and analytical results.

Measured data on the performance characteristics of the new antenna element is presented and compared with the characteristics of a conventional microstrip antenna element having the same dimensions. The results obtained from this technique are in good agreement with measurements.

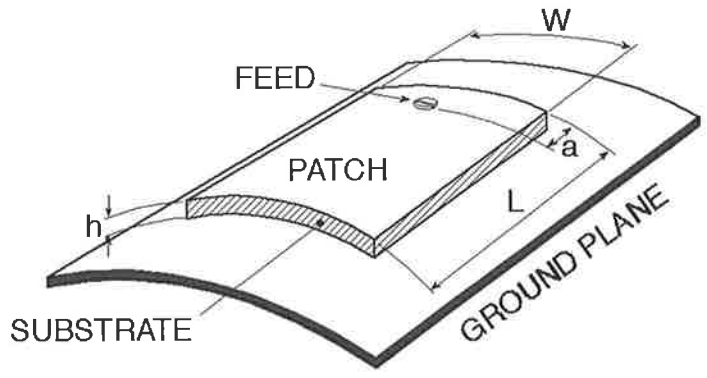

Figure 8.1: Configuration of a broad band microstrip antenna element with dimensional parameters.

Miniaturised antenna elements fitted to the surfaces of space borne vehicles have appropriate mechanical and thermal characteristics and do not result in any aerodynamic drag. Other advantages of these antennae are: the usual configuration with the antenna behind a radome is

eliminated completely, hence the typical pattern distortion effects caused by radomes will not occur, it is also simple to manufacture, and the materials are low cost compared with traditional solutions using high tolerance machining of metal, it requires less space and is light weight, it does not require different processing methods or modification for use on doubly curved surfaces, and it has wider bandwidth, higher gain and it can be mounted on and/or embedded into the bodies of a surface and space borne vehicles.

This antenna can be used as single antenna element or as an element of a large planar phased array, where single antenna or array size is a major concern.

8.2 Physical Properties

The following physical parameters must be considered and calculated in the process of designing a miniaturised rectangular microstrip antenna element: the length, the width, and the feed point location. The important physical parameters of such antenna elements are illustrated in Figure 8.1.

An accurate calculation of the input resonant resistance of an antenna element is necessary to provide a good match between the element and the feed point. This requires a thorough investigation of the antenna dimensions and feed location as well as their effect on the operating characteristics.

8.2.1 Element Width

The width, W, of the broad band miniaturised antenna element suitable for producing efficient operational properties is given by [81, 95-97]

$$W = 0.45\frac{c_o}{f_r\sqrt{\varepsilon_r}} \tag{8.1}$$

where c_o is the velocity of the electromagnetic waves in the free space and f_r is the resonant frequency.

8.2.2 Element Length

The resonant length of the broad-band miniaturised elements can be calculated by [81, 95-97]

$$L = \frac{c_o}{2 f_r \sqrt{\varepsilon_r}} = \frac{\lambda_o}{2\sqrt{\varepsilon_r}} \qquad (8.2)$$

where λ_o is the wavelength in free space.

8.2.3 Feed point Location

The miniaturised antenna element is excited from a coaxial feed whose inner conductor (standard 50 Ω feeding line) is fed from the inside through the dielectric material and connected to the outer copper conducting patch surface. The outer conductor is connected to the backplane. The inner conductor or probe perturbs the field inside the antenna, thus causing the element to radiate. The distance to the coaxial feed point from the nearest edge of the patch, **a**, is approximately one-third of the element length. This position of the feed probe provides an optimum impedance match.

8.3 Electrical Properties

8.3.1 Input Impedance

The input impedance, Z_{in}, of an antenna is an essential property which directly affects the efficiency of energy transfer to or from the antenna, as already discussed in Chapter 4. It varies according to antenna physical properties and, owing to its effects on the efficiency of energy transfer, should be gauged with a high degree of accuracy in order to provide a good match between the antenna element and its feed.

The input impedance of the broad-band miniaturised antenna elements may be given in terms of the loaded quality factor, and the inductive reactance of the probe as outlined in Chapter 4 [81, 95, 96, 97, 108] as

$$Z_{in} = \frac{R_{in}}{X} + jX_L \tag{8.3}$$

with

$$X = 1 - jQ_T\left(\frac{f_r}{f}\right) \tag{8.4}$$

where R_{in} is the input resistance at resonance, f the operating frequency of the antenna and Q_T is the total quality factor which includes all quality factors associated with conductor loss, dielectric loss and loss due to the radiated power. The Q_T can be calculated from equation 2.53.

The lumped series reactance, X_L may be approximated by [58].

$$X_L = \frac{R_o\, f_r\, h}{c_o} \ln\left(\frac{c_o}{d_o\, \pi\, f_r\, \sqrt{\varepsilon_r}}\right) \tag{8.5}$$

where $R_o = 120\pi\ \Omega$ is the vacuum medium resistance and d_o is the diameter of the probe.

As discussed in Chapter 4, the resonant input resistance for the broad band miniaturised antenna element can be given by [1, 81, 95, 96, 97]

$$R_{in} = \frac{Q_T}{\pi\, \varepsilon_o\, \varepsilon_r\, f_r} \frac{h}{WL} \cos^2\left(\frac{a\pi}{L}\right) \tag{8.6}$$

where $\varepsilon_o = 8.854\ 10^{-12}$ F/m, is the permittivity of vacuum.

8 3.2 Resonant Frequency

The resonant frequency of a microstrip antenna is defined to be the frequency at which the input impedance is purely real ($Z_{in} = R_{in}$) as discussed in Chapter 5. Experimentally, the resonance occurs

at a minimum in the measured VSWR corresponding to a minimum in the magnitude of the reflection coefficient.

The expression for the resonant frequency of the miniaturised antenna element is obtained using the rectangular cavity model assuming the cavity is driven at its fundamental TM_{10} mode as [17, 81, 95, 96, 97]

$$f_r = \frac{c_o}{2L\sqrt{\varepsilon_r}} \tag{8.7}$$

This expression has been used to calculate the resonant frequencies of these antenna elements.

8.3.3 Bandwidth

The impedance bandwidth of an antenna is related to the VSWR and a value of VSWR = 2 is a common standard as a range over which the bandwidth of microstrip antenna element can be evaluated. As discussed in Chapter 6, many antenna characteristics including gain, beamwidth, sidelobe level, polarisation, and impedance are determined by the frequency. The variation of any of these characteristics may limit the useful frequency band of the antenna. Therefore, the bandwidth must be determined accurately.

The return loss characteristics of the miniaturised antenna elements were measured to determine the resonant frequency and the bandwidth, similar to that in Figures 8.2 and 8.3. The following frequency relationship is defined to obtain the bandwidth of this antenna elements

$$BW = \frac{f_2 - f_1}{f_r} 100\% \tag{8.8}$$

where f_1 and f_2 are the lower and the upper band edges for S_{11} = -9 dB which is equivalent to VSWR = 2.1.

8.3.4 The Radiation Patterns

The radiation pattern describes the relative strength of the radiated field in various directions from the antenna. The source of radiation for the antenna is the electric field that is excited between the edges of the element and the ground plane. The far field E- and H-plane radiation patterns are calculated using the two slot model shown in Figure 7.1.

As discussed in Chapter 7, for two slots spaced a distance L apart, the E-plane radiation pattern may be expressed as [16, 81, 95, 96, 97]

$$F_\theta(\theta)\Big|_{\phi=0} = \frac{\sin\left(\frac{\pi h}{\lambda_o}\right)}{\frac{\pi h}{\lambda_o}\sin\theta}\cos\left(\frac{\pi L}{\lambda_o}\right) \qquad (8..9)$$

The H-plane radiation pattern is given by

$$E_\phi(\theta)\Big|_{\phi=\frac{\pi}{2}} = \frac{\sin\left(\frac{\pi W}{\lambda_o}\right)}{\frac{\pi W}{\lambda_o}\sin\theta}\cos\theta \qquad (8.10)$$

The half power beamwidth has also been obtained as the angular width between directions where the radiated field reduces to $(2)^{-0.5}$ of the maximum value, or the gain decreases by 3 dB.

8.4 Results and Discussion

The novel miniaturised microstrip antenna element is fabricated on a PTFE woven fibre glass microwave substrate material of relative permittivity ε_r = 2.55 as shown in Figure 8.1. The dimension and feed point location of these antenna elements are given in Table 8.1.

The return loss, input impedance, E- and H-plane radiation patterns and bandwidth are measured as a function of the dimension of the patch and the thickness of the dielectric substrate.

The return loss versus frequency of each of the new elements listed in Table 8.1 for the coaxial feed positioned 3.40 mm and 4.30 from the nearest edge of the elements are shown in Figures 8.2 and 8.3 respectively. This suggests that impedance matching of the feed usually occurs at approximately 1/3 of the element length. It is seen from the return loss plots that the resonance of the proposed elements occurs at 8.650 and 7.230 GHz, corresponding to an error of 0.17 % and 1.2 % in comparison with the predicted frequency using equation 8.7 respectively.

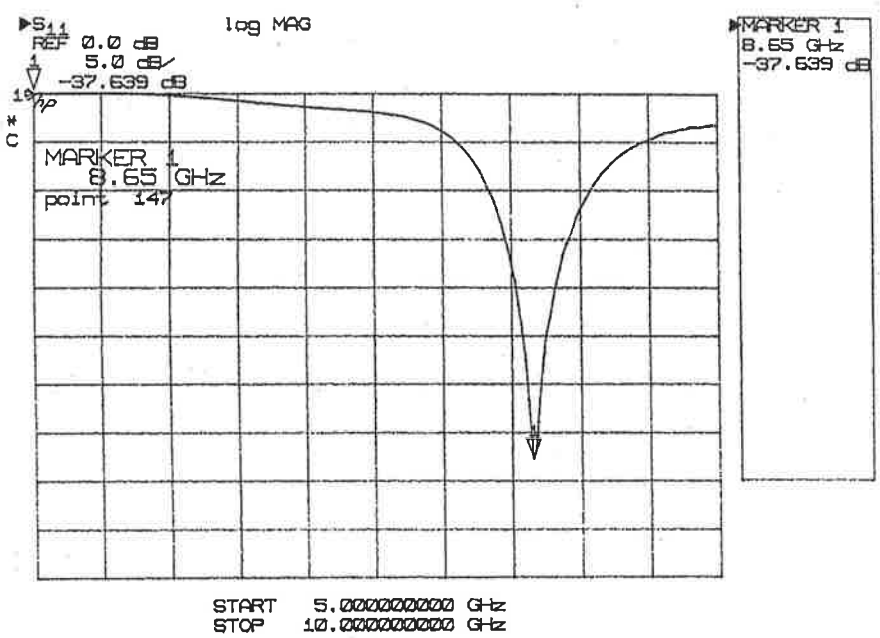

Figure 8.2: Measured return loss characteristics as a function of frequency of the broad antenna number 1 given in Table 8.1.

The fractional bandwidth is also determined from these return loss characteristics, as the frequency difference between points where the loss is -9dB and the maximum loss occurring at the centre frequency (resonant frequency), is the fractional bandwidth. Experimental results confirm that for VSWR = 2.1 bandwidth of the order of 9.3% and 9% are available with these antenna elements respectively compared to the 4.3% of a conventional microstrip antenna of the same dimension.

It is seen from the corresponding Smith charts of Figures 8.4 and 8.5 and Table 8.1, that a good impedance match has been obtained with the loops at the 50 Ω point for both miniaturised antenna

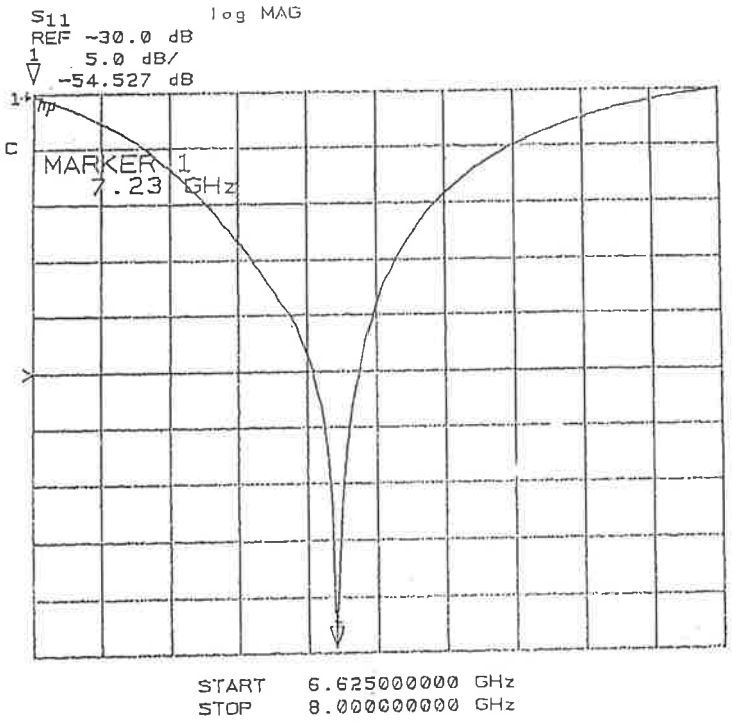

Figure 8.3: Measured return loss characteristics as a function of frequency of the broad antenna number 2 given in Table 8.1.

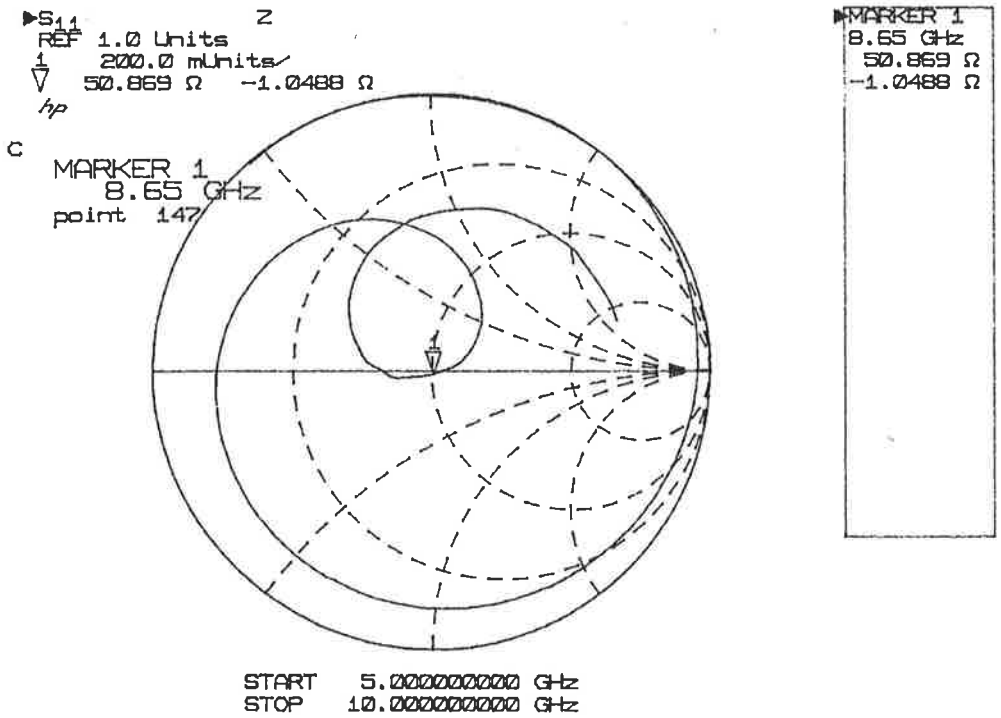

Figure 8.4: Measured input impedance characteristics as a function of frequency of the broad antenna element number 1 in Table 8.1.

elements. The measured input resistances at resonant frequencies of both elements are 50.8 and 50 Ω, corresponding to an error of 3 % and -2%, in comparison with the calculated resistances using equation 8.6 respectively. The results are given in columns nine and ten of Table 8.1. These discrepancies are again attributable to small differences in the element dimensions and feed point locations and secondly, to minor variations in ε_r.

The E-plane radiation patterns for both antenna elements were measured respectively at 8.650 and 7.230 GHz and compared with results obtained from equation 8.9. The excellent agreement between the results obtained from this equation and the measured results are easily seen in Figures 8.6 and 8.7.

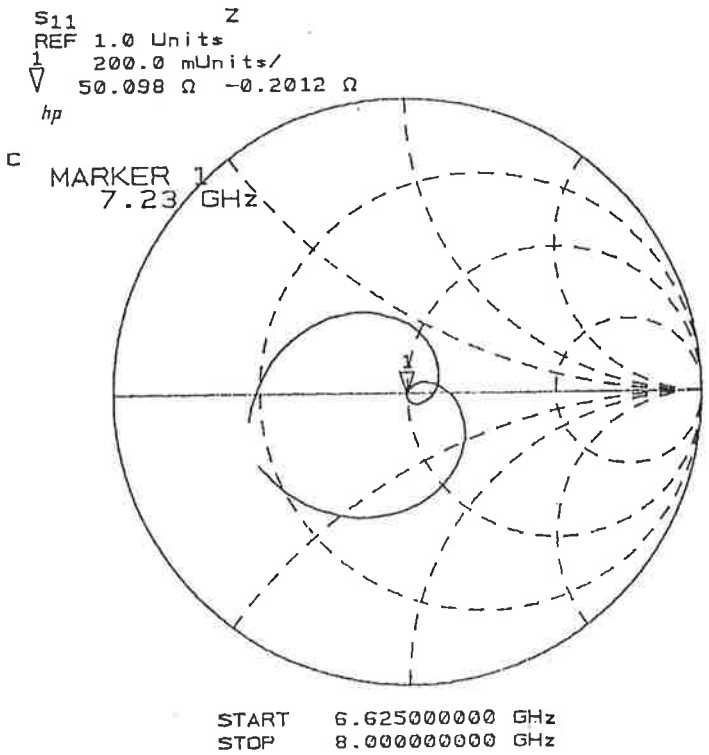

Figure 8.5: Measured input impedance characteristics as a function of frequency of the broad antenna element number 2 in Table 8.1.

The H-plane radiation patterns for both antenna elements were measured at 8.650 GHz and compared with results obtained from equation 8.10. The excellent agreement between the results obtained from this formula and the measured results are easily seen in Figure 8.8.

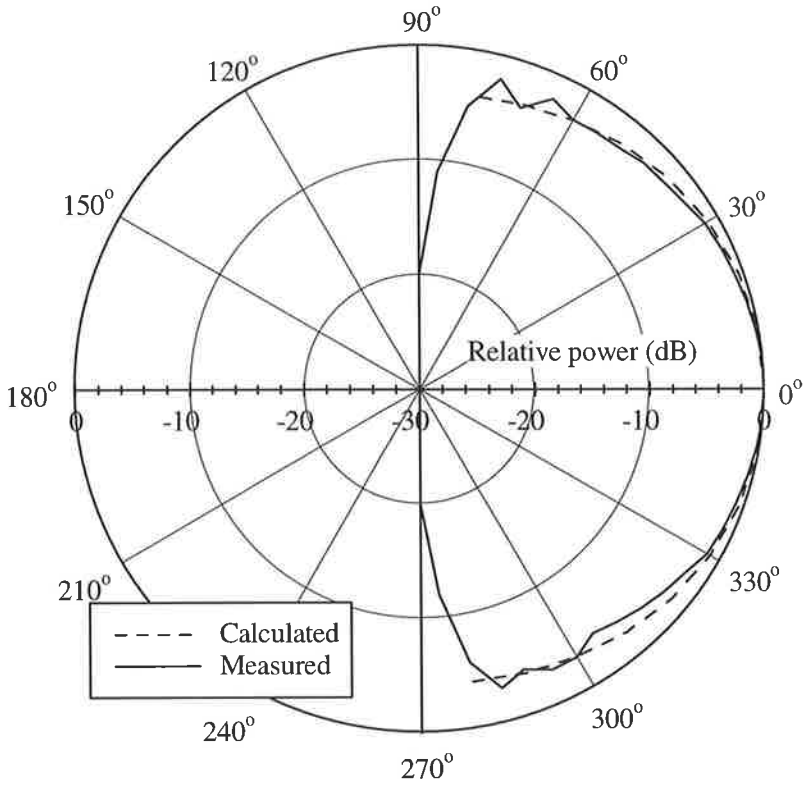

Figure 8.6: Measured far-field radiation pattern in the E-plane at 8.650 GHz for antenna element number 1 in Table 8.1 compared with results obtained from equation 8.9.

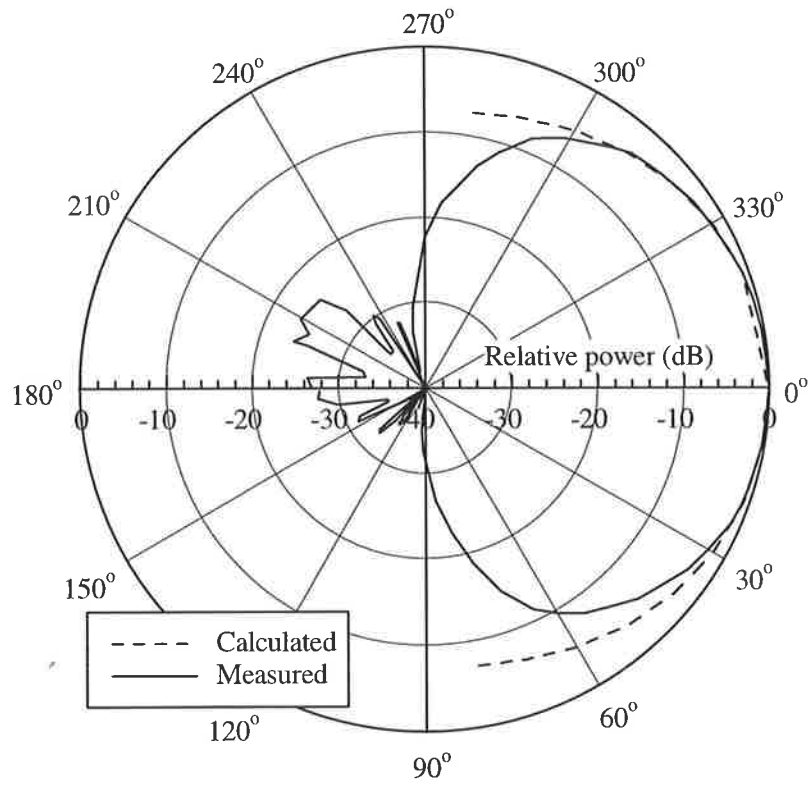

Figure 8.7: Measured far-field radiation pattern in the E-plane at 7.230 GHz for antenna element number 2 in Table 8.1 compared with results obtained from equation 8.9.

Table 8.1 Comparison of physical properties for the novel and conventional antenna elements

	L (mm)	W (mm)	a (mm)	h (mm)	Measured f_r (GHz)	Calculated f_r (GHz)
Block Nr. 1	10.00	9.80	3.40	1.63	8.650	8.635
Block Nr. 2	13.15	11.9	4.30	1.58	7.230	7.143
Conventional microstrip element	13.15	11.9	4.30	1.58	7.100	7.143

Cont.

	Measured R_{in} (Ω)	Calculated R_{in} (Ω)	Bandwidth %	E-plane Beamwidth (Degrees)	H-plane Beamwidth (Degrees)
Block Nr. 1	50.8	49.3	9.3	91	79
Block Nr. 2	50.0	51.0	9.0	77	N/A
Conventional microstrip element	50.0	50.0	4.3	78	N/A

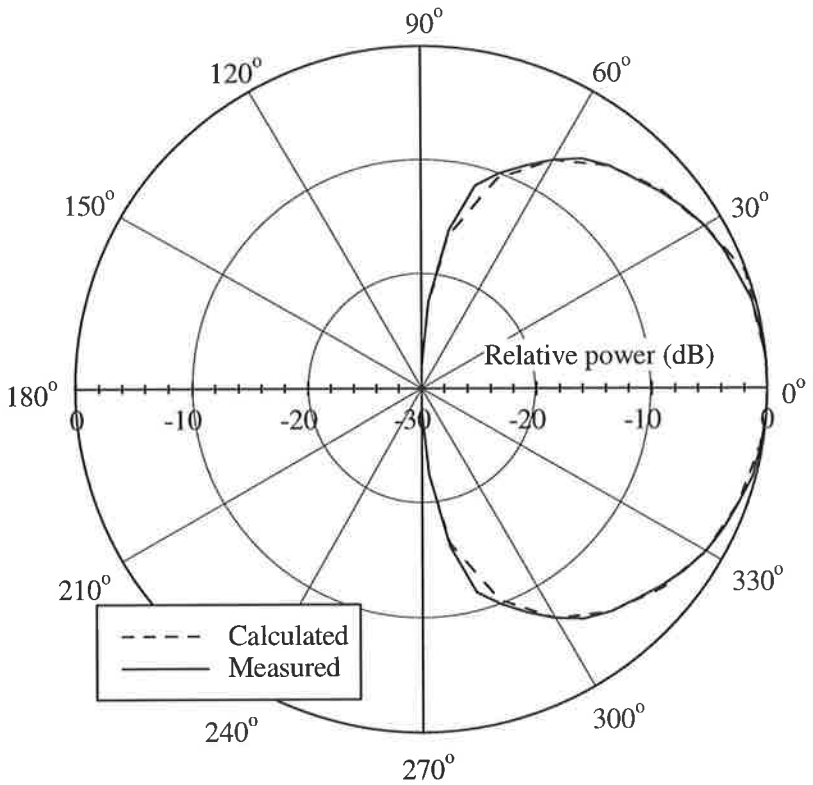

Figure 8.8: Measured far-field radiation pattern in the H-plane at 8.650 GHz for antenna element number 1 in Table 8.1 compared with results obtained from equation 8.10.

In addition, accurate measurement of far field radiation patterns involve the consideration of a number of factors, such as physical dimensions, operational frequency band and the operational environment. The measured half-power beamwidth at resonant frequency of each of these antenna elements are respectively 91° and 76°.

The results obtained for the bandwidth show that using a miniaturised antenna element is an excellent way of widening the bandwidth. An investigation of the far field radiation patterns indicates that the increased bandwidth is obtained without any pattern degradation.

A comparison has been made between the proposed antenna elements and a conventional microstrip antenna element of the same dimension to highlight the merit of the former in respect of bandwidth. The results are listed in Table 8.1.

8.5 Conclusion

A novel broad-band miniaturised rectangular microstrip antenna element has been developed, designed and implemented. Design details, analysis, calculations and experimental observations of this antenna element have been discussed. The experimental results of these antenna elements reveal that

- their bandwidth can be broadened to as high as 9.3% which is 2.16 fold the bandwidth of a conventional microstrip antennae having the same patch dimensions,
- they are capable of very good performance with regard to important design parameters,
- their overall reduction in the size is as high as 70% of a corresponding rectangular patch antenna,
- they are very simple to manufacture and are very economical,
- they are capable of being mounted on and/or embedded into the bodies of surface and space-borne vehicles,
- they can be used as single antenna or in an array environment.

Among the important contributions of the work described in this chapter are:

- The review of some of the more useful practical techniques for microstrip antenna bandwidth enhancement.

- The introduction, design and implementation of a novel miniaturised rectangular microstrip antenna element which may also be called microstrip block antenna element.

- The development of an accurate and computationally efficient method for the analysis of these antenna elements.

- Discovery of the effects of the reduction size of substrate material to the same size as the metal patch.

- The development of a broad-band antenna by using a single layer of substrate and a single feed point.

The analysis that has been developed and applied takes account of all the physical parameters of the antenna, and has revealed that this antenna has the potential to offer excellent performance characteristics.

The research presented in this chapter has therefore, elucidated engineering design opportunities for a novel broad-band antenna element not previously available.

Chapter 9

A Novel Dual-Band Miniaturised Rectangular Microstrip Antenna Element

9.1 Introduction

A dual-band antenna is useful in situations where it is required to operate in two distinct frequencies which may be too far apart for a conventional microstrip antenna to perform efficiently at both frequencies.

The search for new microstrip antenna configurations for dual frequency operation has been a dominant feature of recent research where several methods of obtaining dual-band operations have been developed and discussed in the literature. Some of these methods include

- multilayer patches [170 - 173],
- stacked patches [145, 173 - 176],
- terminated microstrip patch radiators [176],
- parasitic elements coupled to the main patch [145, 168],
- a single layer rectangular patch loaded by two slots which are etched close to the radiating edges [166],
- disc resonant radiators with small tabs attached to the edge [177],
- dual-band microstrip antennae with reactive loading [178],
- log-periodic or quasi-log periodic antennae [138, 179],

- patch antenna with a spur-line band-stop filter [180],
- patch antenna with an inclined slot [181,
- patch antenna with inhomogeneously filled dielectric substrate [182],
- reactively loaded patches with varactor diodes [183] short pins (posts) [184] or optically controlled pin diodes [185],
- stagger-tuned resonators developed either to perform dual frequency operation or to increase the bandwidth [186].

Unfortunately, there are some disadvantages associated with each of these methods, such as (once they are designed and etched):

- The design of the patches is complicated by the added components such as varactor diodes, optically controlled pin diodes etc. and their associated biasing circuit. For high frequencies (eg frequencies greater 10 GHz), the patch sizes are small and it is difficult to accommodate the diodes and shorting posts underneath each patch. In addition, the precise positions of shorting posts are also important.
- The added components in design multiply for an array consisting of a large number of elements.
- The multi layer and stacked structures are thicker than the single patch and the low profile characteristics of the microstrip antenna are slightly compromised. These structures bring problems in the design and manufacture stages along with an increase in height. In addition, increasing the substrate thickness increases the excitation of surface waves resulting in lowered efficiency.

These are just a few of the attempts already made to perform dual frequency operational microstrip antennae. A closer investigation of these examples, however, reveals that it is still desirable to obtain a dual frequency antenna element without increasing either its height or the size, or adding any component.

The analysis design, fabrication and testing of a novel dual-band microstrip antenna resonating at frequencies 6.850 and 7.190 GHz is introduced and discussed in this chapter. It consists of a metal patch on one side of a dielectric sheet in which the dielectric substrate is restricted to the same size as the metal patch, and a ground plane on the other side, Figure 8.1. The antenna is fed by a coaxial line from the back through the ground plane [81, 82, 95, 96, 97]

A novel numerical technique is also developed for the dimensions and operational properties for these antennas. Measured performance data of miniaturised antenna elements are presented and compared with the calculated results. Very good agreement between theory and experiment was achieved.

In many applications, only a few distinct frequency bands are needed, rather than a continuous spectrum of operating frequency such as in the Global Positioning System (GPS). The novel dual-band miniaturised antenna element occupies a minimum space. It can be distributed and/or embedded over or in the surface of surface and space borne vehicles, eg. aircraft, ships, missiles, etc. It is also applicable to satellite systems where two channels are needed to receive/transmit the telecommand and telemetry signals. Phased arrays based on these antennas can be easily designed for use in Space-Borne Imaging or Synthetic-Aperture and Secondary Surveillance Radar systems.

9.2 Physical Properties

The following physical parameters must be considered and calculated in the process of designing a dual band miniaturised microstrip antenna element: the length, L, the width, W, and the feed point location, a. The important physical parameters of this element are illustrated in Figure 8.1. These factors will be discussed individually in the following sections.

9.2.1 Element Width

The width of the miniaturised dual band antenna element suitable for producing efficient operational properties can be given as in Chapter 3 and [81]

$$W = \sqrt{h\lambda_d}\left[\ln\left(\frac{\lambda_d}{h}\right) - 1\right] \tag{9.1}$$

where h is the substrate thickness and λ_d is the wavelength in the dielectric substrate material.

9.2.2 Element Length

The length of the dual-band miniaturised microstrip antenna element suitable for producing efficient operational properties can be calculated from [18]

$$L = 0.49 \frac{\lambda_o}{\sqrt{\varepsilon_r}} \tag{9.2}$$

where λ_o is the free-space wavelength and ε_r is the relative permittivity of the substrate.

9.2.3 Feed Point Location

The dual-band miniaturised microstrip antenna element is excited from a coaxial feed whose inner conductor (standard 50 Ω feeding line) is fed from the inside through the dielectric material and connected to the outer copper conducting surface. The outer conductor is connected to the back plane. This configuration is shown in Fig. 8.1. The inner conductor or probe perturbs the field inside the antenna, thus causing this antenna element to radiate. The distance to the coaxial feed point from the nearest edge of the patch, **a**, is approximately one-third of the element length. This position of the feed probe provides an optimum impedance match.

9.3 Electrical Properties

9.3.1 Input Impedance

The input resistance at both frequencies of the antenna elements can be obtained from Chapters 4 and 8 [81, 82, 95, 96, 87]

$$R_{in} = \frac{Q_T}{\pi \varepsilon_o \varepsilon_r f_r} \frac{h}{WL} \cos^2\left(\frac{a\pi}{L}\right) \tag{9.3}$$

where ε_o =8.854 10^{-12} F/m, is the permittivity of vacuum. The factor Q_T is the total of all quality factors associated with antenna losses, which include conductor loss, dielectric loss and loss due to the radiated power. It can be calculated from formula 2.53.

9.3.2 Resonant Frequency

The resonant frequency of a microstrip antenna is defined to be the frequency at which the input impedance is purely real ($Z_{in} = R_{in}$), as discussed in Chapters 5 and 8. Experimentally, the resonance occurs at a minimum in the measured voltage standing wave ratio, VSWR, corresponding to a minimum in the magnitude of the reflection coefficient.

The frequency of the first resonance is calculated using the transmission line model [1, 81, 82]

$$f_{r1} = \frac{c_o}{2(L + 2\Delta W)\sqrt{\varepsilon_{ew}}} \tag{9.4}$$

where ε_{ew} is the effective relative permittivity of the substrate as obtained from formula 2.10 and ΔW is the line extension obtained from formula 2.11.

The second resonant frequency is calculated using the rectangular cavity model assuming the cavity is driven at its fundamental TM_{10} mode as discussed in reference 17 and Chapter 5

$$f_{r2} = \frac{c_o}{2L\sqrt{\varepsilon_r}} \tag{9.5}$$

Note that the values of both frequencies depend strongly on the element length and the permittivity of the dielectric material.

9. 3.3 The Radiation Patterns

The radiation pattern describes the relative strength of the radiated field in various directions from the antenna. The source of radiation for the antenna is the electric field that is excited between the edges of the element and the ground plane. The far field E-plane radiation pattern is calculated

using the two slot model shown in Figure 7.1 or the cavity model as discussed in Chapters 7 and 8. It may be expressed as [16, 81, 82, 95, 96, 97]

$$F_\theta(\theta)\Big|_{\phi=0} = \frac{\sin\left(\frac{\pi h}{\lambda_o}\right)}{\frac{\pi h}{\lambda_o}\sin\theta}\cos\left(\frac{\pi L}{\lambda_o}\right) \tag{9.6}$$

The half power beamwidth has also been obtained as the angular width between directions where the radiated field reduces to $(2)^{-0.5}$ of the maximum value, or the gain decreases by 3 dB.

9.4 Results and Discussion

An element was fabricated by cutting a 11.93 mm by 13.19 mm block of a PTFE woven fibre glass laminate with a nominal relative permittivity of 2.55, dielectric loss tangent, tanδ, of 0.002, and thickness of 1.58 mm. The dimensions and feed point location are listed in Table 9.1. The return loss characteristics as a function of the frequency is shown in Figure 9.1. It is seen from this figure that the dual-band frequencies of the element occur at 6.850 and 7.190 GHz. The first and second resonant mode frequencies correspond to an error of 1.69% and 0.95% respectively in comparison to the predicted result using equations 9.4 and 9.5. These small discrepancies are attributed to small differences in element length and secondly, to minor variations in the relative dielectric constant of the substrate material.

It is seen from the corresponding Smith chart of Figure 9.2 and Table 9.1 that the measured input resistances at both frequencies of the dual-band element are 56 and 52 Ω. The discrepancies between the measured results and those obtained from equation 9.3 are 2.6% and -0.2%, respectively. These discrepancies are again attributable to small differences in the element widths and feed point locations and secondly, to minor variations in ε_r.

The far-field radiation pattern in the E-plane of the dual-band antenna element were measured at 7.190 GHz and compared with calculated results. The excellent agreement between the results obtained from equation 9.6 and the measured results can be observed in Figure 9.3. In this case the pattern was measured for angles from -180° to 180°. Despite the reduction in the size of substrate

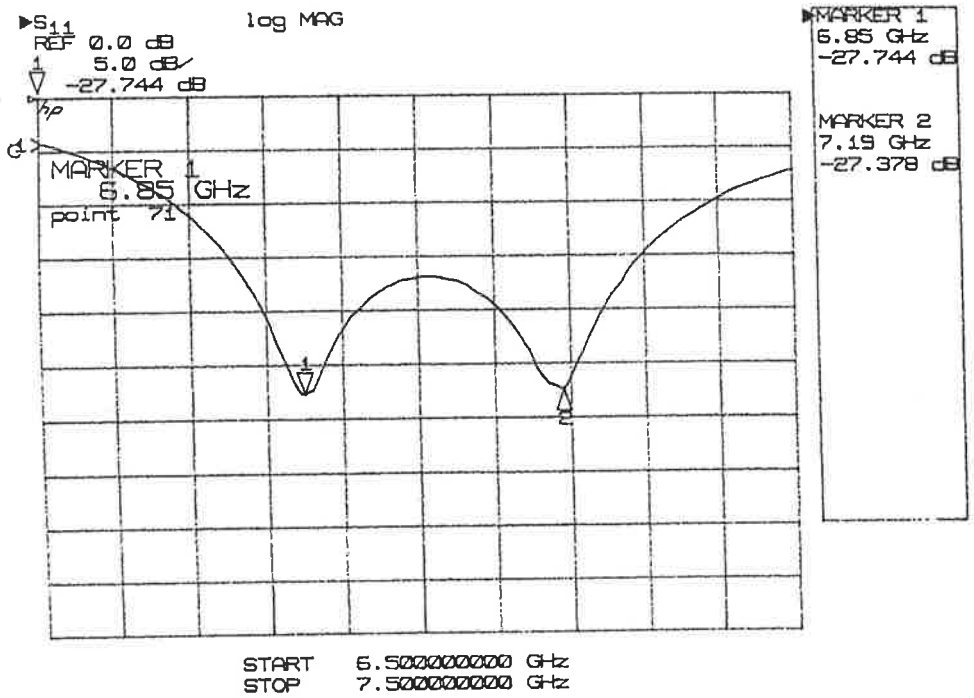

Figure 9.1: Measured return loss characteristics as a function of frequencies of the dual-band microstrip antenna element.

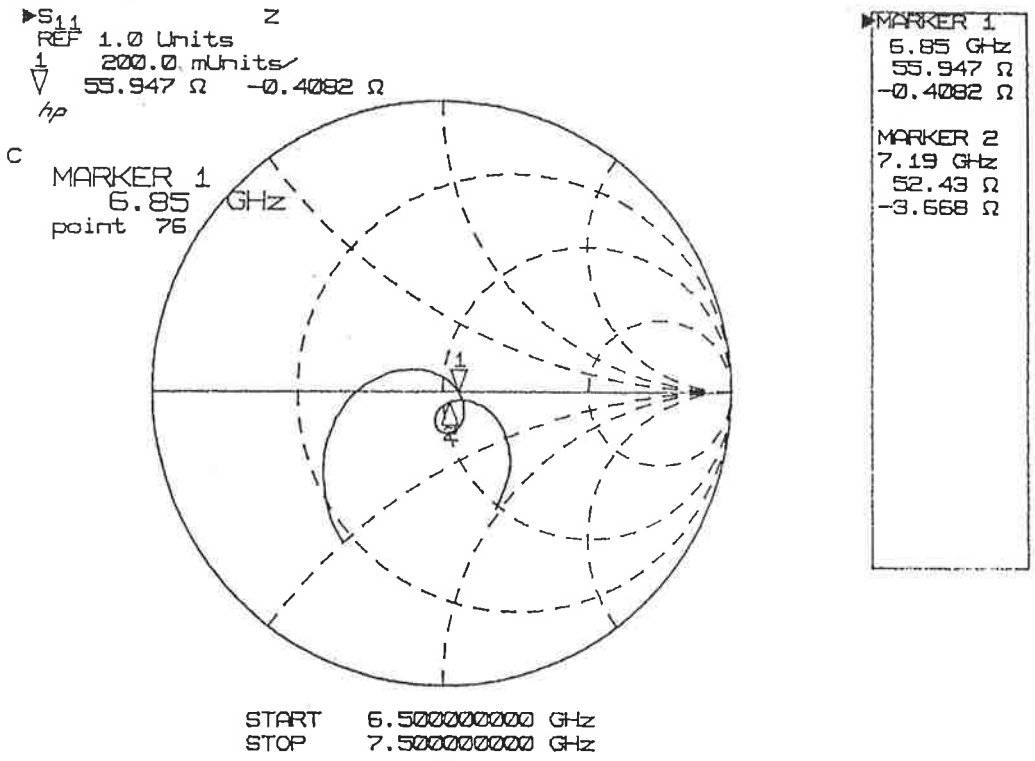

Figure 9.2: Measured input impedance characteristics as a function of frequencies of the dual-band microstrip antenna element.

material to the same size as the metal patch and the use of a 700 mm by 700 mm small ground plane, the dual antenna element exhibited a very good and symmetrical E-plane radiation pattern as can be observed in Figure 9.3. In addition, accurate measurement of far field radiation patterns involve the consideration of a number of factors, such as physical dimensions, the operational frequency band and the operational environment. The measured half-power beamwidth at the second frequency is 80° and the gain is 7dBi ±1.5dB. Note, that Table 9.2 presents the measured and calculated frequencies of the first mode, f_{r1}, and second mode, f_{r2}, the input resistances of the first mode, R_{in1}, and the second mode, R_{in2}.

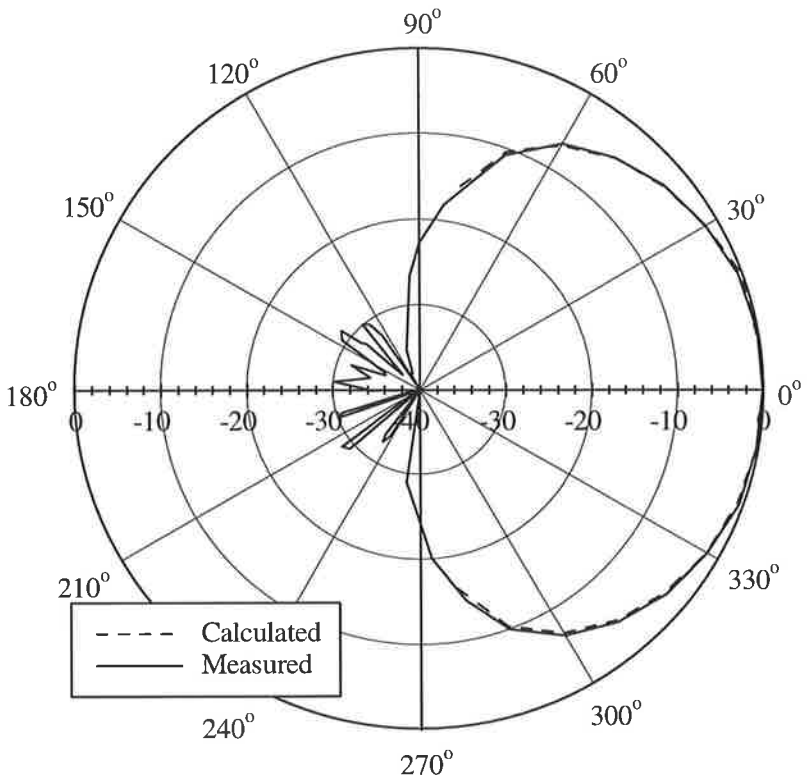

Figure 9.3: Measured H-plane radiation pattern for the dual-band microstrip antenna element at 7.190 GHz.

Table 9.1: Measured and calculated physical and electrical characteristics for the dual-band microstrip antenna element.

L (mm)		W (mm)		a (mm)		h (mm)	
13.19		11.93		4.29		1.58	
measured f_r (GHz)		calculated f_r(GHz)		measured R_{in} (Ω)		calculated R_{in}(Ω)	
f_{r1}	f_{r2}	f_{r1}	f_{r2}	R_{in1}	R_{in2}	R_{in1}	R_{in2}
6.850	7.190	6.734	7.525	56	52.4	57.5	52.3

9.5 Conclusion

A novel dual-band miniaturised rectangular microstrip antenna element which performs efficiently at two distinct frequencies has been developed, designed, manufactured and tested.

Design details, analysis, calculations and experimental observations of this antenna element have been discussed. The experimental results of this antenna elements reveal that

- this antenna operates at two distinct frequencies which are 340 MHz apart,
- they are capable of good performance with regard to important design parameters,
- their overall reduction in the size (area) is as high as 70% of a corresponding rectangular patch antenna,
- they are capable of being mounted on and/or embedded into the bodies of a surface and space borne vehicles,
- they are very simple to manufacture and are very economical.

Among the important contributions of the work described in this chapter are:

- The review of some of the more useful practical techniques of obtaining dual-band operations.
- The introduction, design, implementation and measurement of a novel miniaturised rectangular microstrip antenna element which may also be called dual microstrip block antenna element.
- The development of an accurate and computationally efficient method for the analysis of these antenna elements.
- Discovery of the effects of the reduction in size of substrate material to the same size as the metal patch.

- The development of a dual-band operation by using a single layer of substrate and a single feed point.

The analysis that has been developed and applied takes account of all the physical parameters of the antenna, and has revealed that this antenna has the potential to offer excellent performance characteristics.

The research presented in this chapter has therefore, elucidated engineering design opportunities for a novel miniaturised rectangular microstrip antenna element not previously available.

Chapter 10

A Novel Miniaturised Microstrip Ring Antenna Element

10.1 Introduction

The search for novel microstrip antenna designs with wider bandwidth and better physical and operational properties has been a dominant feature of the literature, because conventional microstrip antenna designs inherently have very a narrow impedance bandwidth [1 - 11], Chapters 6 and 8. The typical size of conventional microstrip antennae can be quite large for some surface and space borne vehicle applications. A study of published microstrip antenna designs reveals that it is still desirable to reduce size without sacrificing performance properties.

This Chapter describes a novel design for a broad-band miniaturised microstrip ring antenna, consisting of a metal ring on one side of a dielectric sheet, in which the dielectric substrate is restricted to the same size as the metal ring, and a ground plane on the other side, like that shown in Figure 10.1. The ring antenna is fed by a coaxial line from the back through the ground plane.

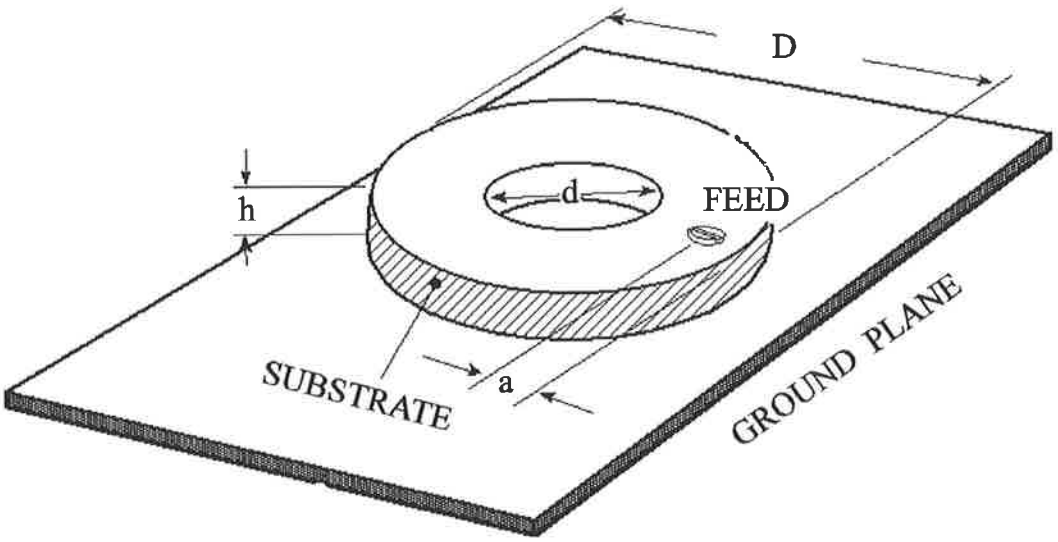

Figure 10.1: Configuration of a miniaturised microstrip ring antenna element with dimensional parameters.

Also reported is a simple and accurate design procedure for this antenna, together with experimental and analytical results [84, 95].

This antenna occupies a minimum space, and can be distributed or embedded over or in the surface of surface and space borne vehicles.

The design, fabrication, testing and analysis of a novel miniaturised microstrip ring antenna is described. A novel analytical technique is developed for the dimensions and operational properties for this antenna. Measured performance data of the ring antenna is presented and compared with calculated results. Very good agreement between theory and experiment was achieved.

10.2 Physical Properties

The goal of this section is to determine the dimensions of the ring antenna element necessary to satisfy the specific performance characteristics over the required frequency band. The required inner and outer diameters and feed point location have been obtained by a trial-and-error design

technique, because there are no formulae to calculate them. The design procedure takes the line extension into account.

10.2.1 The Inner Diameter

The resonant inner diameter of the ring antenna suitable for producing efficient operational properties can be expressed by [84, 95] as

$$d = \frac{\lambda_d}{2} - h \tag{10.1}$$

where h is the thickness of the substrate and λ_d the wavelength in the dielectric substrate given by

$$\lambda_d = \frac{c_o}{f_r\sqrt{\varepsilon_r}} \tag{10.2}$$

where c_o is the velocity of the electromagnetic waves in free space, f_r the resonant frequency and ε_r the relative dielectric constant of the substrate. The open-end extension due to the fringing effects is incorporated into equation 10.1. Here the line extension is assumed to be the same as the substrate thickness, h.

10.2.2 The Outer Diameter

The outer diameter of the ring antenna suitable for producing efficient operational properties can be calculated from [84, 95]:

$$D = \frac{\lambda_d}{2} + \frac{d}{2\sqrt{\varepsilon_r - 1}} \tag{10.3}$$

where D is the outer diameter of the ring.

10.2.3 Feed Point Location

The miniaturised ring antenna is excited from a coaxial feed whose inner connector (standard 50 Ω feeding line) is fed from the inside through the dielectric material and connected to an outer copper conducting surface. The outer conductor is connected to the back plane. This configuration is shown in Figure 10.1. The distance **a** between the coaxial feed probe and the nearest edge of the ring antenna is obtained from [84, 95]

$$a \approx \frac{W}{2\sqrt{\pi}} \tag{10.4}$$

where W is the width of the ring which can be given as

$$W = D - d \tag{10.5}$$

This position of the feed probe provides an optimum impedance match.

10.3 Electrical Properties

10.3.1 Resonant Frequency

As discussed in Chapters 5, 8 and 9, the resonant frequency is defined to be the frequency at which the Voltage Standing Wave Ratio, VSWR, corresponds to a minimum in the magnitude of the reflection coefficient (return loss). The resonant frequency is calculated using the transmission line model [84, 95]

$$f_r = \frac{c_o}{2\pi W \sqrt{\varepsilon_{ew} - 1}} \tag{10.6}$$

where ε_{ew} is the effective relative permittivity as a function of the ring width W and obtained from equation 2.10.

10.3.2 Input Impedance

Similar to Chapters 4, 8 and 9 the resonant input resistance can be obtained from [84, 95]

$$R_{in} = \frac{Q_T}{\pi \varepsilon_o \varepsilon_r f_r} \frac{h}{A} \cos^2\left(\frac{a\pi}{W}\right) \tag{10.7}$$

where A is the surface area of the ring antenna

$$A = 2\pi(R^2 - r^2) \tag{10.8}$$

The factor Q_T is the total of all quality factors associated with antenna losses, which includes conductor loss, dielectric loss and loss due to radiated power. It is given in Chapters 2 and 4 as

$$Q_T = \left(Q_r^{-1} + Q_c^{-1} + Q_d^{-1}\right)^{-1} \tag{10.9}$$

the contribution of the radiation is given by [137]

$$Q_r = \frac{\lambda_o}{4h}\sqrt{\varepsilon_{ew}} \tag{10.10}$$

where λ_o is the free space wavelength.

The loss in the dielectric, Q_d, is the same as the loss tangent, $(\tan\delta)^{-1}$, of the substrate material. The loss in the conductors is given by [134]

$$Q_c = 0.786 \frac{Z_{ow}}{P_w} h(\text{mm}) \sqrt{f_r(\text{GHz})} \tag{10.11}$$

P_W is given for W/h>2

$$P_w = \frac{2\pi\left[\frac{W}{h} + \frac{W}{\pi h}\left(0.94 + \frac{W}{2h}\right)^{-1}\right]\left(1 + \frac{h}{W}\right)}{\left\{\frac{W}{h} + \frac{2}{\pi}\ln\left[2e\pi\left(0.94 + \frac{W}{2h}\right)\right]\right\}^2} \qquad (10.12)$$

where Z_{ow} is the characteristic impedance of an air-filled microstrip line of width W derived from the characteristic impedance of a substrate filled line of width W given in equation 2.4 by setting $\varepsilon_r = 1$. The resulting equation for W/h>3.3 is

$$Z_{ow} = 60\pi\left[\frac{W}{2h} + 0.903 + \frac{1}{\pi}\ln\left(0.94 + \frac{W}{2h}\right)\right]^{-1} \qquad (10.13)$$

Note that the width of the ring was assumed to be equal to width of the stripline in equations 10.12 and 10.13.

10.3.3 The Radiation Patterns

The far field radiation patterns in E- and H-plane are calculated using the two slot model shown in Figure 2.4. For two slots spaced a distance πW apart, the E-plane radiation pattern may be expressed for $-90° < \phi < 90°$ as [84, 95]

$$F_E(\phi) = \frac{\sin\left(\frac{\pi h}{\lambda_o}\right)}{\frac{\pi h}{\lambda_o}\sin\phi}\cos\left(\frac{\pi(\pi W)}{\lambda_o}\right) \qquad (10.14)$$

and for the H-plane radiation pattern

$$E_\phi(\theta)\Big|_{\phi=\frac{\pi}{2}} = \frac{\sin\left(\frac{\pi D}{\lambda_o}\sin\theta\right)}{\frac{\pi D}{\lambda_o}\sin\theta}\cos\theta \qquad (10.15)$$

The half power beamwidth has also been obtained as the angular width between directions where the radiated field reduces to $(2)^{-0.5}$ of the maximum value, or the gain decreases by 3 dB.

10.4 Results and Discussion

An antenna was fabricated by cutting a ring of outer diameter 17.01 mm and inner diameter 10.98 mm of a PTFE woven fibre glass laminate with a nominal dielectric constant, ε_r, of 2.55, dielectric loss tangent, tanδ, of 0.002, and thickness of 1.63 mm. Figure 10.1 shows the important physical parameters of this antenna element. The measured return loss characteristics of the ring antenna versus frequency for a coaxial feed positioned 1.7 mm from the nearest edge of the element is shown in Figure 10.2. Note from this plot that resonant frequency of the ring occurs at 7.450 GHz, corresponding to an error of 2%, in comparison with the calculated resonant frequency from equation 10.6. This small error is attributed once again to a small differences in element physical parameters and to a minor variation in the relative permittivity of the substrate material.

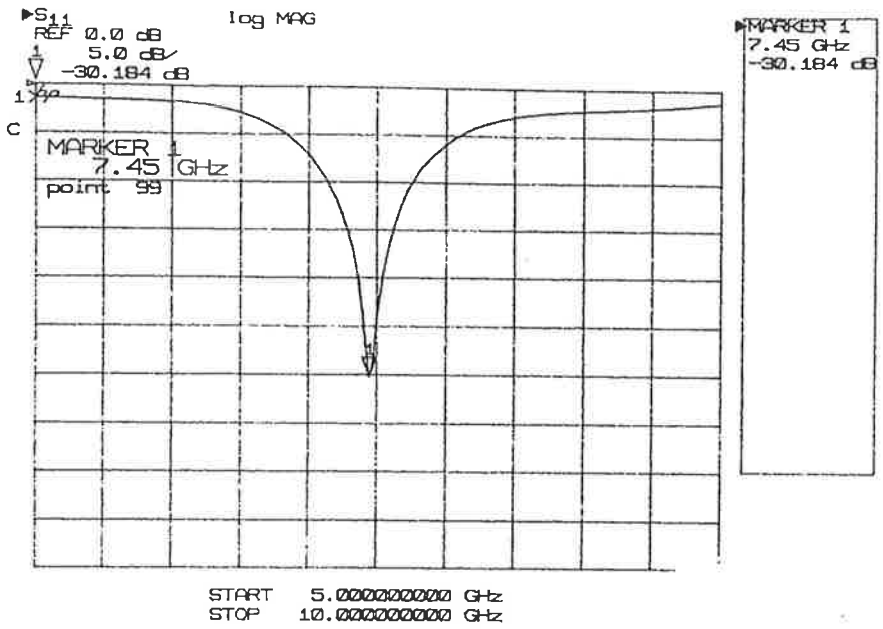

Figure 10.2: Measured return loss characteristics as a function of frequency of the miniaturised microstrip ring antenna element

The fractional bandwidth is determined from the return loss characteristics shown in Figure 10.2 as the frequency difference between points where the loss is -9dB and the maximum loss occurred at the centre frequency. Experimental results confirm that VSWR =2.1; bandwidth of the order of 9.8% is available with this antenna compared to about 5.3% for a conventional microstrip ring antenna of similar dimensions.

It is seen from the corresponding Smith chart of Figure 10.3 that a good impedance match has been obtained with the loop (locus) at 48 Ω. The measured input resistance at resonant frequency is 48 Ω, corresponding to an error of -0.2% in comparison with calculated input resistance from equation 10.7.

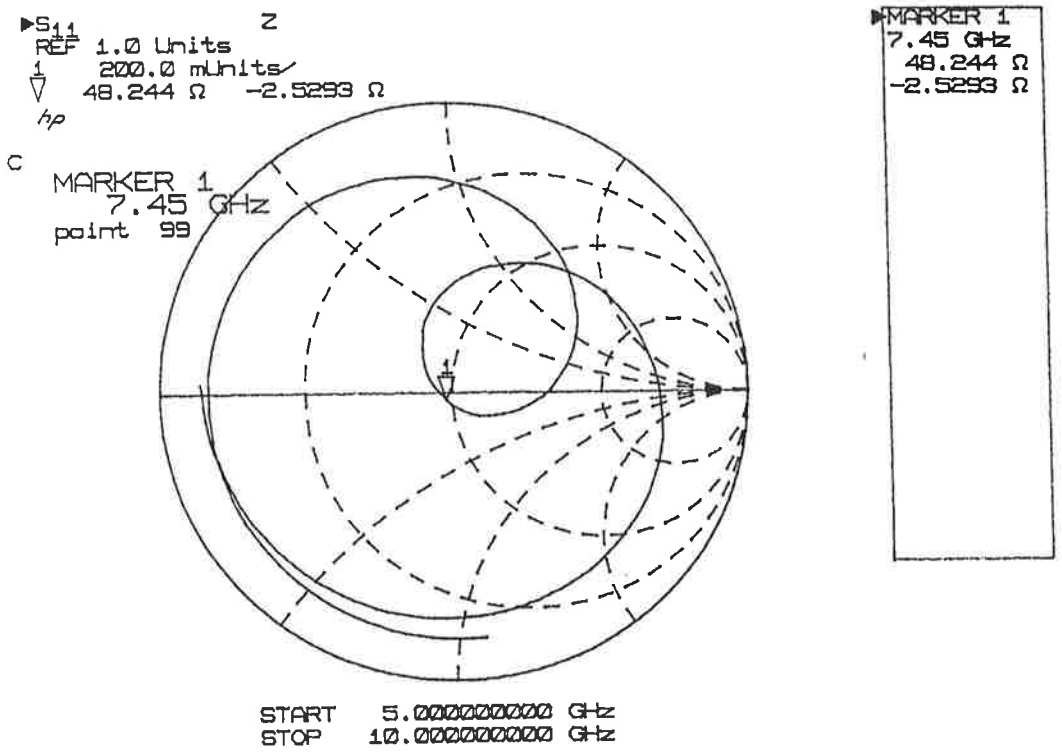

Figure 10.3: Measured input impedance characteristics as a function of frequency of the miniaturised microstrip ring antenna elements

The E- and H-plane radiation patterns for this antenna elements were also measured at 7.450 GHz and compared with results obtained from equations 10.14 and 10.15 respectively. The excellent agreement between the results obtained from these equations and the measured results are easily seen in Figures 10.4 and 10.5.

In addition, accurate measurement of far field radiation patterns involve the consideration of a number of factors, such as physical dimensions, operational frequency band and the operational environment. The measured half-power beamwidths at resonant frequency for E- and H-plane are respectively 71° and 67°.

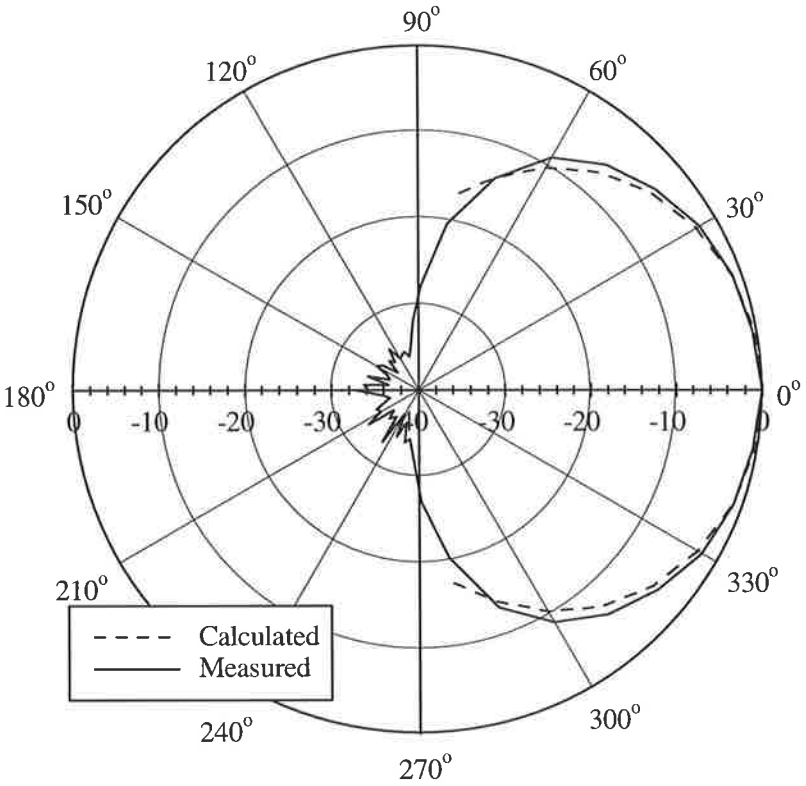

Figure 10.4: Measured far-field radiation pattern in the E-plane at 7.450 GHz compared with results obtained from equation 10.14.

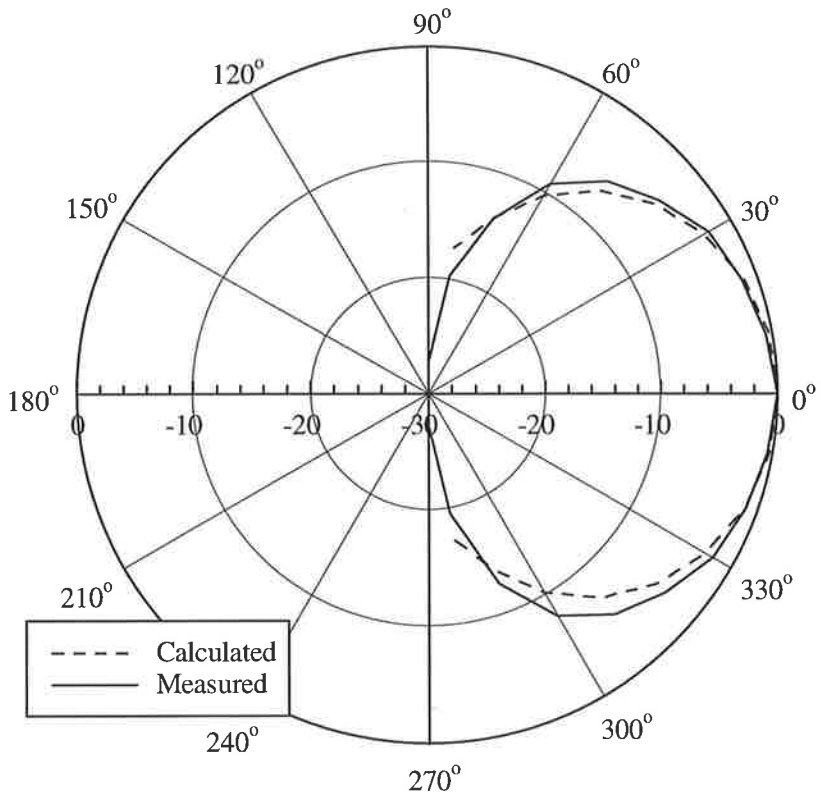

Figure 10.5: Measured far-field radiation pattern in the H-plane at 7.450 GHz compared with results obtained from equation 10.15.

The results obtained for the bandwidth show that using a miniaturised antenna element is an excellent way of widening the bandwidth. An investigation of the far field radiation patterns indicates that the increased bandwidth is obtained without any pattern degradation.

10.5 Conclusion

A novel broad-band miniaturised microstrip ring antenna element has been developed, designed and implemented. Design details, analysis, calculations and experimental observations of this antenna element have been discussed. Its experimental results reveal that

- its bandwidth can be broadened to as high as 9.8% which is 1.8 fold the bandwidth of conventional microstrip ring antenna having the same ring size,
- it is capable of very good performance with regard to important design parameters,
- its overall reduction in the size is as high as 70% of a corresponding ring antenna,
- it is capable of being mounted on and/or embedded into the bodies of a surface- and space-borne vehicles,
- it is very simple to manufacture and is very economical,
- it can be used as a single element or in an array environment.

Among the important contributions of the work described in this chapter are:

- The introduction, design and implementation of a novel miniaturised microstrip ring antenna element.
- The development of an accurate and computationally efficient method for the analysis of this antenna element.
- Discovery of the effects of the reduction in size of substrate material to the same size as the metal patch.
- The development of a broad-band antenna element simply by using a single layer of substrate.

The analysis that has been developed and applied takes account of all the physical parameters of the antenna, and has revealed that this antenna has the potential to offer excellent performance characteristics

The research presented in this chapter has therefore, elucidated engineering design opportunities for a novel broad-band miniaturised microstrip ring antenna element not previously available.

Chapter 11

The Mutual Coupling Between two Rectangular Microstrip Antenna Elements with Various Substrate Thicknesses

11.1 Introduction and brief overview

In the design of a microstrip array, the individual antenna elements can be either in the E-plane or in the H-plane coupled configuration. In such an array, the elements are close to each other. Hence each active element induces current in its neighbouring elements and this is called mutual coupling.

As part of the array design process, for proper operation of each antenna element of an array, the influence of the nearby elements must be calculated in advance. An understanding of the effect of mutual coupling between antenna elements is of great importance in the design of an array because it can result in mismatches of the individual elements to their feeds, and the degradation of the radiating properties of each of the coupled antenna elements such as radiation patterns, gains and polarisation, variation with scan angle. This is because the impedance of the array element is different from that of the individual element, and therefore the excitation value of each array element cannot be determined independently.

The array designer may require mutual coupling data for many orientations and spacings, therefore a method of calculating the mutual coupling is necessary.

In the last two decades there has been a great deal of interest in arrays consisting of microstrip antenna elements, because their printed circuit constructions make them well suited for use in large scanning arrays. Mutual coupling has been calculated and/or measured by several authors [1 - 5], [9, 18, 28, 42, 85, 98, 121], [187 - 205], with a wide variety of analytical methods. These are complicated, time consuming and are not easily implemented in a CAD package. Moreover, all the calculated results to date have been based upon approximations valid only for substrates in the order of $h \leq 0.0815\dot{} \lambda_o$, where λ_o is the free space wavelength and h is the substrate thickness.

Jedlicka et al [193] and [194] reported measured data on the scattering transfer coefficients as a function of element separation for two coupled L-band 1.58 mm and 3.17 mm thick antenna elements in E-plane and H-plane configurations. Here neither the dimensions or the location of the feed probe, nor the permittivity of the substrate are mentioned

Krowne et al [195] modelled the H-plane mutual coupling between two 1.58 mm thick rectangular antenna elements using a coupled transmission line approach and method of moment technique to compute even and odd mode transmission line parameters, and the E-plane mutual coupling using an equivalent π-network of capacitances, where the capacitance values were then obtained by an approximation to a quasi static formulation of the gap in a microstrip line. Unfortunately the results for the scattering reflection coefficient were not compared with any measurements.

Malcomes [196] evaluated the mutual coupling for two 0.5 mm thick antenna elements using a formula for the mutual impedance based on the reaction concept and the cavity model. The measured and calculated E- and H-plane scattering transfer coefficient agreed to within 4 dB for frequencies up to 10 GHz.

Penard et al [197] calculated the scattering transfer coefficient using the reaction theorem with a cavity model of the patch field of H-plane coupled 1.52 mm thick rectangular microstrip antennas. This method takes into account all the equivalent slots around the patch, but neglects the width of the slots, the surface waves, the radiation of the ideal field distribution on the slots versus frequency and higher cavity modes. The calculated magnitude of the transfer coefficient was shown to agree

with their own measurements to within 1 dB for separations greater than 0.1 λ_o for elements operating on a typical substrate at 2.298 GHz.

Pozar [42] has presented a moment method solution which used an exact Green's function for a dielectric slab above a grounded plane. This is regarded as accurately accounting for surface waves and radiative coupling between 3.17 mm thick patches. The agreement between the calculated mutual coupling and that measured by Jedlicka et al is good; however, the value of the effective dielectric constant was chosen to ensure this agreement. Even the much more sophisticated theory of Pozar brings no major improvement for computing the mutual coupling between antenna elements with thick substrates.

Krowne [198] published work which is an expanded combination of the works reported in [195] and [199] but does not include any comparison with measurements.

Van Lil et al [200] used the transmission line model for the patches using the reaction concept to calculate the mutual admittance between two distinct elements with substrates thinner than 1.57 mm. This model is effectively equivalent to Penard et al [197], with the coupling due to the non radiating wall of the patches being neglected. Hence the computed results generally agree less closely with the experiment than those of [197].

Mohammadian et al [201] adopted an approximate model to calculate the mutual coupling between two 1.59 mm and 3.2 mm thick antenna elements which is based on a cavity model expression. This method is time consuming and does also not bring improvement for computing the mutual coupling between antenna elements with thick substrates.

Dubost [202] used the volume equivalence theorem and classical Schelkunoff theory to calculate the mutual impedance and coupling coefficients between two antenna elements in E- and H-plane configurations for the dominant mode TM_{10}. The agreement between the calculated coupling coefficient between two $0.0075\lambda_o$ thick antenna elements in the H-plane and that measured by Jedlicka et al [194] is good. But the calculated coupling coefficient results between some thicker antenna elements ($h = 0.012\ \lambda_o$) in the H-plane agree less closely with that measured and calculated by Penard et al [197]. The calculated coupling coefficient results between two $0.012\lambda_o$ thick patches in the E- plane agree well with those calculated using the cavity theory reported by Penard [203]. Therefore, the method proposed by Dubost [202] can be categorised as computationally equivalent to cavity theory suggested by Penard [203] and valid for thin microstrip arrays only.

As far as it is known, the mutual coupling results available in the literature are given for antenna arrays with substrates thinner than 3.20 mm. Further, many of these methods are complicated, time consuming, not valid for thicker substrates and are also not easily implemented in a Computer Aided Design, CAD, package.

It is important to note that there is almost no data or details on mutual coupling in the open literature for microstrip arrays with substrates satisfying the criteria $h \geq 0.0815\lambda_o$ [85, 98].

This chapter develops formulae that calculate the mutual coupling coefficients between two identical rectangular antenna elements in E- and H-plane configurations for the dominant TM_{10} mode. These formulae are derived using the volume equivalence theorem and the classical Schelkunoff theory [202] as a basis. The mutual coupling coefficients between two antenna elements with various substrate thicknesses are calculated using these formulae and these coefficients are compared with experimental results. It will be seen that, as the thickness of the substrate increases the differences between the measured and calculated results increases unacceptably. Thus, modifications to these formulae need to be made to increase the accuracy of the predictions for the mutual coupling coefficient [85, 98]. These modifications must take into account the effective properties of the antenna elements, the surface wave and also the mismatch that may occur between the elements for both the E- and H-plane configurations. As described in the preceding chapters, the antenna element is modelled as a transmission line of length L ,and an electrical lengthening of ΔW will occur, due to open-end effect, at both edges of the antenna element. A similar effect will occur at the sides of the antenna element, increasing its width electrically. The effect on the periphery is accounted for by replacing the physical width and length by effective width and effective length.

It is well known that a proportion of the total input power supplied to the antenna is consumed in the excitation of the surface wave. The lost power is dissipated within the dielectric substrate material. Thus, the accurate design of microstrip arrays with thick substrates requires not only the inclusion of the space waves to mutual coupling effects but also the surface waves.

The measured and calculated mutual coupling coefficients are presented as a function of separations between two antenna elements with substrates ranging in electrical thickness, defined as h/λ_d, from 0.0419 to 0.2189 and physical thickness from 1.50 mm to 9.52 mm, in E-and H-plane coupling configurations for the dominant TM_{10} mode, where λ_d is the wavelength in the dielectric substrate. This technique is original, simple, and is easily included in a CAD system.

Measured results are compared with calculations using this technique and published formulae [202, 204]. This comparison shows that the present technique is accurate enough for practical microstrip array analysis and design. The basic differences between the present work and that of Dubost are in the method of computation of the radiation resistance, R_r, the consideration of the physical and effective dimensions of the antenna elements, the permittivity and thickness of the substrate and the method of inclusion of surface wave contributions.

Note that the formulae given in Chapter 3 are applied to determine the dimensions and the feed point locations of the antenna elements used in the array design.

11.2 Experimental Procedure

Verification of new formulae reported herein is provided for rectangular antenna elements of various substrate thicknesses, as well as elements of various dimensions, by comparing computed results for the mutual coupling coefficient with measurements made on two identical element test arrays. Measurements were performed with two antenna elements fabricated on a 100 mm by 200 mm microwave substrate, and mounted on a 700 mm by 700 mm aluminium ground plane with a centre slot cut so that the spacing between adjacent elements could be continuously varied. A continuous substrate was simulated by inserting dielectric spacers of the same substrate material between the elements as shown in Figure 11.1. The substrate material is made of a polytetrafluoroethylene (PTFE) woven fibreglass laminate with a nominal dielectric constant of 2.55, and loss tangent of 0.002.

Specific calibration procedures were followed for the reflection measurements. The resonant frequency was measured for each individual patch and a slight mismatch from the calculated results was noted which was attributed to fabrication tolerances. Matching of each element was obtained by a proper choice of the feed location.

The magnitude of the E-plane and H-plane are measured as a function of the distance between the patch edges, which is normalised with respect to the free-space wavelength λ_o.

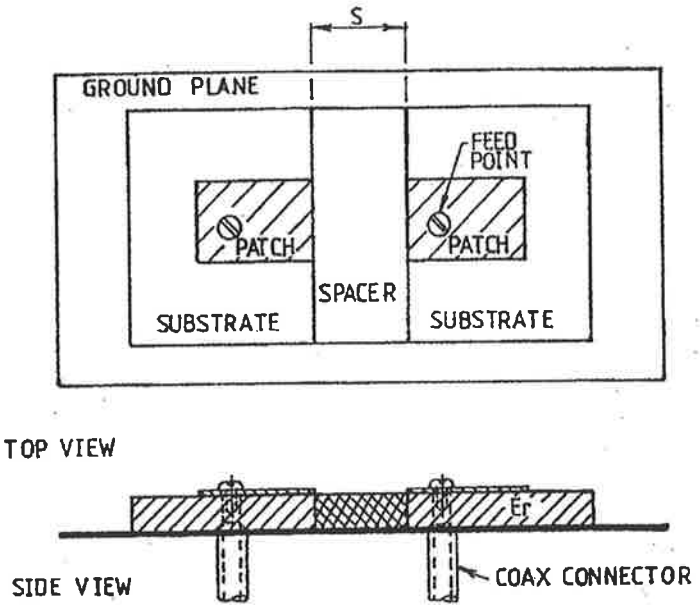

Figure 11.1: Experimental arrangement for the measurement of microstrip antenna array S-parameters.

Mutual coupling between two identical rectangular patch antenna elements is measured by exciting one patch and measuring the relative amplitude, S_{12} (dB), of the power coupled into the other patch antenna at the resonance frequency. The measurements were performed using an HP8410 automatic microwave network analyser system, controlled by an HP9845 desk computer and dedicated computer programs.

The measurements were taken for substrate thicknesses of 1.50, 1.63, 3.00, 4.76, 6.26, 7.76 and 9.52 mm by varying the separation between two antenna elements from 0.2 λ_o to 1.4 λ_o. For each separation the coupling amplitude, $S_{12,}$ was measured in both the E- and the H-plane.

Matching of each element was obtained by a proper choice of the feed location.

11. 3 Formulation and numerical implementation

The test of practical and analytical data has been carried out by means of two identical element arrays consisting of rectangular patch antennas with coaxial feed, shown in Figure 11.1. The analytical expressions for the mutual impedance and coupling coefficients in the E- and H-plane configurations for the dominant TM_{10} mode are obtained using the modified volume equivalence

theorem and the classical Schelkunoff theory suggested by Dubost [202, 204]. The derivation of the expressions is outlined briefly in Appendix B.

The mutual coupling coefficient, C_p, between two microstrip antenna elements at resonance can be calculated from [202] in which radiation resistance R_r is replaced by the total resistance at resonance, R_T, of the antenna. This change takes into consideration the influence of the antenna losses, including radiation out of the walls, heat loss in both the dielectric and conductor (copper) [85, 98]. The mutual coupling coefficient is now given by

$$C_{p\zeta} = 20\log\left(\frac{Z_{12\zeta}}{2R_{T\alpha}}\right) - 40\log\left[\frac{1}{2}\left(\sqrt{\frac{R_{T\alpha}}{R_N}} + \sqrt{\frac{R_N}{R_{T\alpha}}}\right)\right] \tag{11.1}$$

where $Z_{12\zeta}$ is the modular of the mutual impedance and R_N is the normalisation resistance. The subscript ζ has been used to represent either the E- or the H-plane coupling, and α has been used to represent either the patch resonant length, L, or width, W.

At resonance R_T can be calculated from the equation in references [28, 85, 121] in which the subscript α and the surface wave excitation resistance, R_s, have been additionally taken into consideration as follows

$$R_{T\alpha} = R_c + R_d + R_{r\alpha} + R_s \tag{11.2}$$

Note that the subscript α will only be considered when thick antennae are used. The resistance used to account for the power loss in the conductor may be calculated from

$$R_c = 0.00027 Q_r^2 \frac{L}{W}\sqrt{f_r(\text{GHz})} \tag{11.3}$$

where f_r is the resonant frequency and Q_r is the radiation quality factor derived from the transmission line model [1, 22] as

$$Q_r = \frac{\lambda_o}{4h}\sqrt{\varepsilon_{ew}} \tag{11.4}$$

where ε_{ew} the effective permittivity as a function of W and can be calculated from equation 2.10 or equation 3.8. The resistance due to power loss in the dielectric material may be expressed as

$$R_d = 30 \frac{\tan\delta}{\varepsilon_r} \frac{h\lambda_o}{WL} Q_r^2 \tag{11.5}$$

where ε_r is the relative permittivity of the substrate and $\tan\delta$ is the loss tangent of the dielectric substrate.

As defined in Section 4.2 the radiation resistance and the capacitance of the TM_{10} mode at resonance are [1, 28]

$$R_r = \frac{Q_r}{\omega C_{10}} \tag{11.6}$$

with

$$C_{10} = \varepsilon_r \varepsilon_o \frac{L\ W}{2h \cos^2\left(\frac{\pi a}{L}\right)} \tag{11.7}$$

where $\omega = 2\pi f_r$ is the angular frequency and $\varepsilon_o = 8.854 \times 10^{-12}$ Farad per meter (F/m) is the permittivity of free space.

With a microstrip antenna in mind, it is well known that the existence of a dielectric layer over a ground plane is responsible for the excitation of surface waves along the air dielectric interface. These surface waves are guided away by the substrate even though they do not radiate except for producing uncontrolled radiation at substrate edges or at other geometrical discontinuities. The power in the surface waves must therefore be considered along with antenna loss. It is important to note that this work only considers the propagation of the dominant lowest-order TM_o mode which is excited for usual values of the normalised substrate thickness h/λ_d and which has a zero cutoff frequency. The equivalent resistance of the surface waves can be derived from the ratio of the power lost to surface waves, P_s, and radiation power, P_r given by Hall et al [138]

$$\frac{P_s}{P_r} = \frac{R_r}{R_s} = \frac{\varepsilon_r k_1^2 \cos^2(k_1 h)}{\varepsilon_r k_2^2 \cos^2(k_1 h) + k_1^2 h k_2} \tag{11.8}$$

where k_1 and k_2 are surface wave propagation coefficients determined from

$$\tan(k_1 h) = \varepsilon_r \frac{k_2}{k_1} \tag{11.9}$$

and

$$k_1^2 + k_2^2 = k_o^2(\varepsilon_r - 1) \tag{11.10}$$

When $h/\lambda_o \ll 1$, k_1 is found by

$$k_1 = \frac{1}{h\sqrt{2}}\left(-\varepsilon_r^2 + \varepsilon_r\sqrt{\varepsilon_r^2 + 4h^2k_o^2(\varepsilon_r - 1)}\right)^{\frac{1}{2}} \tag{11.11}$$

A Maclaurin's series expansion is used for $\tan(hk_1)$

$$\tan(k_1 h) \approx k_1 h + \frac{1}{3}(k_1 h)^3 + \frac{2}{17}(k_1 h)^5 + \frac{17}{315}(k_1 h)^7 + \cdots \tag{11.12}$$

Combining (11.9) and (11.12) one obtains

$$k_2 = \frac{k_1}{\varepsilon_r}\left[k_1 h + \frac{1}{3}(k_1 h)^3 + \frac{2}{17}(k_1 h)^5 + \frac{17}{315}(hk_1)^7\right] \tag{11.13}$$

Substituting (11.13) into (11.8) yields for R_s

$$R_s = T_m R_{r\alpha} \tag{11.14}$$

with

$$T_m = \left(\frac{hk_1 + T_n}{\varepsilon_r}\right)^2 + \left(\frac{hk_1 + T_n}{\varepsilon_r}\right)hk_1 \cot^2(hk_1) \tag{11.15}$$

and

$$T_n = \frac{1}{3}(k_1 h)^3 + \frac{2}{17}(k_1 h)^5 + \frac{17}{315}(k_1 h)^7 \tag{11.16}$$

A new equation for the calculation of the total input resistance of thick antennae can be given by substituting equation 11.14 into equation 11.2 as

$$R_{T\alpha} = R_{r\alpha}(1 + T_m) + R_c + R_d \qquad (11.17)$$

Note that for a matched antenna $R_{T\alpha}$ is equal to R_N.

11.3.1 Coupling in E-plane (Collinear Position)

The antenna elements are end coupled (E-plane oriented) with the direction of propagation perpendicular to the two adjacent coupled antenna ends, Figure 11.1.

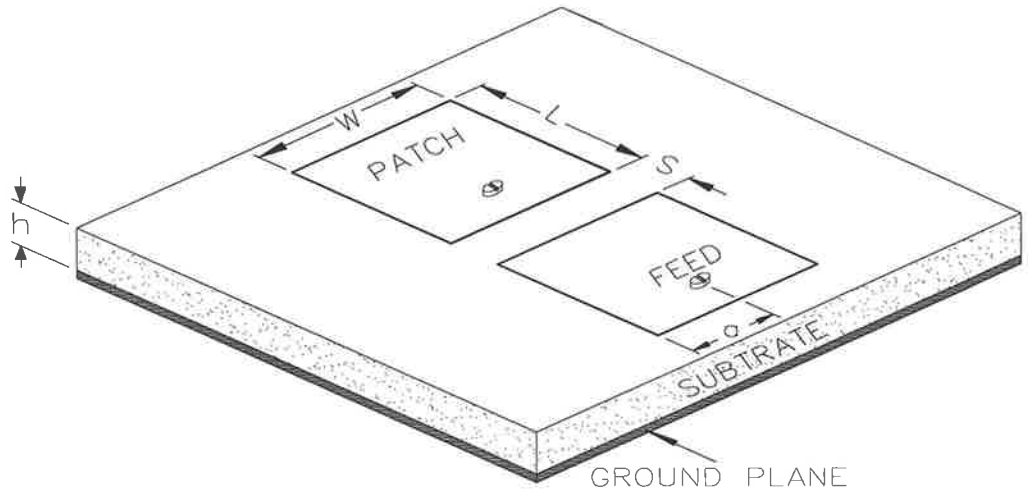

Figure 11.2: Experimental arrangement for the measurement of the mutual coupling in the E-plane between two identical antenna elements.

11.3.1.1 Coupling in E-plane Between two Antenna Elements with Thin Substrates

At resonance the coupling coefficient in E-plane C_{pE} can be calculated from equation 11.1 (by setting ζ = E) in which Z_{12E} is the mutual impedance referred to the feed point location. Z_{12E} can be calculated from the equation given in by Dubost [202], equation B.13 in Appendix B, in which one replaces both the free space wavelength by the wavelength in the dielectric substrate material to take into consideration the influence of the relative permittivity of the substrate and W by L. The resulting formula for Z_{12E} [98] is

$$Z_{12E} = \frac{25\varepsilon_r^2 h R_o \lambda_d^2}{\pi^5 S(\varepsilon_r - 1) L^2}\left[1 + \frac{\lambda_d^2}{4hS\pi^2\varepsilon_r}\right]\cos^2\left(\frac{\pi}{2\sqrt{\varepsilon_r}}\right) \tag{11.18}$$

where $R_o = 120\pi\ \Omega$ is the vacuum medium resistance and S is the distance between two patches. In the following formula R_T is obtained from equation 11.2 by setting $\alpha = L$ and assuming the effect of the surface wave is insignificant ($R_s = 0\ \Omega$) for substrates satisfying the criteria $h \leq 0.0815\ \lambda_o$. The resulting formula for C_{pE} can be given as

$$C_{pE} = 20\log\left\{\frac{25\varepsilon_r^2 R_o}{\pi^5(\varepsilon_r - 1)}\frac{h\lambda_d^2}{SL^2}\frac{1}{R_{TL}}\left(1 + \frac{\lambda_d^2}{4Sh\pi^2\varepsilon_r}\right)\cos^2\left(\frac{\pi}{2\sqrt{\varepsilon_r}}\right)\right\}$$
$$- 40\log\left[\frac{1}{2}\left(\sqrt{\frac{R_{TL}}{50}} + \sqrt{\frac{50}{R_{TL}}}\right)\right] \tag{11.19}$$

As is evident from the good agreement between the measured and calculated coupling coefficient in the E-plane shown in Figures 11.3 - 11.6, the equations 11.1 to 11.19 calculate C_{pE} for antenna arrays with substrates in the thickness range of $h \leq 0.0815\ \lambda_o$ with good accuracy. As the substrate becomes thicker, however, these equations lose accuracy and also applicability, as will be shown in next section.

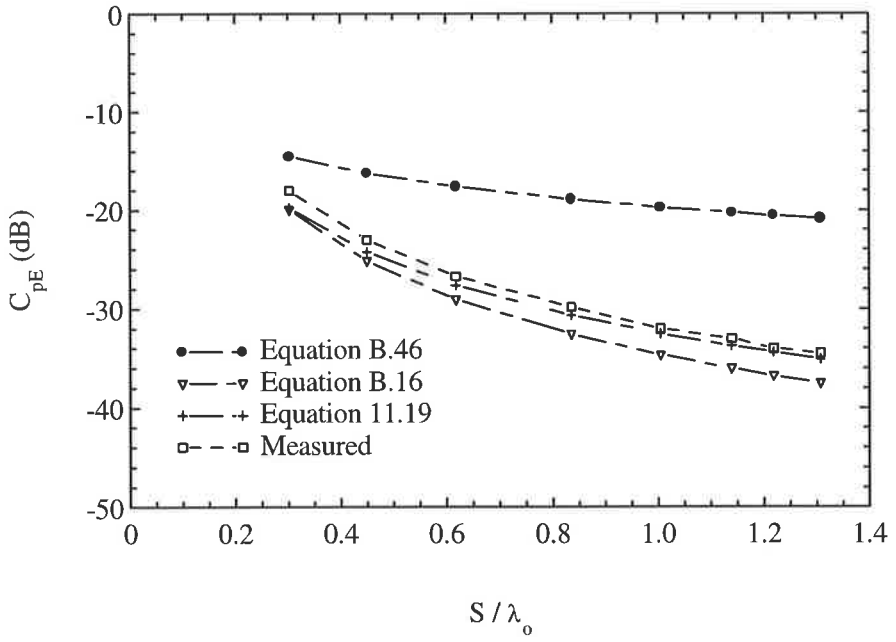

Figure 11.3: Computed and measured E-plane mutual coupling coefficient between two rectangular antenna elements with 1.50 mm thick substrate versus edge spacing normalised with respect to free space wavelength between them (array Nr. 1 of Table 11.1)

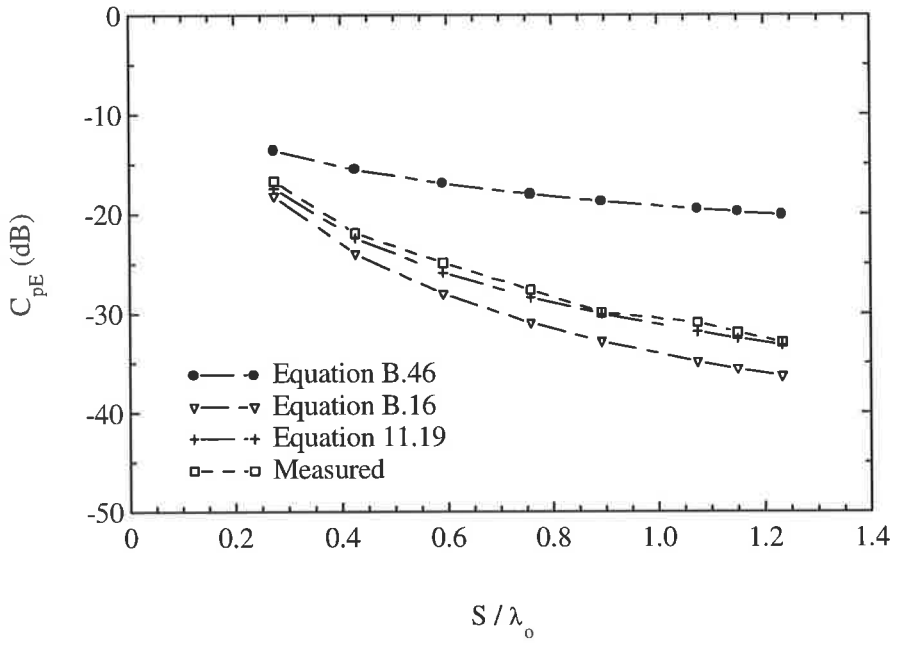

Figure 11.4: Computed and measured E-plane mutual coupling coefficient between two rectangular antenna elements with 1.63 mm thick substrate versus edge spacing normalised with respect to free space wavelength between them (array Nr. 2 of Table 11.1)

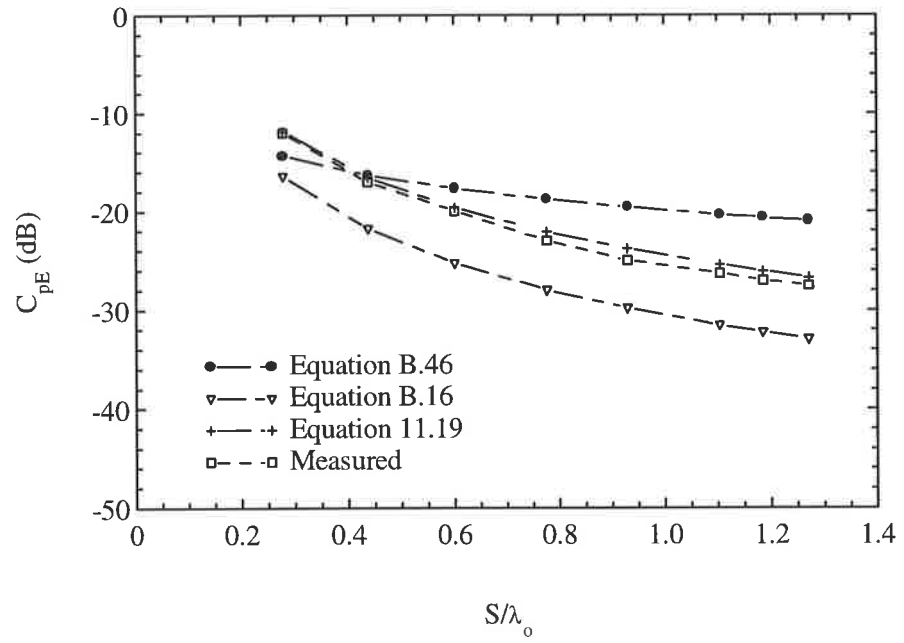

Figure 11.5: Computed and measured E-plane mutual coupling coefficient between two rectangular antenna elements with 3.00 mm thick substrate versus edge spacing normalised with respect to free space wavelength between them (array Nr. 3 of Table 11.1)

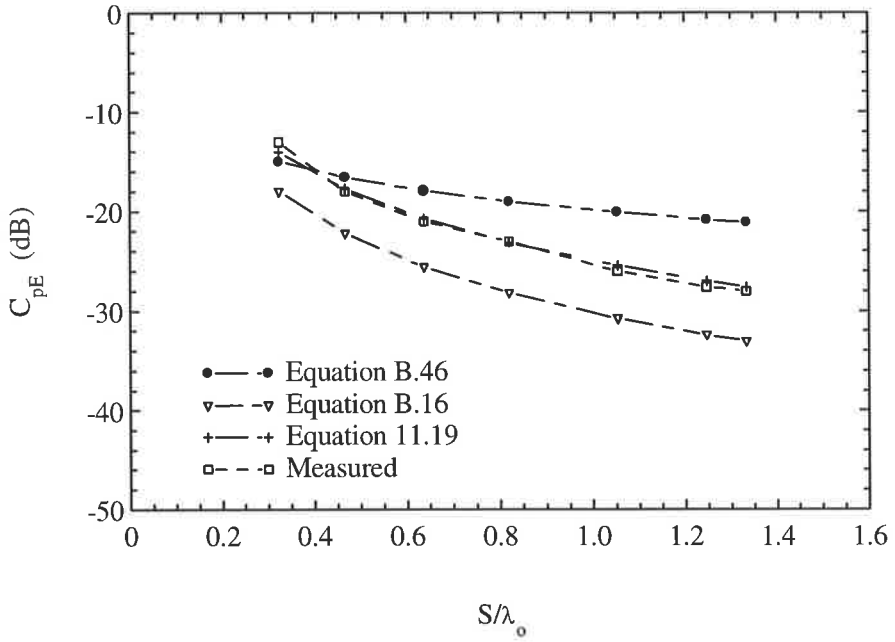

Figure 11.6: Computed and measured E-plane mutual coupling coefficient between two rectangular antenna elements with 3.00 mm thick substrate versus edge spacing normalised with respect to free space wavelength between them (array Nr. 4 of Table 11.1)

Table 11.1 Dimensions of *thin antenna elements* of which mutual couplings in E- and/or H-plane were measured and computed

Array No	h/λ_d	W (mm)	L (mm)	f_r (GHz)	h (mm)	a (mm)	ε_r
1	0.0419	15.85	17.20	5.300	1.50	4.60	2.50
2	0.0434	16.80	18.30	5.000	1.63	5.10	2.55
3	0.0814	15.70	16.80	5.150	3.00	5.00	2.50
4	0.0854	15.00	16.00	5.400	3.00	4.60	2.50

The dimensions, resonant frequencies and substrate thicknesses of the array antenna elements considered for this section are summarised in Table 11.1.

In order to calculate the mutual coupling factor C_{pE} between two antenna elements on thicker substrates, further modifications have been considered in the following section.

11.3.1.2 Coupling in E-plane between two antenna elements with thick substrates

At resonance, the coupling factor C_{pE} between two antenna elements with substrate thicknesses of $h \geq 0.0815\ \lambda_o$ can be calculated from equation 11.1. Z_{12E} is calculated from equation 11.18, in which one replaces both the L and ε_r with effective length, L_{ef}, and effective permittivity, ε_{eL}, to take into account the inhomogeneity of the antenna elements. For this case the resulting formula for Z_{12E} is [85]

$$Z_{12E} = \frac{25\varepsilon_{eL}^2\, R_o h \lambda_d^2}{\pi^5 S(\varepsilon_{eL}-1)L_{ef}^2}\left[1+\frac{\lambda_d^2}{4hS\pi^2\varepsilon_{eL}}\right]\cos^2\left(\frac{\pi}{2\sqrt{\varepsilon_{eL}}}\right) \tag{11.21}$$

Here ε_{eL} is the effective permittivity as a function of L. It can be calculated from equation 2.10 by replacing W with L. A formula for L_{ef} is given in preceding chapters, but for convenience sake it is reproduced here. It takes into account the influences of the fringing field at the patch edges and the dielectric inhomogeneity of the antenna element. It may be obtained from [137]

$$L_{ef} = L + \left(\frac{W_{eq}-W}{2}\right)\left(\frac{\varepsilon_{ew}+0.300}{\varepsilon_{ew}-0.258}\right) \tag{11.22}$$

and W_{eq} is the equivalent patch width [138] calculated from the planar waveguide model:

$$W_{eq} = \frac{R_o h}{Z_{cw}\sqrt{\varepsilon_{ew}}} \tag{11.23}$$

where Z_{cw} is the characteristic impedance of a microstrip line determined by the ε_r, h and W of the stripline. A formula for Z_{cw} is given in preceding chapters, but for convenience sake it is reproduced here [102]

for $W/h \leq 3.3$

$$Z_{cw} = \frac{R_o}{\pi\sqrt{2(\varepsilon_r+1)}}\left[\ln\left(\frac{4h}{W}+\sqrt{2+\frac{16h^2}{W^2}}\right)-\frac{(\varepsilon_r-1)}{(\varepsilon_r+1)}\left(0.2258+\frac{0.1208}{\varepsilon_r}\right)\right] \tag{11.24}$$

and for W/h ≥ 3.3

$$Z_{cw} = \frac{R_o}{2\sqrt{\varepsilon_r}}\left[\frac{W}{2h} + 0.4413 + \frac{0.0823(\varepsilon_r - 1)}{\varepsilon_r^2} + \frac{(\varepsilon_1 + 1)}{\varepsilon_r}\right.$$

$$\left.\cdot\left(0.2310 + 0.1592\ \ln\left(\frac{W}{2h} + 0.94\right)\right)\right]^{-1} \tag{11.25}$$

The radiation resistance of a patch equivalent to a lossy opened line of length L and width W can be given as [85]

$$R_{r\alpha} = \frac{5R_o}{2\pi^3}\left(\frac{\lambda_d}{\alpha + 2\Delta\alpha}\right)^2 \tag{11.26}$$

The differences between equation 11.26 and that of Dubost [202] expression for R_r given as equation B.6 in Appendix B, are in considering the line extensions at the periphery of the patch, in calculating R_r as a function of L or W respectively and in replacing λ_o by λ_d. It is well known that at the immediate vicinity of the patch edges there are fringing fields, $\Delta\alpha$, making the patch dimensions larger than the physical dimensions. The influence of these fringing fields has been taken into account by adding $\Delta\alpha$ to α in equation 11.27. The term $\Delta\alpha$ is given by [85, 105] as

$$\Delta\alpha = 0.412h\ \frac{(\varepsilon_{e\alpha} + 0.300)}{(\varepsilon_{e\alpha} - 0.258)}\ \frac{\left(\frac{\alpha}{h} + 0.264\right)}{\left(\frac{\alpha}{h} + 0.813\right)} \tag{11.27}$$

A closed-form expression for the coupling factor in the E-plane is derived by substituting equations 11.17, 11.21 and equation 11.26 into equation 11.1 and considering the case α = L which is replaced by L_{ef}, $\Delta\alpha = \Delta L$ in equation 11.26 and setting $R_N = 50\ \Omega$ (ie a matched load) [85]

$$C_{pE} = 20\log\left\{\frac{25R_o\varepsilon_{eL}^2}{2\pi^5(\varepsilon_{eL} - 1)}\frac{h\lambda_d^2}{SL_{ef}^2}\frac{1}{R_{TL}}\left[1 + \frac{1}{hS\varepsilon_{eL}}\left(\frac{\lambda_d}{2\pi}\right)^2\right]\cos^2\left(\frac{\pi}{2\sqrt{\varepsilon_{eL}}}\right)\right\}$$

$$- 40\log\left[\frac{1}{2}\left(\sqrt{\frac{R_{TL}}{50}} + \sqrt{\frac{50}{R_{TL}}}\right)\right] \tag{11.28}$$

Equation 11.28 was used to calculate the coupling factors in the E-plane of all antenna elements listed in Table 11.2. As is evident from Figures 11.7- 11.11, this formula gives the required C_{pE} results for antenna elements with thick substrates. The coupling factor results obtained from equation 11.28 agree well with measured results.

The dimensions, resonant frequencies and thicknesses of the substrates of the antennae considered for this section are summarised in Table 11.2.

Table 11.2 Dimensions of *thick antenna elements* for which mutual coupling in E- and H-plane were measured and computed (ε_r=2.55)

Array No.	h/λ_d	W (mm)	L (mm)	f_r (GHz)	h (mm)	a (mm)
1	0.1495	10.60	15.15	5.900	4.76	3.45
2	0.1666	10.00	18.70	5.000	6.26	4.55
3	0.2065	7.51	21.04	5.000	7.76	2.75
4	0.2189	6.20	20.43	5.300	7.76	3.45
5	0.2027	9.48	26.00	4.000	9.52	3.20

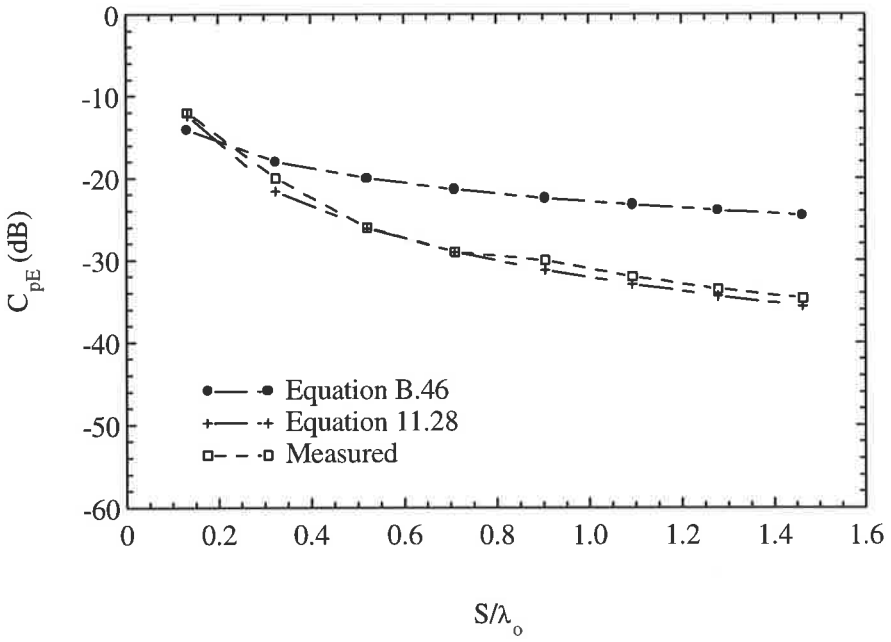

Figure 11.7: Computed and measured E-plane mutual coupling coefficient between two rectangular antenna elements with 4.76 mm thick substrate versus edge spacing normalised with respect to free space wavelength between them (array Nr. 1 of Table 11.2)

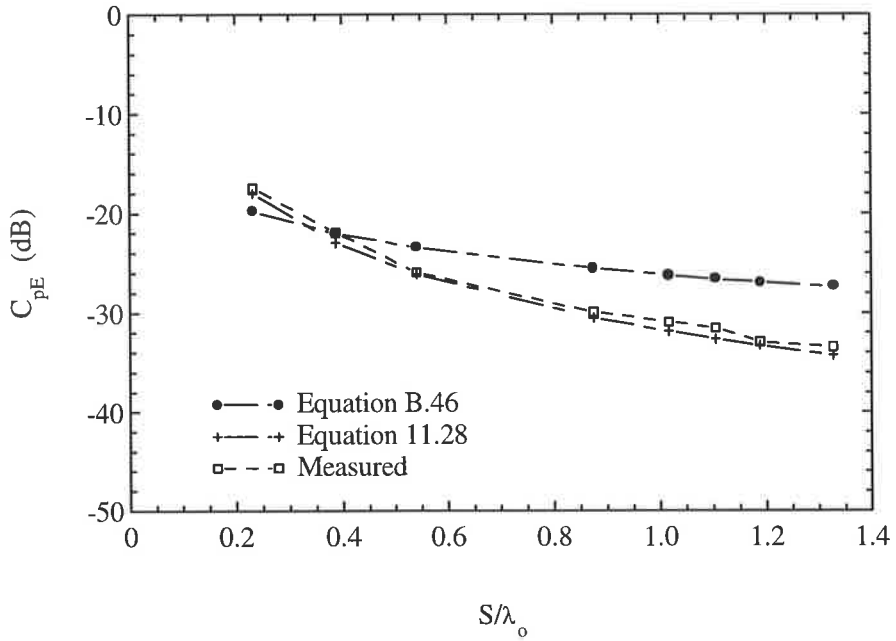

Figure 11.8: Computed and measured E-plane mutual coupling coefficient between two rectangular antenna elements with 6.26 mm thick substrate versus edge spacing normalised with respect to free space wavelength between them (array Nr. 2 of Table 11.2)

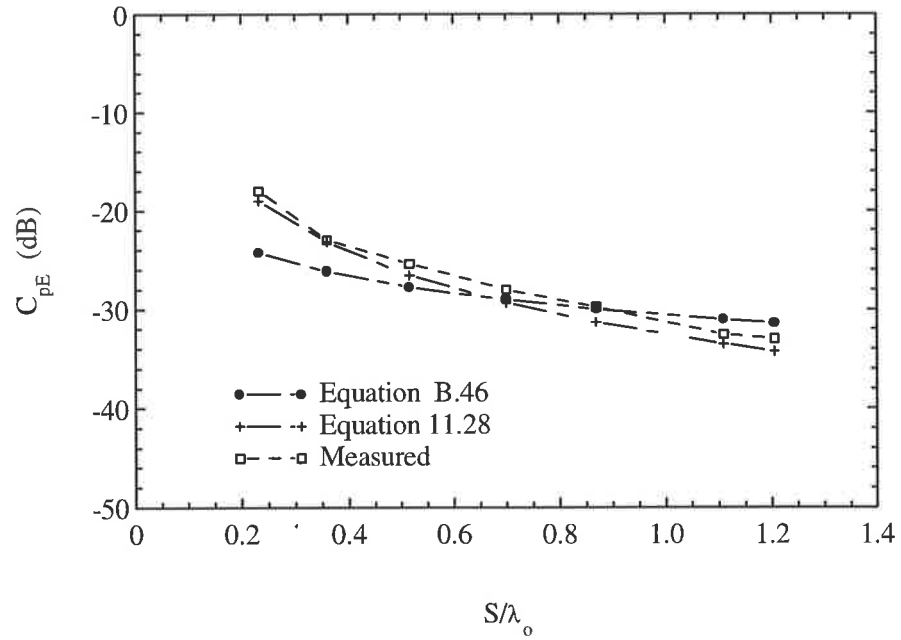

Figure 11.9: Computed and measured E-plane mutual coupling coefficient between two rectangular antenna elements with 7.76 mm thick substrate versus edge spacing normalised with respect to free space wavelength between them (array Nr. 3 of Table 11.2)

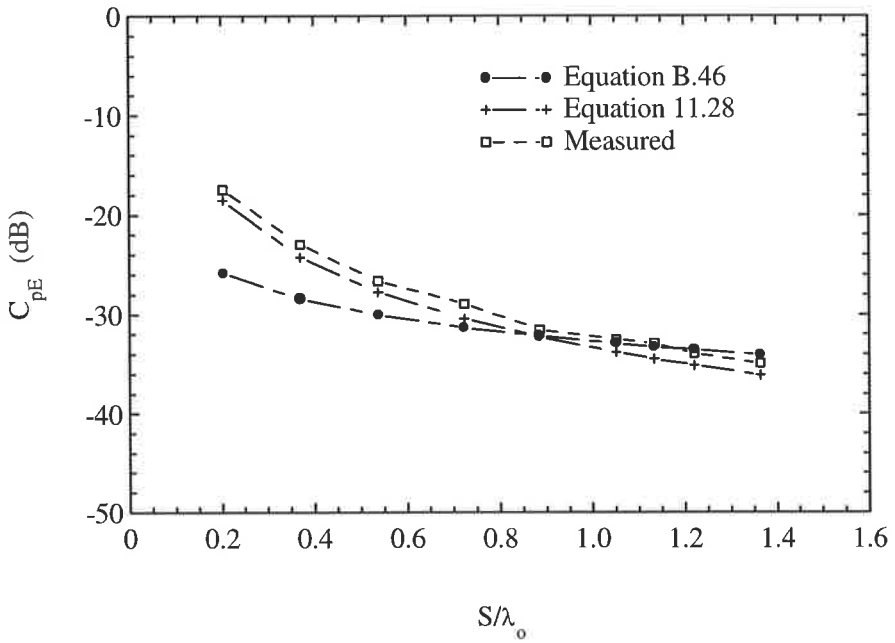

Figure 11.10: Computed and measured E-plane mutual coupling coefficient between two rectangular antenna elements with 7.76 mm thick substrate versus edge spacing normalised with respect to free space wavelength between them (array Nr. 4 of Table 11.2)

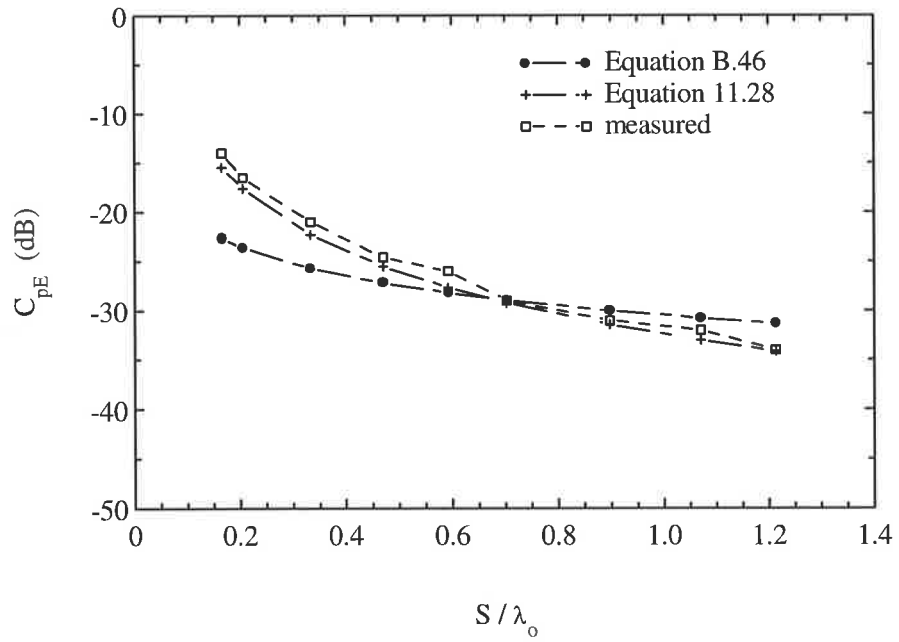

Figure 11.11: Computed and measured E-plane mutual coupling coefficient between two rectangular antenna elements with 9.52 mm thick substrate versus edge spacing normalised with respect to free space wavelength between them (array Nr. 5 of Table 11.2)

11.3.2 Coupling in H-Plane (parallel position)

The two identical probe fed rectangular antenna elements are parallel coupled (H-plane oriented) with the direction of propagation parallel to the coupled antenna edges of length L, as shown in Figure 11.12.

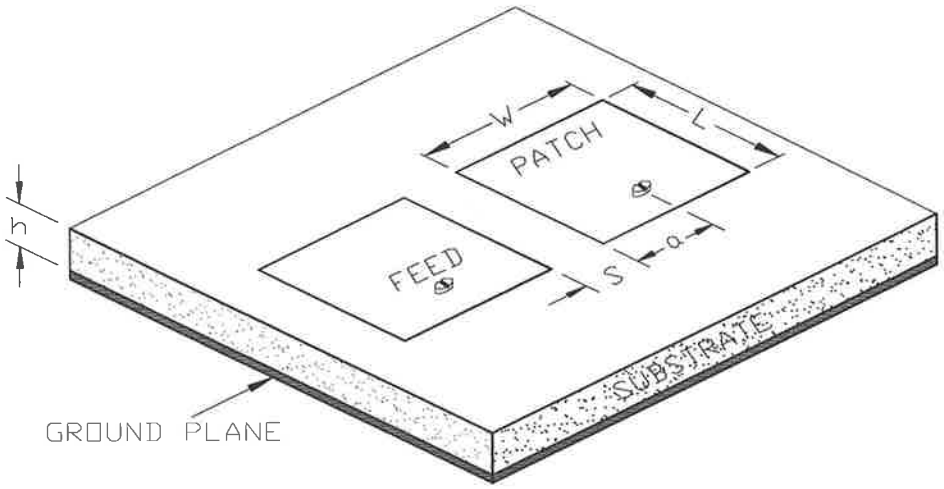

Figure 11.12: Experimental arrangement for the measurement of the mutual coupling in the H-plane between two identical antenna elements.

11.3.2.1 Coupling in H-plane between two antenna elements with thin substrates

At resonance the coupling coefficient in H-plane C_{pH} can be calculated from equation 11.1 (by setting $\zeta = H$) in which Z_{12H} is the mutual impedance referred to the feed point location. Z_{12H} can be calculated from the equation given in by Dubost [202], equation B.21 in Appendix B, in which one replaces both the free space wavelength by the wavelength in the dielectric substrate material to take into consideration the influence of the relative permittivity of the substrate. The resulting formula for Z_{12H} is

$$Z_{12H} = \frac{25R_o \lambda_d^5}{2\pi^8 W^3 S^2} \sin\left(\frac{\pi W}{\lambda_d}\right) \tag{11.29}$$

A formula for C_{pH} was derived by substituting equations 11.2 and 11.29 into 11.1 considering the case of $\alpha = W$ and assuming $R_s = 0$ and $R_N = 50\ \Omega$ (ie. matched load)

$$C_{pH} = 20\log\left[\frac{25R_o}{2\pi^8}\frac{\lambda_d^5}{W^2S^2}\frac{1}{R_{TW}}\sin\left(\frac{\pi W}{\lambda_d}\right)\right] - 40\log\left[\frac{1}{2}\left(\sqrt{\frac{R_{TW}}{50}} + \sqrt{\frac{50}{R_{TW}}}\right)\right] \qquad (11.30)$$

As is evident from the close agreement between the measured and calculated results shown in Figures 11.13 - 11.16, the equation 11.30 calculates C_{pH} for antenna arrays with substrates in the range of $h \leq 0.0815\lambda_o$ with good accuracy. As the substrate becomes thicker, however, these equations lose accuracy and also applicability, as shown in next section.

Similar to Section 11.3.1.2 a modification to equation 11.30 is made to obtain C_{pH} results for arrays with thicker substrates. This modification is given in the following section.

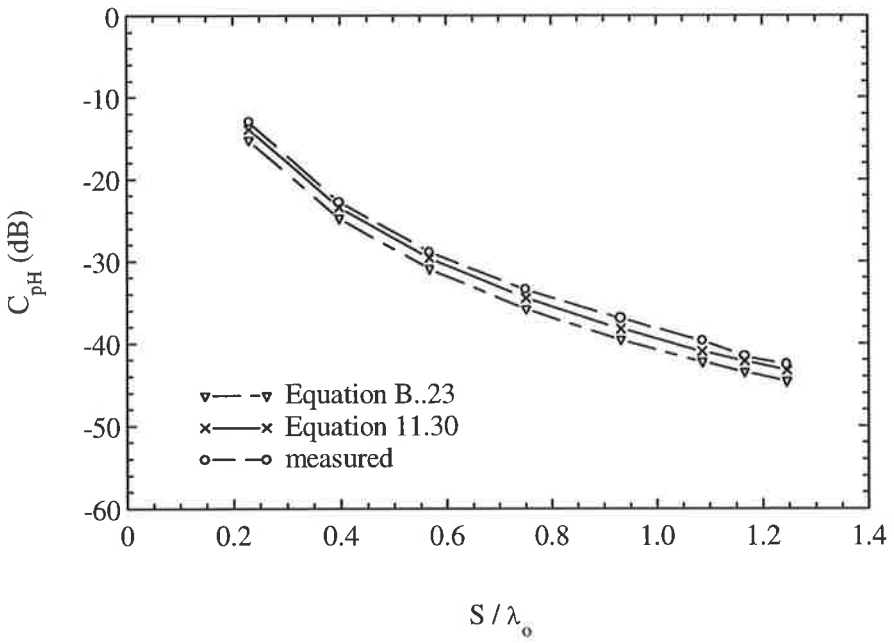

Figure 11.13: Computed and measured H-plane mutual coupling coefficient between two rectangular antenna elements with 1.50 mm thick substrate versus edge spacing normalised with respect to free space wavelength between them (array Nr. 1 of Table 11.1)

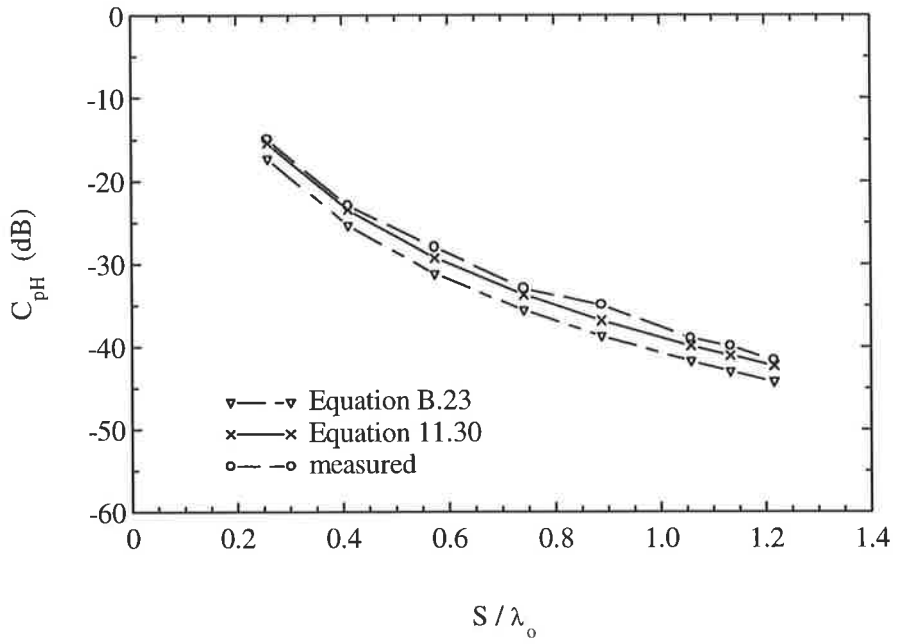

Figure 11.14: Computed and measured H-plane mutual coupling coefficient between two rectangular antenna elements with 1.63 mm thick substrate versus edge spacing normalised with respect to free space wavelength between them (array Nr. 2 of Table 11.1)

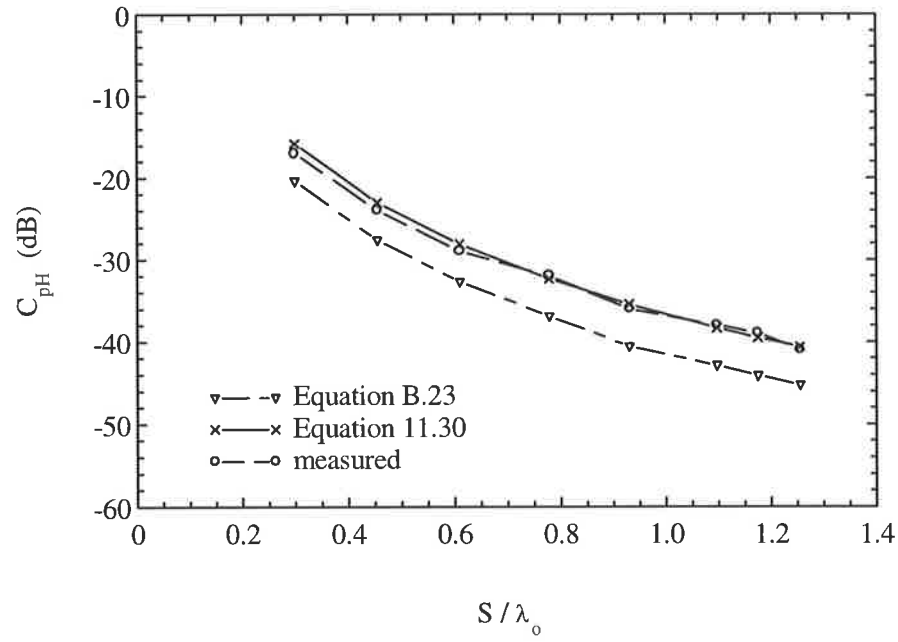

Figure 11.15: Computed and measured H-plane mutual coupling coefficient between two rectangular antenna elements with 3.00 mm thick substrate versus edge spacing normalised with respect to free space wavelength between them (array Nr. 3 of Table 11.1)

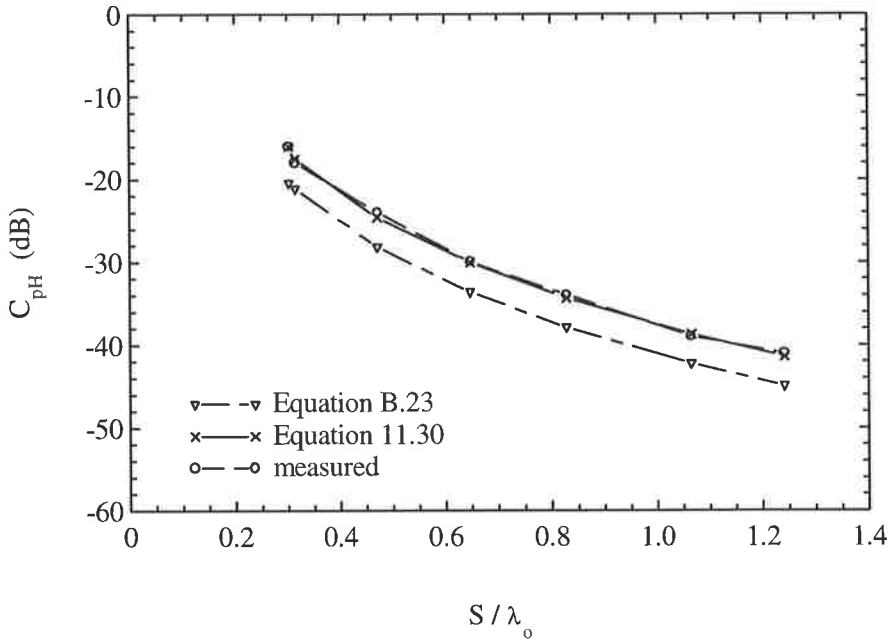

Figure 11.16: Computed and measured H-plane mutual coupling coefficient between two rectangular antenna elements with 3.00 mm thick substrate versus edge spacing normalised with respect to free space wavelength between them (array Nr. 4 of Table 11.1).

11.3.2.2 Coupling in H-plane between two antenna elements with thick substrates

At resonance, the coupling factor C_{pH} between two antenna elements with substrate thicknesses of $h \geq 0.0815\ \lambda_o$ can be calculated from equation 11.1. In this case Z_{12H} is also referred to the feed point location can be calculated from equation 11.29, in which one replaces the W with W_{ef}. The resulting formula for Z_{12H} is [85]

$$Z_{12H} = \frac{25 R_o \lambda_d^5}{2\pi^8 W_{ef}^3 S^2} \sin\left(\frac{\pi W_{ef}}{\lambda_d}\right) \tag{11.31}$$

where W_{ef} is the effective patch width, taking into account the influences of the fringing fields at the edges and the dielectric inhomogeneity of the antenna, similar to equation 11.22, it can be calculated from [137]

$$W_{ef} = W + \left(\frac{L_{eq} - L}{2}\right)\left(\frac{\varepsilon_{eL} + 0.300}{\varepsilon_{eL} - 0.258}\right) \tag{11.32}$$

where L_{eq} is the equivalent patch width calculated from

$$L_{eq} = \frac{h R_o}{Z_{cL}\sqrt{\varepsilon_{eL}}} \tag{11.33}$$

Z_{cL} is the characteristic impedance as a function of the patch length. This can be calculated from equation 11.24 or 11.25 in which L replaces W to account for the lengths of the antenna elements.

The final formula for coupling coefficient in the H-plane is then derived by substituting equations 11.17, 11.26 and 11.31 into 11.1 and considering the cases of $\zeta = H$ and $\alpha = W$ which is replaced by W_{ef} and $\Delta\alpha$ with ΔW in equations 11.26 and 11.27 and setting $R_N = 50\Omega$

$$C_{pH} = 20\log\left[\frac{25R_o}{4\pi^8}\frac{\lambda_o^5}{S^2W_{ef}^3}\frac{1}{R_{TW}}\sin\left(\frac{\pi W_{ef}}{\lambda_o}\right)\right] - 40\log\left[\frac{1}{2}\left(\sqrt{\frac{R_{TW}}{50}} + \sqrt{\frac{50}{R_{TW}}}\right)\right] \tag{11.34}$$

The coupling factor results in the H-plane obtained from equation 11.34 agreeing well with measured results.

As is evident from the close agreement between the measured and calculated C_{pH} coefficients shown in Figures 11.17 - 11.19, the formula 11.34 calculates C_{pH} for antenna arrays with substrates in the range of $h \geq 0.0815\lambda_o$ with good accuracy.

11.4 Results and Discussion

Verification of new formulae reported herein is provided for rectangular antenna elements of various substrate thicknesses and patch dimensions, by comparing computed results for the mutual coupling in the E- and the H-plane with measurements made on two identical element test arrays. Substrate and patch physical characteristics together with their resonant frequencies of the antenna elements used in this chapter are listed in Tables 11.1 and 11.2.

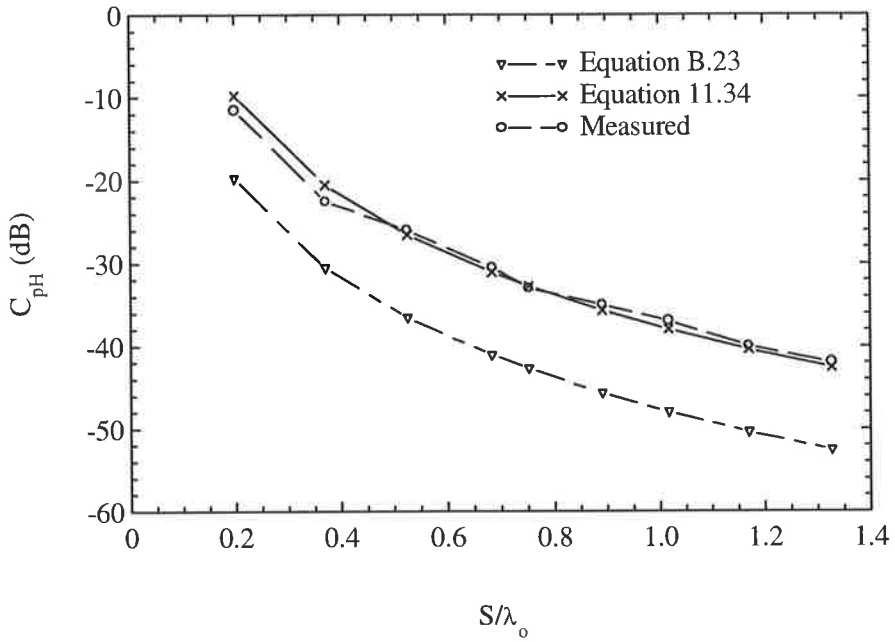

Figure 11.17: Computed and measured H-plane mutual coupling coefficient between two rectangular antenna elements with 6.26 mm thick substrate versus edge spacing normalised with respect to free space wavelength between them (array Nr. 2 of Table 11.2)

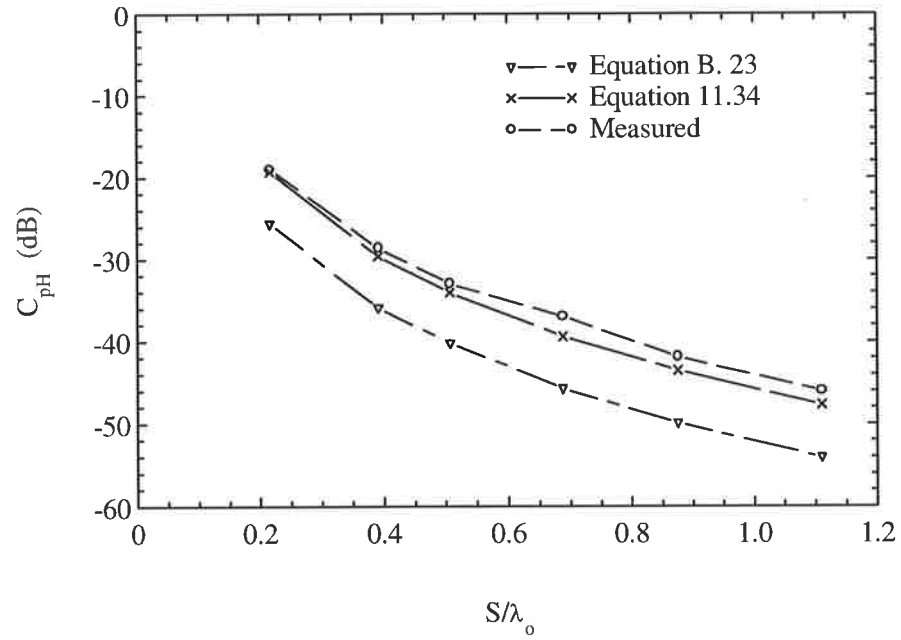

Figure 11.18: Computed and measured H-plane mutual coupling coefficient between two rectangular antenna elements with 7.76 mm thick substrate versus edge spacing normalised with respect to free space wavelength between them (array Nr. 3 of Table 11.2)

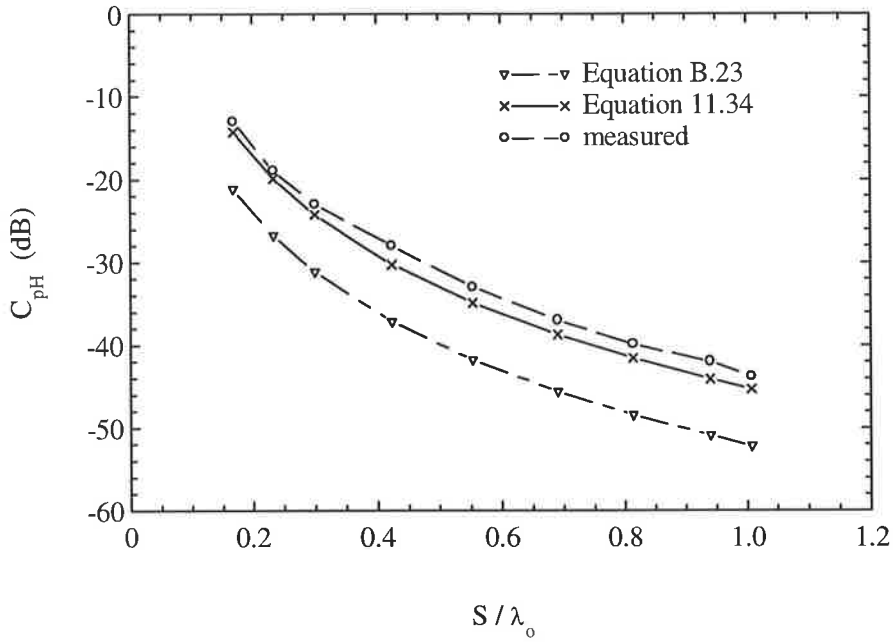

Figure 11.19: Computed and measured H-plane mutual coupling coefficient between two rectangular antenna elements with 9.52 mm thick substrate versus edge spacing normalised with respect to free space wavelength between them (array Nr. 5 of Table 11.2)

Figures 11.3 - 11.6 show the measured mutual coupling results in the E-plane as a function of the normalised separation, S/λ_o, between the edges of two antenna elements and compares these results with those obtained from the new modified equation 11.19 and from equations B.16 and B.46. The dimensions, substrate characteristics and the resonant frequencies of these antenna elements are given in Table 11.1. As can be seen the calculated results using the new equation are in good agreement with the measurements, but, equations B.16 and B.46 fail to accurately predict the coupling factors. Note that the E-plane coupling decreases rapidly for small spacings and slowly for large spacings.

Figures 11.7 - 11.11 show the measured mutual coupling results in the E-plane as a function of the normalised separation, S/λ_o, between the edges of two antenna elements and compares these results with those obtained from the new modified equation 11.28 and from equation B.46. The dimensions, substrate characteristics and the resonant frequencies of these antenna elements are given in Table 11.2. As can be seen the calculated results using the new equation are in good agreement with the measurements, but, equation B.46 fails to satisfactorily predict the coupling factors of these arrays when $S \leq 0.5\ \lambda_o$ and $h \leq 0.2\lambda_d$.

Figures 11.13 - 11.16 show the measured mutual coupling results in the H-plane as a function of the normalised separation, S/λ_o, and compares these results with those obtained from the new modified equation 11.30 and from equation B.23. The dimensions, substrate characteristics and the resonant frequencies of these antenna elements are given in Table 11.1. As can be seen that the results obtained from the new equation 11.30 better agrees with measurements than those results obtained from equation B.23.

Figures 11.17 - 11.19 give the measured H-plane coupling results as a function of the normalised separation, S/λ_o, and compare these results with those obtained from new equation 11.34 and the results obtained from equation B.23. The dimensions of these antenna elements are listed Table 11.2. As can be seen the calculated results using the new equation are in good agreement with the measurements presented while the results obtained from equation B.23 does not yield satisfactory results due to the omission of the effects of relative permittivity and thickness of the substrates, as well as the contribution of surface waves.

Similar to antenna arrays with thin substrates, the H-plane coupling level decreases monotically with separation. However, coupling in the E-plane is much stronger than that in the H-plane, due partly to enhanced coupling to the substrate surface wave modes.

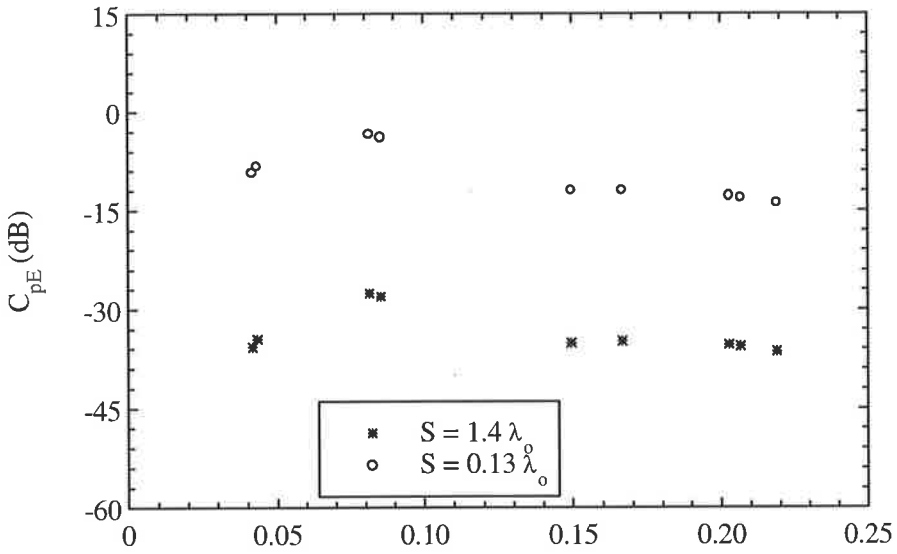

Figure 11.20: E-plane mutual coupling coefficients versus substrate electrical thicknesses of all arrays listed in Tables 11.1 and 11.2 for $S = 0.13\ \lambda_o$ and $S = 1.4\ \lambda_o$ values.

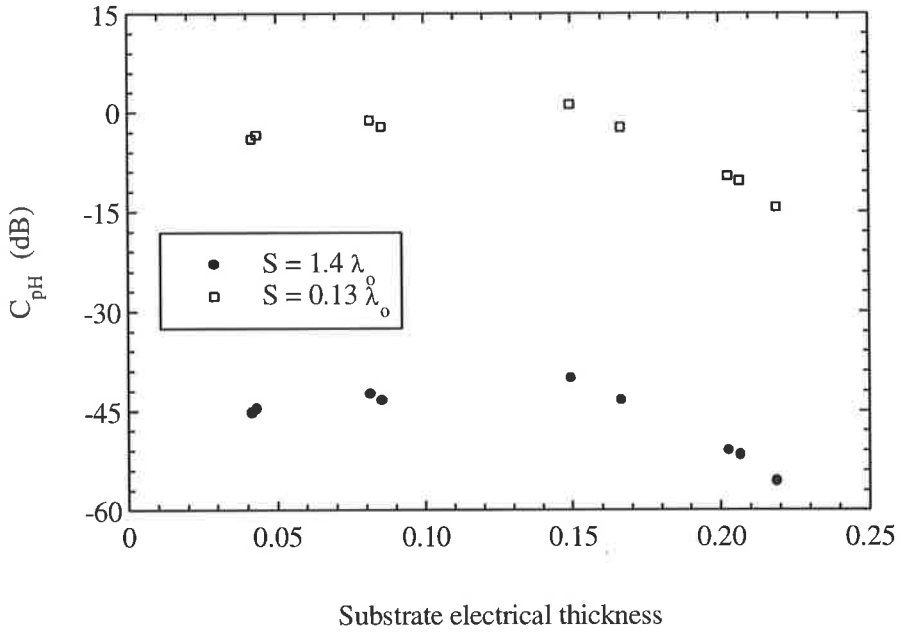

Figure 11.21: H-plane mutual coupling coefficients versus substrate electrical thicknesses of all arrays listed in Tables 11.1 and 11.2 for S = 0.13 λ_o and S = 1.4 λ_o values.

It is known, that a common property of most microsprip antennae is that the antenna launches surface wave modes, in addition to the fields radiated into space. In the case of finite-size substrates, the power launched into the surface waves diffracts from the edges of the substrate, resulting in a disturbance of the radiation characteristics of microstrip antennae and arrays.

The E- and H-plane mutual coupling as a function of substrate thicknesses of all arrays listed in Tables 11.1 and 11.2 are plotted in Figures 11.20 and 11.21 for S = 0.13 λ_o and S = 1.4 λ_o values in order to ascertain whether the surface wave significantly contributes to the coupling. These figures indicate that the excitation of surface waves results in increased mutual coupling between distant antenna elements in both the E- and H-plane, since the surface wave fields decay more slowly with radial distance than do the space wave fields. For these reasons the excitation of surface waves is generally undesirable and can not be neglected.

11.5 Conclusion

The mutual coupling in both the E-and the H-plane are studied from the point of view of mutual coupling where the thickness of substrates of the antenna elements are considered to vary between

$0.0419\ \lambda_d \leq h \leq 0.2189\ \lambda_d$ (1.50 mm $\leq h \leq$ 9.52 mm) and the distance between the edges of the elements between $0.13\ \lambda_o \leq S \leq 1.4\ \lambda_o$.

A set of formulae have been developed for computing the mutual coupling coefficients between two identical probe fed rectangular antenna elements in E- and H-plane configurations by modifying the formulae published by Dubost taking into account the substrate permittivity and thickness, antenna effective dimensions, mismatching, and losses associated with dielectric substrate, conductor, radiation and surface waves.

A number of antenna arrays are designed, manufactured, and tested to validate the developed formulae which lead to a simple, fast and accurate computation of the mutual coupling coefficients in E- and H-plane configurations. Therefore, the method presented here is significant for practical computer aided design of mutual coupling.

The accuracy of the modified formulae was demonstrated by comparing computations with measured results for mutual coupling. Good agreement was obtained between the calculated and measured results for antenna elements with substrates thinner than approximately $0.0815\lambda_o$. Consequently, for antenna elements with thicker substrates Dubost's equations were modified again by taking into account the permittivity and thickness of the substrate and the contribution of the surface waves.

The calculated values of mutual coupling coefficient in the E- and also H-plane of elements with *thicker substrates* are very similar to the measured data. This verifies the accuracy of the modified equations for evaluating the mutual coupling in both the E- and H-plane configurations in the case of thick antenna elements.

The contributions described in this chapter are therefore:

- The study of mutual coupling for rectangular microstrip antenna arrays with various substrate thicknesses.

- The establishment of the threshold of application of the considered method for computing the mutual coupling coefficient.

- The development of a computationally efficient closed form expression for the computation of mutual coupling coefficient in the
    - *E-plane* between two antenna elements with *thin substrates,*
    - *H-plane* between two antenna elements with *thin substrates,*
    - *E-plane* between two antenna elements with *thick substrates,*
    - *H-plane* between two antenna elements with *thick substrates*

- The development of a computationally efficient method which allows accurate mutual coupling prediction for rectangular antenna arrays considerably thicker than those reported elsewhere.

- The conducting of experiments to validate numerical predictions.

- An understanding of the fundamental effects of
    - thin substrates on mutual coupling,
    - thick substrates on mutual coupling,
    - surface waves on mutual coupling.

- The discovery of the small mutual coupling for the widely separated antenna elements with thick substrates.

- The incorporation of the effective dimensions, the effective permittivity, losses associated with dielectric, copper, radiation and surface waves and the mismatch that may occur due to the interaction between two elements as the spacing increases into the mutual coupling coefficient equation.

It is important to note that calculations for the E-plane and the H-plane coupling coefficients are especially sensitive to substrate thickness. It is also apparent that H-plane coupling is stronger than E-plane for small separations. This coupling decreases more rapidly than the E-plane coupling, which is sustained by the surface wave and slightly changes for greater spacings.

Chapter 12

Conclusions and Recommendations

12.1 Conclusions

The aim of this chapter is to summarise the thesis contents, contributions and findings, and highlight some possible directions for future research.

Owing to the great variety of analytical techniques for microstrip antennae this thesis could not provide extensive information about each analytical techniques. But some of these techniques with some indication of limitations and considerations when designing and analysing microstrip antennae at microwave frequencies are briefly discussed without mathematical derivations and formulations, in *Chapter 2*. It was found the majority of the previously proposed analytical techniques are only of academic interest. The use of traditional models such as the transmission line model and the cavity model has been identified as having practical potential and advantages over other techniques in designing and analysing microstrip antenna elements. They have provided good results for thin antennae designs but needed modification for thicker antennae.

This thesis is essentially analytical, numerical and practical in nature. The formulations used aim to fully convey the principles involved but with only as much mathematical detail as is necessary for a clear understanding of the points being made. In addition, the mathematics is used as a tool to explain basic concepts to design and study antenna performance. In fact, some of the material covered represents lessons learned from hardware development.

The suitability and threshold of the applicability of the formulae available in the literature on the design of physical properties of rectangular microstrip antenna elements are demonstrated, and new empirical formulae to aid in the design of these properties are developed in *Chapter 3*. The applicability of a formula based on the TLM for computing the resonant lengths of thin antenna elements is identified and applied. It has been found that antenna elements designed using formulae available in the literature for calculating patch width and feed point locations did not resonate for the range of substrate thickness considered in this thesis. New empirical formulae for computing widths for antenna elements with respectively thin and thick substrates and lengths for antenna elements with thick substrates are devised from the experimental data obtained by a trial-and-error design technique. Feed point locations were also determined experimentally because no formulae are available to compute them.

Because a microstrip antenna has air dielectric above it, an effective permittivity must be computed for use in the design equations. A formula for effective permittivity has been derived from the relationship of the velocity of light in air and the phase velocity in the substrate material.

The influence of substrate thickness on the antenna physical properties is also discussed in Chapter 3.

Three new methods for the calculation of the resonant input resistance of rectangular microstrip antenna elements are presented in *Chapter 4*. The first method is based on the refinement of the cavity model and the transmission line model considering the antenna element in the fundamental modes and is modelled by a simple resonant parallel RLC circuit in series with conductance X_L, which represents the feed probe. The RLC element values are related to the physical parameters, such as patch length, width, feed point location, relative permittivity and thickness of the substrate. Due to the resonant nature of the investigated antenna element, its resonant input resistance is related to the quality factors associated with the system losses.

This technique has been used successfully to calculate the resonant input resistance of rectangular antenna elements with thin substrates.

A second method based on the improved cavity model has been developed for computing the resonant input resistance for antenna elements with thick substrates by considering the antenna in the fundamental mode, modelled by a simple resonant parallel RLC circuit. It takes into account the effective patch dimensions, the substrate dynamic permittivity, the resistance due to power loss in the surface wave, the radiation resistance of the patch, and the resistances due to losses in the conductor and dielectric. A third method is an alternative formula for computing the resonant input resistance for antenna elements with thick substrates. It has been derived empirically using experimentally derived resistance data. A detailed set of graphs based on formulae and experimental data is given for a representative set of parameters, and the predicted results are backed by experimental confirmation.

The applicability of both the TLM, the CM and the magnetic walls models for calculating the resonant frequencies of rectangular microstrip antenna elements is verified in *Chapter 5*. The formula based on the TLM demonstrates its suitability for computing the resonant frequencies of antenna elements with thin substrates. The formulae based on the CM do not yield satisfactory results for the investigated substrate thickness range. For computing the resonant frequency of thick antenna elements, the formula used for thin antennae was modified by adding a new empirically derived correction factor. An alternative formula for computing the resonant frequencies of thick antenna elements is also derived using a curve fitting method. Both formulae, the modified and the alternative formula, give the resonant frequencies for antenna elements with thick substrates correctly, as is evident from the close agreement between the calculated and measured results. An investigation of the relationship between patch lengths and resonant frequencies has also been performed. This has been shown to hold true for various thickness of substrates.

Several formulae based on the CM and the TLM are combined to produce a closed-form expression for calculating the impedance bandwidth of antenna elements with thin substrates in *Chapter 6*. The expression takes into account the effects of radiation, conductor and dielectric losses, with their quality Q-factors. It also provides insight into the fundamental influence of the substrate materials and antenna dimensions on bandwidth. The bandwidth values obtained from this formula confirm those obtained from MSAnt program and from measured return loss plots of all antenna elements investigated in Chapters 3, 4 and 5. This research has also

revealed that increased substrate thickness produces increased bandwidth. For example, a 1.07% bandwidth was measured for VSWR = 2.1 at 7.740 GHz with a 0.0065 λ_d (0.17 mm) substrate thickness, but a 15.90% bandwidth was achieved at 5.100 GHz with a 0.1292 λ_d (4.76 mm) substrate thickness. It has also been demonstrated that electrically thin antenna elements are between 71.3 % and 99.8 % efficient.

A wider bandwidth is usually accomplished by using a thick substrate with low permittivity; yet there is a limit on the maximum useable substrate thickness such that surface waves will not be radiated. Increasing the substrate thickness increases the excitation of surface waves, resulting in lowered efficiency and also lowered bandwidth. For thicker substrates the effect of surface waves is predominant and must be taken into account. Existing methods as well as the proposed formula for computing the bandwidth, are inaccurate for thick substrates. This chapter, a new closed-form expression based on the cavity model and the exact Green's function for a grounded dielectric slab has been developed for computing the bandwidth of rectangular microstrip antenna elements with thick substrates taking into account both the power radiated in the space waves and the power radiated in surface waves and a correction factor. The correction factor was derived by means of a curve-fitting technique and is the ratio of the characteristic impedance of an air filled microstrip line and the characteristic impedance of a substrate filled microstrip line.

The accuracy of this formula has been established by comparing calculated bandwidth results with those obtained from return loss plots of antenna elements investigated in Chapters 3, 4 and 5. It has been shown that the method given here gives results in good agreement with measurements.

This work has also revealed that increased substrate thickness does not produce increased bandwidth as expected. For example, a 17.50% bandwidth was measured for VSWR = 2.1 at 8.000 GHz with a 0.1405 (3.30 mm) thick antenna, but only a 21.60% bandwidth at 3.200 GHz with a 0.2182 λ_d (12.81 mm) thick antenna was achieved. It has also been demonstrated that electrically thick antenna elements are between 58.5 and 69.6 percent efficient.

Chapter 7 discusses formulae based on the two-slots model, the TLM, the CM and the electric surface current model for calculating the far field radiation patterns in the E- and H-plane respectively of rectangular microstrip antenna elements with various substrate thicknesses, and assesses their suitability and threshold of their applicability. It has been

demonstrated that formulae based on the two-slots model, TLM and CM yield the radiation patterns E- plane of antenna elements with thin substrates with good accuracy, but they become increasingly inaccurate as the substrate thickness is increased. For computing the E-plane radiation pattern of antenna elements with thick substrates, the line extension is incorporated in the formula eg based on the two-slot model to account for the inhomogeneity of the medium and fringing field, respectively. This formula gives the E-plane pattern in good agreement with measurement. It has also been demonstrated that the applicability of the formula on the two-slots, the TLM and the CM for calculating the radiation patterns in the H-plane are not restricted to a certain material permittivity and/or thickness of the substrates. They are valid for all antenna elements introduced in this chapter.

A study of the effect of the substrate thickness on the patterns shows these to be quite significant. Generally, the microstrip antenna elements exhibited satisfactory and nearly symmetrical E-and H-plane patterns, but very thick antennae exhibited some variations that could be caused by surface wave diffraction at the substrate edges. The half power beamwidth in the E- and H-plane have also been determined for each of the antenna elements investigated in this thesis.

In electronic warfare, wideband radar and communication systems applications, the antenna must meet particularly demanding specifications. Physically, it must be low profile, light weight, able to withstand thermal stress and be extremely rugged. Moreover, it should neither protrude inwardly to disrupt the mechanical structure, nor disturb the aerodynamic flow across the skin of the platform. The electrical characteristics of the antenna must include high efficiency and wide frequency bandwidth, together with low side-lobes.

The many desirable features of conventional microstrip antennae are well known, as is the fact that narrow intrinsic bandwidth is perhaps the most serious of their limitations. This arises from the fact that the region under the patch is basically a thin resonant cavity with a high quality factor. *Chapter 8* is devoted to a novel miniaturised microstrip antenna element which provides a broad bandwidth as high as 9.3% which is 2.16 fold the bandwidth of a conventional microstrip antenna having the same patch dimensions. It consists of a rectangular metal patch on one side of a dielectric sheet, in which the dielectric substrate is restricted to the same size as the metal patch and a ground plane on the other side. This broad-band antenna is fed by a coaxial line from the back through the ground plane. This antenna offers an overall reduction in the size as high as 70 % and in the cost 90% of a corresponding rectangular patch antenna.

A novel numerical technique based on the TLM and the CM is developed for the calculation of physical and operational properties for this antenna element. Measured data on the performance characteristics of this antenna element are presented and compared with the characteristics of a conventional microstrip antenna element having the same patch dimensions. The results from this technique are in good agreement with measured results.

A dual-band antenna is useful in situations where it is required to operate in two distinct frequencies which may be too far apart for a conventional microstrip antenna to perform efficiently at both frequencies. The design, fabrication, testing and analysis of a novel dual-band miniaturised microstrip antenna is introduced and discussed in *Chapter 9*. It consists of a rectangular metal patch on one side of a dielectric sheet in which the dielectric substrate is restricted to the same size as the metal patch and ground plane on other side. The antenna is fed by a coaxial line from the back through the ground plane.

A numerical method based on the TLM and the CM for computing the dimensions and operational properties for this antenna element is developed. Measured performance data is presented and compared with the calculated results. Good agreement between theory and experiment was achieved. The overall reduction in the size of this antenna element is as high as 70 % and in the cost 90 % of a corresponding dual band antenna element.

In many applications, only a few distinct frequency bands are needed, rather than a continuous spectrum of operating frequency such as in the Global Positioning System. The novel dual-band miniaturised antenna element presented here fulfils the following demands compared to the dual-band antenna elements introduced by other authors: it is economical, occupies a minimum space, improved electrical performance and is capable of being distributed over and/or embedded into the bodies of surface borne and space borne vehicles, eg. aircraft, ships, missiles. It is also applicable to satellite systems where two channels are needed to receive/transmit the telecommand and telemetry signals. Phased arrays based on these antennas can be easily designed for use in Space-Borne Imaging or Synthetic-Aperture and Secondary Surveillance Radar systems. The physical and electrical properties of this antenna element are satisfactorily predicted.

Design details, analysis, calculations and experimental observations of a novel miniaturised microstrip ring antenna element are described in *Chapter 10*. It consists of a metal ring patch on one side of a dielectric sheet, in which the dielectric substrate is restricted to the same size as

the metal ring patch, and a ground plane on the other side. This ring antenna is fed by a coaxial line from the back through the ground plane. Measured performance data is presented and compared with calculated results. Good agreement between numerical results and experiment was achieved.

Miniaturised antenna elements or arrays attached on or embedded in bodies of space borne vehicles have appropriate mechanical and thermal characteristics and do not result in any aerodynamic drag. Other advantages of these antennae are: the usual configuration with the antenna behind a radome is eliminated completely, hence the typical pattern distortion effects caused by radomes will not occur, they are also very simple to manufacture, and the materials are low cost compared with traditional solutions using high tolerance machining of metal, they require less space and are light weight, they do not require different processing methods or modification for use on doubly curved surfaces, and they have wider bandwidth.

In *Chapter 11* several formulae, based on the volume equivalence theorem, classical Schelkunoff theory and a theoretical model equivalent to a lossy transmission line, are combined to produce a closed-form expressions for calculating mutual coupling coefficients between two identical probe fed rectangular microstrip antenna elements in both respectively the E- and H-plane coupling configurations for the dominant TM_{10} mode.

A number of antenna arrays have been designed, constructed, and measured to validate these formulae. The substrate thicknesses of the designed antenna arrays are considered to vary between $0.0419\ \lambda_d \leq h \leq 0.2189\ \lambda_d$ ($1.50\ mm \leq h \leq 9.52\ mm$) and the distance between the edges of the elements between $0.1337\ \lambda_o \leq S \leq 1.364\ \lambda_o$. Good agreement was obtained between the measured results and those obtained from these formulae for antenna arrays with substrates thinner than approximately $0.0815\ \lambda_o$.

As the substrate becomes thick the differences between the measured and calculated results become large. Thus, modifications to these formulae are made, in order to increase the accuracy of the predictions for the mutual coupling coefficient. These modifications take into account the surface wave contribution, mismatching that may occur between the elements, the thickness and relative permittivity of the substrate material and the effective dimensions of the antenna elements. These are applied to a number of antenna arrays that have been designed, constructed, and tested for both the E-and H-plane coupling configurations for the dominant TM_{10} mode resulting in good agreement.

Note that, the formulae given in Chapter 3 are applied to determine the dimensions and the feed point locations of the antenna elements used in the array design.

From the results it is noted that the use of electrically thick dielectric substrates produces antenna elements which exhibit low mutual coupling. This fact is useful for microstrip based array design. It is also found that electrically thick substrates may be employed at lower frequencies to reduce mutual coupling effects. In addition, the method presented here has significant advantages for practical computer aided design of mutual coupling.

12.2 Point Summary of Contributions

In summary, this thesis describes the development of design formulae based on the TLM and CM for microstrip antenna elements and the mutual coupling between two elements with various thicknesses and permittivities of substrate materials. The original contributions of the research are outlined in the body of the thesis, however the main achievements of the work are:

- A brief discussion of existing methods with a view to understanding their merits and limitations.

- For completeness the more common features, advantages, disadvantages and applications of microstrip antennae are briefly described.

- Typical antenna design criteria are listed and the outstanding design problems that are fundamental to microstrip antennae are reviewed.

- The development of efficient computational tools to aid in the physical and electromagnetic design of antenna elements, miniaturised antenna elements and arrays.

- The establishment of design trends for microstrip antennae.

- An understanding of the fundamental effects of substrate thickness on the physical and electromagnetic properties of microstrip antenna elements and arrays.

- The development of formulae for computing the physical and electrical properties of antenna elements with thin and thick substrates by modifying the formulae based on the TLM and CM.

- The design, analysis and exploration of physical and electromagnetic properties of miniaturised broad-band, dual-band and ring antenna elements.

- The development of a method for calculating the mutual coupling coefficient based on the volume equivalence theorem and a theoretical model equivalent to a lossy transmission line, take into account surface wave contribution, mismatching, effective dimensions of the antenna elements, and effective relative permittivity of the substrate materials.

The research represents substantial advances in the design and analysis of microstrip antenna elements with various thickness and relative permittivity of substrate materials, the calculation of mutual coupling coefficients between two antenna elements, and the design of novel miniaturised antenna elements for microwave frequency applications.

12.3 Recommendations for future work

The research presented in this thesis and in the above publications has demonstrated that the introduced method is a viable and effective practical approach to the design of rectangular microstrip antennae, arrays, miniaturised broad-band, dual-band, and ring antenna elements with various thickness and relative permittivity of the substrate materials. However, this conclusion is based on numerical and experimental studies only. In view of the development of a practical design method for circular antenna elements, arrays, miniaturised circular antenna elements, and arrays with various thicknesses and relative permittivities of the substrate materials, there are some theoretical and practical areas in which further research is suggested.

The impetus for future design and development of miniaturised, circular or dual polarised broad-band, and dual-band antenna elements and arrays will be provided by the traditional military oriented applications, as well as commercial applications. Therefore, trends toward super light weight, very cost-effective and easily manufacturable antennae and arrays will

increase. It is appropriate to point out several areas in which further research could be carried out.

Further development of miniaturised antennae is required to achieve:

- circular polarisation operation with a single feed in the proper position,
- dual-polarisation operation obtained by means of four narrow slots close to the edges,
- several applications in radar, missile, satellite and communication systems require the use of a circular or dual polarisation.
- large bandwidth and gain obtained by stacking antenna elements,
- design of miniaturised antenna elements for biomedical applications,
- design of a miniaturised antenna element fed by a microstrip line.

Control of the polarisation properties of microstrip antennae is another area of activity arising largely out of the current awareness for making greater use of the polarisation properties of waves, particularly in radar.

The effect of varying the patch conductor thickness on the electromagnetic properties of rectangular microstrip antenna elements have been investigated.

The effect of varying the thickness of patch conductor on the electromagnetic properties of classical and miniaturised rectangular microstrip antenna elements is another field to be investigated further. As it is documented in a work published by the author [206] using a thick patch on a thin substrate is an excellent way of widening the bandwidth of an antenna element [151, 206].

The methods developed in this thesis are shown to be suitable for the design and analysis of all the significant physical and electrical properties of the conventional rectangular and miniaturised microstrip antenna elements, and the mutual coupling coefficients between two antenna elements with various thickness and permittivity of the substrate materials.

Appendix A

Formulae Based on the Electric Surface Current Model

The electric surface current model [63, 64] primarily depends on an "educated guess" of the current density distribution on the patch surface under the assumption that the radiation is small, ie, the Q of the antenna is high. Assuming the patch is absent the Green's function, which is defined as the electric field generated by a unit current source on the surface on the substrate can be determined. The component of this electric field is parallel to the interface at the plane z = h.

This model uses the Fourier transform domain for the analysis of microstrip antennae. Consider a rectangular microstrip antenna element whose ground plane is at the plane z = 0. The patch surface current J(x, y) is thus related to its two dimensional Fourier transform $J(k_x, k_y)$ by the equation

$$J(x,y) = \frac{1}{4\pi^2} \iint \tilde{J}(k_x, k_y) e^{-j(k_x x + k_y y)} dk_x dk_y \qquad (A.1)$$

where k_x and k_y are parameters in the Fourier domain. Similar relationships hold between E and H fields and their Fourier transforms.

In order to find the field due to an arbitrary current distribution J(x, y) on the surface the wave equation for the electric field can be solved under appropriate boundary conditions. Fourier components of the electric field as a function of the corresponding Fourier component of the current can be shown that [63, 64]

$$\begin{bmatrix} \tilde{E}_x(k_x,k_y) \\ \tilde{E}_y(k_x,k_y) \end{bmatrix} = \begin{bmatrix} \tilde{G}_{xx}(k_x,k_y) & \tilde{G}_{xy}(k_x,k_y) \\ \tilde{G}_{yx}(k_x,k_y) & \tilde{G}_{yy}(k_x,k_y) \end{bmatrix} \begin{bmatrix} \tilde{J}_x(k_x,k_y) \\ \tilde{J}_y(k_x,k_y) \end{bmatrix} \tag{A.2}$$

where the tildes denotes the Fourier transforms, and the elements of the G matrix. The elements of the matrix G are given by

$$\tilde{G}_{xx} = C\left(k_x^2 - k_o^2\right)\gamma_2 \tan\gamma_2 h + j\gamma_1\left(\varepsilon_r^2 k_o^2 - k_x^2\right) \tag{A.3}$$

$$\tilde{G}_{xy} = C\left[-k_x k_y\left(j\gamma_1 - \gamma_2 \tan\gamma_2 h\right)\right] \tag{A.4}$$

$$\tilde{G}_{xy} = C\left[-k_x k_y\left(j\gamma_1 - \gamma_2 \tan\gamma_2 h\right)\right] \tag{A.5}$$

$$\tilde{G}_{yy} = C\left(k_x^2 - k_o^2\right)\gamma_2 \tan\gamma_2 h + j\gamma_1\left(\varepsilon_r^2 k_o^2 - k_x^2\right) \tag{A.6}$$

with

$$C = \frac{\eta_o}{k_o\left(j\gamma_1 \cot\gamma_2 h - \gamma_1\right)\left(j\varepsilon_r\gamma_1 - \gamma_2 \tan\gamma_2 h\right)} \tag{A.7}$$

$$\gamma_1 = \sqrt{k_o^2 - k_x^2 - k_y^2} \tag{A.8}$$

$$\gamma_2 = \sqrt{\varepsilon_r k_o^2 - k_x^2 - k_y^2} \tag{A.9}$$

where $\eta_o = 120\pi\ \Omega$ is the free-space wave impedance; h and ε_r are the thickness and dielectric constant of the substrate, respectively and $j = (-1)^{0.5}$.

Once the Green's function is known, the electric field in the space domain can be calculated by taking the inverse Fourier transform of $\bar{E}(k_x, k_y)$, provided that the patch surface current is known

$$P_{sp} = \left(\frac{V_o}{Z_o}\right)^2 \frac{\eta_o}{2\pi}\varepsilon_{ew}\int_0^{\frac{\pi}{2}}\int_0^{\frac{\pi}{2}} F(\theta,\phi)\,d\phi\,d\theta \tag{A.10}$$

with

$$f(\theta,\phi)=\frac{\cos^2\frac{\pi\sin\theta\cos\phi}{2\sqrt{\varepsilon_{ew}}}}{\left(\sin^2\theta\cos^2\theta-\varepsilon_{ew}\right)^2}\,\mathrm{sinc}^2\left(Wk_o\sin\theta\sin\frac{\phi}{2}\right)\cdot$$

$$\left[\frac{\cos^2\theta\sin\theta\sin^2\phi}{\left(\varepsilon_r-\sin^2\theta\right)\cot^2\left(k_oh\sqrt{\varepsilon_r-\sin^2\theta}\right)+\cos^2\theta}+\frac{\cos^2\theta\sin\theta\left(\varepsilon_r-\sin^2\theta\right)\cos^2\phi}{\left(\varepsilon_r-\sin^2\theta\right)+\varepsilon_r^2\cos^2\theta\cot^2\left(k_oh\sqrt{\varepsilon_r-\sin^2\theta}\right)}\right] \qquad \text{(A.11)}$$

The E- and H-plane patterns can be obtained from the integrand of equation A.10 and the normalised $V_o/Z_o = 1$. The E-plane radiation pattern is functionally expressed as [63, 64]

$$F_E(\theta,\phi=0)=\varepsilon_{ew}\left[1+\varepsilon_r\cot^2\left(k_oh\sqrt{\varepsilon_r}\right)\right]\frac{\cos^2\left(\frac{\pi\sin\theta}{2\sqrt{\varepsilon_{ew}}}\right)}{\left(\sin^2\theta-\varepsilon_{ew}\right)^2}$$
$$\cdot\frac{\cos^2\left(\varepsilon_r-\sin^2\theta\right)}{\left(\varepsilon_r-\sin^2\theta\right)+\varepsilon_r^2\cos^2\theta\cot^2\left(k_oh\sqrt{\varepsilon_r-\sin^2\theta}\right)} \qquad \text{(A.12)}$$

and the H-plane radiation pattern is

$$F_H\left(\theta,\phi=\frac{\pi}{2}\right)=\left[1+\varepsilon_r\cot^2\left(k_oh\sqrt{\varepsilon_r}\right)\right]\mathrm{sinc}^2\left(\frac{Wk_o\sin\theta\sin\phi}{2}\right)$$
$$\cdot\frac{\cos^2\theta}{\left(\varepsilon_r-\sin^2\theta\right)\cot^2\left(k_oh\sqrt{\varepsilon_r-\sin^2\theta}\right)+\cos^2\theta} \qquad \text{(A.13)}$$

The electric surface current model incorporates the surface wave effects in the analysis. Its limitations are the assumption of an infinitely large ground plane, the assumption of a constant transverse current (which may be of questionable accuracy for large W/λ_o values) and the omission of feed location in the calculation of the input impedance.

Appendix B

Mutual Coupling Between two Rectangular Microstrip Antenna Elements

At resonance the coupling coefficient, C_p, between two rectangular antenna elements expressed in decibels is given by

$$C_p = 20\log|S_{12}| \tag{B.1}$$

where S_{12} is the scattering transfer coefficient which may be calculated by [205].

$$|S_{12}| = \left|\frac{2\overline{Z}_{12}}{\left(1+\overline{G}_a\right)^2 - Z_{12}^2}\right| \tag{B.2}$$

where Z_{12} is the normalised mutual impedance, which is equal to

$$\overline{Z}_{12} = \frac{Z_{12}}{R_N} \tag{B.3}$$

where $R_N = 50\Omega$ the normalisation resistance, and Z_{12} is the mutual impedance, which is given by [202]

$$Z_{12} = \frac{U_o}{I_E(0)} \tag{B.4}$$

where $I_E(0)$ is the fed patch input current, U_o is the input induced voltage on the second open-circuited patch, and $\overline{G}_a$ is the normalised radiation conductance which is equal to

$$\overline{G}_a = \frac{R_r}{R_N} \tag{B.5}$$

where R_r is the radiation resistance, related to the feed point located on the patch edge. At resonance it can be calculated by [202, 204]

$$R_r = \frac{5R_o}{2\pi^3}\left(\frac{\lambda_o}{W}\right)^2 \tag{B.6}$$

where $R_o = 120\ \pi\Omega$ is the vacuum medium resistance, λ_o the free space wavelength. When considering two identical rectangular antenna elements in a collinear position at resonance, using equations B.1 and B.2, the coupling factor C_p can be written as

$$C_p = 20\log C_{p_1} - 20\log C_{p_2} \tag{B.7}$$

with

$$C_{p_1} = \left|\frac{\overline{Z}_{12}}{2G_a}\right| \tag{B.8}$$

and

$$C_{p_2} = \left|\frac{1}{2}\left(\sqrt{\overline{G}_a} + \frac{1}{\sqrt{\overline{G}_a}}\right)\right|^2 = \left|\frac{1}{2}\left(\sqrt{\frac{R_r}{R_N}} + \sqrt{\frac{R_N}{R_r}}\right)\right|^2 \tag{B.9}$$

Equation B.8 ignores the feed point location, while equation B.9 takes mismatching into account. For a matched antenna the coupling coefficient reduces to equation B.8, because $R_r = R_N$.

In the next section the E- and H-plane coupling will be separately investigated.

B.1 Coupling in the E-Plane (Collinear Position)

Dubost [202] derived the total electric field induced on the second patch due to the fed patch electric and polarisation currents for $\phi = 0$ and $\theta = h/S$, as

$$(E_\theta)_o = jR_o \frac{5W}{\pi^3\lambda_o}\ \varphi\ I_E(o)\ \cos\left(\frac{\pi}{2\sqrt{\varepsilon_r}}\right)\left[1 + \frac{\varepsilon_r}{(\varepsilon_r - 1)}\left(\frac{h}{S}\right)^2\right]\exp\left(\frac{j\pi}{2\sqrt{\varepsilon_r}}\right) \tag{B.10}$$

with

$$\varphi = \exp\left(-j2\pi\frac{S}{\lambda_o}\right)\frac{1}{S} \tag{B.11}$$

where S is the distance between the two antenna elements.

The polarisation current induced in the second patch is given by [202], as

$$I_D = j\frac{2\pi}{\lambda_o}\frac{1}{R_o}Wh\,\varepsilon_r(E_\theta)_o \tag{B.12}$$

Taking the boundary conditions into account and assuming that h< S, the resolution of the two equivalent transmission line differential equations, from equation B.4 [202] yields

$$Z_{12} = -R_o\frac{10h}{\pi^2 S}\frac{\varepsilon_r^2}{(\varepsilon_r-1)}\cos^2\left(\frac{\pi}{2\sqrt{\varepsilon_r}}\right)\left[1+\frac{\lambda_o^2}{4\pi^2 hS\varepsilon_r}\right]\exp j\left(\frac{\pi}{2\sqrt{\varepsilon_r}}-\frac{2S\pi}{\lambda_o}\right)$$
$$\cdot\left[1+\exp\left(-j\frac{\pi}{\sqrt{\varepsilon_r}}\right)\right] \tag{B.13}$$

Using equation B.8, yields

$$C_{p_1} = 20\log\left\{\frac{10h}{\pi^2 S}\frac{\varepsilon_r^2}{(\varepsilon_r-1)}\left[1+\frac{\lambda_o^2}{4hS\pi^2\varepsilon_r}\right]\cos^2\left(\frac{\pi}{2\sqrt{\varepsilon_r}}\right)\right\} \tag{B.14}$$

Substituting equation B.6 into B.9 one deduces the mismatching coupling factor, C_{p2} as:

$$C_{p_2} = \frac{1}{2}\left(\sqrt{\frac{R_r}{R_N}}+\sqrt{\frac{R_N}{R_r}}\right) \tag{B.15}$$

Then, using equations B.7, B.14 and B.15 one deduces the coupling coefficient, C_p, in the E-plane in dB, as:

$$C_p = 20\log\left\{\frac{10h\varepsilon_r^2}{\pi^2 S(\varepsilon_r-1)}\left[1+\frac{\lambda_o^2}{4hS\varepsilon_r\pi^2}\right]\cos^2\left(\frac{\pi}{2\sqrt{\varepsilon_r}}\right)\right\} - 40\log\left[\frac{1}{2}\left(\sqrt{\frac{R_r}{R_N}}+\sqrt{\frac{R_N}{R_r}}\right)\right] \tag{B.16}$$

B.2 Coupling in the H-Plane (Parallel Position)

The induced voltage, U_o, given in equation B.4 was derived by applying the classical Schelkunoff theory

$$U_o = \frac{(E_\theta)_{\pi/2}}{(\alpha+jk)}\tanh\left[\frac{\lambda_o}{4\sqrt{\varepsilon_r}}(\alpha+jk)\right] \tag{B.17}$$

with

$$\alpha = \frac{4}{5} Wh \left(\frac{\pi}{\lambda_o} \right)^3 \tag{B.18}$$

$$k = \frac{2\pi f}{c_o} \sqrt{\varepsilon_r} \tag{B.19}$$

where $(E_q)p/2$ is the electric field which is parallel by the fed patch electric current distribution. This field was obtained for $\theta = \frac{\pi}{2}$ and $\phi \approx (\frac{\pi}{2} - \frac{h}{S})$ as

$$(E_\theta)_{\pi/2} = j \frac{5}{\pi^4} R_o \psi I_E(0) \frac{h}{S} \left(\frac{\lambda_o}{W} \right)^2 \sin\left(\pi \frac{W}{\lambda_o} \right) \tag{B.20}$$

Using equations B.4, B.21 and B.20, the mutual impedance related to the feed point location was deduced as

$$Z_{12} = \frac{25}{2} \frac{R_o}{\pi^8} \left(\frac{\lambda_o}{W} \right)^3 \left(\frac{\lambda_o}{S} \right)^2 \sin\left(\frac{\pi W}{\lambda_o} \right) \exp\left(-j \frac{2\pi S}{\lambda_o} \right) \tag{B.21}$$

Then, using equations B.7, B.8 and B.21, the mutual coupling, C_p, was deduced as

$$C_p = -20 \log \left[\frac{2\pi^5}{5} \frac{W}{\lambda_o} \left(\frac{S}{\lambda_o} \right)^2 \frac{1}{\sin\left(\frac{\pi W}{\lambda_o} \right)} \right] - 40 \log C_{p_2} \tag{B.22}$$

Then, using equations B22 and B.15, one deduces the mutual coupling in the H-plane as

$$C_p = -20 \log \left\{ \frac{2\pi^5 W}{5\lambda_o} \left(\frac{S}{\lambda_o} \right)^2 \frac{1}{\sin\left(\frac{\pi W}{\lambda_o} \right)} \right\} - 40 \log \left(\sqrt{\frac{R_r}{R_N}} + \sqrt{\frac{R_N}{R_r}} \right) \tag{B.23}$$

Note that equation B.23 is independent of the feed point location, substrate relative permittivity and thickness and it does also not take into account the surface wave contribution.

The following section presents analytical forms, deduced from a rigorous analysis to express the influence of the surface wave upon the coupling between antenna elements.

B.3 Influence of surface wave upon mutual coupling in the E-plane

As the TM_o has a zero cut-off frequency, this mode is always present in the substrate, regardless of the values of the substrate height and dielectric constant [4]. But, James et al [133] estimated that surface wave excitation is not important if $h/\lambda_o < 0.09$ for $\varepsilon_r \approx 2.3$ and $h/\lambda_o < 0.03$ for $\varepsilon_r \approx 10$. A formula for C_{pE} will be given in terms of both space wave and surface wave.

When the volume equivalence theorem is applied, the elementary polarisation current parallel to x axis and located in the xoz - plane is given [204] by the formula:

$$dI_x = j\omega(\varepsilon_r - 1)\varepsilon_o WV(z)\frac{d_z}{h} \tag{B.24}$$

and

$$dB_\phi = j\mu_o\left(\frac{h}{\lambda_o}\right)\left(\frac{dI_x}{\rho}\right) \tag{B.25}$$

In the vacuum medium the magnetic induction field just above the ground plane and due to the elementary electric moment HdI_X is given by equation B.25. When considering a TM mode inside the substrate sheet the magnetic induction at a short distance is expressed as:

$$dB_\phi = -4f\varepsilon_o\mu_o\varepsilon_r A(z)\cos\left(\frac{ux}{h}\right)\left(\frac{dz}{\rho}\right) \tag{B.26}$$

A is a function of z to be determined, u is given by equations B27 and B.28:

$$utgu = v\varepsilon_r \tag{B.27}$$

$$u^2 + v^2 = \left(\frac{2\pi h}{\lambda_o}\right)^2(\varepsilon_r - 1) \tag{B.28}$$

For a TM mode in the substrate sheet, we have the relation:

$$\frac{E_x}{H_\phi} = \frac{\sqrt{\varepsilon_e}}{\varepsilon_r}\sqrt{\frac{\mu_o}{\varepsilon_o}} \tag{B.29}$$

with

$$\varepsilon_e = \varepsilon_r - \left(\frac{u\lambda_o}{2\pi h}\right)^2 \tag{B.30}$$

Expressing the conservation principle of energies in the two mediums, we obtained the A(z) function from equations B,24, B.25, B.26 and B.29 as

$$A(z) = \left(\frac{\pi}{2}\right)(\varepsilon_r - 1)\sqrt[4]{\varepsilon_e}\,\frac{1}{\sqrt{\varepsilon_r}}\,\frac{W}{\lambda_o}\,V(z) \tag{B.31}$$

The electric field dE_x radiated at a distance ρ above the ground plane when $0 \le x \le h$ by the current element located at the origin is equal in cylindrical coordinates and for $\rho >> \lambda_o$ to:

$$dE_x = \beta^2 \frac{\pi}{2}\frac{(\varepsilon_r - 1)}{\sqrt{\varepsilon_r}}\frac{1}{\sqrt[4]{\varepsilon_e}}V(o)\left(\frac{W}{\lambda_o}\right)\sqrt{\frac{2}{\pi\rho\beta}}\exp(-j\rho\beta)\exp\left(-j\frac{\pi}{4}\right)\cos\left(\frac{ux}{h}dz\right) \tag{B.32}$$

with $\beta = 2\pi\dfrac{\sqrt{\varepsilon_e}}{\lambda_o}$. With V(z), is the potential distribution along the antenna acting at the resonance,

$$V(z) = V(o)\frac{\cosh[\gamma(h-z)]}{\cosh(\gamma h)} \tag{B.33}$$

the total electric field into the substrate and due to the polarisation current distribution is equal to:

$$E_x = \int_0^h \frac{V(z)}{V(o)}\exp(j\beta z\cos\phi)dE_x \tag{B.34}$$

When putting $\cosh(\gamma h) \approx \cosh(\alpha h + j\pi) \approx -\cosh(\alpha h) \approx 1$ and with equations B.32, B.33 and B.34 we can write after integration and with $k = \dfrac{2\pi}{\lambda_o}\sqrt{\varepsilon_r}$:

$$E_x = -j\frac{\beta^3\pi}{\sqrt[4]{\varepsilon_e}}\frac{\varepsilon_r - 1}{\sqrt{\varepsilon_r}}\left(\frac{W}{\lambda_o}\right)\exp\left[j\left(\frac{\beta h}{2}\cos\phi - \beta\rho - \frac{\pi}{4}\right)\right]\frac{\cos\phi\cos\left(\dfrac{\beta h\cos\phi}{2}\right)}{k^2 - \beta^2\cos^2\phi}$$
$$\cdot\sqrt{\frac{2}{\pi\beta\rho}}V(o)\cos\left(\frac{ux}{h}\right) \tag{B.35}$$

The electric field tangential component E_ρ is deduced as:

$$E_\rho 2\pi\sqrt{\varepsilon_e} = jutg\left(\frac{ux}{h}\right)\left(\frac{\lambda_o}{h}\right)E_x \tag{B.36}$$

with

$$U_o = \frac{\gamma E_{tan}}{\gamma^2+\beta^2}\frac{\exp(j\beta h)-ch\gamma h}{sh\gamma h} \tag{B.37}$$

and

$$E_{tan} = E_\rho(x=h,\phi=0) \tag{B.38}$$

From

$$\alpha h = \frac{4\pi^3}{5}\frac{LWh}{\lambda_o^3} \tag{B.39}$$

and if: $\frac{Wh}{\lambda_o^2} << \frac{5\sqrt{\varepsilon_r}}{2\pi^2}$, equation B.37 is equal to:

$$|U_o| = \frac{5\lambda_o}{2\pi^4}|E_{tan}|\frac{\varepsilon_{ew}}{\varepsilon_{ew}+\varepsilon_e}\cos\left(\frac{\pi}{2}\sqrt{\frac{\varepsilon_e}{\varepsilon_{ew}}}\right)\frac{\lambda_o^2}{Wh} \tag{B.40}$$

From equation B.4 one can write:

$$\left|\frac{Z_{12}}{2R_r}\right| = \left|\frac{U_o}{2V(o)}\right| \tag{B.41}$$

With equations B.35, B.36, B.38, B.40 and B.41 one can deduce in E-plane:

$$\left|\frac{Z_{12}}{2R_r}\right| = \frac{5}{4\pi^4}.u.\sin u.\left(\frac{\lambda_o}{h}\right)^2\frac{1}{\sqrt{\frac{S}{\lambda_o}}}\cos^2\left(\frac{\pi}{2}\sqrt{\frac{\varepsilon_e}{\varepsilon_{ew}}}\right)\frac{(\varepsilon_r-1)}{\sqrt{\varepsilon_r}}\frac{\varepsilon_{ew}\sqrt{\varepsilon_e}}{\varepsilon_{ew}^2-\varepsilon_e^2} \tag{B.42}$$

S is the distance between the two patches. If $h/\lambda << 1$ from equations B.27 and B.28 one obtains:

$$u\sin u\left(\frac{\lambda_o}{h}\right)^2 \approx 4\pi^2(\varepsilon_r-1) \tag{B.43}.$$

Then equation B.42 becomes:

$$\left|\frac{Z_{12}}{2R_r}\right| = \frac{5}{\pi^2}\frac{(\varepsilon_r - 1)^2}{\sqrt{\varepsilon_r}}\frac{\varepsilon_{ew}\sqrt{\varepsilon_e}}{\varepsilon_{ew}^2 - \varepsilon_e^2}\frac{1}{\sqrt{\frac{S}{\lambda_o}}}\cos^2\left(\frac{\pi}{2}\sqrt{\frac{\varepsilon_e}{\varepsilon_{ew}}}\right) \tag{B.44}$$

Where ε_{ew} is the effective relative permittivity and is given as [104]

$$\varepsilon_{ew} = 0.5\left[(\varepsilon_r + 1) + (\varepsilon_r - 1)\left(1 + \frac{10h}{W}\right)^{-0.5}\right] \tag{B.45}$$

Using equations B.7 and B.44, one can deduce the mutual coupling in the E-plane as a function of the surface wave

$$C_{pE} = 20\log\left\{\frac{5}{\pi^2}\frac{(\varepsilon_r - 1)^2}{\sqrt{\varepsilon_r}}\frac{\varepsilon_{ew}\sqrt{\varepsilon_e}}{\varepsilon_{ew}^2 - \varepsilon_e^2}\frac{1}{\sqrt{\frac{S}{\lambda_o}}}\cos^2\left(\frac{\pi}{2}\sqrt{\frac{\varepsilon_e}{\varepsilon_{ew}}}\right)\right\} - 40\log\left(\sqrt{\frac{R_r}{R_N}} + \sqrt{\frac{R_N}{R_r}}\right) \tag{B.46}$$

Bibliography

[1] I. J. Bahl and P. Bhartia, *Microstrip Antennas.* Dedham: Artech House, 1980.

[2] J. R. James and P. S. Hall, eds., *Handbook of Microstrip Antennas.* Vols I and II, London: Peter Peregrinus, (IEE) 1989.

[3] K. Chang, *Handbook of Microwave and Optical Components.* Vol. I, New York: John Wiley and Sons, 1989.

[4] P. Bhartia, K. Rao and R. Tomar, *Millimeter - Wave Microstrip and Printed Circuit Antennas.* Dedham: Artech House, 1991.

[5] D. M. Pozar and D. H. Schaubert, editors, *Microwave Antennas, The Analysis and Design of Microstrip Antennas and Arrays.* New York: IEEE Press, 1995.

[6] K. Hirasawa and M. Haneishi, eds., *Analysis, Design, and Measurement of Small and Low-Profile Antennas.* Dedham: Artech House, 1992.

[7] G. Dubost, *Flat Radiating Dipoles and Applications to Arrays.* Research Studies Press 1981.

[8] W. F. Richards, "Microstrip Antennas," in Y. T. Lo and S. W. Lee, (eds). *Antenna Handbook.* New York: Van Nostrand Reinhold, 1988.

[9] J. R. James, P. S. Hall and C. Wood, *Microstrip Antenna Theory and Design*. London: Peter Peregrinus (IEE), 1981.

[10] Special Issue, IEEE Transactions on and Antennas Propagation, vol. AP-29, January 1981.

[11] Special Issue, CAD of printed antennas and arrays, Part I and II, in *International Journal of Microwave and Millimeter wave Computer-Aided Engineering*. New York: John Wiley & Sons, 1994.

[12] J. R. Mosig and F. D. Gardiol, "A dynamic radiation model for microstrip structures", *Advances in Electronics and Electron Physics*, vol. 59, Academic Press, pp. 139-227, 1982.

[13] R. C. Johnson and H. Jasik, eds., *Antenna Engineering*. (Chapter 7) *Microstrip Antennas*, Second Edition, McGraw-Hill Book Company, 1984.

[14] D. M. Pozar, *Antenna Design Using Personal Computers*. Dedham: Artech House, pp. 121-126, 1985.

[15] K. C. Gupta and A. Benalla, eds., *Microstrip Antenna Design*. Dedham: Artech House, 1988.

[16] D. M. Pozar, *Analyses and Design of Considerations for Printed Phased Array Antennas*. Vol. I of Handbook of Microstrip Antennas, Chapter 12, London: Peter Peregrinus, 1989.

[17] J. Q. Howell, "Microstrip antennas", *IEEE Antennas and Propagation Symposium Digest*, pp. 177-180, 1972.

[18] R. E. Munson, "Conformal microstrip arrays and microstrip phased arrays", *IEEE Transactions on Antennas and Propagation*, pp. 74-78, January 1974.

[19] A. G. Derneryd, "Linearly polarised microstrip antennas", *IEEE Transactions on Antennas and Propagation*, pp. 846-851, November 1976.

[20] A. G. Derneryd, "Microstrip array antenna", *Proceeding 6th European Microwave Conference*, pp. 339-343, 1976.

[21] A. G. Derneryd, "A theoretical investigation of the microstrip antenna element", *IEEE Transactions on Antennas and Propagation*, vol. AP-26, pp. 532-536, July 1978.

[22] J. Vandensande, H. Pues and A. Van de Capelle, "Calculation of the bandwidth of microstrip resonator antennas", *Proceedings. 9th European Microwave Conference*, pp. 116-119, 1979.

[23] D. L. Sengupta, "Transmission line model analysis of rectangular patch antennas", *Electromagnetics*, Vol. 4, pp. 355-376, 1984.

[24] E. Peus and A. Van de Capelle, "Accurate transmission line model for the rectangular microstrip antenna", *IEE Proceedings*, Part H, vol 131, pp. 334-340, December 1984.

[25] A. K. Bhattacharyya and R. Garg, "Generalised transmission line model for microstrip patches", *IEE Proceedings*, Part H, vol. 132, pp. 93-98, April 1985.

[26] L. Murphy, "SEASAT and SIRA-A Microstrip Antennas", *Proceedings Workshop on Printed Circuit Antenna Technology*, paper 18, October 1979.

[27] K. R. Carver and E. L. Coffey, "A modal expansion theory for the microstrip antenna", *IEEE Antennas and Propagation Symposium Digest,* Seattle, pp. 101-104, 1979.

[28] K. R. Carver, "Practical analytical technique for the microstrip antenna", *Proceedings Workshop on Printed Circuit Antenna Technology*, New Mexico State University, Las Cruces, pp. 7.1 - 7.20, October 1979

[29] A. G. Derneryd and A. G. Lind, "Cavity model of the rectangular microstrip antenna", *Proceedings Workshop on Printed Circuit Antenna Technology*, New Mexico State University, Las Cruces, pp. 12.1-12.11, October 1979.

[30] Y. T. Lo, D. Solomon and W. F. Richards, "Theory and experiment of microstrip antennas", *IEEE Transactions on Antennas and Propagation, AP-27*, pp. 137-145, March 1979.

[31] K. R. Carver and E. L. Coffey, "Theoretical investigation of the microstrip antenna", *ARO semi-annual research report*, PT-00929, January 1979.

[32] K. R. Carver and J. W. Mink, "Microstrip antenna technology", *IEEE Transactions on Antennas and Propagation*, vol. AP-29, pp. 2-24, January 1981.

[33] K. R. Carver, "A modal expansion theory for the microstrip antenna", *IEEE Transaction on Antennas and Propagation Symposium*, Seattle, WA, pp. 101-104, June 1979.

[34] W. F. Richards, Y. T. Lo and D. D. Harrison, "An improved theory for microstrip antennas and applications", *IEEE Transactions on Antennas and Propagation*, vol. AP-29, pp. 38-46, January 1981.

[35] A. K. Bhattacharyya and R. Garg, "Input impedance of annular ring microstrip antenna using circuit theory approach", *IEEE Transactions on Antennas and Propagation*, vol. AP-33, pp. 369-374, April 1985.

[36] A. K. Bhattacharyya and R. Garg, "Spectral domain analysis of wall admittance for circular and annular microstrip patches and the effect of surface waves", *IEEE Transactions on Antennas and Propagation*, vol. AP-33, pp. 1067-1073, October 1985.

[37] A. K. Bhattacharyya and R. Garg, "Effect of substrate on the efficiency of an arbitrarily shaped microstrip patch antenna", *IEEE Transactions on Antennas and Propagation*, vol. AP-34, pp. 1181-1188, October 1986.

[38] A. K. Bhattacharyya and R. Garg, "A microstrip array of concentric array of annular rings", *IEEE Transactions on Antennas and Propagation*, vol. AP-33, pp. 655-659, June 1985.

[39] E. H. Newman and P. Tulyathan, "Analysis of microstrip using moment methods", *IEEE Transactions on Antennas and Propagation*, vol. AP-29, pp. 47-53, January 1981.

[40] T. Itoh and W. Menzel, "A full-wave analysis method for open microstrip structures", *IEEE Transactions on Antennas and Propagation*, vol. AP-29, pp. 63-68, January 1981.

[41] K. Araki and T. Itoh, "Hankel transform domain analysis of open circular microstrip radiating structures", IEEE Transactions on Antennas and Propagation, vol. AP-29, pp. 84-89, 1981.

[42] D. M. Pozar, "Input impedance and mutual coupling of rectangular microstrip antennas", *IEEE Transactions on Antennas and Propagation*, vol. AP-30, pp. 1191-1196, 1982.

[43] P. B. Katehi and N. G. Alexopoulos, "On the effect of substrate thickness and permittivity on printed circuit dipole properties", *IEEE Transactions on Antennas and Propagation*, vol. AP-31, pp. 34-39, January 1983.

[44] N. G. Alexopoulos, P. B. Katehi and D. B. Rudledge, "Substrate optimisation for integrated circuit antennas", *IEEE Transactions on Antennas and Propagation*, vol. AP-31, pp. 550-557, July 1983.

[45] D. M. Pozar, "Considerations for millimetre wave printed antennas", *IEEE Transactions on Antennas and Propagation*, vol. AP-31, pp. 740-747, September 1983.

[46] D. M. Pozar, "Improved computational efficiency for the moment method solution of printed dipoles and patches", *Electromagnetics*, vol. 3, pp. 299-309, July-December 1983.

[47] N. G. Alexopoulos, D. R. Jackson and P. B. Katehi, "Criteria for nearly omnidirectional radiation patterns for printed antennas", *IEEE Transactions on Antennas and Propagation*, vol. AP-33, pp. 195-205, February 1985.

[48] M. M. Ney, "Method of moments as applied to electromagnetic problems", *IEEE Transactions on Microwave Theory and Techniques*, vol. MTT-33, pp. 972-980, October 1985.

[49] D. R. Jackson and N. G. Alexopoulos, "Microstrip dipoles on electrically thick substrates", *International Journal of Infrared and Millimeter Waves*, vol. 7, pp. 1-26, January 1986.

[50] P. L. Sullivan and D. H. Schaubert, "Analysis of an aperture coupled microstrip antenna", *IEEE Transactions on Antennas and Propagation*, vol. AP-34, pp. 977-984, August 1986.

[51] D. R. Jackson and N. G. Alexopoulos, "Analysis of planar strip geometry in a substrate-superstrate configuration", *IEEE Transactions on Antennas and Propagation*, vol. AP-34, pp. 1430-1438, December 1986.

[52] D. M. Pozar, "Radiation and scattering from a microstrip patch on a uniaxial substrate", *IEEE Transactions on Antennas and Propagation*, vol. AP-35, pp. 613-621, June 1987.

[53] D. M. Pozar and S. M. Voda, "A rigorous analysis of a microstrip line fed patch antenna", *IEEE Transactions on Antennas Propagation*, vol. AP-35, pp. 1343-1350, December 1987.

[54] H. Nakao, S. R. Kerner and N. G. Alexopoulos, "The moment method Solution for printed wire antennas of arbitrary configuration", *IEEE Transactions on Antennas and Propagation*, vol. AP-36, pp. 1667-1674, December 1988.

[55] J. R. Mosig, "Arbitrarily shaped microstrip structures and their analysis with a mixed potential integral equation", *IEEE Transactions on Microwave Theory and Techniques*, vol. MTT-36, pp. 314-323, February 1988.

[56] T. M. Willis and D. L. Sengupta, "Spectral analysis of microstrip antennas with CG-FFT: two-dimensional results", *IEEE Transactions on Antennas and Propagation*, vol. AP-37, pp. 810-816, July 1989.

[57] N. G. Alexopoulos, N. K. Uzunoglu and I. Rana, "Radiation by Microstrip Patches," IEEE *Antennas and Propagation Symposium Digest*, Seattle, pp. 722-727, 1979.

[58] M. D. Despande and M. C. Bailey, "Input impedance of microstrip antennas", *IEEE Transactions on Antennas and Propagation*, vol. AP-30, pp. 645-650, 1982.

[59] P. K. Agrawal and M. C. Bailey, "An analysis technique for microstrip antennas", *IEEE Transactions on Antennas and Propagation*, vol. AP-25, pp. 756-759, November 1977.

[60] P. C. Sharma and K. C. Gupta, "Analysis and optimised design of single feed circularly polarised microstrip antennas", *IEEE Transactions on Antennas and Propagation*, vol. AP-31, pp. 949-955, 1983.

[61] T. Okoshi and T. Miyoshi, "The planar circuit - an approach to microwave integrated circuitry", *IEEE Transactions on Microwave Theory and Techniques*, vol MTT-20, pp. 245-253, April 1972.

[62] V. Polanisamy and R. Garg, "Analysis of arbitrarily shaped microstrip patch antennas using segmentation technique and cavity model", *IEEE Transactions on Antennas and Propagation*, vol. AP-34, pp. 1208-1213, 1986.

[63] P. Perlmutter, S. Shtrikman and D. Trevers, "Electric surface current model for the analysis of microstrip antennas with application to rectangular elements", *IEEE Transactions on Antennas and Propagation*, vol. AP-33, pp. 301-311, March 1985.

[64] J. Ashkenazy, S. Shtrikman and D. Treves, "Electric surface current model for the analysis of microstrip antennas on cylindrical bodies", *IEEE Transactions on Antennas and Propagation*, vol. AP-33, pp. 295-300, March 1985.

[65] J. R. Mosig and F. E. Gardiol, "The near field of a open microstrip structure", *IEEE Antennas and Propagation Symposium Digest*, Seattle, pp. 379-381, 1979.

[66] N. K. Uzunoglu, N. G. Alexopoulos and J. G. Fikioris, "Radiation properties of microstrip dipoles", *IEEE Transactions on Antennas and Propagation*, vol. AP-27, pp. 853-858, November 1979, and corrections, AP-30, p. 526, May 1982.

[67] F. J. German, L. S. Gothard, L. S. Riggs and M. E. Baginski, "Analysis of microstrip antennas using the TLM method", *Applied Computational Electromagnetics*, Conference Proceedings, pp. 645 - 691, 1989.

[68] L. Napoli and J. Hughes, "Foreshortening of microstrip open circuits on alumina substrate", *IEEE Transactions on Microwave Theory and Techniques*, vol. MTT-19, pp. 559-561, 1971.

[69] H. Araki, H. Ueda and T. Masayuki, "Numerical analysis of circular diskmicrostrip antennas with parasitic elements", *IEEE Transactions on Antennas and Propagation*, vol. AP-34, pp. 1390-1394, December 1986.

[70] J. R. James and C. J. Wilson, "Microstrip antennas and arrays. Part I- fundamental action and limitations", *IEE Journal Microwaves, Optics and Acustics*, vol. 1, pp. 165-174, 1977.

[71] A. G. Derneryd, "Analysis of the microstrip disk antenna element", *IEEE Transaction on Antennas and Propagation*, vol. AP-27, pp. 660-664, 1979.

[72] D. M. Pozar, "A reciprocity method of analysis for printed slot and slot coupled microstrip antennas", *IEEE Transactions on Antennas and Propagation*, vol. AP-34, pp. 1439-1446, 1986.

[73] R. M. Martinson and E. F. Kuester, "Accurate analysis of arbitrarily shaped patch resonators on thin substrates", *IEEE Transactions on Microwave Theory and Techniques*", MTT-36, pp. 324-331, February 1988.

[74 Y. Suzuki and T. Chiba, "Computer analysis method for arbitrarily shaped microstrip antenna with multiterminals", *IEEE Transactions on Antennas and Propagation*, vol. AP-32, pp. 585-590, June 1984.

[75] W. C. Chew and J. A. Kong, "Analysis of a circular microstrip disk antenna with a thick dielectric substrate", *IEEE Transactions on antennas and Propagation*, vol. AP-29, pp. 68-76, January 1981.

[76] C. Wood, "Analysis of microstrip circular patch antennas", *IEE Proceedings* Part H, vol. 128 H, pp. 69 - 76, 1981.

[77] M. Kara, "Design principles of physically thick microstrip antenna elements for missile applications", *Third Australian Symposium on Antennas*, Sydney, Australia, 1991.

[78] M. Kara, "A new method for computing the physical parameters of rectangular microstrip antenna element", *Proceedings of IREECON International Convention*, Melbourne, Australia, pp. 642-645, September 1989.

[79] M. Kara, "Formulae for the computation of the physical properties of rectangular microstrip antenna elements with various substrate thicknesses", to be published in *Microwave and Optical Technology Letters*.

[80] M. Kara, "A new formula for patch resonant length", to be published in *International Journal of Electronic.*

[81] M. Kara, "A novel broad-band rectangular microstrip antenna element", *Microwave and Optical Technology Letters*, vol. 7, pp. 685-687, October 1994.

[82] M. Kara, "Novel dual-band rectangular microstrip antenna element", *International Journal of Electronics*, vol. 78, pp. 417-422, 1995.

[83] M. Kara, "Effective permittivity of rectangular microstrip antenna elements with various thicknesses of substrates", *Microwave and Optical Technology Letters*, vol. 10, pp. 244-247, November 1995

[84] M. Kara, "A novel tiny microstrip ring antenna element", *Microwave and Optical Technology Letters*, vol. 10, pp. 259-261, December 1995.

[85] M. Kara, "Novel technique for computation of mutual coupling between two rectangular microstrip antenna elements with thick substrates", to be published in *IEE Proceedings, Microwaves, Antennas and Propagation.*

[86] M. Kara, "Considerations for X- and Ku band rectangular microstrip antenna elements", *Proceedings of IREECON International Convention,* Sydney, Australia, pp. 688-691, 1991.

[87] M. Kara, "The resonant frequency of rectangular microstrip antenna elements with various substrates thicknesses", M*icrowave and Optical Technology Letters,* vol 11, pp. 55-59, February 1996.

[88] M. Kara, "Closed-form expression for the resonant frequency of rectangular microstrip antenna elements with thick substrates", has been accepted for publication in *Microwave and Optical Technology Letters* and will appear in the June 20, 1996 issue.

[89] M. Kara, "A simple technique for the calculation of bandwidth of rectangular Microstrip antenna elements with various substrate thicknesses", *Microwave and Optical Technology Letters*, Vol. 12, No. 1, pp. 16-20, May 1996.

[90] M. Kara, "A novel technique for computation the bandwidth of rectangular microstrip antenna elements with thick substrate", has been accepted for publication in *Microwave and Optical Technology Letters* and will appear in the June 5, 1996 issue.

[91] D. W. Griffin and M. Kara, "Experimental evidence that microstrip patches and flat dipoles on grounded substrates are same type of element", *IEEE Antennas and Propagation Symposium Digest,* Syracuse, USA, pp. 458-461, June 1988.

[92] M. Kara and D. W. Griffin, "An investigation of microstrip patch antennas using various thickness of dielectric", *Proceedings of IREECON International Convention,* Sydney, Australia, pp. 339-342, September, 1987.

[93] M. Kara, "Examination of far field characteristics of rectangular microstrip antenna elements", *Proceedings of* RADARCON *International Convention*, Adelaide, Australia, pp. 407-414, April 1990.

[94] M. Kara, "Effects of substrate thickness on performance characteristics of rectangular microstrip antenna elements", Asia-Pacific Microwave Conference, Adelaide, Australian, pp. 203-206, August 1992.

[95] M. Kara, "Miniaturised microstrip antenna elements", *Fifth Australian Symposium on Antennas*, p. 18, Sydney, Australia, February, 1996.

[96] M. Kara, "Novel microstrip antenna elements for radar and satellite systems applications", *Workshop on Applications of Radio Science*, Canberra, Australia June 1995.

[97] M. Kara, "Miniaturised microstrip antenna elements for surface and space borne vehicles applications", to be published in *Journal of Electrical and Electronics Engineering, Australia.*

[98] M. Kara, "A simple technique for the computation of the mutual coupling between two rectangular microstrip antenna elements with various substrate thicknesses", *Fifth Australian Symposium on Antennas,* p. 14, Sydney, Australia, February, 1996.

[99] R. W. Dearnly and A. R. F. Barel, "A broad-band transmission line model for a rectangular microstrip antenna", IEEE Transactions on Antennas and Propagation, vol AP-37, pp. 6-15, January 1989.

[100] G. Dubost, "Linear transmission line model analysis of arbitrary shape patch antennas", *Electronics Letters*, vol. 22, pp. 798-799, 1986.

[101] J. R. James, "Printed antennas-new research frontiers", *Asia-Pacific Microwave Conference Proceedings*, pp. 21-26, August 1992

[102] R. P. Owens, "Accurate analytical determination of quasi-static microstrip line parameters", *Radio and Electronic Engineer*, vol. 46, pp. 360-364, 1976.

[103] R. F. Harrington, *Time-Harmonic Electromagnetic Fields*, New York, McGraw-Hill, 1961, p.183.

[104] M. V. Schneider, "Microstrip lines for microwave integrated circuits", *Bell Systems Technical Journal*, vol. 48, pp. 1421-1444, May-June 1969.

[105] E. O. Hammerstad, "Equations for microstrip circuits design", Proceeding *5th European Microwave Conference*, pp. 268-272, September 1975.

[106] A. G. Derneryd and A. G. Lind, "Extended analysis of rectangular microstrip resonator antennas", *IEEE Transactions on Antennas and Propagation*, vol. AP-27, pp. 846-849, November 1979.

[107] W. F. Richards, Y. T. Lo, P. Simon and D. D. Harrison, "Theory and applications for microstrip antennas", *Proceeding Workshop on Printed Circuit Antenna Technology*, New Mexico State University, Las Cruces, pp. 8.1-8.23, October 1979.

[108] S. Long, L. C. Shen and P. B. Morel, "Theory of the circular-disc printed - circuit antennas", *IEE Proceedings*, Part H, vol. 125, pp. 925-928, 1978.

[109] A. K. Skrivervik and J. R. Mosig, "Impedance matrix of multiport microstrip discontinuity including radiation effects", *Archiv fur Elektrotechnik und Ubertragungstechnik*, 44 (6) pp. 453-461, 1990.

[110] J. Huang, "The finite ground plane effect on the microstrip antenna radiation patterns", *IEEE Transactions on Antennas and Propagation*, vol. AP-31, pp. 649-653, 1983.

111] M. Kominami, D. M., Pozar and D. H Schaubert, "Dipole and slot elements and arrays on semi-infinite substrates", *IEEE Transactions on Antennas and Propagation*, vol. AP-33, pp. 660-607, June 1985.

[112] A. Reineix and B. Jecko," Analysis of microstrip patch antennas using finite difference time domain method", *IEEE Transactions on Antennas and Propagation*, vol. AP-37, pp. 1361-1369, 1989.

[113] P. Leveque, A. Reineix and B. Jecko, "Modelling dielectric losses in microstrip patch antennas application of FDTD method", *Electronics Letters*, vol. 6, pp. 539-540, 1992.

[114] C. Wu, K. L. Wu, Z. Q. Bi and J. Litva, "Accurate characterisation of planar printed antennas using finite difference time domain method", *IEEE Transactions on Antennas and Propagation*, vol. AP-40, pp. 526 -533, 1992.

[115] T. Kashiwa, T. Onihi, and I. Fukai, "Analysis of microstrip antennas on a curved surface using the conformal grids FD-TD method", *IEEE Transactions on Antennas and Propagation*, vol. AP-42, pp. 423-427, 1994.

[116] A. Reineix, J. Paillol, and B. Jacko, "FDTD method applied to the study of radar cross section of microstrip patch antennas: *des Telecommunications*, 48, 11/12, pp. 589 - 593, 1993.

[117] K. Uehara and K. Kagoshima, "FDTD method analysis of mutual coupling between microstrip antennas", *IEICE Transactions on Communications*, E76-B, 7, pp. 762-764, 1993

[118] J. R. Mosig and F. E. Gardiol, "The near field of an open microstrip structure", *IEEE Antennas and Propagation Symposium Digest*, Seattle, pp. 379-381, 1979.

[119] P. Hammer, D. Van Bouchaute, D. Verschraeven and A. Van De Capelle, "A model for calculating the radiation field of microstrip antennas", *IEEE Transactions on Antennas and Propagation*, vol. AP-27, pp. 267-270, March 1979.

[120] H. D. Weinschel, "Measurements of various microstrip parameters," *Proceedings Workshop on Printed Circuit Antennas Technology,* New Mexico State University, USA, pp. 2.1 - 2.15, October 1979.

[121] I. J. Bahl, "Build microstrip antennas with paper-thin dimensions", Microwaves, vol. 18, pp. 50-63, October 1979.

[122] K. G. Schroeder, "Miniature slotted cylinder antennas", *Microwaves*, pp. 28-37, December 1964.

[123] I. Wolff and N. Knoppik, "Rectangular and circular microstrip disc capacitors and resonators", *IEEE Transactions on Microwave Theory and Techniques*, vol. MTT-22, pp. 857-864, October 1974.

[124] E. H. Newman, J. H. Richmond and G. W. Kwan, "Mutual impedance computation between microstrip antennas", *IEEE Transactions on Microwave Theory and Techniques*, vol. MTT-31, pp. 941-945, November 1983.

[125] D. H. Schaubert, D. M. Pozar and A. Adrian, "Effect of microstrip antenna substrate thickness and permittivity: comparison of theories with experiment", *IEEE Transactions on Antennas and Propagation*, AP-37, pp. 677-682, June 1989.

[126] J. R. Mosig and F. E. Gardiol, "General integral equation formulation for microstrip antennas and scatterers", *IEE Proceedings* Part H, vol. 132, No. 7, pp. 424-432, 1985.

[127] R. C. Hall and J. R. Mosig, "The analysis of coaxially fed microstrip antenna with electrically thick substrates", *Electrmagnetics*, vol. 9, pp. 367-384, 1989.

[128] L. Barlatey, J. R. Mosig, and T. Sphicopoulos, "Analysis of stacked microstrip patches with a mixed potential integral equation", *IEEE Transactions on Antennas and Propagation*, vol. AP-38, pp. 608-615, 1990.

[129] J. T. Aberle and D. M. Pozar, "Analysis of infinite arrays of probe-fed rectangular micristrip patches using a rigorous feed model", *IEE Proceedings* Part H, vol. 136, pp. 110-119, 1989.

[130] E. Chang, S. A. Long and W. F. Richards, "An experimental investigation of electrically thick rectangular microstrip antennas", *IEEE Transactions on Antennas and Propagation*, vol. AP-34, pp. 767-772, June 1986.

[131] M. Kara, "The input resistance of rectangular microstrip antenna elements with various substrate thicknesses", to be published in *Microwave and Optical Technology Letters.*

[132] M. Kara, "An efficient technique for the computation of the input resistance of rectangular microstrip antenna elements with thick substrates", to be published in *Microwave and Optical Technology Letters.*

[133] J. R. James and A. Henderson, "High frequency behaviour of microstrip open circuit terminations", *IEE Journal Microwaves, Optics and Acustics*, vol. 3, pp. 205-218, September 1979.

[134] J. R. Henderson and P. H. Hall, "Microstrip antenna performance is determined by substrate constraints", *Microwave Systems News*, vol. 12, pp. 73-84, August 1982.

[135] N. Knoppik, "The Q factor of microstrip resonators", *Archiv fur Elektrotechnik und Ubertragungstechnik, v*ol. 30, pp. 49-58, February 1976.

[136] H. Pues, J. Bogaers, R. Pieck and A. Van de Capelle, "Wideband quasi-log-periodic microstrip antennas", *IEE Proceedings*, Part H, vol. 128, pp. 159-163, June 1981.

[137] R. Garg and S. A. Long, "Resonant frequency of electrically thick rectangular microstrip antenna", *Electronics Letters*, vol. 23, pp. 1149-1151, 1987.

[138] P. S. Hall and J. R. James, "Cross polarisation behaviour of series-fed microstrip linear array", *IEE Proceedings*, Part H, vol. 131, pp. 247-257, August 1984.

[139] A. G. Derneryd, "Circular and Rectangular Microstrip Antenna Elements", *Ericsson Technics,* No. 3, pp. 160-171, 1978.

[140] J. Q. Howell, "Microstrip antennas", *IEEE Transactions on Antennas and Propagation*, vol. AP-23, pp. 90-93, January 1975.

[141] E. Penard and J. P. Daniel, "Open and hybrid microstrip antennas", *IEE Proceedings*, Part H, vol. 131, pp. 38-44, 1981.

[142] J. F. Zurcher, "The SSFIP: a global concept for high performance broad band antenna", *Electronics Letters*, vol. 24, pp. 1433-1435, November 1988.

[144] D. M. Pozar and B. Kaufman, "Increasing the bandwidth of a microstrip antenna by proximity coupling", *Electronics Letters*, vol. 23, pp. 368-369, April 1987.

[145] G. Kumar and K. C. Gupta, "Broadband microstrip antennas using additional resonators gap coupled to the radiating edges", *IEEE Transactions on Antennas Propagation*, vol. AP-32, pp. 1375-1379, December 1984.

[146] H. K. Smith and P. E. Mayes, "Stacking resonators to increase the bandwidth of low profile antennas", *IEEE Transactions on Antennas and Propagation*, vol. AP-35, pp. 1473-1476, December 1987.

[147] A. N. Tulintseff, S. M. Ali and J. A. Kong, "Input impedance of probe-fed stacked circular microstrip antenna", *IEEE Transactions on Antennas and Propagation*, vol. AP-39, pp. 381-390, March 1991.

[148] A. Sabban, "New broadband stacked two layer microstrip antenna", *IEEE Antennas and Propagation Symposium Digest*, Houston, Tx. pp. 63-66, 1983.

[149] R. B. Waterhouse and N. V. Shuley, "Analysis of microstrip patch antennas with broad bandwidth and frequency agility using shottkey barrier diodes", *Proceedings, 3rd Int. Symposium on Recent Advances in Microwave Technology*, Reno, 1977, pp. 277-280, 1991

[150] C. Wood, "Curved microstrip lines as compact wideband circularly polarised antennas", *IEE Journal Microwaves, Optics and Acustics*, vol. 3, pp. 5-13, 1979

[151] M. Kara, "Thick patch on a thin substrate improves the bandwidth of microstrip antennas", *Fourth Australian Symposium on Antennas*, Sydney, Australia, February 1994.

[153] IEEE Standard Dictionary of Electrical and Electronics Terms, third Edition, 1984

[154] A. G. Derneryd, "The circular microstrip antenna element", *IEE Proceedings International Conferance Publication Antennas and Propagation*, Part I, pp. 307-310, November 1978.

[155] D. M. Pozar, "Rigorous closed-form expressions for the surface wave loss of printed antennas," *Electronics Letters*, vol. 26, pp. 954-956, June 1990.

[156] G. Dubost, "Far field radiated by rectangular patch microstrip antenna", *Electronics Letters*, vol. 18, pp. 991-993, November 1982.

[157] H. F. Pues, and A. R. Van De Capelle, "An impedance-matching technique for increasing the bandwidth of microstrip antennas", *IEEE Transactions on Antennas and Propagation*, vol. AP-37, pp. 1345-1354, 1989.

[158] D. A. Paschen, "Practical examples of integral broadband matching of microstrip antenna element," *Proceedings of Antenna Applications Symposium*, pp. 199-217, 1986.

[159] A. J. Svitak, D. M. Pozar, and R. W. Jackson, "Optically fed aperture coupled microstrip patch antennas", *IEEE Transactions on Antennas and Propagation*, vol. AP. 40, pp. 85-90, January 1992.

[160] H. An, B. Nauwelaers, and A. Van de Capelle, "Broadband active microstrip array antennas," Electronics Letters, vol. 27, pp. 2378-2379, 5, 1991.

[161] P. S. Hall, "Probe compensation in thick microstrip patches," *Electronics Letters*, vol. 21, pp. 606-607, May 1987.

[162] D. M. Pozar and B. Kaufman, "Increasing the bandwidth of a microstrip antenna by proximity coupling", *Electronics Letters*, vol. 23, pp. 368-369, April 1987.

[163] H. Legay and L. Shafai, "New stacked microstrip antenna with large bandwidth and high gain", *IEE Proceeding Microwave Antennas Propagation*, vol. 141, pp. 199-204, June 1994.

[164] P. S. Hall, C. Wood and C. Garrett, "Wide bandwidth microstrip antennas for circuit integration", *Electronics Letters*, vol. 15, pp. 458 - 460, 1979.

[165] G. Kossiavas and A. Papiernik, "A circularly or linearly polarised broadband microstrip antenna operating in L-band", *Microwave Journal*, pp. 266-272, May 1992.

[166] F. Croq and D. M. Pozar, "Millimeter wave design of wide-band aperture coupled stacked microstrip antennas", *IEEE Transactions on Antennas and Propagation*, vol. AP-39, pp. 1770 -1776, December 1991.

[167] C. Wood, "Improved bandwidth of microstrip antennas using parasitic elements", *IEE Proceedings*, Part H, vol. 127, pp. 231-234, 1980.

[168] G. Kumar and K. C. Gupta, "Non-radiating edges and four-edges gap-oupled with multiple resonator, broadband microstrip antennas", *IEEE Transactions on Antennas and Propagation*, vol. AP-33, pp. 173-178, 1985.

[169] Y. Suzuki, N. Miyano and T. Chiba, "Expanding the frequency bandwidth of a microstrip antenna", *IEEE Antennas and Propagation Symposium*, pp. 617-620, 1980.

[170] H. S. Johns, D. H. Schaubert and F. G. Farrar, "Dual frequency piggyback antenna", *US. patent* No 4, 162 499, 24 July 1979.

[171] N. W. Montgomery, "Triple frequency stacked microstrip element", *IEEE Antennas and Propagation Symposium*, Boston, MA, pp. 255- 258, June 1984.

[172] S. A. Long and W. D. Walton, "A dual frequency stacked circular disc antenna", *IEEE Transactions on Antennas and Propagation*, vol. AP-27, pp. 270-273, 1979.

[173] J. S. Dahele and K. F. Lee, "A dual frequency stacked microstrip antenna", *IEEE Antennas and Propagation Symposium Digest*, pp. 308-311, 1982.

[174] J. S. Dahele, K. F. Lee and D. P. Wong, "Dual-frequency stacked annular-ring Microstrip Antenna", *IEEE Transactions on Antennas and Propagation*, vol. AP-35, pp. 1281-1285, 1987.

[175] J. Wang, R. Fralich, C. Wu and J. Litva, "Multi-functional aperture coupled stacked antenna", *Electronics Letters*, vol. l.26, pp. 2067-2068, 1990.

[176] D. H. Schaubert and F. G. Farrar, "Some conformal, printed circuit antenna designs", *Proceedings Workshop on Printed Circuit Antennas*, New Mexico State University, pp. 5.1-5.21, October 1979.

[177] J. McIlvenna and N. Kernweis, "Modified circular microstrip antenna elements", *Electronics Letters*, vol. 15, pp. 207-208, 1979.

[178] S. E. Davidson, S. A. Long and W. F. Richards, "Dual-band microstrip antennas with monolithic reactive loading", *Electronics Letters*, vol. 21, pp. 936-937, 1985.

[179] P. S. Hall, "New wideband microstrip antenna using log-periodic technique", *Electronics Letters*, vol. 16, pp. 127-128, February 1980.

[180] C. S., V. Nalbandian and F. Schwering, "Planar dual- band microstrip antenna", IEEE Transaction on Antennas and Propagation, vol. AP-43, pp. 892-894, August 1995.

[181] Y. M. M. Antar, A. I. Ittipiboon, and A. K. Bhattacharyya, "A dual-frequency antenna using a single patch and an inclined slot", *Microwave and Optical Technology Letters*, vol. 8, pp. 309-311, 1995.

[182] C. S. Lee, V. Nalbandian and F. Schwering, "Dual-frequency microstrip antenna with inhomogeneously filled dielectric substrate", *Microwave and Optical Technology Letters*, vol. 6, pp. 629-632, 1993.

[183] P. Bhartia and I. Bahl, "A frequency agile microstrip antenna", *IEEE Antennas and Propagation Symposium Digest*, New Mexico, pp. 304-307, 1982.

[184] D. H. Schaubert, F. G. Farrar, A. Sindoris and S. T. Hayes, "Microstrip antennas with frequency agility and polarisation diversity", *IEEE Transactions on Antennas and Propagation*, vol. AP-29, pp. 118-124, January 1984.

[185] A. S. Daryoush, K. Bontzos and P. R. Hercsfeld, "Optically tune patch antenna for phased array applications", *IEEE Antennas and Propagation Symposium Digest*, Philadelphia, pp. 361-364, 1986.

[186] H. Pues, J. Vandensande and A. Van de Capelle, "Broadband microstrip resonator antennas", *IEEE Antennas and Propagation Symposium Digest*, Washington, pp. 268-271, May 1978.

[187] R. J. Mailloux, J. F. McIlbenna and N. P. Kernweis, "Microstrip array technology", *IEEE Transactions on Antennas and Propagation*, vol. AP-29, pp. 25-37, 1981.

[188] A. R. Sindoris and C. M. Krowne, " Calculation of H-plane mutual coupling between rectangular microstrip antennas", *IEEE Antennas and Propagation Symposium Digest*, pp. 738-742, June 1980.

[189] N. G. Alexopoulos, I. E. Rana, "Mutual impedance computation between printed dipoles", *IEEE Transactions on Antennas and Propagation*, vol. AP-29, pp. 106-111, January 1981.

[190] E. H. Van Lil and A. R. Van De Capelle, "Comparison of models for calculating mutual coupling in microstrip arrays", *IEEE Antennas and Propagation Symposium Digest*, Boston, pp. 745-748, 1984.

[191] E. Penard and J. P. Daniel, "Mutual coupling between microstrip antennas", *Electronics Letters*, vol. 18, pp. 605-607, 1982.

[192] V. J. H. Pues and A. Van De Capelle, "Calculation of the bandwidth of microstrip resonator antennas", *Proceedings 9th European Microwave Conference*, pp. 116-119, 1979.

[193] R. P. Jedlicka, and K. R. Carver, "Mutual coupling between microstrip antennas", *Proceedings Workshop on Printed Circuit Antenna Technology*, New Mexico State University, Las Cruces, pp. 4 1-4.19, October 1979,

[194] R. P. Jedlicka, M. T. Poe and K. R. Carver, "Measured mutual coupling between microstrip antennas", *IEEE Transactions on Antennas and Propagation*, vol. AP-29, pp. 147-149, January 1981.

[195] C. M. Krowne, A. R. Sindoris, "H-plane coupling between rectangular microstrip antennas", *Electronics Letters*, vol. 16, pp. 211-213, 1980.

[196] M. Malkomes, "Numerische Und Experimentelle Analyse Gedruckter Microstrip Antennen Und Verkoppelter Antennengruppen", Ph.D dissertation, Fakultat fur Electrotechnik der Rheinisch-Westfalschen Technishcen Hochschule Aachen W. Deutschland 1982.

[197] E. Penard and J. P. Daniel, "Mutual coupling between microstrip antennas", *Electronics Letters*, vol. 18, pp. 605-607, July 1982.

[198] C. M. Krowne, "Dielectric and width effect on H-plane and E-plane coupling between rectangular microstrip antennas", *IEEE Transactions on Antennas and Propagation*, vol. AP-31, pp. 39-47, January 1983.

[199] C. M. Krowne, "E-plane coupling between two rectangular microstrip antennas", *Electronics Letters*, vol. 16, pp. 635-636, 1980.

[200] E. H. Van Lil and A. R. Van de Capelle, "Transmission line model for mutual coupling between microstrip antennas", *IEEE Transactions on Antennas and Propagation*, vol. AP-32, pp. 816-821, 1984.

[201] A. H. Mohammadian, N. M. Martin and D. W. Griffin, "A Theoretical and experimental study of mutual coupling in microstrip antenna arrays", *IEEE Transactions and Antennas and Propagation*, pp. 1217-1223, 1989.

[202] G. Dubost, "Mutual impedance and coupling coefficient between two patches expressed through analytical forms", *Electronics Letters*, pp. 1099-1101, November 1985.

[203] E. Penard, "Etude d'antennes imprimeès par la mèthode de la cavitè. Application au couplagè", Thèse 3è Cycle Universitè de Rennes I, December 1982.

[204] G. Dubost, "Influence of surface wave upon efficiency and mutual coupling between rectangular microstrip antennas", *IEEE Antennas and Propagation Symposium Digest*, Dallas, USA, pp. 660-663, 1990.

[205] D. R. Jackson, et al., "An exact mutual coupling theory for microstrip patches", *IEEE Antennas and Propagation Symposium Digest,* pp. 790-793, June 1987.

[206] M. Kara, "Microstrip block antenna elements with thick patch conductor", to be published in *Electronics Letters*